

NASA TECHNICAL NOTE



NASA TN D-6617

c.1

NASA TN D-6617

LOAN COPY: RETURN TO  
AFWL (DO NOT)  
KIRTLAND AFB



ELECTROSTATIC-PROBE MEASUREMENTS  
OF PLASMA PARAMETERS FOR  
TWO REENTRY FLIGHT EXPERIMENTS  
AT 25 000 FEET PER SECOND

*by W. Linwood Jones, Jr., and Aubrey E. Cross*  
*Langley Research Center*  
*Hampton, Va. 23365*





0133161

1. Report No. NASA TN D-6617	2. Government Accession No.	3. Recipient's Catalog No.	
4. Title and Subtitle ELECTROSTATIC-PROBE MEASUREMENTS OF PLASMA PARAMETERS FOR TWO REENTRY FLIGHT EXPERIMENTS AT 25 000 FEET PER SECOND		5. Report Date February 1972	6. Performing Organization Code
		8. Performing Organization Report No. L-7984	10. Work Unit No. 115-21-01-01
7. Author(s) W. Linwood Jones, Jr., and Aubrey E. Cross		11. Contract or Grant No.	13. Type of Report and Period Covered Technical Note
9. Performing Organization Name and Address NASA Langley Research Center Hampton, Va. 23365		14. Sponsoring Agency Code	
		12. Sponsoring Agency Name and Address National Aeronautics and Space Administration Washington, D.C. 20546	
15. Supplementary Notes With appendix B by Lorraine F. Satchell and appendix C by William L. Weaver. Part of the information presented herein was included in a dissertation, "Probe Measurements of Electron Density Profiles During a Blunt-Body Reentry" by W. Linwood Jones, Jr., presented in partial fulfillment of the requirements for the degree of Doctor of Philosophy in Electrical Engineering, Virginia Polytechnic Institute and State University, Blacksburg, Virginia, June 1971.			
16. Abstract Unique plasma diagnostic measurements at high altitudes from two geometrically similar blunt-body reentry spacecraft using electrostatic probe rakes are presented. The probes measured the positive-ion density profiles (shape and magnitude) during the two flights. The probe measurements were made at eight discrete points (1 cm to 7 cm) from the vehicle surface in the aft flow field of the spacecraft over the altitude range of 85.3 to 53.3 km (280 000 to 175 000 ft) with measured densities of $10^8$ to $10^{12}$ electrons/cm <sup>3</sup> , respectively. Maximum reentry velocity for each spacecraft was approximately 7620 meters/second (25 000 ft/sec). In the first flight experiment, water was periodically injected into a flow field which was contaminated by ablation products from the spacecraft nose region. The nonablative nose of the second spacecraft thereby minimized flow-field contamination. Comparisons of the probe-measured density profiles with theoretical calculations are presented with discussion as to the probable cause of significant disagreement. Also discussed are the correlation of probe measurements with vehicle angle-of-attack motions and the good high-altitude agreement between electron densities inferred from the probe measurements, VHF antenna measurements, and microwave reflectometer diagnostic measurements.			
17. Key Words (Suggested by Author(s)) Reentry communications; plasma diagnostics; electrostatic (Langmuir) probes; blackout alleviation; microwave reflectometer; body motions; electron concentration		18. Distribution Statement Unclassified - Unlimited	
19. Security Classif. (of this report) Unclassified	20. Security Classif. (of this page) Unclassified	21. No. of Pages 129	22. Price* \$3.00



## CONTENTS

	Page
SUMMARY . . . . .	1
INTRODUCTION . . . . .	1
SYMBOLS . . . . .	2
EXPERIMENT DESCRIPTION . . . . .	6
Flight Objectives . . . . .	6
Launch Vehicles . . . . .	6
Payloads . . . . .	7
Electrostatic Probe System . . . . .	8
RAM C-I Water-Injection System . . . . .	12
RAM C-II Microwave Reflectometer System . . . . .	12
VHF System . . . . .	13
ELECTROSTATIC PROBE THEORY . . . . .	13
FLIGHT DATA RESULTS AND DISCUSSION . . . . .	14
Measured Electrostatic Probe Ion Currents . . . . .	14
Thermocouple Probe Results . . . . .	15
Electron Densities Inferred by Electrostatic Probe . . . . .	15
Effects of Ablation Impurities on Electron Density . . . . .	16
Effects of Vehicle Angle-of-Attack Perturbations on Electron Density . . . . .	16
Effects of Water Injection on Electron Density . . . . .	17
Microwave Reflectometer Measurements . . . . .	18
VHF Antenna Measurements . . . . .	18
Comparison of Inferred Electron Densities for the RAM-C Flights . . . . .	19
Comparison of Theoretical and Experimental Electron Density Profiles . . . . .	19
CONCLUSIONS . . . . .	21
APPENDIX A – ELECTROSTATIC PROBE THEORY . . . . .	22
Flowing Plasmas . . . . .	22
Directed Flow Parallel to Probe . . . . .	23
Directed Flow Normal to Probe . . . . .	26
Interpretation of RAM-C Fixed-Bias Electrostatic Probe Data . . . . .	29
Sample Calculation . . . . .	29
APPENDIX B – ELECTROSTATIC-PROBE AUTOMATIC DATA REDUCTION PROCEDURE AND LISTINGS . . . . .	31

	Page
APPENDIX C – ANALYSIS OF SPACECRAFT MOTIONS AND WIND ANGLES . . .	56
Determination of Wind Angles . . . . .	56
Summary of Wind-Angle Analysis . . . . .	58
REFERENCES . . . . .	59
TABLES . . . . .	62
FIGURES . . . . .	67

ELECTROSTATIC-PROBE MEASUREMENTS OF PLASMA PARAMETERS  
FOR TWO REENTRY FLIGHT EXPERIMENTS AT  
25 000 FEET PER SECOND\*

By W. Linwood Jones, Jr., and Aubrey E. Cross  
Langley Research Center

SUMMARY

Unique plasma diagnostic measurements at high altitudes from two geometrically similar blunt-body reentry spacecraft using electrostatic probe rakes are presented. The probes measured the positive-ion density profiles (shape and magnitude) during the two flights. The probe measurements were made at eight discrete points (1 cm to 7 cm) from the vehicle surface in the aft flow field of the spacecraft over the altitude range of 85.3 to 53.3 km (280 000 to 175 000 ft) with measured densities of  $10^8$  to  $10^{12}$  electrons/cm<sup>3</sup>, respectively. Maximum reentry velocity for each spacecraft was approximately 7620 meters/second (25 000 ft/sec).

In the first flight experiment, water was periodically injected into a flow field which was contaminated by ablation products from the spacecraft nose region. The nonablative nose of the second spacecraft thereby minimized flow-field contamination.

Comparisons of the probe-measured density profiles with theoretical calculations are presented with discussion as to the probable cause of significant disagreement. Also discussed are the correlation of probe measurements with vehicle angle-of-attack motions and the good high-altitude agreement between electron densities inferred from the probe measurements, VHF antenna measurements, and microwave reflectometer diagnostic measurements.

INTRODUCTION

The plasma sheath (ionized gas) which envelops a spacecraft during entry into an atmosphere can disrupt radio communications and cause "radio blackout." This phenomenon has received much attention (refs. 1 and 2) from both the U.S. Department of Defense and the National Aeronautics and Space Administration because of the serious problems

---

\* Part of the information presented herein was included in a dissertation, "Probe Measurements of Electron Density Profiles During a Blunt-Body Reentry" by W. Linwood Jones, Jr., presented in partial fulfillment of the requirements for the degree of Doctor of Philosophy in Electrical Engineering, Virginia Polytechnic Institute and State University, Blacksburg, Virginia, June 1971.

that it causes for mission planners. For instance, in manned flight missions there is a significant increase in the complexity of such onboard systems as navigation, guidance, and control due to the reduction of ground systems support during critical blackout periods. In other instances, provisions for onboard data storage and delayed playback, or even a recoverable package, may be required for data retrieval after blackout. Also, terminal-phase systems such as altimeters, landing radars, homing devices, and electronic countermeasures may be compromised for lack of real-time signal transmission. Consequently, a requirement exists for a fundamental understanding of the reentry plasma sheath and its interaction with spacecraft electromagnetic systems.

A project called "Radio Attenuation Measurements (RAM)" has been conducted at Langley Research Center where flow-field plasma characteristics and the resulting attenuation of propagating electromagnetic waves have been investigated both experimentally and theoretically. (See ref. 3.) Experiments have been performed in both ground facilities and on reentry flights to determine radio-frequency plasma attenuation and flow-field electron density and collision-frequency distribution.

This report presents electron density profiles (absolute magnitude and shape) inferred from electrostatic probe measurements during two blunt-body reentries at 7620 meters/second (25 000 ft/sec). A rake of eight negatively biased probes, located near the aft section of each spacecraft, collected positive ion current out to a normal distance of 7 cm (2.75 in.) and over an altitude range of 85.3 km (280 000 ft) to 53.3 km (175 000 ft). In addition, inferred electron densities are presented from VHF antenna measurements during both flights and from microwave reflectometer measurements during the second flight. Comparisons are made between the experimentally derived electron densities and theoretically calculated values to assess the validity of present plasma flow-field models. Also the effects on electron density profiles of material injection (during the first flight) and spacecraft motions are discussed.

Also included in this report are a discussion of electrostatic probe theory in appendix A, a description of the probe-data-reduction procedure and a listing of RAM C-I and C-II current and inferred density as a function of altitude and time for all probes in appendix B by Lorraine F. Satchell, and an analysis of spacecraft motions and wind angles in appendix C by William L. Weaver.

## SYMBOLS

Values are given in both SI and U.S. Customary Units. The measurements and calculations in the text and appendix A were made in SI Units; those in appendixes B and C, in U.S. Customary Units.

A	current, amperes; also projected area of probe, cm <sup>2</sup>
A <sub>n</sub>	accelerometer-measured accelerations (normal)
a	radius of probe sheath, R <sub>p</sub> + d <sub>s</sub> , cm
a <sub>y</sub> , a <sub>n</sub>	accelerometer-measured accelerations due to aerodynamic force along Y-axis (tangential) and negative Z-axis (normal)
D	body nose diameter, cm
d <sub>s</sub>	sheath thickness, cm
e	magnitude of electronic charge, 1.5921 × 10 <sup>-19</sup> coulomb
H	ratio of modified potential energy to kinetic energy, $\frac{\chi_p}{1 + S^2}$
H <sub>l</sub>	lateral angular momentum
H <sub>t</sub>	total angular momentum
H <sub>X</sub>	roll angular momentum (about X-axis), I <sub>X</sub> p
I, I <sub>+</sub>	positive ion current collected by a probe, amperes
I <sub>d</sub>	directed current into probe, nev <sub>f</sub> (2R <sub>p</sub> L), amperes
I <sub>l</sub>	lateral moment of inertia, $\frac{I_Y + I_Z}{2}$
I <sub>n</sub>	normalized probe current, $\frac{I_+}{I_r}$
I <sub>r</sub>	random ion current calculated for a probe, $\frac{nev_+}{4}(2\pi R_p L)$ , amperes
I <sub>X</sub> , I <sub>Y</sub> , I <sub>Z</sub>	moments of inertia about spacecraft axes, kg-m <sup>2</sup>
J <sub>i</sub>	saturation positive ion current density, 0.4nev <sub>+</sub> , amperes-cm <sup>-2</sup>
k	Boltzmann's constant, 1.38044 × 10 <sup>-23</sup> joule-K <sup>-1</sup>



L	probe length, cm
$\vec{L}$	angular impulse
M	ion mass, g
$N_e$	electron density, electrons-cm <sup>-3</sup>
n	electron density, electrons-cm <sup>-3</sup> , or ion density, ions-cm <sup>-3</sup>
p,q,r	rotation rates about X-axis (roll), Y-axis (pitch), and Z-axis (yaw), rad-sec <sup>-1</sup>
R	modified normalized probe current, $\frac{I_n}{\sqrt{1+S^2}}$ , amperes
$R_p$	probe radius, cm
$r_a$	radius at which particles will just be collected, cm
S	ion speed ratio, $\frac{v_f}{v_+}$
$T_e$	mean electron temperature, K
V	probe potential, volts; also spacecraft velocity or wind axis
V'	absolute magnitude of applied probe bias, volts
$V_0$	initial energy of ion entering sheath, $\frac{kT_e}{e}$ , joule-coulomb <sup>-1</sup>
$V_\infty$	plasma potential, volts
$v_+$	random thermal velocity of ions entering sheath, $\sqrt{\frac{8kT_e}{\pi M}}$ , cm-sec <sup>-1</sup>
$v_f$	normal component of flow velocity, cm-sec <sup>-1</sup>
$v_{flow}$	flow velocity of ion flux past probe, cm-sec <sup>-1</sup>
X,Y,Z	spacecraft body-axis system
x	distance from nose along body axis, cm

$y$	distance from body along normal to body surface, cm
$\alpha, \beta, \eta$	wind angles: angle of attack, sideslip angle, total wind angle, deg
$\gamma$	ratio of probe-sheath radius to probe radius, $\frac{a}{R_p}$
$\epsilon$	permittivity of free space
$ \Delta\eta $	absolute variation in total wind angle
$\Theta$	inverted form of the Child-Langmuir 3/2-power law, $\frac{\text{volts}^{3/2}}{\text{ampere}}$
$\theta$	precession cone half-angle; also angle between flow velocity and probe axis, deg
$\lambda_D$	Debye length, $\frac{\epsilon_0 k T_e}{e^2 n}$ , cm
$\nu_b$	precession frequency of vector $\omega_l$ about body axis
$\nu_H$	precession frequency of X-axis about angular momentum vector
$\rho$	charge density
$\phi$	angular coordinate for payload referenced to electrostatic probe rake, deg
$\chi_p$	normalized potential difference between probe and plasma, $\frac{e(V - V_\infty)}{kT_e}$
$\omega_l$	lateral angular velocity, $\sqrt{q^2 + r^2}$ , rad-sec <sup>-1</sup>

Subscripts:

cr	critical
o	initial

An arrow over a symbol denotes a vector.

## EXPERIMENT DESCRIPTION

Three flight experiments were conducted in the medium velocity (7620 meters/second (25 000 ft/sec)) reentry region to obtain quantitative measurements of plasma parameters about a hemisphere-cone body and to test radio-attenuation alleviation techniques. Only the first two flights are discussed herein, since the analysis of probe data for the third flight is incomplete. (Descriptions of the third flight and the preliminary probe results are found in refs. 4 and 5.) This section provides a brief description of the flight objectives, launch vehicles, and payload experiments. A description of the electrostatic probe system is given which includes the mechanical construction of the probe rake, the electronic circuitry, characteristics of the circuit components, and data format. Also described briefly are other plasma diagnostic experiment systems onboard the respective payloads.

### Flight Objectives

The primary objectives of the first flight (RAM C-I) were to test the effectiveness of water injection as an alleviation technique and to establish the operational system injection parameters (mass flow, penetration distance, and injection orifice size and location) necessary to achieve a required level of signal recovery. During this flight, electrostatic probes were the principal diagnostic instrumentation for assessing the plasma alleviation. In the second flight (RAM C-II), the primary objective was to measure the electron density time and altitude histories at several locations along the spacecraft using microwave reflectometers and electrostatic probes. Flight details are discussed in reference 6 for RAM C-I and in reference 7 for RAM C-II.

### Launch Vehicles

Similar four-stage solid-fuel Scout vehicles were used to launch the RAM C-I and C-II payloads from the NASA Wallops Island Station in Virginia. The two Scout vehicles designated S-159 and S-168, ready for launching, are shown in the composite photograph of figure 1. Pertinent vehicle-payload identification and launch information are given in the following table:

Designation		Launch	
Scout	Payload	Date	Time, GMT
S-159	RAM C-I	10-19-67	17:33:00
S-168	RAM C-II	8-22-68	15:16:00

Approximate staging sequencing applicable to the RAM C-I and C-II launch vehicles and payloads with important events is shown in figure 2(b). The launch vehicles transported their respective payloads to apogees greater than 220.5 km (720 000 ft) before propelling them back into the earth's atmosphere. To minimize lateral rotations and trajectory dispersion during the thrusting of the fourth-stage motor which was unguided, the motor and spacecraft were spin-stabilized just prior to motor ignition. Tip-off moments produced by the separation of the expended fourth-stage motor at an altitude of about 113 km (370 000 ft) caused coning of the spacecraft and a resulting oscillatory relative wind angle. The earth-relative reentry flight-path angle was a nominal  $-15^{\circ}$ , and both payloads reached their maximum velocities at an altitude of 67.0 km (220 000 ft). Some pertinent dynamic characteristics for each payload are given in the following table:

Payload	Spin rate		Maximum velocity		Total wind angle over probe data period, deg
	rad/sec	rps	m/sec	ft/sec	
RAM C-I	18.5	2.95	7670	25 165	5.0
RAM C-II	19.1	3.04	7678	25 193	4.0

The reentry data periods occurred just north of Bermuda as shown in the RAM C-II ground track. (See fig. 2(a).) The RAM C-I and C-II payloads flew nearly identical reentry trajectories, as indicated in figure 3 and in table I; and for this reason, the RAM C-I trajectory was used in the data reduction for both flights. Although the use of the RAM C-I trajectory produced approximately a 365.8-meter (1200-ft) bias error in the altitude for all RAM C-II probe data, this procedure introduced negligible errors in the inferred electron and ion densities.

### Payloads

The payload geometries were essentially identical and are shown in figure 4. Each payload consisted of an approximately 15-cm (6-in.) radius hemispherical nose followed by a  $9^{\circ}$  half-angle cone and had an overall length of about 130 cm (51 in.). The physical characteristics of each payload are given in the following table:

Payload	Nose material	Nose diameter		Body length		Weight before launch		Afterbody material
		cm	in.	cm	in.	kg	lb	
RAM C-I	NARMCO 4028 (Phenolic-graphite charring ablator)	31.90	12.56	130.25	51.28	121.1	267.0	Teflon
RAM C-II	Beryllium nose cap*	30.48	12.00	129.54	51.00	121.8	268.5	Teflon

\* Ejected at time of electrostatic-probe retraction.

RAM C-I had a phenolic-graphite charring ablator on the hemispherical nose, whereas the nose of RAM C-II was covered by a beryllium-cap heat sink. Since RAM C-I was primarily a material-injection experiment, the ability to maintain the integrity of the injection orifices during the ablation period was mandatory; therefore, the phenolic-graphite material was selected. (See ref. 8; RAM-CA designation is synonymous with RAM C-I.) An analysis of a sample of the NARMCO 4028 used to fabricate the heat shield showed that it contained about 1100  $\mu\text{g/g}$  sodium. The analysis was incapable of detecting potassium, if present, at less than 3600  $\mu\text{g/g}$  which means that the ablator could have contained up to 4700  $\mu\text{g/g}$  of alkali. The beryllium nose cap and the teflon were found to be free of any significant amounts of alkaline impurities. For a sample of teflon, the analysis showed the alkali content to be less than 5  $\mu\text{g/g}$ . Thus, during the RAM C-I reentry, the ablation of the nose fed easily ionizable alkali metals into the flow-field boundary layer. Since the primary objective of the RAM C-II flight was plasma flow-field diagnostics, the nonablative beryllium cap was selected to keep the flow field free of ablative contaminants so that a comparison could be made of measured plasma characteristics with pure-air theoretical calculations. The beryllium cap was ejected at an altitude of 56.4 km (185 000 ft) prior to the surface melting, and thus exposed a teflon-covered nose. For both flights, the effects of teflon ablation from the afterbodies are believed to be negligible at altitudes above 56.4 km (185 000 ft) (refs. 7 and 9) since the teflon had a low-alkali-metal contamination level; also, the ablation rates there were much less than those for the nose.

The location of the electrostatic and thermocouple probe rakes, the various radio-frequency antennas (diagnostic and instrumentation) on both payloads, and the water-injection orifices on the RAM C-I payload are shown in figure 5. Table II gives exact coordinate location and position of the various system sensors for both payloads.

### Electrostatic Probe System

Design philosophy. - Realistic predictions of the electromagnetic wave attenuation to be experienced during atmospheric entry are dependent upon several factors, the foremost of which is the physical nature of the plasma itself. The requirement for accurate knowledge of gas composition is more stringent for an analysis of this problem than for other reentry problems such as heat transfer or aerodynamic flow. The reason for this requirement is that the free electrons, which control the electrical conductivity of the gas, are a trace species and, as such, require a comprehensive nonequilibrium flow-field analysis including finite-rate chemistry to determine the degree of gas ionization. For example, approximately 40 finite-rate chemical kinetic reactions involving 11 plasma species (free electrons, molecular and atomic ions, molecules, and atoms) must be considered in theoretical calculations of electron concentration. In addition, the dominant chemical kinetic process is dependent upon the velocity and body shape of the reentering spacecraft.

Moreover, calculations are more difficult to perform as one moves aft from the stagnation region because not only is a complete understanding of the local gas conditions required, but also of the entire gas history from the shock-entry point of each streamline to the location of interest.

The objective of the RAM-C electrostatic probe experiment for both flights was to determine experimentally the electron density profiles in the aft flow field in order to assess the validity of the theoretical calculations and to provide experimental data upon which to improve the analytical model used. The design of the RAM-C electrostatic probe system and the calibration testing in ground plasma facilities are discussed in detail in reference 4.

Configuration of electrostatic probe rakes on RAM C-I and C-II. - A photograph of the electrostatic probe rake is shown in figure 6(a); and the exterior configuration, a sectional view of the leading edge, and standoff dimensions of the ion collectors are shown in figure 6(b). Each of the iridium ion collectors extended 0.0254 cm (0.010 in.) beyond the wedge-shaped beryllium oxide leading edge of the rake. The two larger iridium pieces, one on each side of the rake, were electrically common and served as electron collectors. Iridium was chosen as the probe collector material because of its high melting temperature, high electronic work function, and negligible oxidation property. The beryllium oxide leading-edge material was a high-temperature insulator which mechanically and electrically separated the ion collectors and the electron collectors. The beryllium oxide leading edge was a 60° wedge with a leading-edge radius of 0.0254 cm (0.010 in.) and was inclined at an angle of 45° with respect to the payload surface. The main body of the probe was constructed of a phenolic fiber-glass ablation material.

Probe circuitry. - A fixed bias of -5.0 volts, referenced to the electron collectors, was applied simultaneously to all ion collectors to attract positive ions. Figure 7 gives a schematic drawing of the probe electronic system on both the RAM C-I and RAM C-II payloads. As each probe continuously collected plasma current, the mechanical commutator sampled the voltage developed across the probe load resistors and calibrate resistors and fed the signals to the logarithmic amplifier at the rate of 300 samples per second. The voltage developed across the probe load resistor was converted by the logarithmic amplifier to drive a telemetry subcarrier oscillator. A photograph of typical flight components is shown in figure 8.

For the RAM C-I experiment, the output of the logarithmic amplifier was connected single-ended to the input of the subcarrier oscillator; whereas on the RAM C-II experiment the output of the amplifier was connected to a differential-input subcarrier oscillator. This modification in the electronic system was made to correct an anomaly which occurred during the RAM C-I flight. The occurrence of the anomaly was ascertained during the onboard calibration of the logarithmic amplifier. The problem presented itself at an alti-

tude of about 67.0 km (220 000 ft) when the logarithmic amplifier output including all calibrate levels unexpectedly went to zero. During water injection, the amplifier returned to normal operation; however, after the injection stopped, the output returned to zero. Approximately 3 seconds later at 61.0 km (200 000 ft), the amplifier returned to normal and continued so for the remainder of the flight. The anomaly was analyzed and it could be reproduced in the laboratory by connecting a -1.85-volt potential between the electron collector and the payload ground. It is surmised that during the flight the electron collectors and the spacecraft metallic skin assumed different floating potentials in the plasma. This condition caused the internal input diodes of the logarithmic amplifier to conduct and thereby reduced the amplifier output to zero. The differential connection used on the RAM C-II system corrected the situation by effectively adding a large resistance (10 megohms) in series with this unwanted potential and thus prevented the diodes from conducting.

Logarithmic amplifier. - The solid-state logarithmic amplifier was developed specifically for the electrostatic probe experiments. The device was a low-level input, adjustable high gain, chopper-stabilized dc amplifier which converted a differential high-impedance input into a differential low-impedance output. Figure 9(a) shows the dynamic (commutated at 300 samples/sec) input-output voltage characteristics of the amplifiers used for flight. As can be seen from the figure, the device provided an output proportional to the logarithm of the input voltage for greater than a three-decade range. The amplifier gain was adjusted so that the voltage developed by an input current from the probes of at least  $10^{-6}$  ampere, across the load resistor of 400 ohms, would be on the reasonably linear section of the characteristic curve. The maximum input current was  $10^{-3}$  ampere and the minimum current value was determined by system noise (approximately  $5 \times 10^{-7}$  ampere for the RAM C-I experiment and  $10^{-7}$  ampere for the RAM C-II experiment). The amplifier characteristics shown in figure 9(a) were obtained just prior to flight by calibrating the entire probe system as installed in the spacecraft. This calibration technique used a range of known resistances that were externally connected in sequence across the biased probe electrodes and thereby simulated a range of plasma currents. This calibration should not be confused with the onboard calibration the main purpose of which was to provide certain pulse levels in each data frame for automatic data reduction requirements.

Since the signal to the amplifier was commutated at 300 samples per second, good dynamic response was needed to reproduce the input accurately. Figure 9(b) shows a typical pulse-response curve of the amplifiers. With a delay time of less than 100 microseconds and rise and fall times of less than 75 microseconds each, the response was sufficient for data samples of approximately 3 milliseconds duration. For data-reduction purposes, only the center 50 percent of the pulse width was used.

Probe-experiment characteristics and data format. - The format used for electrostatic probe information from the logarithmic amplifier output, including currents from the probes and from the calibrates, is presented in figure 10. Shown in figure 10 is one complete data frame which has a duration of 100 milliseconds. There are five calibrate levels for each frame, which correspond to currents of 0.1, 1.0, 10.0, 100.0, and 1000.0 microamperes. Between the calibrate sequences are three consecutive samplings of the eight ion collectors. One profile measurement represents about 26.4 milliseconds or about 8 percent of a complete payload roll motion. The sampling rate of 300 samples per second was selected so that at least two data formats would be completed during the off time of the water-addition cycling system on RAM C-I. The same sampling rate was maintained for the RAM C-II experiment.

Thermocouple probes. - On both of the RAM-C payloads, a rake of thermocouples was located diametrically opposite the electrostatic probe rake to monitor the temperature of the leading edge. On RAM C-I, both the thermocouple and electrostatic probes were in line with the water-injection sites to insure similar heating environments. The external configuration of the thermocouple probe fin was the same as that of the electrostatic probe fin and is shown in figure 11. Instead of electrodes, however, three thermocouples were embedded 0.0635 to 0.1016 cm (0.025 to 0.040 in.) from the leading edge of the wedge. The thermocouples were platinum-platinum+13-percent-rhodium and were located 2, 4, and 6 cm (0.79, 1.57, and 2.36 in.) from the payload surface. The useful measurement range of the thermocouples was from 255 to 1977 K (0° to 3100° F).

At elevated temperatures, the insulating properties of the beryllium oxide degraded, and unwanted leakage currents flowed between ion collectors and between ion and electron collectors. The thermocouple probe was used therefore to determine the altitude at which probe heating became significant. The electrical resistivity degradation affected the accuracy of the inferred electron density because the leakage currents added to the measured plasma current and thereby caused a higher than actual electron density to be inferred. In reference 6, the electrostatic probe data were considered to be unusable in an absolute sense once the local probe temperature exceeded 811 K (1000° F). An improved analysis given in reference 4 estimated that the leakage current was on the order of 100 microamperes for a thermocouple temperature of 1366 K (2000° F). For both RAM-C flights the inferred plasma density was greater than  $10^{11}$  electrons/cm<sup>3</sup> when the local temperature for a given probe exceeded 1366 K; thus, the error in the inferred density at that point was less than a factor of two. For higher leading-edge temperatures, the leakage current probably exceeded the plasma current; therefore, above 1366 K the data were considered to be degraded for useful plasma-density interpretation purposes.



Retraction of probe rakes. - Although it was desirable to make electrostatic probe measurements over the entire blackout data period from 85.3 to 24.4 km (280 000 to 80 000 ft), certain restrictions were imposed. The high heating rates predicted for the intermediate altitude range from 61.0 to 30.5 km (200 000 to 100 000 ft) would result in structural failure of the probes which could endanger the stability of the payload itself. Therefore, the rakes (electrostatic and thermocouple) were simultaneously retracted into the base region of the payload at a predetermined altitude by programmer action. The RAM C-I rakes were retracted at an altitude of 53.6 km (176 000 ft). RAM C-II probe retraction was initiated simultaneously with the beryllium cap ejection at 56.4 km (185 000 ft), but the effects of retraction on the inferred density were not noted until 55.9 km (183 400 ft).

#### RAM C-I Water-Injection System

During the RAM C-I flight, water was periodically injected into the flow field from the spacecraft nose to provide for electron density reductions in the peak attenuating layer of the flow field. The water was injected at varying flow rates with specific penetrations over an altitude range of 83.2 to 33.8 km (273 000 to 111 000 ft). The injection locations are shown on the payload sketch in figure 5. Locations and positions of the nozzles are also given in table II. The electrostatic probe rake and two VHF slot antennas were located in line with the injection sites and were the principal diagnostic instrumentation for assessing the plasma alleviation.

The resultant programmed variation of flow rates for the RAM C-I experiment is given in table III, with the altitude shown for the start of each pulse. Typical water flow-rate pulses are shown as a sequence of valve-on times. One complete injection cycle is shown and the cycles were repeated every 4 seconds. The valve-on times were 230 milliseconds and the valves were opened at 0.5-second intervals. A more detailed description of the RAM C-I water-injection system can be found in reference 6.

#### RAM C-II Microwave Reflectometer System

A four-frequency microwave reflectometer system was used to infer the peak electron density time and altitude histories about the RAM C-II spacecraft. A plasma-density measurement range of three decades ( $10^{10}$  to  $10^{13}$  electrons/cm<sup>3</sup>) was provided by the reflectometer system. The microwave reflectometer technique used the reflectivity of the plasma to infer the electron density and phase measurements to infer the electron density profile shape. Microwave antennas for the four frequencies (L-, S-, X-, and K<sub>a</sub>-bands) were located at each of the four body stations (except station 1, L-band excluded), for a total of 15 antennas (fig. 5). Antenna locations are listed in table II. Greater detail on the microwave reflectometer system may be found in reference 7 and in table II.

## VHF System

It has been shown that significant pattern changes can occur for plasma-clad cylindrical antennas when the electron density passes through the critical value. (See ref. 10.) These pattern changes are also accompanied by rapid changes in input impedance or input voltage standing wave ratio (VSWR). Received signal strength and onboard antenna VSWR were monitored during the RAM C-I and C-II flights and were used to determine the occurrence of the VHF critical electron density. The antenna VSWR was monitored by onboard directional couplers, and the antenna patterns were reconstructed by use of the signal received from the spinning spacecraft. There were several ground, airborne, and shipborne receiving stations with different look angles; thus, patterns were obtained in several planes. The arrangement of receiving stations for RAM C-II is shown in figure 2(a).

Two types of VHF antennas (cavity-backed slots and circumferential slot arrays) were used for the flights, as shown in figure 5. For the RAM C-I payload, two diametrically opposed, axially oriented, 259.7-MHz cavity-backed slot antennas transmitted the real-time telemetry, and an aft-positioned circumferential slot array (ring) antenna transmitted the delayed-time telemetry. In comparison, on the RAM C-II payload, the real-time and delayed-time telemetry systems utilized a pair of aft-located circumferential slot arrays (ring antennas). The axially oriented slot antennas on RAM C-I were in line with the material-injection orifices and the electrostatic probes. The ring antennas for all payloads were just forward of the electrostatic probes. A more complete description of the VHF antennas on RAM C-I may be found in references 6 and 11 and in table IV.

## ELECTROSTATIC PROBE THEORY

The RAM-C electrostatic probe measurements were interpreted by use of a free-molecular cylindrical probe theory modified to account for a directed-ion flux due to the plasma flow. This theory was developed by Scharfman (refs. 12 and 13) based on the works of Hok et al. and Smetana (refs. 14 and 15, respectively) and is summarized in appendix A.

The configuration of the RAM-C probe rake is such that in relation to the flowing plasma, each ion collector appears to be a cylindrical wire 0.0254 cm (0.010 in.) in diameter and 0.5385 cm (0.212 in.) long, which is inclined at an angle of  $45^{\circ}$  with respect to the plasma flow. Experimental programs were performed at Langley Research Center, Stanford Research Institute, and Cornell Aeronautical Laboratories to verify that the RAM-C electrostatic probe rake could be used to infer accurate localized ambient plasma electron densities. (See refs. 4, 13, 16, and 17.) Typical results from references 13 and 17 are shown in figure 12. The conclusion based on this work is that free-stream electron density can be inferred within  $\pm 20$  percent by using the described theory for the

RAM-C flight conditions for plasma densities from  $10^{10}$  to  $10^{11}$  electrons/cm<sup>3</sup> and within a factor of two over the  $10^9$  to  $10^{13}$  electrons/cm<sup>3</sup> range.

## FLIGHT DATA RESULTS AND DISCUSSION

### Measured Electrostatic Probe Ion Currents

Ion currents measured by each of the eight electrostatic probes onboard the RAM C-I and C-II flights are presented as a function of altitude from 85.3 to 53.3 km (280 000 to 175 000 ft) in figures 13 and 14, respectively, and are listed in appendix B. (Altitudes for RAM C-II are too low by 0.3658 km (1200 ft).) In the figures, the measured probe-current data points are represented by the symbols which have been interconnected in order to show small variations clearly. Probes for both flights indicate an initial measurable current at an altitude of about 85.3 km (280 000 ft). Lowest measurable current for the probe electronic systems was about  $10^{-7}$  A. Likewise, system saturation current was  $10^{-3}$  A.

Figures 13(a) to 13(d) show the currents measured by the electrostatic probes aboard RAM C-I. The effects of periodic water injection into the flow field can be seen as respective periods of greatly reduced measured currents for all eight probes. The anomaly period, discussed in an earlier section, occurred between 67.1 and 61.0 km (220 000 and 200 000 ft). The data shown in the figures during the anomaly period are considered to be valid since they were selected only when the onboard calibrators indicated normal amplifier operation. All data are valid after the anomaly period. The probes aboard RAM C-I were retracted at 53.6 km (176 000 ft) from the aft-flow-field region into the payload base region. The probes continued to make measurements after retraction, but the analysis of these data is not presented in this report. Immediately after retraction, the outermost probes still indicated system saturation current because of electrical degradation of the beryllium-oxide probe insulator induced by aerodynamic heating.

Figures 14(a) to 14(d) show the electrostatic-probe-measured ion currents for RAM C-II. Effects of retraction can be seen at about 55.5 km (182 000 ft) in figures 14(a) to 14(c) as a steep dropoff of measured current. Again, the outermost probes of figure 14(d) were still saturated immediately after retraction because of leakage current through the degraded probe insulator.

The small sinusoidal-type variation superimposed on the curves shown in figures 13 and 14 are variations in the plasma density due to spacecraft motion. These variations will be discussed in detail in a later section and in appendix C.

## Thermocouple Probe Results

An accurate knowledge of the probe-rake leading-edge temperature during reentry was necessary for valid interpretation of the fixed-bias probe currents because at thermocouple temperatures greater than 1366 K (2000° F), the insulating properties of the dielectric wedge were degraded to the point that the inferred plasma densities were questionable. Therefore, the first task in the data-reduction procedure was to examine the thermocouple data and to identify those probe data for which this threshold had been exceeded.

Measured thermocouple temperatures for both the RAM C-I and C-II reentries are presented in figure 15. Overall, for corresponding thermocouples at identical altitudes, the temperatures of RAM C-I were less than those of RAM C-II most likely because of the cooling effects of water injection which can be seen on the RAM C-I curves. Water-injection cycles for RAM C-I are shown at the top of the figure. The RAM C-I and RAM C-II data are presented in figure 16 as constant-temperature profiles of normal standoff distance  $y$  to a given temperature boundary plotted against altitude.

At any altitude, the temperature at any probe location on the leading edge may be determined from the intersection of a horizontal-probe location line, a vertical-altitude line, and a constant-temperature contour. When, for a given probe, this intersection occurs above the 1366 K (2000° F) contour, the interpretation of these data is questionable.

## Electron Densities Inferred by Electrostatic Probe

By use of the probe interpretation discussed in appendix A, the collected ion currents given in figures 13 and 14 were converted into respective ion (electron) densities for the two flights. (Flow-field calculations (ref. 9) indicate that positive-ion and electron densities are very nearly equal for the RAM-C trajectory.) The electron densities for RAM C-I are shown in figure 17 and for RAM C-II in figure 18. The electron densities plotted against time and altitude are also tabulated for both flights in appendix B. The RAM C-I and RAM C-II results after probe retraction should be disregarded since no temperature and velocity data are presently available to allow proper interpretation of the ion current.

Flow-field electron-density profiles (electron density plotted against standoff distance  $y$ ) were determined during both flights. Typical results are shown in figure 19 for selected altitudes during the RAM C-I flight where no water-injection effects were present and in figure 20 for similar altitudes on RAM C-II. The data represent the time-averaged electron density (averaged over one spacecraft revolution) at a given altitude for each probe, and the bars in figure 20 represent the peak-to-peak density change due to body

motions, to be discussed in a later section. The profiles for RAM C-I and RAM C-II flights are similar, although there was a slight difference in the absolute level at the specified altitudes. These differences are also observed in overlays of electron density plotted against altitude for RAM C-I and RAM C-II given in figure 21.

#### Effects of Ablation Impurities on Electron Density

Since the nose materials for the two RAM spacecraft were different (charring ablator for RAM C-I, nonablating heat sink for RAM C-II), a comparison can be made between contaminated and noncontaminated reentry plasma flow fields. The electron-density histories for RAM C-I and RAM C-II are superimposed for comparison in figure 21. The electron density for RAM C-I is approximately a factor of 2 higher than that for RAM C-II for the altitude range of 85.3 to 73.2 km (280 000 to 240 000 ft). Below this altitude, RAM C-II results are slightly greater than those for RAM C-I, although the RAM C-I anomaly period and the effects of material addition make a quantitative comparison less meaningful. The differences in measured electron density between these flights could be attributed to ablation product contamination effects because the payloads were nearly geometrically identical and they flew nearly identical trajectories. The RAM C-I charring phenolic-graphite nose fed easily ionizable alkali metals (sodium and potassium constituted approximately 1000 to 4000  $\mu\text{g/g}$  in the virgin material) into the flow-field boundary layer, whereas the nonablating beryllium nose cap on RAM C-II did not contaminate the flow. For both spacecraft the teflon afterbody did ablate slightly; however, additional ionization was not probable because here the alkali metal content was kept below 5 ppm of teflon. A detailed discussion of alkali ablation product contamination of the RAM-C flow field is given in reference 9.

#### Effects of Vehicle Angle-of-Attack Perturbations on Electron Density

An analysis of the accelerometer data (appendix C) revealed that each payload underwent small angle-of-attack oscillations which produced variations in the ion current collected by all probes and variations in the microwave reflectometer measurements (RAM C-II). This effect is more clearly observed in the RAM C-II results (fig. 18) since these results are not disturbed by water injection. Variations in electron density at the probe station were produced because the payload was at an angle of attack (unsymmetrical flow field about payload) while spinning at 18.84 rad/sec (3 rps). When the payload experienced a positive angle of attack (positive normal acceleration), the electrostatic probes were on the windward side of the payload and sensed a compression of the flow field. Conversely, for a negative angle of attack (negative normal acceleration), the probes sensed the leeward (less dense) side of the flow field.

A comparison of the RAM C-II vehicle angle-of-attack motions (determined by accelerometer data) with electron density (inferred from electrostatic probe 1) is shown for the altitude region from 59.4 to 55.8 km (195 000 to 183 000 ft) in figure 22. As seen in the figure, small angle-of-attack motions produced peak-to-peak density fluctuations in the aft part of the flow field approaching a factor of three. The sizable density variations close to the payload for relatively small changes in angle of attack can be one of the reasons that signal-attenuation models do not always accurately predict plasma-caused signal losses when normal zero angle-of-attack plasma profiles are used.

#### Effects of Water Injection on Electron Density

The effectiveness of water injection as a plasma alleviant in the RAM C-I flow field was assessed by means of two VHF slot antennas and the electrostatic probe rake located in line with the injection sites. The probe measurements provided an excellent means of determining injectant penetration distances as well as the resultant magnitudes of the suppressed plasma.

The amount of plasma suppression due to water injection on the RAM C-I plasma electron density is seen in figure 23. In the upper part of the figure, the water injection pulses are shown with varying magnitude. (Flow rates are given in table III.) Each pulse caused corresponding decreases in measured electron density. Cycle 1 (not shown in the figure) had no flow because of a slow fill rate in the lines. The very low flow rates of cycle 2 produced no detectable plasma alleviation for any of the probes. The larger flow rates of cycle 3, particularly the side-injection flow rates 3 and 4, caused appreciable electron-density reduction for all probes. Electron-density profiles for the various lateral injection flow rates of cycle 3 are shown in figure 24. Here, it is clearly seen that increasing flow rates are more effective in reducing electron density and in penetrating farther out into the flow. The electron-density profiles during stagnation injection (cycle 4, flow rate 5) are shown in figure 25 for selected altitudes over the 593 meter (1947 ft) altitude range.

The probe electronic system anomaly occurred immediately after cycle 4, flow rate 6, and persisted through cycle 4, flow rate 4. For intervals during the periods of water injection, however, the amplifier returned to normal operation and allowed reliable probe measurements.

The effectiveness of the water-injection technique was assessed by comparing density profiles with water injection against those without water for the same altitude range. Alleviation effects of water injection were noted by the ground stations on the signals received from all the onboard radio-frequency systems and good correlation was found between the probe electron-density profile changes and the observed attenuation changes of the signal strengths.

## Microwave Reflectometer Measurements

The location and magnitude of the peak electron density inferred by the station 4 microwave reflectometers agree with the electron-density profiles inferred by the electrostatic probes for the RAM C-II flight. This good agreement lends credence to both measurements since both measured and theoretical electron-density gradients along the aft payload surface are small (refs. 7 and 9, respectively).

The microwave phase data (fig. 35 of ref. 7) indicate that there was a strong density gradient between the payload surface and a normal distance into the flow of 1 to 2 cm. Beyond this distance the profile appeared to be nearly uniform for another several centimeters.

The magnitudes of the electron density inferred by the probes and microwaves are also strongly correlated as shown in the longitudinal profiles of peak electron density for constant altitude. (See fig. 26.) In figure 26, the time-averaged peak electron densities as indicated by the reflectometer are plotted against distance along the body, where zero on the abscissa corresponds to the payload nose. Also shown in the figure for purposes of comparison are the time-averaged electron densities (averaged over one body revolution) for probes 1 and 8 (innermost and outermost probes, respectively). The bar on the probe data represents the peak-to-peak density fluctuation due to body motions.

## VHF Antenna Measurements

The received VHF signal strengths (recorded at the Bermuda and U.S. Navy Ship (USNS) Twin Falls Victory stations) and the reflected power for the onboard antennas for RAM C-I are presented in figures 27 and 28 and for RAM C-II in figure 29. The Bermuda station was located approximately broadside to the payload during the data period and the Twin Falls Victory station was directly down range. (See fig. 2(a).)

The peak electron density at a given antenna location was inferred from the region where the received signal strength ripple pattern (due to spinning payload) and the onboard antenna reflected power changed abruptly. In reference 10, these changes were shown to occur at the critical electron density; however, since the RAM-C experimental conditions were slightly different than those in reference 10, the peak electron density is estimated to be the critical value within a factor of two uncertainty.

For the RAM C-I records, the time period of interest is from 385 to 394 seconds. In the Bermuda 225.7-MHz record, the pattern ripple is about 30 dB prior to the critical electron-density region (indicated by the arrows) which is in agreement with the measured free-space patterns in the equatorial plane. The ripple structure diminishes markedly in the critical electron-density region and then resumes as attenuation due to an overdense plasma occurs. The same sequential change was also noted by the Bermuda station in the 259.7-MHz antenna pattern ripple structure during a similar time frame.

A related change in the pattern ripple structure was also observed for both antennas in the signal received at the USNS Twin Falls Victory station between 386 and 394 seconds. At 386 seconds, the plasma electron density over the antennas is negligible and the antenna pattern ripple is about  $\pm 2$  dB. Also the mean level of the signal received at the two frequencies is different by about 16 to 20 dB in absolute level. Both the magnitude of the pattern ripple and the absolute power levels agree very well with those predicted from the nose-on free-space absolute antenna patterns. During the time period from 390 to 392 seconds, the 225.7-MHz record experiences a 20-dB dip in the received signal level as the plasma goes through critical density. A similar but smaller signal-level dip also occurs at 259.7 MHz. The time of occurrence of these amplitude dips in the received nose-on signal closely correspond to the time period where a significant decrease in pattern ripple was observed from the broadside direction.

The records of reflected power to both the 225.7-MHz and the 259.7-MHz antennas are shown in the lower parts of figures 27 and 28. The sharp rise or increase in reflected power with the simultaneous occurrence of critical electron density over the antenna aperture corresponds to that altitude range where the pattern ripple changes were noted. For RAM C-II, nearly identical antenna effects were observed, as shown in figure 29.

#### Comparison of Inferred Electron Densities for the RAM-C Flights

The plasma diagnostic results for both flights are shown in figure 30 for the purpose of comparison. They include electron density as a function of altitude inferred from the RAM C-II electrostatic probes, RAM C-II microwave reflectometers, and the RAM C-I and RAM C-II VHF antenna measurements. The data presented for electromagnetic techniques are time-averaged peak electron densities. The probe data represent the envelope of maximum to minimum values for all probes. All inferred densities are corrected for body location and are referred to the probe station by use of the appropriate longitudinal profile in figure 26.

#### Comparison of Theoretical and Experimental Electron Density Profiles

Calculated electron density profiles for the RAM-C flights were provided by the authors of reference 9. These calculations began with pressure distributions derived from equilibrium inviscid flow-field solutions for sphere-cone shapes. A nonequilibrium streamtube method provided temperature, density, and composition (including electron concentration). Streamline positions were determined by means of mass flow conservation. An equilibrium thin boundary-layer solution was adapted for use with nonequilibrium edge conditions, and the combined viscous-inviscid solution was iterated to account for vorticity and displacement thickness. Inviscid streamline values were discarded upon entry into the boundary layer and were replaced by calculations based on conditions in the



boundary layer. The flow-field solutions described are not valid at altitudes above about 70.1 km (230 000 ft). It should be noted that ambipolar diffusion of the charged particles, which cannot be included in this treatment, was estimated in reference 9 to become an important influence at altitudes higher than 70.1 km (230 000 ft).

For RAM C-II the clean-air assumption should have been valid down to 56.4 km (185 000 ft) where the beryllium nose cap was ejected, but for RAM C-I the flow field was contaminated by ablation products from the phenolic-graphite nose. For both bodies the teflon afterbody did ablate to some extent, but no additional ionization would result because the alkali metal content was kept below 5 ppm in the heat shield. There is, however, an unanswered question concerning the reduction of the electron density due to the electrophilic action of teflon ablation products.

When the measured electron-density profiles shown in figures 19 and 20 were compared with the calculated profiles previously mentioned, the measured profiles were found to be lower and flatter than the calculated ones. Also the measurements appeared to extend to greater distances from the body surface than had been anticipated. A typical comparison is shown in figure 31 with the RAM C-II data bars representing the envelope of probe data (due to body motions). Comparison of the probe data with other available plasma flow-field calculations (ref. 18) also indicates this significant disagreement between experiment and theory in absolute magnitude and in shape of the electron-density profiles.

In an effort to resolve these differences above 71.0 km (233 000 ft), the effects of ambipolar diffusion were considered. Since the analytical model used a streamtube approach, the effects could not be handled directly; rather an ion diffusion correction factor was determined (ref. 9) which accounts for the reduction in the magnitude of the peak electron density. Unfortunately, no theoretical means is available for predicting the spreading of the electron-density profiles; conceptually, however, ambipolar diffusion should decrease the absolute magnitude of density and reduce its gradients.

The theoretical peak electron density and the RAM C-I and RAM C-II envelopes of time-averaged inferred densities from probe 8 are shown in figure 32. The RAM C-II data should provide a better comparison with the "pure air" plasma calculations because the RAM C-II beryllium nose cap minimized flow-field contamination down to an altitude of 56.4 km (185 000 ft). At 85.3 km (280 000 ft) the inviscid calculation of peak electron density must be reduced by approximately two decades because of the ambipolar diffusion correction factor. This correction goes to zero near 70.1 km (230 000 ft), and below this altitude both the inviscid calculations and the inviscid calculations corrected for boundary layer yield identical results and according to reference 9 are believed to be correct. The good agreement between the inviscid calculations corrected for ambipolar diffusion and the experimental measurements above 70.1 km supports the hypothesis that ambipolar

diffusion is a principal mechanism for shaping the high-altitude electron-density profiles. The RAM C-II electron densities from the inviscid calculations corrected for boundary layer, the microwave reflectometer measurements, and the electrostatic probe measurements are given for different body locations in figure 33. Although both the experimental and theoretical curves show a leveling of the electron density below 70.1 km (230 000 ft), the experimental values are greater. The electrostatic probe data envelope shown in the figure includes only those data that are below the 1366 K (2000° F) critical temperature. Although the probe data might be suspect below 70.1 km because of aerodynamic heating, the microwave reflectometer technique does not suffer from this effect.

### CONCLUSIONS

Unique high-altitude electrostatic probe measurements have been made on the aft section of two high-velocity reentry spacecraft. Good agreement between the two RAM-C flight probe experiments with strong correlative data from microwave reflectometer and VHF antenna measurements support the following conclusions:

1. High-altitude (above 70 km (230 000 ft) for RAM-C configurations) calculations of electron-density profiles using an inviscid streamtube approach corrected for boundary layer are inadequate and modifications including ambipolar diffusion effects are necessary.
2. Increases in ionization due to phenolic-graphite ablation products in the aft-flow-field boundary layer were no greater than a factor of two over an altitude range of 56.4 to 82.3 km (185 000 to 270 000 ft).
3. Small angle-of-attack motions produce significant peak-to-peak density fluctuations in the aft parts of the flow field. These variations in electron-density profiles can be useful in qualitatively indicating vehicle angle of attack in the high altitudes where accelerometer data are limited.
4. The use of water addition into the flow field as a plasma alleviant is effective in reducing the electron density in the flow field and in alleviating radio blackout.

Langley Research Center,  
National Aeronautics and Space Administration,  
Hampton, Va., December 20, 1971.

## APPENDIX A

### ELECTROSTATIC PROBE THEORY

Simplicity makes the electrostatic probe attractive for plasma diagnostics; however, the theoretical interpretation of its current-voltage characteristics is extremely complicated. The difficulty stems from the fact that a probe represents a boundary to a plasma and near this boundary the equations which describe the motion of the charged particles change their character. At the surface of the probe, one polarity of charged particle is collected while the other is repelled; thus, a charge separation region or sheath is created where ion and electron densities differ and hence where large electric fields can be present. A fundamental result of the original theoretical interpretation of probes by Langmuir (ref. 19) is that under many experimental conditions, the sheath may be considered as a thin layer near the probe surface and the plasma appears to be field-free and electrically neutral up to the edge of this well-defined boundary. In recent years considerable progress has been made by the application of computer numerical integration techniques to the analysis of the collection of charged particles in the collisionless case for cylindrical and spherical probes in nonflowing plasmas (refs. 20 to 24). Thus, the artifice of a sheath boundary has been eliminated and the continuous transition from probe surface to ambient plasma is adequately described. Currently, the most realistic collisionless or free-molecular probe theory has been developed by Laframboise (ref. 20) who used the analytical model of Bernstein and Rabinowitz (ref. 21) to calculate the entire probe characteristic for both cylindrical and spherical probes in a Maxwellian plasma at rest. His plasma model consists of positive and negative species of charged particles, each having a Maxwellian velocity distribution with its own characteristic temperature. The analysis was based on the collisionless Boltzmann or Vlasov equations for two species coupled by Poisson's equation for the electric field. These equations are valid for only those conditions where binary collisions are negligible; that is, the collision mean free path is much greater than the probe radius and the plasma Debye length. The electric field, consistent with Poisson's equation, is therefore the dominant influence on the motion of the charged particles.

#### Flowing Plasmas

The theory for interpreting the response of an electrostatic probe in a plasma with directed flow is considerably more primitive than the classical probe theory just discussed. The available theories for including the effects of flow are oversimplified and their experimental verification are for the most part cursory. Fortunately, positive ion collection with an "infinitely long" cylindrical probe (long enough for end effects to be neglected) aligned parallel to the flow can be interpreted by use of the theory of

## APPENDIX A – Continued

Laframboise for nonflowing plasmas. Also, for most experimental conditions, this theory should be applicable for electron collection with any probe orientation because the random velocity of electrons is usually large compared with the directed velocity of the flowing plasma. However, this theory is not applicable for the interpretation of positive ion collection with a cylindrical probe of arbitrary orientation in a flowing plasma. In the following sections, an interpretation for cylindrical probes under these conditions by Scharfman (ref. 12), based on the works of Hok et al. (ref. 14) and Smetana (ref. 15), is presented.

### Directed Flow Parallel to Probe

The ion current part of a cylindrical electrostatic probe characteristic has been numerically evaluated by Hok et al. (ref. 14) over a large range of ion densities and electron temperatures for a nonflowing plasma which is also applicable to a plasma with the directed flow parallel to the axis of the probe. For the flowing plasma case, it is advantageous to use this theory because it can easily be modified to account for an arbitrary probe orientation. These results are shown graphically in figure 34 as the variation of the normalized current  $I_n$  with the normalized potential difference  $\chi_p$  between the probe and the plasma for selected values of ratio  $\gamma$  of sheath radius  $a$  to probe radius  $R_p$ . The normalized current is the ratio of the current  $I_+$  collected by a probe to the random ion current  $I_r$ . The random ion current is defined by Hok et al. to be the product of the saturation ion current density and the area of the probe and is given by

$$I_r = \frac{nev_+}{4}(2\pi R_p L)$$

where

$n$	electron density or ion density
$e$	magnitude of electronic charge
$R_p$	probe radius
$L$	probe length
$v_+$	velocity of ions entering sheath

## APPENDIX A – Continued

The velocity  $v_+$  is defined to be

$$v_+ = \sqrt{\frac{8kT_e}{\pi M}} \quad (A1)$$

where

$k$  Boltzmann's constant

$T_e$  mean electron temperature

$M$  ion mass

It is to be noted that in equation (A1) the electron temperature  $T_e$  is used rather than the ion temperature. This departure from the classical definition for the mean thermal speed is the result of incomplete shielding of the probe sheath. Thus, a total potential drop of order of magnitude  $kT_e$  exists in the plasma and accelerates the ions into the probe sheath (ref. 25).

The normalized potential difference  $\chi_p$  between the probe and the plasma is a dimensionless parameter defined as

$$\chi_p = \frac{e(V - V_\infty)}{kT_e}$$

where

$V$  probe potential

$V_\infty$  plasma potential

Before Hok's results (fig. 34) can be used to interpret experimental probe data, the ratio  $\gamma$  of sheath to probe radii must be known. The ion sheath radius  $a$  is defined as

$$a = R_p + d_s$$

where  $d_s$  is the sheath thickness. For a planar probe geometry, the sheath thickness varies directly as the probe potential and inversely as the ion density and is given by

$$d_s = \lambda_D \chi_p^{3/4}$$

where  $\lambda_D$  is the Debye length and is defined as

APPENDIX A – Continued

$$\lambda_D = \left( \frac{\epsilon_0 k T_e}{e^2 n} \right)^{1/2}$$

where  $\epsilon_0$  is the permittivity of free space.

The approximation of a planar solution for sheath thickness is applicable to cylindrical probes only when the sheath thickness is small compared with the probe radius. When this is not the case, the ratio  $\gamma$  of the sheath to probe radius may be obtained from an inverted form of the Child-Langmuir 3/2-power law for space-charge-limited current flow. This relation has been derived by Hok for cylindrical probes and is plotted in figure 35 as  $\gamma - 1$  against  $\Theta$  where  $\Theta$  is defined as

$$\Theta = \frac{L}{I_+ R_p} \left( V' + \frac{5kT_e}{e} \right)^{3/2} \left( 1 + \frac{2.66}{\sqrt{\chi_p}} \right) \quad (A2)$$

and

$I_+$  measured probe current

$V'$  absolute magnitude of applied probe bias

To give more physical significance to the current collection curves shown in figure 34, the following asymptotic cases are given:

Case I; thin sheath,  $\gamma \approx 1$ ;  $\chi_p < -1$ :

$$I_+ = 2\pi R_p L J_i \quad (A3)$$

where  $J_i$  is the saturation positive ion current density for a collisionless Maxwellian plasma at rest and is given approximately by Bohm et al. (ref. 26) as

$$J_i = 0.4 n e v_+ \quad (A4)$$

Note that equation (A3) is independent of the applied probe bias.

Case II; moderate to thick sheaths,  $\gamma > 1$ ; large negative probe bias,  $\chi_p \ll -\gamma$ :

$$I_+ = \gamma 2\pi R_p L J_i \quad (A5)$$

This current varies directly as the applied bias because of  $\gamma$ .

## APPENDIX A – Continued

Case III; extremely thick sheaths,  $\gamma \gg |\chi_p|$ ; moderate negative probe bias,  $\chi_p < -2$ :

$$I_+ = \frac{2}{\sqrt{\pi}} \sqrt{|\chi_p| + 1} (2\pi R_p L J_i) \quad (A6)$$

In this region the current is approximately proportional to the square root of applied probe bias.

### Directed Flow Normal to Probe

The effect of a normally directed ion flux (ions/unit area) on the current collected by free molecular cylindrical probes has been analyzed by several investigators. (See refs. 12, 15, 27, and 28.) If it is assumed that the flow does not distort the form of the ion sheath around the probe, the current density is the result of a superposition of random and directed ion fluxes (ref. 12). This effect is illustrated by figure 36, a curve of the normalized current  $I_n$  collected by a cylindrical probe not aligned with the flow plotted against the ion speed ratio  $S$ . The speed ratio is defined as the normal component  $v_f$  of the flow velocity  $v_{\text{flow}}$  divided by the random thermal velocity  $v_+$

$$S = \frac{v_f}{v_+} \quad (A7)$$

In figure 36 there are two asymptotes shown as dashed lines. The horizontal asymptote represents the value of current collected by a thin-sheathed ( $\gamma \approx 1$ ) probe in a nonflowing plasma and is equal to the random current  $I_r$  or to a normalized current of unity. The other asymptote represents the superposition of the random current  $I_r$  and a directed current  $I_d$ . The directed current is

$$I_d = ne v_f (2R_p L) = \rho v_f A \quad (A8)$$

where

$\rho$             charge density

$A$             projected area of probe

When the normal component of the flow velocity is small ( $S \ll 1$ ), the probe current is approximately that collected in a nonflowing plasma. For larger values of the normal component of flow velocity, that is,  $S > 3$ , the current collected by the probe approaches the value given in equation (A8).

When the ion sheath is not thin, that is,  $\gamma > 1$ , the problem is more complicated because the ability of the relatively weak electrostatic potential field around the probe to

APPENDIX A – Continued

capture ions with increased inertial energy due to the flow is reduced. This problem was treated by Smetana (ref. 15) and the results are shown in figure 37.

Scharfman (ref. 12) gives the following qualitative explanation of Smetana's results: For the nonflowing plasma case ( $S = 0$ ) with low values of applied bias ( $\chi_p > -1$ ) and a large sheath thickness ( $\gamma \gg 1$ ), the attraction of the probe's potential field is weak; consequently, most of the ions that enter the sheath orbit past the probe and are not collected. By using simple orbital theory, the radius  $r_a$  at which particles will just be collected is

$$r_a = R_p \left( 1 + \frac{V}{V_0} \right)^{1/2}$$

where

$V$  probe potential

$V_0$  initial energy of ion entering sheath,  $kT_e/e$

Thus, the current is proportional to the flux (ions/unit area) entering the sheath at the radius  $r_a$  and is proportionally given as

$$I_+ \propto nV_0^{1/2} R_p \left( 1 + \frac{V}{V_0} \right)^{1/2}$$

In the limit of large applied potential ( $\chi_p \ll -1$ ),

$$I_+ \propto V^{1/2} R_p$$

When a directed velocity is included ( $S > 0$ ), the flux is proportional to  $SV_0^{1/2}$  and the capture radius becomes

$$r_a = R_p \left( 1 + \frac{V}{S^2 V_0} \right)^{1/2}$$

Thus, the effective capture radius for ions decreases while the flux increases. Therefore,

$$I_+ \propto nSV_0^{1/2} R_p \left( 1 + \frac{V}{S^2 V_0} \right)^{1/2}$$

In the limit of large applied potentials ( $\chi_p \ll -S^2$ ), this relationship reduces to the same value as when  $S = 0$ ; that is,



APPENDIX A – Continued

$$I_+ \propto V^{1/2} R_p$$

In the limit of large directed velocity ( $S \gg 1$ ),  $I_n$  approaches  $S$  in value, and the current  $I_+$  is approximately given by equation (A8).

With this understanding of current collection under directed velocity conditions and with the asymptotic solutions for  $S = 0$  and  $S \gg 1$ , the works of Hok and Smetana can be combined by a transformation of the coordinates of figure 34. This result from Scharfman is replotted in figure 38 as the variation of  $R$  with  $H$  where

$$R = \frac{I_n}{(1 + S^2)^{1/2}} \quad (\text{A9})$$

$$H = \frac{\chi_p}{1 + S^2} \quad (\text{A10})$$

where

$R$             modified normalized probe current

$H$             ratio of modified potential energy to kinetic energy

The results presented in figure 38 can be readily used to infer positive ion density  $n$  by the following algorithm:

- (1) Determine  $T_e$
- (2) Measure the probe current  $I_+$  at  $V'$  volts below floating potential
- (3) Calculate the normalized probe to plasma potential

$$\chi_p = \left( \frac{eV'}{kT_e} \right) + 5 \pm 0.5 \quad (\text{A11})$$

- (4) Calculate  $\Theta$  by use of equation (A2)
- (5) Obtain the appropriate value of  $\gamma$  from figure 35
- (6) Calculate  $v_+$  by using equation (A1)
- (7) Calculate  $S$  by using equation (A7)
- (8) Calculate  $H$  by using equation (A10)

APPENDIX A – Continued

(9) Obtain the appropriate value of  $R$  from figure 38

(10) Calculate the positive ion density from

$$n = \frac{I_+}{\sqrt{1 + S^2 R \sqrt{\pi} e v_+ R_p L}}$$

Interpretation of RAM-C Fixed-Bias Electrostatic Probe Data

The configuration of the RAM-C electrostatic probe is shown in figure 6(b). In relation to the flowing plasma, each ion collector appears to be a cylindrical wire 0.0254 cm (0.010 in.) in diameter and 0.5385 cm (0.212 in.) long, which is inclined at an angle of 45° with respect to the plasma flow. To illustrate the data-reduction procedure, a sample calculation is presented.

Sample Calculation

The following factors are given in the sample calculation:

Altitude, km (ft) . . . . .	76.2 (250 000)
Ion collector . . . . .	8
Potential of probe below floating potential, $V'$ , volts . . . . .	5
Temperature, $T$ , K . . . . .	7500
Flow velocity, $v_{flow}$ , km/sec (ft/sec) . . . . .	5160 (16 930)
Angle between flow velocity and probe axis, $\theta$ , deg . . . . .	45
Ion mass ( $NO^+$ ), $M$ , g . . . . .	$49.88 \times 10^{-24}$
Measured current, $I_+$ , $\mu A$ . . . . .	50
Probe length, $L$ , cm (in.) . . . . .	0.5385 (0.212)
Probe radius, $R_p$ , cm (in.) . . . . .	0.0127 (0.005)
Boltzmann constant, $k$ , J/K . . . . .	$1.38044 \times 10^{-23}$
Electronic charge, $e$ , coulombs . . . . .	$1.5921 \times 10^{-19}$

For an altitude of 76.2 km (250 000 ft) and ion collector 8, the temperature was calculated to be 7500 K. The electron temperature is assumed to be equal to the local gas temperature. A plot of gas temperature as a function of altitude for the ion collector locations is shown in figure 39. These temperature data, as well as the flow velocity data given in figure 40, were generated by a nonequilibrium boundary-layer-corrected flow-field analysis of the RAM C-I trajectory.

## APPENDIX A – Concluded

The first factor to be calculated is the normalized potential difference between the probe and the plasma by using equation (A11)

$$\chi_p = \frac{eV'}{kT_e} + 5 = 12.69$$

Next, the ratio of ion sheath radius to probe radius  $\gamma$  is estimated by using figure 35 and equation (A2)

$$\Theta = \frac{L}{I_+ R_p} \left( V' + \frac{5kT_e}{e} \right)^{3/2} \left( 1 + \frac{2.66}{\sqrt{\chi_p}} \right)$$

For a measured current of  $50 \mu\text{A}$ , the value of  $\Theta$  is  $3.51 \times 10^7 \text{ volts}^{3/2}/\text{ampere}$ . The corresponding ratio of sheath radius to probe radius  $\gamma$  is 2.61.

The modified normalized probe current  $R$  is now determined. Figure 38 is a plot of  $R$  as a function of the ratio of modified potential energy to kinetic energy  $H$  (eq. (A10)) which is defined as

$$H = \frac{\chi_p}{1 + S^2}$$

The velocity of ions entering the sheath  $v_+$  is calculated (eq. (A1)) to be

$$v_+ = \left( \frac{2kT_e}{M} \right)^{1/2} = 2.037 \times 10^5 \text{ cm/sec}$$

The ion speed ratio  $S$  is (from eq. (A7))

$$S = \frac{v_f}{v_+} = \frac{v_{\text{flow}} \sin \theta}{v_+}$$

From equation (A7),  $S = 1.791$  and thus the value of  $H$  is 3.015. The corresponding value of  $R$  is 1.93 from figure 38.

Solving for the density  $n$  yields

$$n = \frac{I_+}{\sqrt{1 + S^2} R \sqrt{\pi} e v_+ R_p L} = 3.21 \times 10^{10} \text{ cm}^{-3}$$

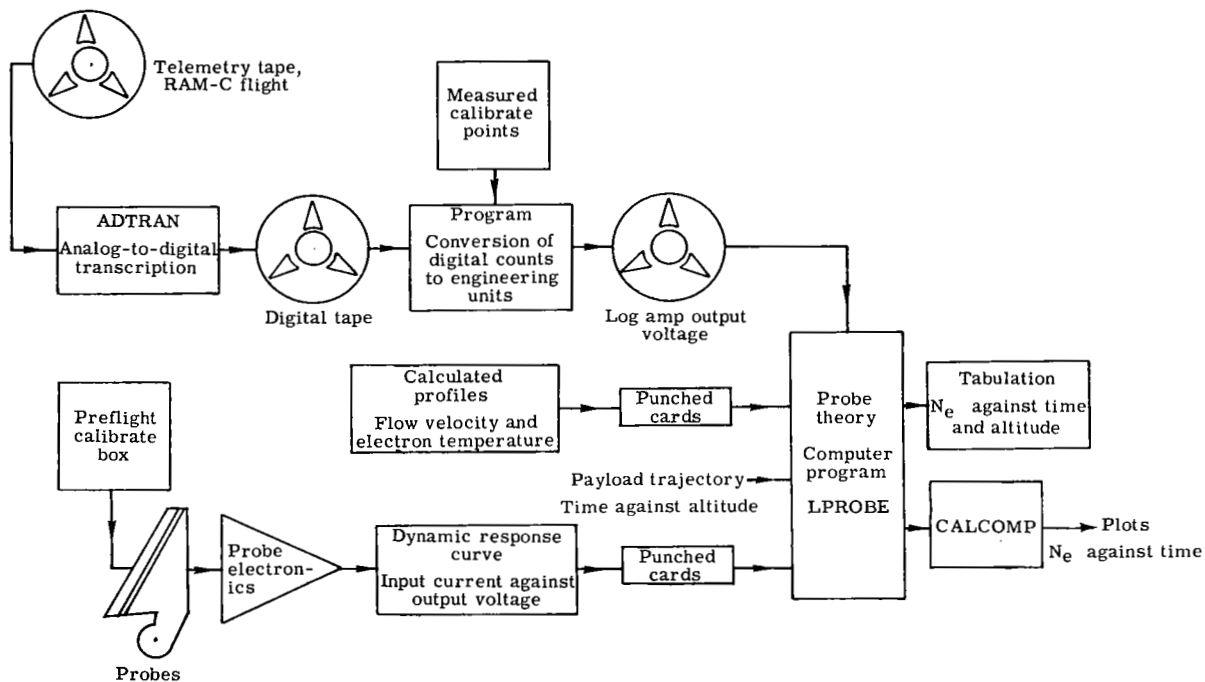
## APPENDIX B

### ELECTROSTATIC-PROBE AUTOMATIC DATA REDUCTION

#### PROCEDURE AND LISTINGS

By Lorraine F. Satchell  
Langley Research Center

This appendix outlines the method for inferring electron density from telemetry data for the RAM-C flight experiments. The theoretical interpretation used was that of Scharfman (based on the works of Smetana and Hok) as presented in appendix A. A flow chart that illustrates the data-reduction procedure follows:



Telemetry signals containing the electrostatic probe data were recorded by ground receiving stations on magnetic tape. These data were in an analog—frequency-modulation form which consisted of subcarrier oscillator frequency deviations as a function of logarithmic amplifier output voltage. The format for this commutated probe data is given in figure 10. An analog-to-digital transcription made from magnetic telemetry tape data was converted to engineering units to be used as inputs to the probe theory computer program named LPROBE. LPROBE also required, as input data, theoretical flow-field velocities

## APPENDIX B – Continued

and electron temperatures for each probe location, as functions of elapsed flight time and altitude, and preflight probe-electronic system calibration. Sufficient points from curves of these input data were tabulated and a second-order interpolation using FTLUP, a table look-up subroutine, provided the desired accuracy.

LPROBE was written in Fortran IV language for the Control Data 6000 series computer. The formats for the program inputs were flight time (FLTIME), delta time (DELTA), synchronization code (ISYNC), and 24 channels of voltage and 24 channels of current. DNSTY was a subroutine with all tabular data listed internally. LPROBE provided the data in the call sequence and DNSTY computed the electron density. The outputs of LPROBE were CALCOMP plots (figs. 13, 14, 17, and 18) and/or tabulations of electron density (electrons/cm<sup>3</sup>) as a function of time for each probe.

Presented in this appendix are: a listing of the program, logarithmic amplifier calibrates (output voltage as a function of input current in microamperes) for the two flights, tables of computed gas temperatures (for altitudes in thousands of feet), flow velocity calculations (as a function of time) for each of the probes, and tabulations of computed electron density as a function of time for each of the probes for both RAM C-I and RAM C-II.

```

C          #CALL SEQUENCE FOR SUBROUTINE DNSTY*                                LFS 250
C                                                                                   LFS 260
C  TE=ELECTRON TEMPERATURE,DEGREES KELVIN(COMPUTED FROM TABLES VS. TIME)      LFS 270
C                                                                                   LFS 280
C  TI=ION TEMPERATURE(NOT USED-DUMMY IN CALL STATEMENT)                         LFS 290
C                                                                                   LFS 300
C  PDMILL(DIAMETER OF PROBE)=10.0 MILLS                                          LFS 310
C                                                                                   LFS 320
C  PLMILL(LENGTH OF PROBE)=212.0 MILLS                                          LFS 330
C                                                                                   LFS 340
C  AV POTENTIAL CC IS MEASURED WITH RESPECT TO PLASMA POTENTIAL.                 LFS 350
C                                                                                   LFS 360
C  CC ION SATURATION CURRENT,MICRCAMPS (COMPUTED VALUES).                      LFS 370
C                                                                                   LFS 380
C  AMU(ION MASS)=28.0 AMU                                                         LFS 390
C                                                                                   LFS 400
C  ANG(ORIENTATION ANGLE OF PROBE)=45.0 DEGREES OR .78539816 RADIANS           LFS 410
C                                                                                   LFS 420
C  FLOVEL(FLOW-VELOCITY) IN M/SEC. (COMPUTED FROM TABLES VS. TIME)            LFS 430
C                                                                                   LFS 440
C  AV(ELECTRON DENSITY) COMPUTED USING SUBROUTINE DNSTY.                         LFS 450
C                                                                                   LFS 460
C  THERE ARE 8 PROBES-EACH SAMPLES THE DATA 3 TIMES PER FLIGHT TIME.          LFS 470
C  SEE FIGURE 11 AND TABLE BELOW.                                              LFS 480
C  DATA(1,09,17) ARE PROBE 1 (FTLUP USES CORRECTED TIME,TEMP1 AND VF 1)        LFS 490
C  DATA(2,10,18) ARE PROBE 2 (FTLUP USES CORRECTED TIME,TEMP2 AND VF 2)        LFS 500
C  DATA(3,11,19) ARE PROBE 3 (FTLUP USES CORRECTED TIME,TEMP3 AND VF 3)        LFS 510
C  DATA(4,12,20) ARE PROBE 4 (FTLUP USES CORRECTED TIME,TEMP4 AND VF 4)        LFS 520
C  DATA(5,13,21) ARE PROBE 5 (FTLUP USES CORRECTED TIME,TEMP5 AND VF 5)        LFS 530
C  DATA(6,14,22) ARE PROBE 6 (FTLUP USES CORRECTED TIME,TEMP6 AND VF 6)        LFS 540
C  DATA(7,15,23) ARE PROBE 7 (FTLUP USES CORRECTED TIME,TEMP7 AND VF 7)        LFS 550
C  DATA(8,16,24) ARE PROBE 8 (FTLUP USES CORRECTED TIME,TEMP8 AND VF 8)        LFS 560
C                                                                                   LFS 570
C          REAL N3(600)                                                            LFS 580
C                                                                                   LFS 590

```

## APPENDIX B - Continued

```

DIMENSION VGLTS(50),CUR(50),TIMEA(40),ALTA(40),TEMP(40,8),TIMEB(40LFS 600
1),ALTB(40),VF(40,8),FLTIME(200),VOLTAGE(200,24),CURRENT(200,24), LFS 610
1ISYNC(200),DELTAT(200),TIME(600),CLRR(600) LFS 620
C LFS 630
EQUIVALENCE (TIMEA,TIMEB),(ALTA,ALTB) LFS 640
C LFS 650
INITIALIZE PLOTTER. LFS 660
CALL CALCCMP LFS 670
C LFS 680
USE PAPER 300 - SET PEN ON RIGHT MARGIN - SET ORIGIN. LFS 690
CALL CALPLT(C.0,1.0,-3) LFS 700
C LFS 710
PRINT CONSTANTS. LFS 720
SIZE=.1 LFS 730
SIZED2=SIZE/2.0 LFS 740
W=(6./7.)*SIZE LFS 750
SIZED=SIZE+SIZED2 LFS 760
C LFS 770
DATA CONSTANTS $ CAYOEP=K/EPSILCN LFS 780
PDMILL=1C.0 LFS 790
PLMILL=212.0 LFS 800
AMII=28.0C LFS 810
ANG=.78539816 LFS 820
E=5.0 LFS 830
CAYOEP=.0C0138054/1.60210 LFS 840
C LFS 850
READ,STORE AND WRITE VOLTAGE VS. CURRENT FROM LOG-AMP CURVES(814 LFS 860
RAM C-I AND 813 RAM C-II)(DYNAMIC INPUT-OUTPUT CURVES) LFS 870
WRITE(6,1) LFS 880
1 FORMAT(*1 VOLTAGE CURRENT LOG-AMP 814*/) LFS 890
CO 10 I=1,50 LFS 900
READ(5,3)VOLTS(I),CUR(I) LFS 910
3 FORMAT(2F10.3) LFS 920
WRITE(6,3)VOLTS(I),CUR(I) LFS 930
10 CONTINUE LFS 940
C LFS 950
READ,STORE AND WRITE TIME AND ALTITUDE VS. TEMPERATURE (1 THRU 8) LFS 960
C (COMPUTED ELECTRON OR GAS TEMPERATURE AS A FUNCTION OF ALTITUDE LFS 970
FOR ELECTROSTATIC PROBE LOCATIONS ON RAM C-I AND RAM C-II) LFS 980
C LFS 990
WRITE(6,11) LFS 1000
11 FORMAT(*1 TIME ALT TEMP1 TEMP2 TEMP3 TEM LFS 1010
1F4 TEMP6 TEMP7 TEMP8*/) LFS 1020
CO 20 I=1,40 LFS 1030
READ(5,12)TIMEA(I),ALTA(I),(TEMP(I,J),J=1,8) LFS 1040
12 FORMAT(2F8.1,8F8.3) LFS 1050
WRITE(6,13)TIMEA(I),ALTA(I),(TEMP(I,J),J=1,8) LFS 1060
13 FORMAT(2F10.1,8F10.3) LFS 1070
20 CONTINUE LFS 1080
C LFS 1090
READ,STORE AND WRITE TIME AND ALTITUDE VS. FLOW VELOCITY (1 THRU 8) LFS 1100
C (COMPUTED VELOCITY AS A FUNCTION OF ALTITUDE). LFS 1110
WRITE(6,21) LFS 1120
21 FORMAT(*1 TIME ALT VF1 VF2 VF3 VLFS 1130
1F4 VF5 VF6 VF7 VF8*/) LFS 1140
CO 30 I=1,40 LFS 1150
READ(5,12)TIMEB(I),ALTB(I),(VF(I,J),J=1,8) LFS 1160
WRITE(6,13)TIMEB(I),ALTB(I),(VF(I,J),J=1,8) LFS 1170
30 CONTINUE LFS 1180
C LFS 1190
READ AND STORE DATA FROM FLIGHTS (RAM C-I REEL 214009 AND RAM CII LFS 1200
REEL 314026). LFS 1210
I=1 LFS 1220
60 READ(8)FLTIME(I),ISYNC(I),DELTAT(I),(VOLTAGE(I,J),J=1,24),(CURRENT LFS 1230
1(I,J),J=1,24) LFS 1240
IF(EOF,8)75,65 LFS 1250
65 I=I+1 LFS 1260
GO TO 60 LFS 1270

```

APPENDIX B - Continued

	75 REWIND 8	LFS 1280
	CALL EVICT(5LTAPE8)	LFS 1290
	IPTS=I	LFS 1300
C		LFS 1310
C	CCOMPUTE DATA BY PROBES	LFS 1320
	CO 300 IPROBE=1,8	LFS 1330
C		LFS 1340
C	HEADINGS FOR DATA	LFS 1350
	NPTS=0	LFS 1360
	WRITE(6,76)	LFS 1370
	76 FORMAT(*1PROBE DIMETER=10 MILS PROBE LENGTH=212 MILS IJN MASL	LFS 1380
	IS=28 AMU ORIENTATION ANGLE=.78539816 RADIANS*/)	LFS 1390
	WRITE(6,77)	LFS 1400
	77 FORMAT(*OPROBE FL TIME SYNC VOLTAGE CURRENT ALTITUDE TEMPERLFS	LFS 1410
	1ATURE F-VELOCITY AV TIME ELECTRON DNSTY LOG(N3)*))LFS	LFS 1420
	IF(IPROBE.EQ.1)GO TO 81	LFS 1430
	IF(IPROBE.EQ.2)GO TO 82	LFS 1440
	IF(IPROBE.EQ.3)GO TO 83	LFS 1450
	IF(IPROBE.EQ.4)GO TO 84	LFS 1460
	IF(IPROBE.EQ.5)GO TO 85	LFS 1470
	IF(IPROBE.EQ.6)GO TO 86	LFS 1480
	IF(IPROBE.EQ.7)GO TO 87	LFS 1490
	IF(IPROBE.EQ.8)GO TO 88	LFS 1500
	81 M1=1	LFS 1510
	M2=17	LFS 1520
	NO=-11	LFS 1530
	GO TO 90	LFS 1540
	82 M1=2	LFS 1550
	M2=18	LFS 1560
	NO=-12	LFS 1570
	GO TO 90	LFS 1580
	93 M1=3	LFS 1590
	M2=19	LFS 1600
	NO=-13	LFS 1610
	GO TO 90	LFS 1620
	84 M1=4	LFS 1630
	M2=20	LFS 1640
	NO=-14	LFS 1650
	GO TO 90	LFS 1660
	95 M1=5	LFS 1670
	M2=21	LFS 1680
	NO=-15	LFS 1690
	GO TO 90	LFS 1700
	86 M1=6	LFS 1710
	M2=22	LFS 1720
	NO=-16	LFS 1730
	GO TO 90	LFS 1740
	87 M1=7	LFS 1750
	M2=23	LFS 1760
	NO=-17	LFS 1770
	GO TO 90	LFS 1780
	88 M1=8	LFS 1790
	M2=24	LFS 1800
	NO=-18	LFS 1810
C		LFS 1820
C	TI IS A DUMMY IN CALL STATEMENT TO SUBROUTINE DNSTY.	LFS 1830
	90 TI=1.0	LFS 1840
	IS=1	LFS 1850
	CC 100 I=1,IPTS	LFS 1860
	IF(ISYNC(I).EQ.1)GO TO 100	LFS 1870
	IF(ISYNC(I).EQ.2)GO TO 100	LFS 1880
	CO 98 J=M1,M2,8	LFS 1890
	JJ=J	LFS 1900
	IF(VOLTAGE(I,J).LT.(-.C80))GO TO 98	LFS 1910
	IF(VOLTAGE(I,J).GT.(5.264))GO TO 98	LFS 1920

APPENDIX B - Continued

```

IF(CURRENT(I,J).LT.(.100))GO TO 98          LFS 1930
IF(CURRENT(I,J).GT.(1000.))GO TO 98        LFS 1940
IF(LEGVAR(VOLTAGE(I,J)))98,91,98           LFS 1950
91 IF(LEGVAR(CURRENT(I,J)))98,92,98        LFS 1960
92 ATIME=FLTME(I)+(FLOAT(JJ))*DELTAT(I)    LFS 1970
IF(ATIME.GT.(406.000))GO TO 98            LFS 1980
NPTS=NPTS+1                                LFS 1990
TIME(NPTS)=ATIME                            LFS 2000
CALL FTLUP(ATIME,ALT,2,40,TIMEB,ALTB)      LFS 2010
ALT=ALT*1000.                               LFS 2020
CC=CURRENT(I,J)                             LFS 2030
CURR(NPTS)=CURRENT(I,J)                    LFS 2040
CALL FTLUP(ATIME,TE,2,40,TIMEA,TEMP(1,IPRCBE)) LFS 2050
TE=TE*1000.                                 LFS 2060
AV=E+5.0*CAYQEP*TE                          LFS 2070
CALL FTLUP(ATIME,FLOVEL,2,40,TIMEB,VF(1,IPROBE)) LFS 2080
FLOVEL=FLOVEL*1000.                         LFS 2090
CALL DNSTY(TE,TI,PDMILL,PLMILL,CC,AV,AMII,ANG,FLOVEL,AN) LFS 2100
N3(NPTS)=ALOG10(AN)                         LFS 2110
WRITE(6,96)IPROBE,J,FLTME(I),ISYNC(I),VCLTAGE(I,J),CC,ALT,TE, LFS 2120
IFLOVEL,AV,TIME(NPTS),AN,N3(NPTS)          LFS 2130
96 FORMAT(I2,I4,F9.3,I5,2F10.3,F10.1,2F13.3,F10.3,FR.3,E16.6,F12.6) LFS 2140
KPTS=NPTS                                    LFS 2150
IF(MOD(NPTS,40))98,97,98                   LFS 2160
97 WRITE(6,76)                               LFS 2170
WRITE(6,77)                                 LFS 2180
93 CCNTINUE                                  LFS 2190
100 CONTINUE                                 LFS 2200
NPTS=KPTS                                    LFS 2210
C                                             LFS 2220
C SCALE DATA TO BE PLOTTED                  LFS 2230
DO 110 I=1,NPTS                             LFS 2240
TIME(I)=TIME(I)-386.C                       LFS 2250
N3(I)=(N3(I)-7.0)*2.5                       LFS 2260
CURR(I)=(1.0+ALOG10(CURR(I)))*2.5          LFS 2270
110 CONTINUE                                 LFS 2280
C                                             LFS 2290
C PLOT TIME VS. ELECTRON DENSITY (N3) AND TIME VS. CURRENT (CURR). LFS 2300
DO 200 IPLOT=1,2                            LFS 2310
C                                             LFS 2320
C DRAW X-AXIS AND LOGRID                    LFS 2330
CALL AXES(0.0,0.0,0.0,0.0,21.0,386.,1.0,1.0,.5,9HTIME,SEC.,.15,-9) LFS 2340
CALL LOGRID(21.0,2.5,-1.6,0.C,1.0,.5,.2)   LFS 2350
C                                             LFS 2360
C GENERAL IDENTIFICATION OF Y-AXIS          LFS 2370
CALL CALPLT(0.0,15.0,2)                    LFS 2380
CALL CALPLT(0.0,0.0,3)                     LFS 2390
CALL NOTATE(-.3,0.0,SIZE,6HPROBE ,90.0,6)  LFS 2400
NPROBE=IPROBE                              LFS 2410
XPROBE=NPROBE                              LFS 2420
CALL NUMBER(-.3,(0.0+(5.0*W)),SIZE,XPROBE,90.0,-1) LFS 2430
CALL NCTATE(-.75,0.,SIZE,7HRAM C-A,90.0,7) LFS 2440
IF(IPLOT.EQ.2)GO TO 140                    LFS 2450
CALL NCTATE(-.2,6.5,.15,8HELECTRON,90.0,8) LFS 2460
CALL NOTATE(-.2,7.7,.15,7HDENSITY,90.0,7)  LFS 2470
C                                             LFS 2480
C TIME VS. N3                               LFS 2490
DO 120 I=1,NPTS                             LFS 2500
CALL FNTPLT(TIME(I),N3(I),NO,IS)           LFS 2510
120 CONTINUE                                 LFS 2520
GO TO 190                                    LFS 2530
C                                             LFS 2540
C TIME VS. CURRENT                          LFS 2550
140 CALL NCTATE(-.2,7.1,.15,7HCURRENT,90.0,7) LFS 2560
DO 180 I=1,NPTS                             LFS 2570
CALL PNTPLT(TIME(I),CURR(I),NO,IS)        LFS 2580
180 CONTINUE                                 LFS 2590
C                                             LFS 2600

```



APPENDIX B - Continued

```

C      MOVE TO NEW PLOTTING AREA                                LFS 2610
19J CALL CALPLT(24.0,C.0,-3)                                    LFS 2620
20J CONTINUE                                                    LFS 2630
C      CLEAR CORE FOR NEXT PRJBE.                                LFS 2640
      DC 250 I=1,NPTS                                           LFS 2650
      TIME(I)=0.0                                               LFS 2660
      N3(I)=0.C                                                LFS 2670
      CURR(I)=0.0                                              LFS 2680
25J CCNTINUE                                                    LFS 2690
30J CONTINUE                                                    LFS 2700
C      RELEASE PLOTTER AND STOP.                                  LFS 2710
C      CALL CALPLT(0.0,C.0,999)                                  LFS 2720
      STCP                                                       LFS 2730
      END                                                         LFS 2740
      SURROUTINE DNSTY(TE,TI,PDMILL,PLMILL,CC,AV,AMII,ANG,FLOVEL,AN) LFS 2750
      DIMENSION R(6),C(6),EIF(9)                                LFS 2760
      DIMENSION D(9),E1P5(9),E2(9),E3(9),E5(9),E1C(9),E2C(9),E5C(9) LFS 2770
      DIMENSION G(8),H(8)                                       LFS 2780
      DATA R/5.2,6.,7.,8.,9.,10./                               LFS 2790
      DATA C/-1.,-.61,-.0926,.463,1.083,1.786/                 LFS 2800
      DATA D/-1.,-.5,C.,.5,1.,1.5,2.,2.5,3./                 LFS 2810
      DATA E1P5/.031,.036,.136,6*.175/                       LFS 2820
      DATA E2/.031,.073,.167,.253,5*.300/                    LFS 2830
      DATA E3/.031,.074,.171,.316,.428,4*.475/              LFS 2840
      DATA E5/.031,.074,.191,.35,.521,.654,3*.7/            LFS 2850
      DATA E1C/.031,.074,.191,.37,.58,.755,.919,.988,1./    LFS 2860
      DATA E2C/.031,.074,.191,.37,.58,.802,1.04,1.19,1.29/  LFS 2870
      DATA E5C/.031,.074,.191,.37,.58,.81,1.05,1.28,1.32/  LFS 2880
      DATA EIF/.031,.074,.191,.37,.58,.81,1.06,1.20,1.55/  LFS 2890
      DATA G/.175,.300,.475,.7,1.,1.3,1.7,10./              LFS 2900
      FL=PLMILL*2.54E-5                                         LFS 2910
1 AC=ABS(CC)*1.E-6                                             LFS 2920
C PR=PDMILL*2.54E-5/2. $AMI=AMII*1.672E-27                    LFS 2930
FR=.5*PDMILL*2.54E-5 $AMI=AMII*1.672E-27                    LFS 2940
C A=AV*11604./TE                                              LFS 2950
A=ABS(AV*11604./TE)                                           LFS 2960
T=PL*AV**1.5*(1.+2.66/SQRT(A))/(PR*AC)                       LFS 2970
T=ALOG10(T)                                                    LFS 2980
CALL DISCCT(T,T,B,C,C,-20,6,0,ANS)                             LFS 2990
2 ADR=1.+10.**ANS                                              LFS 3000
3 VP=SQRT(2.*1.38E-23*TE/AMI)                                  LFS 3010
4 S=FLOVEL*SIN(ANG)/VP                                         LFS 3020
T=A/(1.+S*S)                                                  LFS 3030
T=ALOG10(T)                                                    LFS 3040
CALL DISCCT(T,T,D,E1P5,E1P5,-20,9,0,ANS1P5)                   LFS 3050
CALL DISCCT(T,T,D,E2 ,E2 ,-20,9,0,ANS2 )                      LFS 3060
CALL DISCCT(T,T,D,E3 ,E3 ,-20,9,0,ANS3 )                      LFS 3070
CALL DISCCT(T,T,D,E5 ,E5 ,-20,9,0,ANS5 )                      LFS 3080
CALL DISCCT(T,T,D,E10,E10,-20,9,0,ANS10)                      LFS 3090
CALL DISCCT(T,T,D,E20,E20,-20,9,0,ANS20)                      LFS 3100
CALL DISCCT(T,T,D,E5C,E50,-20,9,0,ANS50)                     LFS 3110
CALL DISCCT(T,T,D,EIF,EIF,-20,9,0,ANSIF)                      LFS 3120
F(1)=ANS1P5 $ H(2)=ANS2 $ H(3)=ANS3 $ H(4)=ANS5 $ H(5)=ANS10  LFS 3130
F(6)=ANS2C $ H(7)=ANS50 $ H(8)=ANSIF                          LFS 3140
ACR=ALOG10(ACR)                                               LFS 3150
CALL DISCCT(ADR,ADR,G,H,H,-20,8,0,ANS)                         LFS 3160
ANS=10.**ANS                                                    LFS 3170
F=ANS*SQRT(1.+S*S)                                            LFS 3180
AREA=6.28*PR*PL                                              LFS 3190
5 AN=4.*AC/(AREA*F*1.6E-19*SQRT(8.*1.38E-23*TE/(3.14159*AMI))) LFS 3200
AN=AN*1.E-6                                                  LFS 3210
RETURN                                                         LFS 3220
END                                                            LFS 3230

```

## APPENDIX B – Continued

### PRE-FLIGHT CALIBRATION OF LOGARITHMIC AMPLIFIERS

RAM C-I		RAM C-II	
Logarithmic amplifier, serial number 814		Logarithmic amplifier, serial number 813	
VOLTAGE	CURRENT	VOLTAGE	CURRENT
-.080	.100	-.136	.100
-.060	.570	0.000	.298
-.040	.695	.090	.370
0.000	.754	.240	.450
.055	.830	.495	.580
.150	.922	.780	.720
.305	1.020	.925	.790
.400	1.085	1.115	.870
.545	1.175	1.375	.990
.700	1.260	1.540	1.090
.850	1.340	1.725	1.240
1.055	1.480	1.825	1.340
1.210	1.625	1.950	1.480
1.300	1.725	2.025	1.600
1.480	1.980	2.140	1.800
1.600	2.185	2.215	2.000
1.710	2.450	2.310	2.300
1.800	2.695	2.375	2.550
1.900	3.030	2.500	3.200
1.990	3.400	2.605	4.000
2.100	3.890	2.651	4.500
2.250	4.810	2.715	5.200
2.300	5.220	2.765	6.000
2.385	6.010	2.810	7.000
2.500	7.640	2.865	8.500
2.635	10.490	2.905	10.000
2.800	13.800	2.940	11.000
3.065	20.700	2.980	12.500
3.200	24.900	3.040	14.500
3.300	28.600	3.130	18.500
3.460	33.400	3.175	21.000
3.600	36.600	3.230	23.500
3.750	49.500	3.330	28.500
3.900	58.900	3.430	34.000
4.000	65.500	3.535	40.000
4.200	80.500	3.725	53.000
4.325	92.700	3.880	65.000
4.400	104.500	4.030	79.000
4.530	133.000	4.110	90.000
4.600	162.500	4.170	100.000
4.700	226.000	4.185	132.000
4.755	274.000	4.190	105.000
4.800	302.000	4.225	120.000
4.900	392.000	4.265	140.000
5.000	505.000	4.330	180.000
5.055	579.000	4.480	277.000
5.100	626.000	4.520	310.000
5.170	717.000	4.615	390.000
5.200	770.000	4.770	550.000
5.264	1000.000	5.023	1000.000

## RAM C-I AND C-II COMPUTED GAS TEMPERATURES FOR PROBES 1 - 8

TIME	ALT	TEMP1	TEMP2	TEMP3	TEMP4	TEMP5	TEMP6	TEMP7	TEMP8
386.5	302.6	5.870	7.060	8.530	9.900	10.630	11.160	11.690	12.220
387.0	299.2	5.760	7.030	8.500	9.850	10.570	11.120	11.670	12.220
387.5	295.9	5.660	6.990	8.460	9.760	10.490	11.060	11.630	12.200
388.0	292.6	5.570	6.970	8.400	9.660	10.420	10.990	11.560	12.130
388.5	289.4	5.470	6.920	8.360	9.560	10.340	10.900	11.460	12.020
389.0	286.1	5.380	6.880	8.270	9.450	10.250	10.800	11.350	11.900
389.5	282.8	5.280	6.830	8.200	9.320	10.150	10.680	11.210	11.740
390.0	279.6	5.190	6.780	8.120	9.190	10.030	10.570	11.110	11.650
390.5	276.3	5.100	6.720	8.050	9.060	9.850	10.460	11.070	11.550
391.0	273.0	5.000	6.660	7.940	8.900	9.650	10.250	10.850	11.450
391.5	269.8	4.900	6.580	7.840	8.750	9.440	10.050	10.660	11.270
392.0	266.5	4.810	6.510	7.720	8.590	9.220	9.760	10.300	10.840
392.5	263.3	4.700	6.430	7.620	8.440	9.010	9.470	9.930	9.850
393.0	260.0	4.600	6.330	7.490	8.260	8.770	9.120	9.100	8.920
393.5	256.8	4.510	6.230	7.370	8.070	8.530	8.800	8.610	8.380
394.0	253.5	4.400	6.130	7.230	7.870	8.280	8.470	8.200	7.930
394.5	250.3	4.310	6.030	7.080	7.690	8.050	8.180	7.870	7.580
395.0	247.0	4.200	5.910	6.920	7.480	7.760	7.860	7.540	7.240
395.5	243.7	4.100	5.780	6.750	7.260	7.500	7.540	7.230	6.920
396.0	240.4	4.000	5.660	6.670	7.040	7.220	7.230	6.940	6.630
396.5	237.1	3.890	5.520	6.380	6.810	6.930	6.920	6.670	6.360
397.0	233.9	3.800	5.360	6.180	6.550	6.640	6.630	6.360	6.090
397.5	230.6	3.680	5.200	5.970	6.300	6.340	6.350	6.150	5.840
398.0	227.3	3.580	5.040	5.770	6.050	6.070	6.070	5.920	5.620
398.5	224.1	3.480	4.860	5.530	5.770	5.820	5.820	5.710	5.400
399.0	220.8	3.380	4.660	5.280	5.510	5.550	5.550	5.460	5.160
399.5	217.6	3.270	4.460	5.020	5.230	5.300	5.300	5.240	4.940
400.0	214.3	3.180	4.260	4.760	4.950	5.050	5.020	5.020	4.720
400.5	211.0	3.070	4.020	4.460	4.660	4.770	4.800	4.800	4.500
401.0	207.7	2.970	3.770	4.140	4.370	4.490	4.560	4.560	4.280
401.5	204.7	2.870	3.530	3.830	4.090	4.250	4.320	4.320	4.080
402.0	201.1	2.760	3.250	3.480	3.720	3.980	4.110	4.110	3.860
402.5	197.9	2.660	2.960	3.110	3.500	3.750	3.900	3.900	3.650
403.0	194.6	2.550	2.640	2.730	3.210	3.480	3.690	3.690	3.430
403.5	191.4	2.460	2.350	2.380	2.950	3.270	3.490	3.490	3.270
404.0	188.1	2.350	1.990	1.990	2.660	3.030	3.290	3.290	3.030
404.5	184.9	2.240	1.580	1.580	2.360	2.820	3.100	3.100	2.820
405.0	181.6	2.140	1.250	1.250	2.100	2.610	2.910	2.910	2.590
405.5	178.3	2.040	.920	.920	1.840	2.360	2.750	2.750	2.420
406.0	175.1	1.940	.610	.610	1.600	2.120	2.570	2.570	2.200

APPENDIX B - Continued

RAM C-I AND C-II COMPUTED FLOW VELOCITY FOR PROBES 1 - 8

TIME	ALT	VF1	VF2	VF3	VF4	VF5	VF6	VF7	VF8
386.5	302.6	.850	1.070	1.170	1.240	1.310	1.360	1.420	1.470
387.0	299.2	.845	1.110	1.230	1.340	1.440	1.520	1.640	1.720
387.5	295.9	.840	1.140	1.300	1.450	1.600	1.700	1.850	1.970
388.0	292.6	.830	1.180	1.360	1.560	1.730	1.900	2.060	2.230
388.5	289.4	.825	1.200	1.430	1.660	1.880	2.060	2.275	2.450
389.0	286.1	.820	1.240	1.500	1.770	2.010	2.230	2.470	2.660
389.5	282.8	.818	1.270	1.570	1.870	2.150	2.420	2.710	2.910
390.0	279.6	.815	1.300	1.630	1.980	2.310	2.620	2.920	3.160
390.5	276.3	.810	1.330	1.700	2.080	2.430	2.770	3.120	3.400
391.0	273.0	.808	1.370	1.770	2.190	2.570	2.970	3.350	3.590
391.5	269.8	.805	1.400	1.830	2.300	2.720	3.140	3.560	3.860
392.0	266.5	.804	1.430	1.880	2.400	2.850	3.310	3.750	4.110
392.5	263.3	.810	1.460	1.980	2.500	2.980	3.450	3.940	4.350
393.0	260.0	.830	1.490	2.020	2.570	3.070	3.590	4.120	4.580
393.5	256.8	.850	1.520	2.070	2.630	3.160	3.720	4.300	4.780
394.0	253.5	.880	1.560	2.130	2.710	3.260	3.850	4.490	4.980
394.5	250.3	.910	1.600	2.200	2.790	3.370	3.990	4.660	5.180
395.0	247.0	.950	1.650	2.280	2.880	3.480	4.140	4.830	5.380
395.5	243.7	1.000	1.720	2.370	2.980	3.610	4.280	4.990	5.530
396.0	240.4	1.050	1.790	2.470	3.100	3.730	4.430	5.140	5.680
396.5	237.1	1.120	1.880	2.570	3.220	3.880	4.590	5.300	5.840
397.0	233.9	1.180	1.960	2.690	3.360	4.010	4.740	5.440	5.980
397.5	230.6	1.260	2.070	2.830	3.510	4.180	4.890	5.590	6.120
398.0	227.3	1.320	2.180	2.970	3.670	4.340	5.050	5.730	6.230
398.5	224.1	1.410	2.300	3.130	3.840	4.520	5.210	5.860	6.350
399.0	220.8	1.500	2.440	3.320	4.030	4.720	5.370	5.990	6.460
399.5	217.6	1.600	2.600	3.490	4.230	4.900	5.530	6.120	6.570
400.0	214.3	1.700	2.760	3.700	4.460	5.090	5.700	6.230	6.660
400.5	211.0	1.800	2.950	3.940	4.700	5.310	5.860	6.340	6.750
401.0	207.7	1.930	3.150	4.200	4.970	5.540	6.020	6.450	6.830
401.5	204.4	2.050	3.370	4.480	5.250	5.770	6.190	6.550	6.920
402.0	201.1	2.170	3.630	4.800	5.580	6.020	6.370	6.670	6.980
402.5	197.9	2.290	3.780	5.020	5.760	6.150	6.480	6.750	7.020
403.0	194.6	2.420	3.940	5.230	5.870	6.230	6.570	6.800	7.050
403.5	191.4	2.530	4.050	5.380	5.950	6.290	6.620	6.830	7.070
404.0	188.1	2.640	4.160	5.490	6.030	6.350	6.650	6.870	7.090
404.5	184.9	2.760	4.250	5.570	6.090	6.400	6.680	6.890	7.100
405.0	181.6	2.880	4.330	5.640	6.130	6.440	6.710	6.900	7.110
405.5	178.3	2.990	4.410	5.700	6.170	6.480	6.730	6.910	7.110
406.0	175.1	3.110	4.490	5.740	6.200	6.500	6.750	6.920	7.110

APPENDIX B - Continued

APPENDIX B - Continued

TABULATIONS OF CURRENT AND INFERRED ELECTRON DENSITY FOR

RAM C-I, PROBE 1

Table with columns: ELAPSED TIME, SECONDS; ALTITUDE, FEET; CURRENT, MICROAMPS; ELECTRON DENSITY, ELECTRONS PER CUBIC CENTIMETER. Data points range from 386.785 to 393.370.

Table with columns: ELAPSED TIME, SECONDS; ALTITUDE, FEET; CURRENT, MICROAMPS; ELECTRON DENSITY, ELECTRONS PER CUBIC CENTIMETER. Data points range from 393.356 to 396.805.

Table with columns: ELAPSED TIME, SECONDS; ALTITUDE, FEET; CURRENT, MICROAMPS; ELECTRON DENSITY, ELECTRONS PER CUBIC CENTIMETER. Data points range from 396.830 to 402.422.

Table with columns: ELAPSED TIME, SECONDS; ALTITUDE, FEET; CURRENT, MICROAMPS; ELECTRON DENSITY, ELECTRONS PER CUBIC CENTIMETER. Data points range from 402.402 to 409.586.

1 meter = 0.3048 feet

APPENDIX B - Continued

TABLATIONS OF CURRENT AND INFERRED ELECTRON DENSITY FOR  
RAM C-I, PROBE 2

ELAPSED TIME, SECONDS	ALTITUDE, FEET	CURRENT, MICROAMPS	ELECTRON DENSITY PER CUBIC CENTIMETER
(a)	(b)	(c)	(d)
386.64	281897	0.70	3.93E+08
386.66	281720	0.70	2.76E+08
386.73	281260	0.70	3.93E+08
386.78	280700	0.49	2.07E+08
386.82	280084	0.72	4.23E+08
386.85	280319	0.60	3.70E+08
386.86	280324	0.40	2.11E+08
386.92	280064	0.70	4.11E+08
386.94	279839	0.73	4.29E+08
386.96	279600	0.70	4.21E+08
386.98	279441	0.70	3.96E+08
386.99	279206	0.70	3.78E+08
386.99	279127	0.64	3.26E+08
386.99	279127	0.60	3.76E+08
386.121	278816	0.70	4.23E+08
386.147	278602	0.70	4.11E+08
386.173	278411	0.70	4.11E+08
386.218	278121	0.60	3.40E+08
386.244	277854	0.70	4.59E+08
386.269	277628	0.70	4.47E+08
386.312	277321	0.70	4.05E+08
386.329	277123	0.70	4.47E+08
386.365	276840	0.79	4.59E+08
386.412	276551	0.60	4.04E+08
386.437	276272	0.55	3.00E+08
386.462	276000	0.60	3.94E+08
386.487	275740	0.60	3.82E+08
386.512	275484	0.60	3.82E+08
386.537	275232	0.60	3.82E+08
386.562	274984	0.60	3.82E+08
386.587	274740	0.60	3.82E+08
386.612	274500	0.60	3.82E+08
386.637	274264	0.60	3.82E+08
386.662	274032	0.60	3.82E+08
386.687	273804	0.60	3.82E+08
386.712	273580	0.60	3.82E+08
386.737	273360	0.60	3.82E+08
386.762	273144	0.60	3.82E+08
386.787	272932	0.60	3.82E+08
386.812	272724	0.60	3.82E+08
386.837	272520	0.60	3.82E+08
386.862	272320	0.60	3.82E+08
386.887	272124	0.60	3.82E+08
386.912	271932	0.60	3.82E+08
386.937	271744	0.60	3.82E+08
386.962	271560	0.60	3.82E+08
386.987	271380	0.60	3.82E+08
387.012	271204	0.60	3.82E+08
387.037	271032	0.60	3.82E+08
387.062	270864	0.60	3.82E+08
387.087	270700	0.60	3.82E+08
387.112	270540	0.60	3.82E+08
387.137	270384	0.60	3.82E+08
387.162	270232	0.60	3.82E+08
387.187	270084	0.60	3.82E+08
387.212	269940	0.60	3.82E+08
387.237	269800	0.60	3.82E+08
387.262	269664	0.60	3.82E+08
387.287	269532	0.60	3.82E+08
387.312	269404	0.60	3.82E+08
387.337	269280	0.60	3.82E+08
387.362	269160	0.60	3.82E+08
387.387	269044	0.60	3.82E+08
387.412	268932	0.60	3.82E+08
387.437	268824	0.60	3.82E+08
387.462	268720	0.60	3.82E+08
387.487	268620	0.60	3.82E+08
387.512	268524	0.60	3.82E+08
387.537	268432	0.60	3.82E+08
387.562	268344	0.60	3.82E+08
387.587	268260	0.60	3.82E+08
387.612	268180	0.60	3.82E+08
387.637	268104	0.60	3.82E+08
387.662	268032	0.60	3.82E+08
387.687	267964	0.60	3.82E+08
387.712	267900	0.60	3.82E+08
387.737	267840	0.60	3.82E+08
387.762	267784	0.60	3.82E+08
387.787	267732	0.60	3.82E+08
387.812	267684	0.60	3.82E+08
387.837	267640	0.60	3.82E+08
387.862	267600	0.60	3.82E+08
387.887	267564	0.60	3.82E+08
387.912	267532	0.60	3.82E+08
387.937	267504	0.60	3.82E+08
387.962	267480	0.60	3.82E+08
387.987	267460	0.60	3.82E+08
388.012	267444	0.60	3.82E+08
388.037	267432	0.60	3.82E+08
388.062	267424	0.60	3.82E+08
388.087	267420	0.60	3.82E+08
388.112	267420	0.60	3.82E+08
388.137	267424	0.60	3.82E+08
388.162	267432	0.60	3.82E+08
388.187	267444	0.60	3.82E+08
388.212	267460	0.60	3.82E+08
388.237	267480	0.60	3.82E+08
388.262	267504	0.60	3.82E+08
388.287	267532	0.60	3.82E+08
388.312	267564	0.60	3.82E+08
388.337	267600	0.60	3.82E+08
388.362	267640	0.60	3.82E+08
388.387	267684	0.60	3.82E+08
388.412	267732	0.60	3.82E+08
388.437	267784	0.60	3.82E+08
388.462	267840	0.60	3.82E+08
388.487	267900	0.60	3.82E+08
388.512	267964	0.60	3.82E+08
388.537	268032	0.60	3.82E+08
388.562	268104	0.60	3.82E+08
388.587	268180	0.60	3.82E+08
388.612	268260	0.60	3.82E+08
388.637	268344	0.60	3.82E+08
388.662	268432	0.60	3.82E+08
388.687	268524	0.60	3.82E+08
388.712	268620	0.60	3.82E+08
388.737	268720	0.60	3.82E+08
388.762	268824	0.60	3.82E+08
388.787	268932	0.60	3.82E+08
388.812	269044	0.60	3.82E+08
388.837	269160	0.60	3.82E+08
388.862	269280	0.60	3.82E+08
388.887	269404	0.60	3.82E+08
388.912	269532	0.60	3.82E+08
388.937	269664	0.60	3.82E+08
388.962	269800	0.60	3.82E+08
388.987	269940	0.60	3.82E+08
389.012	270084	0.60	3.82E+08
389.037	270232	0.60	3.82E+08
389.062	270384	0.60	3.82E+08
389.087	270540	0.60	3.82E+08
389.112	270700	0.60	3.82E+08
389.137	270864	0.60	3.82E+08
389.162	271032	0.60	3.82E+08
389.187	271204	0.60	3.82E+08
389.212	271380	0.60	3.82E+08
389.237	271560	0.60	3.82E+08
389.262	271744	0.60	3.82E+08
389.287	271932	0.60	3.82E+08
389.312	272124	0.60	3.82E+08
389.337	272320	0.60	3.82E+08
389.362	272520	0.60	3.82E+08
389.387	272724	0.60	3.82E+08
389.412	272932	0.60	3.82E+08
389.437	273144	0.60	3.82E+08
389.462	273360	0.60	3.82E+08
389.487	273580	0.60	3.82E+08
389.512	273804	0.60	3.82E+08
389.537	274032	0.60	3.82E+08
389.562	274264	0.60	3.82E+08
389.587	274500	0.60	3.82E+08
389.612	274740	0.60	3.82E+08
389.637	275000	0.60	3.82E+08
389.662	275264	0.60	3.82E+08
389.687	275532	0.60	3.82E+08
389.712	275804	0.60	3.82E+08
389.737	276080	0.60	3.82E+08
389.762	276360	0.60	3.82E+08
389.787	276644	0.60	3.82E+08
389.812	276932	0.60	3.82E+08
389.837	277224	0.60	3.82E+08
389.862	277520	0.60	3.82E+08
389.887	277820	0.60	3.82E+08
389.912	278124	0.60	3.82E+08
389.937	278432	0.60	3.82E+08
389.962	278744	0.60	3.82E+08
389.987	279060	0.60	3.82E+08
390.012	279380	0.60	3.82E+08
390.037	279704	0.60	3.82E+08
390.062	280032	0.60	3.82E+08
390.087	280364	0.60	3.82E+08
390.112	280700	0.60	3.82E+08
390.137	281040	0.60	3.82E+08
390.162	281384	0.60	3.82E+08
390.187	281732	0.60	3.82E+08
390.212	282084	0.60	3.82E+08
390.237	282440	0.60	3.82E+08
390.262	282800	0.60	3.82E+08
390.287	283164	0.60	3.82E+08
390.312	283532	0.60	3.82E+08
390.337	283904	0.60	3.82E+08
390.362	284280	0.60	3.82E+08
390.387	284660	0.60	3.82E+08
390.412	285044	0.60	3.82E+08
390.437	285432	0.60	3.82E+08
390.462	285824	0.60	3.82E+08
390.487	286220	0.60	3.82E+08
390.512	286620	0.60	3.82E+08
390.537	287024	0.60	3.82E+08
390.562	287432	0.60	3.82E+08
390.587	287844	0.60	3.82E+08
390.612	288260	0.60	3.82E+08
390.637	288680	0.60	3.82E+08
390.662	289104	0.60	3.82E+08
390.687	289532	0.60	3.82E+08
390.712	289964	0.60	3.82E+08
390.737	290400	0.60	3.82E+08
390.762	290840	0.60	3.82E+08
390.787	291284	0.60	3.82E+08
390.812	291732	0.60	3.82E+08
390.837	292184	0.60	3.82E+08
390.862	292640	0.60	3.82E+08
390.887	293100	0.60	3.82E+08
390.912	293564	0.60	3.82E+08
390.937	294032	0.60	3.82E+08
390.962	294504	0.60	3.82E+08
390.987	294980	0.60	3.82E+08
391.012	295460	0.60	3.82E+08
391.037	295944	0.60	3.82E+08
391.062	296432	0.60	3.82E+08
391.087	296924	0.60	3.82E+08
391.112	297420	0.60	3.82E+08
391.137	297920	0.60	3.82E+08
391.162	298424	0.60	3.82E+08
391.187	298932	0.60	3.82E+08
391.212	299444	0.60	3.82E+08
391.237	299960	0.60	3.82E+08
391.262	300480	0.60	3.82E+08
391.287	301004	0.60	3.82E+08
391.312	301532	0.60	3.82E+08
391.337	302064	0.60	3.82E+08
391.362	302600	0.60	3.82E+08
391.387	303140	0.60	3.82E+08
391.412	303684	0.60	3.82E+08
391.437	304232	0.60	3.82E+08
391.462	304784	0.60	3.82E+08
391.487	305340	0.60	3.82E+08
391.512	305900	0.60	3.82E+08
391.537	306464	0.60	3.82E+08
391.562	307032	0.60	3.82E+08
391.587	307604	0.60	3.82E+08
391.612	308180	0.60	3.82E+08
391.637	308760	0.60	3.82E+08
391.662	309344	0.60	3.82E+08
391.687	309932	0.60	3.82E+08
391.712	310524	0.60	3.82E+08
391.737	311120	0.60	3.82E+08
391.762	311720	0.60	3.82E+08
391.787	312324	0.60	3.82E+08
391.812	312932	0.60	3.82E+08
391.837	313544	0.60	3.82E+08
391.862	314160	0.60	3.82E+08
391.887	314780	0.60	3.82E+08

APPENDIX B - Continued

TABULATIONS OF CURRENT AND INFERRED ELECTRON DENSITY FOR RAM C-I, PROFILE 3

Table with columns: ELAPSED TIME, ALTITUDE, CURRENT, ELECTRON DENSITY. Rows 389-557.

Table with columns: ELAPSED TIME, ALTITUDE, CURRENT, ELECTRON DENSITY. Rows 593-855.

Table with columns: ELAPSED TIME, ALTITUDE, CURRENT, ELECTRON DENSITY. Rows 916-1213.

Table with columns: ELAPSED TIME, ALTITUDE, CURRENT, ELECTRON DENSITY. Rows 1296-1557.

1 meter = 3.2808 feet

# APPENDIX B - Continued

## TABLATIONS OF CURRENT AND INFERRED ELECTRON DENSITY FOR RAM C-I, PROBE 4

ELAPSED TIME, SECONDS	ALTITUDE, FEET (a)	CURRENT, MICROAMPS	ELECTRON DENSITY, ELECTRONS PER CUBIC CENTIMETER	ELAPSED TIME, SECONDS	ALTITUDE, FEET (a)	CURRENT, MICROAMPS	ELECTRON DENSITY, ELECTRONS PER CUBIC CENTIMETER	ELAPSED TIME, SECONDS	ALTITUDE, FEET (a)	CURRENT, MICROAMPS	ELECTRON DENSITY, ELECTRONS PER CUBIC CENTIMETER	ELAPSED TIME, SECONDS	ALTITUDE, FEET (a)	CURRENT, MICROAMPS	ELECTRON DENSITY, ELECTRONS PER CUBIC CENTIMETER
389.446	281855	843	4.54E+08	353.172	258886	21.935	1.43E+10	350.718	235694	1.002	5.61E+08	402.338	199140	42.000	2.78E+10
389.472	281847	803	4.23E+08	353.218	259654	16.452	1.00E+10	356.744	235928	1.100	6.15E+08	402.406	199511	540.000	4.40E+11
389.498	281510	780	4.22E+08	353.263	258120	8.812	4.36E+09	358.780	235924	1.817	8.54E+08	402.431	199345	655.000	6.10E+11
389.746	282228	803	4.33E+08	353.269	258291	14.171	6.88E+09	356.816	235100	1.312	7.33E+08	402.457	199179	710.000	6.30E+11
389.769	282091	763	4.10E+08	353.314	259003	11.368	6.70E+09	378.240	234993	1.613	8.62E+08	402.502	197887	710.000	6.25E+11
389.794	282928	823	4.31E+08	353.340	257836	10.374	6.42E+09	378.240	234993	1.613	8.62E+08	402.528	197719	880.000	6.40E+11
389.836	286843	863	4.66E+08	353.366	257670	12.737	7.69E+09	366.911	234478	34.127	2.42E+10	402.554	197551	520.000	4.48E+11
389.864	286434	884	4.84E+08	353.411	257557	22.333	1.43E+10	358.937	234311	23.688	1.46E+10	402.599	197256	345.000	2.85E+11
389.890	282313	903	4.86E+08	353.436	257131	27.370	1.88E+10	356.982	234018	34.424	2.49E+10	402.624	197028	31.900	1.40E+10
389.935	280033	893	4.81E+08	353.462	257004	30.105	2.10E+10	357.007	233852	62.832	4.97E+10	402.650	196920	25.900	1.26E+10
389.960	279587	843	4.54E+08	353.507	256755	30.775	2.13E+10	357.007	233852	62.832	4.97E+10	402.676	196824	41.300	6.32E+09
389.986	279691	907	4.87E+08	353.533	256587	30.937	2.17E+10	357.106	233223	87.887	7.38E+10	402.721	196552	5.300	3.14E+09
390.031	279400	903	4.87E+08	353.559	256418	29.238	2.03E+10	357.130	233054	85.784	7.57E+10	402.747	196420	13.000	7.47E+08
390.056	279233	843	4.55E+08	353.604	256122	24.758	1.68E+10	357.175	232758	7.01	4.28E+08	402.793	195955	11.000	1.49E+10
390.082	279086	903	4.88E+08	353.630	255935	22.333	1.60E+10	357.226	232421	1.203	6.74E+08	402.818	195787	21.000	1.31E+10
390.108	278940	913	4.95E+08	353.656	255783	13.402	5.7E+09	357.271	232114	1.053	6.42E+08	402.844	195619	694.000	4.78E+10
390.133	278800	923	5.01E+08	353.701	255487	16.359	1.05E+10	357.296	231945	1.053	6.42E+08	402.889	195324	345.000	2.84E+11
390.179	278428	943	5.12E+08	353.726	255318	16.928	1.04E+10	357.305	231602	14.253	6.92E+08	402.915	195155	430.000	3.62E+11
390.225	278130	913	5.08E+08	353.752	255124	21.073	1.40E+10	357.321	231784	1.083	6.07E+08	402.941	194986	800.000	4.81E+11
390.250	277963	933	5.36E+08	353.797	254829	27.952	1.93E+10	357.390	231323	29.600	2.05E+10	402.989	194691	21.000	1.31E+10
390.275	277783	993	5.62E+08	353.823	254663	29.388	2.00E+10	357.416	231156	31.000	2.16E+10	403.038	194333	1000.000	9.02E+11
390.320	277498	923	5.10E+08	353.848	254493	30.774	2.16E+10	357.461	230858	31.000	2.16E+10	403.108	193998	870.000	7.28E+11
390.346	277318	993	5.49E+08	353.873	254326	30.937	2.17E+10	357.487	230687	39.000	2.48E+10	403.134	193713	4.900	2.84E+09
390.372	277147	1.003	5.55E+08	353.918	254029	30.937	2.17E+10	357.558	230219	67.000	6.78E+10	403.170	193433	14.200	8.46E+08
390.417	276849	1.023	5.67E+08	353.945	253860	30.409	2.14E+10	357.583	230050	71.000	8.10E+10	403.231	193111	2.650	1.57E+09
390.442	276680	1.023	5.67E+08	353.969	253698	30.435	2.14E+10	357.613	229818	41.000	8.34E+09	403.292	192797	21.000	1.31E+10
390.468	276511	1.063	5.90E+08	354.015	253400	31.099	2.18E+10	357.654	229584	87.000	7.43E+10	403.351	192483	51.000	3.80E+10
390.513	276217	1.043	5.79E+08	354.041	253234	31.259	2.20E+10	357.682	229413	89.000	7.42E+10	403.377	192215	51.000	3.80E+10
390.538	276046	1.043	5.79E+08	354.068	253068	31.259	2.20E+10	357.717	229250	83.669	6.88E+10	403.402	191947	21.000	1.31E+10
390.563	275886	1.073	5.93E+08	354.113	252778	31.773	2.27E+10	357.753	229085	81.942	6.71E+10	403.457	191651	51.000	3.80E+10
390.588	275715	1.053	5.82E+08	354.137	252613	31.375	2.23E+10	357.787	228922	77.000	6.24E+10	403.527	191333	51.000	3.80E+10
390.607	275544	1.053	5.82E+08	354.181	252327	31.962	2.31E+10	357.803	228750	77.000	6.24E+10	403.577	191040	51.000	3.80E+10
390.633	275424	1.043	5.78E+08	354.206	252168	25.492	1.76E+10	357.803	228592	84.000	5.02E+10	403.602	190870	51.000	3.80E+10
390.659	275253	1.083	6.00E+08	354.250	251878	25.790	1.79E+10	357.824	228428	90.210	5.24E+10	403.638	190700	51.000	3.80E+10
390.704	274960	1.063	5.89E+08	354.275	251714	25.400	1.77E+10	357.844	228264	94.718	5.38E+10	403.684	190530	51.000	3.80E+10
390.729	274790	1.063	5.89E+08	354.300	251549	27.500	1.90E+10	357.864	228100	95.210	5.42E+10	403.730	190360	51.000	3.80E+10
390.754	274620	1.063	5.89E+08	354.371	251136	31.000	2.18E+10	357.900	227950	36.553	2.00E+10	403.786	190190	51.000	3.80E+10
390.779	274450	1.033	5.74E+08	354.400	250971	31.100	2.19E+10	357.944	227800	84.553	6.88E+10	403.842	189920	51.000	3.80E+10
390.805	274285	1.187	1.54E+09	354.422	250806	30.400	2.18E+10	357.977	227648	84.553	6.88E+10	403.898	189750	51.000	3.80E+10
390.831	274120	1.187	1.54E+09	354.467	250518	42.000	3.11E+10	358.029	227500	113.486	9.16E+10	403.913	189580	51.000	3.80E+10
390.856	273955	1.187	1.54E+09	354.492	250353	42.000	3.11E+10	358.059	227352	117.600	1.02E+11	403.939	189410	51.000	3.80E+10
390.882	273790	1.133	1.42E+09	354.518	250188	34.300	2.44E+10	358.090	227204	67.500	4.48E+10	403.988	189240	51.000	3.80E+10
390.907	273625	1.133	1.42E+09	354.543	250023	31.000	2.18E+10	358.135	227056	72.250	4.81E+10	404.037	189070	51.000	3.80E+10
390.932	273460	1.133	1.42E+09	354.568	249858	32.430	2.30E+10	358.181	226908	80.445	5.41E+10	404.086	188900	51.000	3.80E+10
390.957	273295	1.133	1.42E+09	354.593	249693	31.000	2.18E+10	358.226	226760	7.250	4.00E+08	404.135	188730	51.000	3.80E+10
390.982	273130	1.133	1.42E+09	354.618	249528	26.500	1.98E+10	358.271	226612	75.750	6.05E+10	404.184	188560	51.000	3.80E+10
391.007	272965	1.133	1.42E+09	354.643	249363	26.500	1.98E+10	358.316	226464	72.250	4.00E+08	404.233	188390	51.000	3.80E+10
391.032	272800	1.133	1.42E+09	354.668	249198	26.500	1.98E+10	358.361	226316	8.045	4.46E+08	404.282	188220	51.000	3.80E+10
391.057	272635	1.133	1.42E+09	354.693	249033	26.500	1.98E+10	358.406	226168	2.492	1.06E+08	404.331	188050	51.000	3.80E+10
391.082	272470	1.133	1.42E+09	354.718	248868	26.500	1.98E+10	358.451	226020	4.378	1.21E+08	404.380	187880	51.000	3.80E+10
391.107	272305	1.133	1.42E+09	354.743	248703	26.500	1.98E+10	358.496	225872	57.284	6.37E+10	404.429	187710	51.000	3.80E+10
391.132	272140	1.133	1.42E+09	354.768	248538	26.500	1.98E+10	358.541	225724	67.500	4.48E+10	404.478	187540	51.000	3.80E+10
391.157	271975	1.133	1.42E+09	354.793	248373	26.500	1.98E+10	358.586	225576	79.600	6.42E+10	404.527	187370	51.000	3.80E+10
391.182	271810	1.133	1.42E+09	354.818	248208	26.500	1.98E+10	358.631	225428	72.250	4.00E+08	404.576	187200	51.000	3.80E+10
391.207	271645	1.133	1.42E+09	354.843	248043	26.500	1.98E+10	358.676	225280	81.581	6.57E+10	404.625	187030	51.000	3.80E+10
391.232	271480	1.133	1.42E+09	354.868	247878	26.500	1.98E+10	358.721	225132	70.254	5.25E+10	404.674	186860	51.000	3.80E+10
391.257	271315	1.133	1.42E+09	354.893	247713	26.500	1.98E+10	358.766	224984	31.000	2.16E+10	404.723	186690	51.000	3.80E+10
391.282	271150	1.133	1.42E+09	354.918	247548	26.500	1.98E+10	358.811	224836	1.940	1.94E+08	404.772	186520	51.000	3.80E+10
391.307	270985	1.133	1.42E+09	354.943	247383	26.500	1.98E+10	358.856	224688	2.940	2.16E+08	404.821	186350	51.000	3.80E+10
391.332	270820	1.133	1.42E+09	354.968	247218	26.500	1.98E+10	358.901	224540	4.900	2.38E+08	404.870	186180	51.000	3.80E+10
391.357	270655	1.133	1.42E+09	354.993	247053	26.500	1.98E+10	358.946	224392	6.860	2.60E+08	404.919	186010	51.000	3.80E+10
391.382	270490	1.133	1.42E+09	355.018	246888	26.500	1.98E+10	358.991	224244	101.300	8.51E+11	404.968	185840	51.000	3.80E+10
391.407	270325	1.133	1.42E+09	355.043	246723	26.500	1.98E+10	359.036	224096	116.614	9.82E+11				



TABULATIONS OF CURRENT AND INFERRED ELECTRON DENSITY FOR RAM C-I, PROBE 5

Table with columns: ELAPSED TIME, SECONDS; ALTITUDE, FEET; CURRENT, MICROAMPS; ELECTRON DENSITY, ELECTRONS PER CUBIC CENTIMETER. Contains data for the first set of measurements.

Table with columns: ELAPSED TIME, SECONDS; ALTITUDE, FEET; CURRENT, MICROAMPS; ELECTRON DENSITY, ELECTRONS PER CUBIC CENTIMETER. Contains data for the second set of measurements.

Table with columns: ELAPSED TIME, SECONDS; ALTITUDE, FEET; CURRENT, MICROAMPS; ELECTRON DENSITY, ELECTRONS PER CUBIC CENTIMETER. Contains data for the third set of measurements.

Table with columns: ELAPSED TIME, SECONDS; ALTITUDE, FEET; CURRENT, MICROAMPS; ELECTRON DENSITY, ELECTRONS PER CUBIC CENTIMETER. Contains data for the fourth set of measurements.

\*1 meter = 0.3048 feet

APPENDIX B - Continued

TABULATIONS OF CURRENT AND INFERRED ELECTRON DENSITY FOR  
 RAM C-I, PROBE 6

ELAPSED TIME, SECONDS	ALTITUDE, FEET (a)	CURRENT, MICROAMPS	ELECTRON DENSITY, ELECTRONS PER CUBIC CENTIMETER
189.653	281813	782	4.03E+08
189.679	281645	767	3.62E+08
189.705	281477	752	3.20E+08
189.750	281188	763	3.93E+08
189.775	281056	813	4.18E+08
189.801	280885	800	4.13E+08
189.845	280601	863	4.44E+08
189.871	280574	902	4.55E+08
189.896	280271	903	4.65E+08
189.941	279882	863	4.44E+08
189.967	279811	860	4.41E+08
189.992	279645	810	4.18E+08
190.037	279359	802	4.13E+08
190.063	279191	843	4.34E+08
190.088	279024	863	4.44E+08
190.134	278728	930	4.80E+08
190.160	278557	893	4.50E+08
190.186	278385	915	4.70E+08
190.231	278089	980	4.95E+08
190.256	277908	963	4.95E+08
190.282	277741	1000	5.16E+08
190.328	277446	980	4.95E+08
190.352	277275	980	4.95E+08
190.378	277106	1002	5.16E+08
190.423	276807	1013	5.21E+08
190.449	276638	1023	5.26E+08
190.474	276469	1040	5.36E+08
190.519	276174	1072	5.52E+08
190.544	276005	1073	5.52E+08
190.569	275835	1093	5.62E+08
190.613	275542	1050	5.42E+08
190.639	275371	1023	5.26E+08
190.665	275202	1033	5.31E+08
190.710	274911	1043	5.36E+08
190.736	274741	1185	5.98E+08
190.762	274575	1223	6.24E+08
190.787	274405	1123	5.52E+08
190.812	274236	1122	5.52E+08
190.857	273943	1143	5.73E+08
190.883	273774	1185	6.04E+08
190.927	273474	1205	7.15E+08
190.953	273305	1245	7.46E+08
190.998	273016	1351	6.97E+08
191.024	272846	1336	6.87E+08
191.050	272677	1387	7.15E+08
191.095	272383	1405	7.15E+08
191.121	272214	1387	7.15E+08
191.166	271919	1584	8.01E+08
191.191	271749	2238	1.15E+09
191.217	271579	2440	1.25E+09
191.242	271409	2238	1.15E+09
191.268	271239	2237	1.15E+09
191.313	270944	2356	1.25E+09
191.339	270774	2381	1.25E+09
191.364	270605	2465	1.35E+09
191.410	270310	2421	1.25E+09
191.436	270140	2421	1.25E+09
191.462	269970	2416	1.25E+09
191.507	269675	2483	1.25E+09
191.532	269505	2482	1.25E+09
191.577	269210	2478	1.25E+09
191.603	269040	2554	1.35E+09
191.628	268870	2611	1.45E+09
191.673	268575	2694	1.55E+09
191.718	268280	2760	1.55E+09
191.744	268110	2904	1.65E+09
191.770	267940	2910	1.65E+09
191.795	267770	2982	1.75E+09
191.821	267600	2980	1.75E+09
191.866	267305	3111	2.06E+09
191.892	267135	3102	2.06E+09
191.918	266965	3108	2.06E+09
191.963	266670	3108	2.06E+09
191.989	266500	3190	2.16E+09
192.034	266205	3108	2.06E+09
192.060	266035	3108	2.06E+09
192.105	265740	3108	2.06E+09
192.131	265570	3151	2.16E+09
192.157	265400	3151	2.16E+09
192.202	265105	3151	2.16E+09
192.228	264935	3108	2.06E+09
192.273	264640	3108	2.06E+09
192.299	264470	3108	2.06E+09
192.344	264175	3108	2.06E+09
192.370	264005	3147	2.16E+09
192.405	263710	3108	2.06E+09
192.431	263540	3108	2.06E+09
192.476	263245	3108	2.06E+09
192.502	263075	3108	2.06E+09
192.528	262905	3108	2.06E+09
192.573	262610	3108	2.06E+09
192.600	262440	3108	2.06E+09
192.645	262145	3108	2.06E+09
192.671	261975	3108	2.06E+09
192.717	261680	3108	2.06E+09
192.743	261510	3108	2.06E+09
192.788	261215	3108	2.06E+09
192.814	261045	3108	2.06E+09
192.860	260750	3108	2.06E+09
192.886	260580	3108	2.06E+09
192.931	260285	3108	2.06E+09
192.957	260115	3108	2.06E+09
193.003	259820	3108	2.06E+09
193.029	259650	3108	2.06E+09
193.055	259480	3108	2.06E+09
193.081	259310	3108	2.06E+09
193.127	259015	2983	1.96E+09

1 meter = 3.28084 feet

ELAPSED TIME, SECONDS	ALTITUDE, FEET (a)	CURRENT, MICROAMPS	ELECTRON DENSITY, ELECTRONS PER CUBIC CENTIMETER
193.153	259012	26.465	1.62E+10
193.179	258844	23.338	1.41E+10
193.224	258553	16.940	1.01E+10
193.250	258389	17.030	1.03E+10
193.275	258230	14.917	8.58E+09
193.320	257924	13.572	7.74E+09
193.346	257765	12.757	7.23E+09
193.372	257608	12.740	7.23E+09
193.417	257313	29.934	1.85E+10
193.443	257171	31.773	1.98E+10
193.468	257025	33.756	2.12E+10
193.513	256713	33.619	2.11E+10
193.539	256544	34.026	2.14E+10
193.585	256236	33.194	2.08E+10
193.610	256068	30.774	1.91E+10
193.636	255911	28.140	1.76E+10
193.681	255614	25.902	1.57E+10
193.707	255445	20.620	1.23E+10
193.733	255276	22.333	1.36E+10
193.758	255082	28.876	1.78E+10
193.783	254917	32.473	2.01E+10
193.829	254614	33.480	2.10E+10
193.854	254451	33.619	2.11E+10
193.880	254286	31.158	2.05E+10
193.925	253987	34.929	2.20E+10
193.951	253824	34.421	2.16E+10
193.996	253525	34.678	2.18E+10
194.022	253358	33.993	2.14E+10
194.047	253192	31.963	2.04E+10
194.092	252892	34.788	2.19E+10
194.118	252727	34.453	2.17E+10
194.143	252562	34.718	2.18E+10
194.188	252262	31.619	2.11E+10
194.214	252097	31.467	2.10E+10
194.217	251930	29.412	1.92E+10
194.281	251713	30.500	2.02E+10
194.307	251548	29.500	1.95E+10
194.332	251384	31.600	2.18E+10
194.377	251084	41.500	2.69E+10
194.403	250919	41.718	2.71E+10
194.428	250754	53.000	3.49E+10
194.473	250454	76.000	4.81E+10
194.499	250288	53.000	3.49E+10
194.524	250121	49.500	3.25E+10
194.549	249956	44.948	2.97E+10
194.594	249657	37.200	2.30E+10
194.620	249492	34.000	2.13E+10
194.645	249327	31.600	1.95E+10
194.671	249162	30.750	1.88E+10
194.720	248862	26.200	1.50E+10
194.746	248697	21.092	1.10E+10
194.792	248397	36.308	2.33E+10
194.818	248232	45.900	2.99E+10
194.863	247932	62.478	4.28E+10
194.889	247767	66.337	4.58E+10
194.934	247467	56.241	3.76E+10
194.960	247302	51.546	3.47E+10
195.005	246992	44.708	2.97E+10
195.031	246827	46.313	3.03E+10
195.056	246662	44.101	2.87E+10
195.082	246497	45.841	2.95E+10
195.108	246332	48.003	3.10E+10
195.153	246032	45.800	2.90E+10
195.179	245867	49.845	3.18E+10
195.205	245702	49.848	3.18E+10
195.250	245402	32.733	2.03E+10
195.276	245237	29.588	1.83E+10
195.301	245072	22.333	1.35E+10
195.346	244774	22.621	1.36E+10
195.372	244609	69.337	4.09E+10
195.398	244444	72.026	4.30E+10
195.443	244144	74.290	4.52E+10
195.469	243979	66.324	4.24E+10
195.494	243814	65.593	4.18E+10
195.540	243514	51.918	3.48E+10
195.566	243349	47.167	3.10E+10
195.611	243049	40.821	2.65E+10
195.637	242884	46.028	2.98E+10
195.682	242584	55.225	3.71E+10
195.708	242419	58.983	4.05E+10
195.753	242119	58.365	4.00E+10
195.779	241954	44.909	2.99E+10
195.824	241654	75.128	5.12E+10
195.850	241489	79.605	5.58E+10
195.881	241324	66.005	4.63E+10
195.926	241024	64.005	4.45E+10
195.952	240859	63.542	4.39E+10
195.978	240694	58.317	3.90E+10
196.023	240394	60.372	4.10E+10
196.049	240229	62.632	4.29E+10
196.075	240064	61.187	4.03E+10
196.120	239764	72.626	5.00E+10
196.146	239599	72.544	4.99E+10
196.191	239299	71.822	4.91E+10
196.217	239134	69.400	4.73E+10
196.243	238969	67.800	4.62E+10
196.288	238669	67.400	4.60E+10
196.314	238504	67.400	4.60E+10
196.360	238204	67.400	4.60E+10
196.386	238039	67.400	4.60E+10
196.431	237739	67.400	4.60E+10
196.457	237574	67.400	4.60E+10
196.502	237274	67.400	4.60E+10
196.528	237109	67.400	4.60E+10
196.573	236809	67.400	4.60E+10
196.600	236644	67.400	4.60E+10
196.645	236344	67.400	4.60E+10
196.671	236179	67.400	4.60E+10
196.716	235879	67.400	4.60E+10
196.742	235714	67.400	4.60E+10
196.787	235414	67.400	4.60E+10
196.813	235249	67.400	4.60E+10
196.858	234949	67.400	4.60E+10
196.884	234784	67.400	4.60E+10
196.929	234484	67.400	4.60E+10
196.955	234319	67.400	4.60E+10
197.000	234019	67.400	4.60E+10
197.026	233854	67.400	4.60E+10
197.071	233554	67.400	4.60E+10
197.097	233389	67.400	4.60E+10
197.142	233089	67.400	4.60E+10
197.168	232924	67.400	4.60E+10
197.213	232624	67.400	4.60E+10
197.239	232459	67.400	4.60E+10
197.284	232159	67.400	4.60E+10
197.310	231994	67.400	4.60E+10
197.355	231694	67.400	4.60E+10
197.381	231529	67.400	4.60E+10
197.426			

APPENDIX B - Continued

TABULATIONS OF CURRENT AND INFERRED ELECTRON DENSITY FOR  
RAM C-I, PROBE 7

ELAPSED TIME, SECONDS	ALTITUDE, FEET	CURRENT, MICROAMPS	ELECTRON DENSITY, ELECTRONS PER CUBIC CENTIMETER
399.656	281792	4.643	3.25E+07
399.662	281824	4.643	3.25E+07
399.768	281856	4.643	3.25E+07
399.753	281192	4.710	2.39E+07
399.778	281030	4.707	3.55E+08
399.824	282307	4.733	3.70E+07
399.848	280881	4.863	4.30E+07
399.874	280847	4.902	4.20E+07
399.900	280251	4.903	4.50E+07
399.924	279791	4.930	4.51E+07
399.970	279785	4.936	4.36E+07
399.996	279629	4.983	4.20E+07
399.990	279537	4.950	4.21E+07
399.996	279172	4.870	4.41E+07
399.992	279003	4.903	4.31E+07
399.137	278701	4.914	4.41E+07
399.163	278535	4.914	4.81E+07
399.188	278363	4.920	4.96E+07
399.234	278007	4.928	5.30E+07
399.259	277887	4.943	5.20E+07
399.285	277722	4.972	5.41E+07
399.330	277424	4.930	5.11E+07
399.335	277254	4.982	5.00E+07
399.381	277053	4.983	4.90E+07
399.426	276784	4.973	4.46E+07
399.452	276617	4.983	4.06E+07
399.478	276451	4.983	4.06E+07
399.522	276155	4.983	4.06E+07
399.547	275998	4.983	4.06E+07
399.572	275824	4.983	4.06E+07
399.617	275534	4.983	4.06E+07
399.642	275370	4.983	4.06E+07
399.668	275189	4.983	4.06E+07
399.714	274900	4.983	4.06E+07
399.739	274718	4.983	4.06E+07
399.765	274530	4.983	4.06E+07
399.780	274343	4.983	4.06E+07
399.815	274079	4.983	4.06E+07
399.860	273913	4.983	4.06E+07
399.905	273722	4.983	4.06E+07
399.950	273525	4.983	4.06E+07
399.958	273384	4.983	4.06E+07
399.972	273241	4.983	4.06E+07
399.993	273098	4.983	4.06E+07
399.058	272922	4.983	4.06E+07
399.124	272747	4.983	4.06E+07
399.150	272572	4.983	4.06E+07
399.154	272444	4.983	4.06E+07
399.220	272180	4.983	4.06E+07
399.244	272011	4.983	4.06E+07
399.291	271742	4.983	4.06E+07
399.311	271578	4.983	4.06E+07
399.316	271422	4.983	4.06E+07
399.388	271158	4.983	4.06E+07
399.413	270993	4.983	4.06E+07
399.439	270829	4.983	4.06E+07
399.484	270665	4.983	4.06E+07
399.510	270501	4.983	4.06E+07
399.536	270337	4.983	4.06E+07
399.562	270173	4.983	4.06E+07
399.588	270009	4.983	4.06E+07
399.614	269845	4.983	4.06E+07
399.640	269681	4.983	4.06E+07
399.666	269517	4.983	4.06E+07
399.692	269353	4.983	4.06E+07
399.718	269189	4.983	4.06E+07
399.744	269025	4.983	4.06E+07
399.770	268861	4.983	4.06E+07
399.796	268697	4.983	4.06E+07
399.822	268533	4.983	4.06E+07
399.848	268369	4.983	4.06E+07
399.874	268205	4.983	4.06E+07
399.900	268041	4.983	4.06E+07
399.926	267877	4.983	4.06E+07
399.952	267713	4.983	4.06E+07
399.978	267549	4.983	4.06E+07
399.004	267385	4.983	4.06E+07
399.030	267221	4.983	4.06E+07
399.056	267057	4.983	4.06E+07
399.082	266893	4.983	4.06E+07
399.108	266729	4.983	4.06E+07
399.134	266565	4.983	4.06E+07
399.160	266401	4.983	4.06E+07
399.186	266237	4.983	4.06E+07
399.212	266073	4.983	4.06E+07
399.238	265909	4.983	4.06E+07
399.264	265745	4.983	4.06E+07
399.290	265581	4.983	4.06E+07
399.316	265417	4.983	4.06E+07
399.342	265253	4.983	4.06E+07
399.368	265089	4.983	4.06E+07
399.394	264925	4.983	4.06E+07
399.420	264761	4.983	4.06E+07
399.446	264597	4.983	4.06E+07
399.472	264433	4.983	4.06E+07
399.498	264269	4.983	4.06E+07
399.524	264105	4.983	4.06E+07
399.550	263941	4.983	4.06E+07
399.576	263777	4.983	4.06E+07
399.602	263613	4.983	4.06E+07
399.628	263449	4.983	4.06E+07
399.654	263285	4.983	4.06E+07
399.680	263121	4.983	4.06E+07
399.706	262957	4.983	4.06E+07
399.732	262793	4.983	4.06E+07
399.758	262629	4.983	4.06E+07
399.784	262465	4.983	4.06E+07
399.810	262301	4.983	4.06E+07
399.836	262137	4.983	4.06E+07
399.862	261973	4.983	4.06E+07
399.888	261809	4.983	4.06E+07
399.914	261645	4.983	4.06E+07
399.940	261481	4.983	4.06E+07
399.966	261317	4.983	4.06E+07
399.992	261153	4.983	4.06E+07
399.018	260989	4.983	4.06E+07
399.044	260825	4.983	4.06E+07
399.070	260661	4.983	4.06E+07
399.096	260497	4.983	4.06E+07
399.122	260333	4.983	4.06E+07
399.148	260169	4.983	4.06E+07
399.174	260005	4.983	4.06E+07
399.200	259841	4.983	4.06E+07
399.226	259677	4.983	4.06E+07
399.252	259513	4.983	4.06E+07
399.278	259349	4.983	4.06E+07
399.304	259185	4.983	4.06E+07
399.330	259021	4.983	4.06E+07
399.356	258857	4.983	4.06E+07
399.382	258693	4.983	4.06E+07
399.408	258529	4.983	4.06E+07
399.434	258365	4.983	4.06E+07
399.460	258201	4.983	4.06E+07
399.486	258037	4.983	4.06E+07
399.512	257873	4.983	4.06E+07
399.538	257709	4.983	4.06E+07
399.564	257545	4.983	4.06E+07
399.590	257381	4.983	4.06E+07
399.616	257217	4.983	4.06E+07
399.642	257053	4.983	4.06E+07
399.668	256889	4.983	4.06E+07
399.694	256725	4.983	4.06E+07
399.720	256561	4.983	4.06E+07
399.746	256397	4.983	4.06E+07
399.772	256233	4.983	4.06E+07
399.798	256069	4.983	4.06E+07
399.824	255905	4.983	4.06E+07
399.850	255741	4.983	4.06E+07
399.876	255577	4.983	4.06E+07
399.902	255413	4.983	4.06E+07
399.928	255249	4.983	4.06E+07
399.954	255085	4.983	4.06E+07
399.980	254921	4.983	4.06E+07
399.006	254757	4.983	4.06E+07
399.032	254593	4.983	4.06E+07
399.058	254429	4.983	4.06E+07
399.084	254265	4.983	4.06E+07
399.110	254101	4.983	4.06E+07
399.136	253937	4.983	4.06E+07
399.162	253773	4.983	4.06E+07
399.188	253609	4.983	4.06E+07
399.214	253445	4.983	4.06E+07
399.240	253281	4.983	4.06E+07
399.266	253117	4.983	4.06E+07
399.292	252953	4.983	4.06E+07
399.318	252789	4.983	4.06E+07
399.344	252625	4.983	4.06E+07
399.370	252461	4.983	4.06E+07
399.396	252297	4.983	4.06E+07
399.422	252133	4.983	4.06E+07
399.448	251969	4.983	4.06E+07
399.474	251805	4.983	4.06E+07
399.500	251641	4.983	4.06E+07
399.526	251477	4.983	4.06E+07
399.552	251313	4.983	4.06E+07
399.578	251149	4.983	4.06E+07
399.604	250985	4.983	4.06E+07
399.630	250821	4.983	4.06E+07
399.656	250657	4.983	4.06E+07
399.682	250493	4.983	4.06E+07
399.708	250329	4.983	4.06E+07
399.734	250165	4.983	4.06E+07
399.760	250001	4.983	4.06E+07
399.786	249837	4.983	4.06E+07
399.812	249673	4.983	4.06E+07
399.838	249509	4.983	4.06E+07
399.864	249345	4.983	4.06E+07
399.890	249181	4.983	4.06E+07
399.916	249017	4.983	4.06E+07
399.942	248853	4.983	4.06E+07
399.968	248689	4.983	4.06E+07
399.994	248525	4.983	4.06E+07
399.020	248361	4.983	4.06E+07
399.046	248197	4.983	4.06E+07
399.072	248033	4.983	4.06E+07
399.098	247869	4.983	4.06E+07
399.124	247705	4.983	4.06E+07
399.150	247541	4.983	4.06E+07
399.176	247377	4.983	4.06E+07
399.202	247213	4.983	4.06E+07
399.228	247049	4.983	4.06E+07
399.254	246885	4.983	4.06E+07
399.280	246721	4.983	4.06E+07
399.306	246557	4.983	4.06E+07
399.332	246393	4.983	4.06E+07
399.358	246229	4.983	4.06E+07
399.384	246065	4.983	4.06E+07
399.410	245901	4.983	4.06E+07
399.436	245737	4.983	4.06E+07
399.462	245573	4.983	4.06E+07
399.488	245409	4.983	4.06E+07
399.514	245245	4.983	4.06E+07
399.540	245081	4.983	4.06E+07
399.566	244917	4.983	4.06E+07
399.592	244753	4.983	4.06E+07
399.618	244589	4.983	4.06E+07
399.644	244425	4.983	4.06E+07
399.670	244261	4.983	4.06E+07
399.696	244097	4.983	4.06E+07
399.722	243933	4.983	4.06E+07
399.748	243769	4.983	4.06E+07
399.774	243605	4.983	4.06E+07
399.800	243441	4.983	4.06E+07
399.826	243277	4.983	4.06E+07
399.852	243113	4.983	4.06E+07
399.878	242949	4.983	4.06E+07
399.904	242785	4.983	4.06E+07
399.930	242621	4.983	4.06E+07
399.956	242457	4.983	4.06E+07
399.982	242293	4.983	4.06E+07
399.008	242129	4.983	4.06E+07
399.034	241965	4.983	4.06E+07
399.060	241801	4.983	4.06E+07
399.086	241637	4.983	4.06E+07
399.112	241473	4.983	4.06E+07
399.138	241309	4.983	4.06E+07
399.164	241145	4.983	4.06E+07
399.190	240981	4.983	4.06E+07
399.216			

APPENDIX B - Continued

TABULATIONS OF CURRENT AND INFERRED ELECTRON DENSITY FOR RAM C-I, PROBE 8

ELAPSED TIME, SECONDS	ALTITUDE, FEET	CURRENT, MICROAMPS	ELECTRON DENSITY, ELECTRONS PER CUBIC CENTIMETER
389.459	281771	+493	2.45E+08
389.756	281172	+470	2.35E+08
389.807	280640	+483	2.30E+08
389.852	280560	+512	2.42E+08
389.877	280359	+523	2.45E+08
389.903	280233	+493	2.40E+08
389.948	279940	+522	2.48E+08
389.973	279774	+489	2.38E+08
389.999	279600	+483	2.38E+08
390.044	279310	+500	2.46E+08
390.069	279145	+493	2.42E+08
390.095	278982	+492	2.42E+08
390.120	278815	+483	2.38E+08
390.146	278541	+522	2.48E+08
390.172	278342	+500	2.46E+08
390.197	278160	+522	2.48E+08
390.223	277986	+500	2.46E+08
390.248	277800	+523	2.45E+08
390.273	277625	+500	2.46E+08
390.299	277430	+523	2.45E+08
390.324	277233	+500	2.46E+08
390.349	277045	+523	2.45E+08
390.375	276855	+500	2.46E+08
390.400	276675	+523	2.45E+08
390.426	276480	+500	2.46E+08
390.451	276295	+523	2.45E+08
390.477	276105	+500	2.46E+08
390.502	275920	+523	2.45E+08
390.527	275735	+500	2.46E+08
390.553	275550	+523	2.45E+08
390.578	275365	+500	2.46E+08
390.604	275180	+523	2.45E+08
390.629	275000	+500	2.46E+08
390.654	274820	+523	2.45E+08
390.680	274645	+500	2.46E+08
390.705	274470	+523	2.45E+08
390.730	274300	+500	2.46E+08
390.756	274135	+523	2.45E+08
390.781	273970	+500	2.46E+08
390.806	273810	+523	2.45E+08
390.832	273655	+500	2.46E+08
390.857	273500	+523	2.45E+08
390.882	273350	+500	2.46E+08
390.908	273205	+523	2.45E+08
390.933	273060	+500	2.46E+08
390.958	272920	+523	2.45E+08
390.984	272785	+500	2.46E+08
391.009	272650	+523	2.45E+08
391.034	272520	+500	2.46E+08
391.059	272395	+523	2.45E+08
391.085	272270	+500	2.46E+08
391.110	272150	+523	2.45E+08
391.135	272035	+500	2.46E+08
391.160	271920	+523	2.45E+08
391.185	271810	+500	2.46E+08
391.210	271705	+523	2.45E+08
391.235	271605	+500	2.46E+08
391.260	271510	+523	2.45E+08
391.285	271420	+500	2.46E+08
391.310	271335	+523	2.45E+08
391.335	271255	+500	2.46E+08
391.360	271180	+523	2.45E+08
391.385	271110	+500	2.46E+08
391.410	271045	+523	2.45E+08
391.435	270985	+500	2.46E+08
391.460	270935	+523	2.45E+08
391.485	270890	+500	2.46E+08
391.510	270850	+523	2.45E+08
391.535	270815	+500	2.46E+08
391.560	270785	+523	2.45E+08
391.585	270755	+500	2.46E+08
391.610	270725	+523	2.45E+08
391.635	270695	+500	2.46E+08
391.660	270670	+523	2.45E+08
391.685	270645	+500	2.46E+08
391.710	270625	+523	2.45E+08
391.735	270605	+500	2.46E+08
391.760	270590	+523	2.45E+08
391.785	270575	+500	2.46E+08
391.810	270565	+523	2.45E+08
391.835	270555	+500	2.46E+08
391.860	270550	+523	2.45E+08
391.885	270545	+500	2.46E+08
391.910	270545	+523	2.45E+08
391.935	270545	+500	2.46E+08
391.960	270545	+523	2.45E+08
391.985	270545	+500	2.46E+08
392.010	270545	+523	2.45E+08
392.035	270545	+500	2.46E+08
392.060	270545	+523	2.45E+08
392.085	270545	+500	2.46E+08
392.110	270545	+523	2.45E+08
392.135	270545	+500	2.46E+08
392.160	270545	+523	2.45E+08
392.185	270545	+500	2.46E+08
392.210	270545	+523	2.45E+08
392.235	270545	+500	2.46E+08
392.260	270545	+523	2.45E+08
392.285	270545	+500	2.46E+08
392.310	270545	+523	2.45E+08
392.335	270545	+500	2.46E+08
392.360	270545	+523	2.45E+08
392.385	270545	+500	2.46E+08
392.410	270545	+523	2.45E+08
392.435	270545	+500	2.46E+08
392.460	270545	+523	2.45E+08
392.485	270545	+500	2.46E+08
392.510	270545	+523	2.45E+08
392.535	270545	+500	2.46E+08
392.560	270545	+523	2.45E+08
392.585	270545	+500	2.46E+08
392.610	270545	+523	2.45E+08
392.635	270545	+500	2.46E+08
392.660	270545	+523	2.45E+08
392.685	270545	+500	2.46E+08
392.710	270545	+523	2.45E+08
392.735	270545	+500	2.46E+08
392.760	270545	+523	2.45E+08
392.785	270545	+500	2.46E+08
392.810	270545	+523	2.45E+08
392.835	270545	+500	2.46E+08
392.860	270545	+523	2.45E+08
392.885	270545	+500	2.46E+08
392.910	270545	+523	2.45E+08
392.935	270545	+500	2.46E+08
392.960	270545	+523	2.45E+08
392.985	270545	+500	2.46E+08
393.010	270545	+523	2.45E+08
393.035	270545	+500	2.46E+08
393.060	270545	+523	2.45E+08
393.085	270545	+500	2.46E+08
393.110	270545	+523	2.45E+08
393.135	270545	+500	2.46E+08
393.160	270545	+523	2.45E+08
393.185	270545	+500	2.46E+08
393.210	270545	+523	2.45E+08
393.235	270545	+500	2.46E+08
393.260	270545	+523	2.45E+08
393.285	270545	+500	2.46E+08
393.310	270545	+523	2.45E+08
393.335	270545	+500	2.46E+08
393.360	270545	+523	2.45E+08
393.385	270545	+500	2.46E+08
393.410	270545	+523	2.45E+08
393.435	270545	+500	2.46E+08
393.460	270545	+523	2.45E+08
393.485	270545	+500	2.46E+08
393.510	270545	+523	2.45E+08
393.535	270545	+500	2.46E+08
393.560	270545	+523	2.45E+08
393.585	270545	+500	2.46E+08
393.610	270545	+523	2.45E+08
393.635	270545	+500	2.46E+08
393.660	270545	+523	2.45E+08
393.685	270545	+500	2.46E+08
393.710	270545	+523	2.45E+08
393.735	270545	+500	2.46E+08
393.760	270545	+523	2.45E+08
393.785	270545	+500	2.46E+08
393.810	270545	+523	2.45E+08
393.835	270545	+500	2.46E+08
393.860	270545	+523	2.45E+08
393.885	270545	+500	2.46E+08
393.910	270545	+523	2.45E+08
393.935	270545	+500	2.46E+08
393.960	270545	+523	2.45E+08
393.985	270545	+500	2.46E+08
394.010	270545	+523	2.45E+08
394.035	270545	+500	2.46E+08
394.060	270545	+523	2.45E+08
394.085	270545	+500	2.46E+08
394.110	270545	+523	2.45E+08
394.135	270545	+500	2.46E+08
394.160	270545	+523	2.45E+08
394.185	270545	+500	2.46E+08
394.210	270545	+523	2.45E+08
394.235	270545	+500	2.46E+08
394.260	270545	+523	2.45E+08
394.285	270545	+500	2.46E+08
394.310	270545	+523	2.45E+08
394.335	270545	+500	2.46E+08
394.360	270545	+523	2.45E+08
394.385	270545	+500	2.46E+08
394.410	270545	+523	2.45E+08
394.435	270545	+500	2.46E+08
394.460	270545	+523	2.45E+08
394.485	270545	+500	2.46E+08
394.510	270545	+523	2.45E+08
394.535	270545	+500	2.46E+08
394.560	270545	+523	2.45E+08
394.585	270545	+500	2.46E+08
394.610	270545	+523	2.45E+08
394.635	270545	+500	2.46E+08
394.660	270545	+523	2.45E+08
394.685	270545	+500	2.46E+08
394.710	270545	+523	2.45E+08
394.735	270545	+500	2.46E+08
394.760	270545	+523	2.45E+08
394.785	270545	+500	2.46E+08
394.810	270545	+523	2.45E+08
394.835	270545	+500	2.46E+08
394.860	270545	+523	2.45E+08
394.885	270545	+500	2.46E+08
394.910	270545	+523	2.45E+08
394.935	270545	+500	2.46E+08
394.960	270545	+523	2.45E+08
394.985	270545	+500	2.46E+08
395.010	270545	+523	2.45E+08
395.035	270545	+500	2.46E+08
395.060	270545	+523	2.45E+08
395.085	270545	+500	2.46E+08
395.110	270545	+523	2.45E+08
395.135	270545	+500	2.46E+08
395.160	270545	+523	2.45E+08
395.185	270545	+500	2.46E+08
395.210	270545	+523	2.45E+08
395.235	270545	+500	2.46E+08
395.260	270545	+523	2.45E+08
395.285	270545	+500	2.46E+08
395.310	270545	+523	2.45E+08
395.335	270545	+500	2.46E+08
395.360	270545	+523	2.45E+08
395.385	270545	+500	2.46E+08
395.410	270545	+523	2.45E+08
395.435	270545	+500	2.46E+08
395.460	270545	+523	2.45E+08
395.485	270545	+500	2.46E+08
395.510	270545	+523	2.45E+08
395.535	270545	+500	2.46E+08
395.560	270545	+523	2.45E+08
395.585	270545	+500	2.46E+08
395.610	270545	+523	2.45E+08
395.635	270545	+500	2.46E+08
395.660	270545	+523	2.45E+08
395.685	270545	+500	2.46E+08
395.710	270545	+523	2.45E+08
395.735	270545	+500	2.46E+08
395.760	270545	+523	2.45E+08
395.785	270545	+500	2.46E+08
395.810	270545	+523	2.45E+08
395.835	270545	+500	2.46E+08
395.860	270545	+523	2.45E+08
395.885	270545	+500	2.46E+08
395.910	270545	+523	2.45E+08
395.935	270545	+500	2.46E+08
395.960	270545	+523	2.45E+08
395.985	270545	+500	2.46E+08
396.010	270545	+523	2.45E+08

ELAPSED TIME, SECONDS	ALTITUDE, FEET	CURRENT, MICROAMPS	ELECTRON DENSITY, ELECTRONS PER CUBIC CENTIMETER
393.185	258802	33.943	2.01E+08
393.231	258512	30.275	1.77E+08
393.256	258373	26.062	1.59E+08
393.282	258250	21.360	1

TABLATIONS OF CURRENT AND INFERRED ELECTRON DENSITY FOR RAM C-II, PROBE 1

Table with columns: ELAPSED TIME, ALTITUDE, CURRENT, ELECTRON DENSITY. Contains 100 rows of data for probe 1.

Table with columns: ELAPSED TIME, ALTITUDE, CURRENT, ELECTRON DENSITY. Contains 100 rows of data for probe 1.

Table with columns: ELAPSED TIME, ALTITUDE, CURRENT, ELECTRON DENSITY. Contains 100 rows of data for probe 1.

Table with columns: ELAPSED TIME, ALTITUDE, CURRENT, ELECTRON DENSITY. Contains 100 rows of data for probe 1.

\* meter = 0.3048 feet

APPENDIX B - Continued

TABULATIONS OF CURRENT AND INFERRED ELECTRON DENSITY FOR  
 RAM C-II, PROBE 2

ELAPSED TIME, SECONDS	ALTITUDE, FEET	CURRENT, MICROAMPS	ELECTRON DENSITY, ELECTRONS PER CUBIC CENTIMETER
389.736	281278	1.03	5.85E+C7
389.763	281129	1.03	5.85E+C7
389.790	280980	1.03	5.85E+C7
389.818	280831	1.03	5.85E+C7
389.845	280682	1.03	5.85E+C7
389.872	280533	1.03	5.85E+C7
389.899	279384	1.03	5.85E+C7
389.926	279235	1.03	5.85E+C7
389.953	279086	1.03	5.85E+C7
389.980	278937	1.03	5.85E+C7
390.007	278788	1.03	5.85E+C7
390.034	278639	1.03	5.85E+C7
390.061	278490	1.03	5.85E+C7
390.088	278341	1.03	5.85E+C7
390.115	278192	1.03	5.85E+C7
390.142	278043	1.03	5.85E+C7
390.169	277894	1.03	5.85E+C7
390.196	277745	1.03	5.85E+C7
390.223	277596	1.03	5.85E+C7
390.250	277447	1.03	5.85E+C7
390.277	277298	1.03	5.85E+C7
390.304	277149	1.03	5.85E+C7
390.331	276999	1.03	5.85E+C7
390.358	276850	1.03	5.85E+C7
390.385	276701	1.03	5.85E+C7
390.412	276552	1.03	5.85E+C7
390.439	276403	1.03	5.85E+C7
390.466	276254	1.03	5.85E+C7
390.493	276105	1.03	5.85E+C7
390.520	275956	1.03	5.85E+C7
390.547	275807	1.03	5.85E+C7
390.574	275658	1.03	5.85E+C7
390.601	275509	1.03	5.85E+C7
390.628	275360	1.03	5.85E+C7
390.655	275211	1.03	5.85E+C7
390.682	275062	1.03	5.85E+C7
390.709	274913	1.03	5.85E+C7
390.736	274764	1.03	5.85E+C7
390.763	274615	1.03	5.85E+C7
390.790	274466	1.03	5.85E+C7
390.817	274317	1.03	5.85E+C7
390.844	274168	1.03	5.85E+C7
390.871	274019	1.03	5.85E+C7
390.898	273870	1.03	5.85E+C7
390.925	273721	1.03	5.85E+C7
390.952	273572	1.03	5.85E+C7
390.979	273423	1.03	5.85E+C7
391.006	273274	1.03	5.85E+C7
391.033	273125	1.03	5.85E+C7
391.060	272976	1.03	5.85E+C7
391.087	272827	1.03	5.85E+C7
391.114	272678	1.03	5.85E+C7
391.141	272529	1.03	5.85E+C7
391.168	272380	1.03	5.85E+C7
391.195	272231	1.03	5.85E+C7
391.222	272082	1.03	5.85E+C7
391.249	271933	1.03	5.85E+C7
391.276	271784	1.03	5.85E+C7
391.303	271635	1.03	5.85E+C7
391.330	271486	1.03	5.85E+C7
391.357	271337	1.03	5.85E+C7
391.384	271188	1.03	5.85E+C7
391.411	271039	1.03	5.85E+C7
391.438	270890	1.03	5.85E+C7
391.465	270741	1.03	5.85E+C7
391.492	270592	1.03	5.85E+C7
391.519	270443	1.03	5.85E+C7
391.546	270294	1.03	5.85E+C7
391.573	270145	1.03	5.85E+C7
391.600	269996	1.03	5.85E+C7
391.627	269847	1.03	5.85E+C7
391.654	269698	1.03	5.85E+C7
391.681	269549	1.03	5.85E+C7
391.708	269400	1.03	5.85E+C7
391.735	269251	1.03	5.85E+C7
391.762	269102	1.03	5.85E+C7
391.789	268953	1.03	5.85E+C7
391.816	268804	1.03	5.85E+C7
391.843	268655	1.03	5.85E+C7
391.870	268506	1.03	5.85E+C7
391.897	268357	1.03	5.85E+C7
391.924	268208	1.03	5.85E+C7
391.951	268059	1.03	5.85E+C7
391.978	267910	1.03	5.85E+C7
392.005	267761	1.03	5.85E+C7
392.032	267612	1.03	5.85E+C7
392.059	267463	1.03	5.85E+C7
392.086	267314	1.03	5.85E+C7
392.113	267165	1.03	5.85E+C7
392.140	267016	1.03	5.85E+C7
392.167	266867	1.03	5.85E+C7
392.194	266718	1.03	5.85E+C7
392.221	266569	1.03	5.85E+C7
392.248	266420	1.03	5.85E+C7
392.275	266271	1.03	5.85E+C7
392.302	266122	1.03	5.85E+C7
392.329	265973	1.03	5.85E+C7
392.356	265824	1.03	5.85E+C7
392.383	265675	1.03	5.85E+C7
392.410	265526	1.03	5.85E+C7
392.437	265377	1.03	5.85E+C7
392.464	265228	1.03	5.85E+C7
392.491	265079	1.03	5.85E+C7
392.518	264930	1.03	5.85E+C7
392.545	264781	1.03	5.85E+C7
392.572	264632	1.03	5.85E+C7
392.599	264483	1.03	5.85E+C7
392.626	264334	1.03	5.85E+C7
392.653	264185	1.03	5.85E+C7
392.680	264036	1.03	5.85E+C7
392.707	263887	1.03	5.85E+C7
392.734	263738	1.03	5.85E+C7
392.761	263589	1.03	5.85E+C7
392.788	263440	1.03	5.85E+C7
392.815	263291	1.03	5.85E+C7
392.842	263142	1.03	5.85E+C7
392.869	262993	1.03	5.85E+C7
392.896	262844	1.03	5.85E+C7
392.923	262695	1.03	5.85E+C7
392.950	262546	1.03	5.85E+C7
392.977	262397	1.03	5.85E+C7
393.004	262248	1.03	5.85E+C7
393.031	262099	1.03	5.85E+C7
393.058	261950	1.03	5.85E+C7
393.085	261801	1.03	5.85E+C7
393.112	261652	1.03	5.85E+C7
393.139	261503	1.03	5.85E+C7
393.166	261354	1.03	5.85E+C7
393.193	261205	1.03	5.85E+C7
393.220	261056	1.03	5.85E+C7
393.247	260907	1.03	5.85E+C7
393.274	260758	1.03	5.85E+C7
393.301	260609	1.03	5.85E+C7
393.328	260460	1.03	5.85E+C7
393.355	260311	1.03	5.85E+C7
393.382	260162	1.03	5.85E+C7
393.409	260013	1.03	5.85E+C7
393.436	259864	1.03	5.85E+C7
393.463	259715	1.03	5.85E+C7
393.490	259566	1.03	5.85E+C7
393.517	259417	1.03	5.85E+C7
393.544	259268	1.03	5.85E+C7
393.571	259119	1.03	5.85E+C7
393.598	258970	1.03	5.85E+C7
393.625	258821	1.03	5.85E+C7
393.652	258672	1.03	5.85E+C7
393.679	258523	1.03	5.85E+C7
393.706	258374	1.03	5.85E+C7
393.733	258225	1.03	5.85E+C7
393.760	258076	1.03	5.85E+C7
393.787	257927	1.03	5.85E+C7
393.814	257778	1.03	5.85E+C7
393.841	257629	1.03	5.85E+C7
393.868	257480	1.03	5.85E+C7
393.895	257331	1.03	5.85E+C7
393.922	257182	1.03	5.85E+C7
393.949	257033	1.03	5.85E+C7
393.976	256884	1.03	5.85E+C7
394.003	256735	1.03	5.85E+C7
394.030	256586	1.03	5.85E+C7
394.057	256437	1.03	5.85E+C7
394.084	256288	1.03	5.85E+C7
394.111	256139	1.03	5.85E+C7
394.138	255990	1.03	5.85E+C7
394.165	255841	1.03	5.85E+C7
394.192	255692	1.03	5.85E+C7
394.219	255543	1.03	5.85E+C7
394.246	255394	1.03	5.85E+C7
394.273	255245	1.03	5.85E+C7
394.300	255096	1.03	5.85E+C7
394.327	254947	1.03	5.85E+C7
394.354	254798	1.03	5.85E+C7
394.381	254649	1.03	5.85E+C7
394.408	254500	1.03	5.85E+C7
394.435	254351	1.03	5.85E+C7
394.462	254202	1.03	5.85E+C7
394.489	254053	1.03	5.85E+C7
394.516	253904	1.03	5.85E+C7
394.543	253755	1.03	5.85E+C7
394.570	253606	1.03	5.85E+C7
394.597	253457	1.03	5.85E+C7
394.624	253308	1.03	5.85E+C7
394.651	253159	1.03	5.85E+C7
394.678	253010	1.03	5.85E+C7
394.705	252861	1.03	5.85E+C7
394.732	252712	1.03	5.85E+C7
394.759	252563	1.03	5.85E+C7
394.786	252414	1.03	5.85E+C7
394.813	252265	1.03	5.85E+C7
394.840	252116	1.03	5.85E+C7
394.867	251967	1.03	5.85E+C7
394.894	251818	1.03	5.85E+C7
394.921	251669	1.03	5.85E+C7
394.948	251520	1.03	5.85E+C7
394.975	251371	1.03	5.85E+C7
395.002	251222	1.03	5.85E+C7

ELAPSED TIME, SECONDS	ALTITUDE, FEET	CURRENT, MICROAMPS	ELECTRON DENSITY, ELECTRONS PER CUBIC CENTIMETER
393.844	254520	7.905	5.36E+C8
393.871	254370	7.905	5.36E+C8
393.898	254221	7.905	5.36E+C8
393.925	254072	7.905	5.36E+C8
393.952	253923	7.905	5.36E+C8
393.979	253774	7.905	5.36E+C8
394.006	253625	8.551	5.86E+C8
394.033	253476	8.551	5.86E+C8
394.060	253327	8.551	5.86E+C8
394.087	253178	8.551	5.86E+C8
394.114	253029	8.551	5.86E+C8
394.141	252880	8.551	5.86E+C8
394.168	252731	9.197	6.36E+C8
394.195	252582	9.197	6.36E+C8
394.222	252433	9.197	6.36E+C8
394.249	252284	9.197	6.36E+C8
394.276	252135	9.197	6.36E+C8
394.303	251986	9.197	6.36E+C8
394.330	251837	9.197	6.36E+C8
394.357	251688	9.197	6.36E+C8
394.384	251539	9.197	6.36E+C8
394.411	251390	9.197	6.36E+C8
394.438	251241	9.197	6.36E+C8
394.465	251092	9.197	6.36E+C8
394.492	250943	9.197	6.36E+C8
394.519	250794	9.197	6.36E+C8
394.546	250645	9.197	6.36E+C8
394.573	250496	9.197	6.36E+C8
394.600	250347	9.197	6.36E+C8
394.627	250198	9.197	6.36E+C8
394.654	250049	9.197	6.36E+C8
394.681	249900	9.197	6.36E+C8
394.708	249751	9.197	6.36E+C8
394.735	249602	9.197	6.36E+C8
394.762	249453	9.197	6.36E+C8
394.789	249304	9.197	6.36E+C8
394.816	249155	9.197	6.36E+C8
394.843	249006	9.197	6.36E+C8
394.870	248857	9.197	6.36E+C8
394.897	248708	9.197	6.36E+C8
394.924	248559	9.197	6.36E+C8
394.951	248410	9.197	6.36E+C8
394.978	248261	9.197	6.36E+C8
395.005	248112	9.197	6.36E+C8
395.032	247963	9.197	6.36E+C8
395.059	247814	9.197	6.36E+C8
395.086	247665	9.197	6.36E+C8
395.113	247516	9.197	6.36E+C8
395.140	247367	9.197	6.36E+C8

APPENDIX B - Continued

TABLATIONS OF CURRENT AND INFERRED ELECTRON DENSITY FOR RAM C-II, PROBE 3

Table with columns: ELAPSED TIME, SECONDS; ALTITUDE, FEET; CURRENT, MICRAMPS; ELECTRON DENSITY, ELECTRONS PER CUBIC CENTIMETER. Rows include data points for altitudes from 281527 to 284811 and currents from 1.00 to 8.58.

Table with columns: ELAPSED TIME, SECONDS; ALTITUDE, FEET; CURRENT, MICRAMPS; ELECTRON DENSITY, ELECTRONS PER CUBIC CENTIMETER. Rows include data points for altitudes from 28487 to 288226 and currents from 8.98 to 10.86.

Table with columns: ELAPSED TIME, SECONDS; ALTITUDE, FEET; CURRENT, MICRAMPS; ELECTRON DENSITY, ELECTRONS PER CUBIC CENTIMETER. Rows include data points for altitudes from 28746 to 291476 and currents from 108.613 to 515.000.

Table with columns: ELAPSED TIME, SECONDS; ALTITUDE, FEET; CURRENT, MICRAMPS; ELECTRON DENSITY, ELECTRONS PER CUBIC CENTIMETER. Rows include data points for altitudes from 201293 to 291476 and currents from 950.000 to 1.300.

\* 1 meter = 3.2808 feet.

# APPENDIX B - Continued

## TABULATIONS OF CURRENT AND INFERRED ELECTRON DENSITY FOR

### RAM C-II, PROBE 4

ELAPSED TIME, SECONDS	ALTITUDE, FEET	CURRENT, MICROAMPS	ELECTRON DENSITY, ELECTRONS PER CUBIC CENTIMETER
389.743	2544.75	1.00	5.42E+C7
389.770	281084	1.00	5.40E+C7
389.787	280911	1.00	5.40E+C7
389.843	280860	1.42	5.26E+C7
389.872	280427	1.25	6.49E+C7
389.900	280250	1.00	5.41E+C7
389.948	279939	1.00	5.41E+C7
389.975	279761	1.10	5.42E+C7
390.003	279583	1.10	5.42E+C7
390.051	279271	1.20	6.42E+C7
390.078	279093	1.10	5.49E+C7
390.105	278915	1.20	6.53E+C7
390.153	278603	1.40	7.63E+C7
390.180	278425	1.35	6.17E+C7
390.207	278246	1.00	5.40E+C7
390.255	277919	1.20	6.21E+C7
390.282	277737	1.68	1.00E+C8
390.310	277556	1.28	6.25E+C7
390.338	277374	1.48	6.09E+C7
390.365	277192	1.59	6.22E+C7
390.412	276861	1.29	6.22E+C7
390.440	276680	1.32	6.45E+C7
390.487	276358	1.22	6.17E+C7
390.515	276176	1.24	6.23E+C7
390.563	275855	1.74	6.02E+C7
390.591	275673	1.34	6.01E+C7
390.640	275352	1.92	6.01E+C7
390.668	275170	1.51	6.00E+C7
390.720	274850	1.56	6.00E+C7
390.748	274668	1.56	6.00E+C7
390.793	274347	1.30	6.00E+C7
390.821	274165	1.63	6.00E+C7
390.869	273844	1.55	6.00E+C7
390.896	273662	1.42	6.00E+C7
390.923	273480	1.40	6.00E+C7
390.971	273159	1.53	6.00E+C7
390.998	272977	1.63	6.00E+C7
391.025	272795	1.63	6.00E+C7
391.073	272474	1.20	6.00E+C7
391.100	272292	1.35	6.00E+C7
391.128	272110	1.30	7.03E+C7
391.176	271789	1.20	6.49E+C7
391.203	271607	1.10	6.00E+C7
391.230	271425	1.03	6.00E+C7
391.278	271104	1.12	6.00E+C7
391.306	270922	1.10	6.00E+C7
391.335	270740	1.30	7.03E+C7
391.384	270419	1.20	6.00E+C7
391.411	270237	1.43	7.03E+C7
391.459	270056	1.45	6.00E+C7
391.487	269874	1.40	6.00E+C7
391.514	269692	1.68	6.15E+C7
391.562	269371	1.68	6.15E+C7
391.590	269189	1.76	6.15E+C7
391.617	269007	1.72	6.46E+C7
391.644	268825	1.30	6.00E+C7
391.652	268644	1.30	6.00E+C7
391.719	268323	2.04	6.00E+C7
391.747	268141	1.90	6.00E+C7
391.795	267820	2.12	6.00E+C7
391.822	267638	1.90	6.00E+C7
391.850	267456	2.09	6.00E+C7
391.898	267135	2.27	6.00E+C7
391.925	266953	2.12	6.00E+C7
391.953	266771	2.42	6.00E+C7
391.980	266589	2.12	6.00E+C7
392.028	266268	2.07	6.11E+C7
392.056	266086	2.71	6.00E+C7
392.084	265904	2.66	6.00E+C7
392.131	265583	4.54	6.21E+C7
392.159	265401	4.48	6.46E+C7
392.207	265080	4.30	6.00E+C7
392.234	264898	3.10	6.00E+C7
392.282	264577	3.47	6.00E+C7
392.310	264395	3.20	6.13E+C7
392.337	264213	4.57	6.21E+C7
392.364	264031	4.30	6.00E+C7
392.412	263710	6.17	6.00E+C7
392.439	263528	6.87	6.00E+C7
392.487	263207	6.12	6.00E+C7
392.514	263025	6.50	6.17E+C7
392.562	262704	6.00	6.15E+C7
392.570	262522	5.22	6.00E+C7
392.618	262201	5.37	6.01E+C7
392.645	262019	5.27	6.02E+C7
392.673	261837	5.30	6.27E+C7
392.721	261516	6.50	6.11E+C7
392.748	261334	6.95	6.02E+C7
392.776	261152	6.55	6.02E+C7
392.824	260831	6.55	6.02E+C7
392.851	260649	7.25	6.19E+C7
392.879	260467	7.21	6.19E+C7
392.927	260146	7.61	6.19E+C7
392.954	260004	8.51	6.03E+C7
392.982	259862	8.00	6.15E+C7
393.010	259680	10.79	6.22E+C7
393.057	259360	10.60	6.23E+C7
393.084	259178	10.48	6.18E+C7
393.132	258857	8.72	6.15E+C7
393.159	258675	7.58	6.32E+C7
393.187	258493	7.67	6.43E+C7
393.235	258172	7.25	6.20E+C7
393.262	257990	6.28	6.15E+C7
393.290	257808	8.94	6.33E+C7
393.318	257626	8.18	6.15E+C7
393.365	257305	14.75	6.21E+C7
393.392	257123	15.60	6.16E+C7
393.440	257165	9.91	6.15E+C7
393.467	257013	13.23	6.22E+C7
393.495	256831	11.87	6.28E+C7
393.543	256510	10.79	6.23E+C7
393.570	256328	10.75	6.18E+C7
393.597	256146	9.75	6.15E+C7
393.645	255825	10.38	6.25E+C7
393.673	255643	11.68	6.12E+C7
393.701	255461	12.00	6.11E+C7
393.749	255140	13.90	6.10E+C7
393.777	254958	15.82	6.09E+C7
393.803	254776	14.72	6.34E+C7

\*1 meter = 0.3048 feet









APPENDIX B -- Concluded

TABLATIONS OF CURRENT AND INFERRED ELECTRON DENSITY FOR RAM C-II, Phase 8

Table with columns: ELAPSED TIME, ALTITUDE, CURRENT, ELECTRON DENSITY. Contains data points for various altitudes and currents.

Table with columns: ELAPSED TIME, ALTITUDE, CURRENT, ELECTRON DENSITY. Contains data points for various altitudes and currents.

Table with columns: ELAPSED TIME, ALTITUDE, CURRENT, ELECTRON DENSITY. Contains data points for various altitudes and currents.

Table with columns: ELAPSED TIME, ALTITUDE, CURRENT, ELECTRON DENSITY. Contains data points for various altitudes and currents.

\*1 meter = 0.3048 feet

## APPENDIX C

### ANALYSIS OF SPACECRAFT MOTIONS AND WIND ANGLES

By William L. Weaver  
Langley Research Center

The spacecraft axis system employed and its relation to the wind axis are illustrated in figure 41.

The rate gyro data show coning of the RAM C-I and C-II spacecraft after separation of the expended fourth-stage motors, but the very low dynamic pressures and resulting low accelerations did not permit accurate determinations of the spacecraft wind angles from accelerometer data. Coning of the spacecraft was also indicated by the cyclic variations in the electrostatic probe-measured electron densities observed during both flights. Figure 42 shows the correlation of measured normal aerodynamic acceleration with variations in electron densities measured by probe 1 on RAM C-II during the last few seconds before probe-rake retraction. Figure 43 shows that the electrostatic probe rake was in the same plane as the measured normal acceleration, and thus the correlation of figure 42 suggests that the cyclic variations in measured electron densities were due to displacements of the probe rake from the wind axis in the angle-of-attack ( $\alpha$ ) plane. The variations were generally symmetrical; this symmetry further suggest that the average value of the electron densities corresponded to the zero-angle-of-attack case.

#### Determination of Wind Angles

Prior to separation of the fourth-stage motors, the RAM C-I and C-II spacecraft had roll momenta only with the X-axes fixed in direction. The separation impulses produced uniform coning (precession) of the X-axes about the total angular momentum vectors. The motion is illustrated in figure 44, and the equations which describe it are

$$L = I_l \omega_l \tag{C1}$$

$$\tan \theta = \frac{I_l \omega_l}{I_{X^p}} \tag{C2}$$

$$\nu_H = \frac{I_{X^p}}{I_l} \frac{1}{\cos \theta} \frac{1}{2\pi} \tag{C3}$$

$$\nu_b = \frac{I_X - I_l}{I_l} \frac{p}{2\pi} \tag{C4}$$

## APPENDIX C – Continued

Values computed by these equations for both flights are given in table V. The preflight-measured moments of inertia and the flight-measured rotation rates are given in table VI. It can be seen from figures 41 and 44 that for the case of  $\eta_0 = 0$  (X-axes initially aligned with velocity vectors), the total wind angles will describe the cones of half-angle  $\theta$ . Thus the absolute change in the total wind angle ( $|\Delta\eta|$ ) is given by  $2\theta$ .

To study the spacecraft motions further, a computer-programed set of equations for the angular motions of a rigid body was employed. At about 380 seconds, short-duration (0.01 second) angular impulses were applied; these impulses produced matchups of the gyro-measured lateral rotation rates. Total wind angle was set to zero ( $\eta_0 = 0$ ). Figure 45 shows the comparisons of the measured and program-computed spacecraft rotation rates. The required impulses were

$$L = 3.93 \text{ N-m-sec (2.9 lb-ft-sec)} \quad (\text{RAM C-I})$$

$$L = 3.25 \text{ N-m-sec (2.4 lb-ft-sec)} \quad (\text{RAM C-II})$$

These values are in good agreement with the impulses computed by equation (C1). (See table V.) Figure 45 shows that both the magnitudes and frequencies of the rotation rates are closely matched. The frequencies are identical with the values of  $\nu_b$  given in table V.

Figure 46 shows the histories of the program-computed values of the wind angles for the computer runs which produced the matchup in rotation rates. These values are not the actual histories of the in-flight wind angles. They do represent the characteristic trends, and the frequencies and absolute variations in the angles should closely approximate those in flight. Note that the maximum values of  $\eta$  are twice the values of the cone angles  $\theta$  in table V and that the frequencies of  $\eta$  are identical to those listed for  $\nu_H$  in table V. The component wind angles ( $\alpha, \beta$ ) are seen to have variations approximately equal to  $\pm 2\theta$  because the spacecraft is rolling on the surface of the precession cone as illustrated in figure 44. If it is assumed that the velocity vectors were alined with the spacecraft X-axes at stage separations, the variations in  $\eta$  were

$$0 \cong \eta \cong 5^\circ \quad (\text{for RAM C-I})$$

$$0 \cong \eta \cong 4^\circ \quad (\text{for RAM C-II})$$

and the peak-to-peak variations in the component wind angles were

$$\alpha, \beta = \pm 5^\circ \quad (\text{for RAM C-I})$$

$$\alpha, \beta = \pm 4^\circ \quad (\text{for RAM C-II})$$

## APPENDIX C – Concluded

### Summary of Wind-Angle Analysis

Cyclic changes in the measured electron densities were shown to be due to the displacements of the electrostatic probe from the wind axis in the angle-of-attack ( $\alpha$ ) plane. Peak-to-peak variations in the densities were produced by variations in angle of attack of  $\alpha = \pm 5^\circ$  (for RAM C-I) and  $\alpha = \pm 4^\circ$  (for RAM C-II). The symmetry of the density variation suggests that the average values corresponded to the case where  $\alpha = 0$ .

## REFERENCES

1. Bachynski, M. P.: Electromagnetic Wave Penetration of Reentry Plasma Sheaths. *Radio Sci., J. Res. NBS*, vol. 69D, no. 2, Feb. 1965, pp. 147-154.
2. Anon.: Proceedings of the NASA Conference on Communicating Through Plasmas of Atmospheric Entry and Rocket Exhaust. NASA SP-52, 1964.
3. Akey, Norman D.: Overview of RAM Reentry Measurement Program. The Entry Plasma Sheath and Its Effects on Space Vehicle Electromagnetic Systems, Vol. I, NASA SP-252, 1970, pp. 19-31.
4. Jones, William Linwood, Jr.: Probe Measurements of Electron Density Profiles During a Blunt-Body Reentry. Ph. D. Thesis, Virginia Polytechnic Inst. & State Univ., June 1971.
5. Jones, W. Linwood, Jr.; and Cross, Aubrey E.: Electrostatic Probe Measurements of Plasma Surrounding Three 25 000 Foot Per Second Reentry Flight Experiments. The Entry Plasma Sheath and Its Effects on Space Vehicle Electromagnetic Systems, Vol. I, NASA SP-252, 1970, pp. 109-136.
6. Akey, Norman D.; and Cross, Aubrey E. (With appendix A by Thomas G. Campbell; appendix B by Fred B. Beck; and appendix C by W. Linwood Jones, Jr.): Radio Blackout Alleviation and Plasma Diagnostic Results From a 25 000 Foot Per Second Blunt-Body Reentry. NASA TN D-5615, 1970.
7. Grantham, William L.: Flight Results of a 25 000-Foot-Per-Second Reentry Experiment Using Microwave Reflectometers To Measure Plasma Electron Density and Standoff Distance. NASA TN D-6062, 1970.
8. Sutton, Kenneth; Zoby, Ernest V.; and Butler, David H.: An Evaluation Test of a Full-Scale Replica of the RAM-CA Flight Heat Shield in a Rocket-Engine Exhaust. NASA TM X-1841, 1969.
9. Schexnayder, Charles J., Jr.; Huber, Paul W.; and Evans, John S.: Calculation of Electron Concentration for a Blunt Body at Orbital Speeds and Comparison With Experimental Data. NASA TN D-6294, 1971.
10. Swift, C. T.; Gooderum, P. B.; and Castellow, S. L., Jr.: Experimental Investigation of a Plasma Covered, Axially Slotted Cylinder Antenna. *IEEE Trans. Antennas Propagation*, vol. AP-17, no. 5, Sept. 1969, pp. 598-605.
11. Crowell, William F.; and Jones, W. Linwood, Jr.: Effects of Reentry Plasma on RAM C-I VHF Telemetry Antennas. The Entry Plasma Sheath and Its Effects on Space Vehicle Electromagnetic Systems, Vol. I, NASA SP-252, 1970, pp. 183-201.



12. Scharfman, W. E.: The Use of Langmuir Probes To Determine the Electron Density Surrounding Re-Entry Vehicles. SRI Project 5034 (Contract NAS 1-3942), Stanford Res. Inst., June 1965.
13. Scharfman, W. E.; and Bredfeldt, H. R.: Use of the Langmuir Probe To Determine the Electron Density and Temperature Surrounding Re-Entry Vehicles. SRI Project 5771 (Contract NAS 1-4872), Stanford Res. Inst., Dec. 1966. (Available as NASA CR-66275.)
14. Hok, Gunnar; Spencer, N. W.; Reifman, A.; and Dow, W. G.: Dynamic Probe Measurements in the Ionosphere. AFCRC TN-58-616, U.S. Air Force, Nov. 1958.
15. Smetana, Frederick O.: On the Current Collected by a Charged Circular Cylinder Immersed in a Two-Dimensional Rarefied Plasma Stream. Rarefied Gas Dynamics, Vol. II, J. A. Laurmann, ed., Academic Press, Inc., 1963, pp. 65-91.
16. Dunn, Michael G.: Laboratory Measurements of Electron Density and Electron Temperature With RAM Flight Probes. The Entry Plasma Sheath and Its Effect on Space Vehicle Electromagnetic Systems, Vol. I, NASA SP-252, 1970, pp. 261-276.
17. Dunn, Michael G.: Experimental Plasma Studies. NASA CR-1958, 1972.
18. Webb, H., Jr.; Dresser, H.; Korkan, K.; and Raparelli, R.: Theoretical Flow Field Calculations for Project RAM. NASA CR-1308, 1969.
19. Suits, C. Guy; and Way, Harold E., eds.: The Collected Works of Irving Langmuir. Vol. 4 - Electrical Discharge. Pergamon Press, Inc., c.1961.
20. Laframboise, James G.: Theory of Spherical and Cylindrical Langmuir Probes in a Collisionless, Maxwellian Plasma at Rest. Rep. No. 100, Inst. Aerosp. Studies, Univ. of Toronto, June 1966. (Available from DDC as AD 634 596.)
21. Bernstein, Ira B.; and Rabinowitz, Irving N.: Theory of Electrostatic Probes in a Low-Density Plasma. Phys. Fluids, vol. 2, no. 2, Mar.-Apr. 1959, pp. 112-121.
22. Allen, J. E.; Boyd, R. L. F.; and Reynolds, P.: The Collection of Positive Ions by a Probe Immersed in a Plasma. Proc. Phys. Soc., vol. 70, pt. 3, no. 447B, Mar. 1, 1957, pp. 297-304.
23. Lam, S. H.: The Langmuir Probe in a Collisionless Plasma. AFOSR 64-0353, U.S. Air Force, Mar. 1964. (Available from DDC as AD 434 342.)
24. Chen, Francis F.: Numerical Computations for Ion Probe Characteristics in a Collisionless Plasma. MATT-252 (Contract AT(30-1)-1238), Plasma Phys. Lab., Princeton Univ., Feb. 1964.
25. Chen, Francis F.: Electric Probes. Plasma Diagnostic Techniques, Richard H. Huddlestone and Stanley L. Leonard, eds., Academic Press, 1965, pp. 113-200.

26. Bohm, David.; Burhop, E. H. S.; and Massey, H. S. W.: The Use of Probes for Plasma Exploration in Strong Magnetic Fields. The Characteristics of Electrical Discharges in Magnetic Fields, A. Guthrie and R. K. Wakerling, eds., McGraw-Hill Book Co., Inc., 1949, pp. 13-76.
27. Sonin, A. A.: The Behaviour of Free Molecular Cylindrical Langmuir Probes in Supersonic Flows, and Their Application to the Study of the Blunt Body Stagnation Layer. UTIAS Rep. No. 109, Univ. of Toronto, Aug. 1965.
28. Hoegy, W. R.; and Brace, L. H.: The Dumbbell Electrostatic Ionosphere Probe: Theoretical Aspects. Rep. JS-1 (Contracts AF 19(604)6124, DA-20-018-509-ORD-103, and NASw-139), College Eng., Univ. Michigan, Sept. 1961.

TABLE I.- ALTITUDE, VELOCITY, AND TIME OF RAM C-I AND RAM C-II\* REENTRY TRAJECTORIES

Altitude		Velocity		Time from lift-off, sec	Altitude		Velocity		Time from lift-off, sec
km	ft	m/sec	ft/sec		km	ft	m/sec	ft/sec	
152.4	500 × 10 <sup>3</sup>	7012	23 004	355.98	77.7	255 × 10 <sup>3</sup>	7657	25 121	393.77
150.9	495	7095	23 279	356.83	76.2	250	7661	25 135	394.54
149.4	490	7183	23 567	357.64	74.7	245	7670	25 164	395.30
147.8	485	7277	23 875	358.42	73.2	240	7664	25 143	396.07
146.3	480	7366	24 166	359.19	71.6	235	7660	25 131	396.83
144.8	475	7460	24 476	359.98	70.1	230	7662	25 139	397.59
143.2	470	7527	24 696	360.77	68.6	225	7665	25 148	398.36
141.7	465	7564	24 816	361.57	67.0	220	7670	25 165	399.13
140.2	460	7580	24 872	362.34	65.5	215	7668	25 156	399.89
138.7	455	7579	24 866	363.11	64.0	210	7664	25 145	400.65
137.2	450	7578	24 863	363.87	62.5	205	7657	25 123	401.41
135.6	445	7580	24 872	364.64	61.0	200	7651	25 102	402.18
134.1	440	7587	24 892	365.40	59.4	195	7655	25 115	402.94
132.6	435	7590	24 902	366.18	57.9	190	7653	25 108	403.71
131.1	430	7596	24 920	366.95	56.4	185	7643	25 076	404.48
129.5	425	7597	24 926	367.73	54.9	180	7640	25 064	405.25
128.0	420	7594	24 916	368.49	53.3	175	7630	25 034	406.02
126.5	415	7594	24 914	369.25	51.8	170	7623	25 009	406.79
125.0	410	7597	24 924	370.00	50.3	165	7610	24 967	407.56
123.4	405	7602	24 941	370.75	48.8	160	7596	24 923	408.32
121.9	400	7609	24 965	371.52	47.2	155	7568	24 829	409.09
120.4	395	7614	24 982	372.30	45.7	150	7544	24 752	409.86
118.9	390	7611	24 971	373.08	44.2	145	7517	24 663	410.64
117.3	385	7610	24 967	373.85	42.7	140	7477	24 532	411.42
115.8	380	7610	24 969	374.61	41.4	135	7432	24 384	412.20
114.3	375	7612	24 973	375.37	39.6	130	7363	24 157	412.99
112.8	370	7616	24 986	376.14	38.1	125	7279	23 882	413.80
111.2	365	7617	24 991	376.92	36.6	120	7182	23 563	414.61
109.7	360	7619	24 996	377.70	35.0	115	7072	23 202	415.43
108.2	355	7622	25 008	378.47	33.5	110	6938	22 763	416.26
106.7	350	7626	25 019	379.23	32.0	105	6759	22 176	417.12
105.2	345	7629	25 029	379.99	30.5	100	6539	21 455	418.00
103.6	340	7627	25 024	380.75	29.0	95	6232	20 446	418.91
102.1	335	7629	25 031	381.52	27.4	90	5938	19 483	419.87
100.6	330	7631	25 037	382.29	25.9	85	5555	18 226	420.87
99.1	325	7628	25 026	383.07	24.4	80	5089	16 697	421.96
97.5	320	7628	25 025	383.86	22.9	75	4552	14 935	423.16
96.0	315	7633	25 042	384.63	21.3	70	3945	12 942	424.51
94.5	310	7640	25 065	385.39	19.8	65	3238	10 624	426.12
93.0	305	7650	25 098	386.14	18.3	60	2438	8 000	428.22
91.4	300	7649	25 094	386.88	16.8	55	1739	5 706	430.88
89.9	295	7646	25 087	387.64	15.2	50	1049	3 441	434.69
88.4	290	7642	25 074	388.40	13.7	45	581	1 906	440.26
86.9	285	7645	25 082	389.17	12.2	40	271	890	448.98
85.3	280	7649	25 095	389.93	10.7	35	220	721	459.34
83.8	275	7651	25 103	390.70	9.1	30	239	785	467.88
82.3	270	7649	25 094	391.46	7.6	25	227	744	475.40
80.8	265	7649	25 096	392.23	6.1	20	276	907	484.45
79.2	260	7654	25 113	393.00					

\*For time correlation purposes, between the times of 386.88 and 406.79 seconds, the C-II spacecraft was 365.8 m (1200 ft) higher in altitude than listed in the table with a velocity of approximately 18 m/sec (60 ft/sec) greater than the value listed.

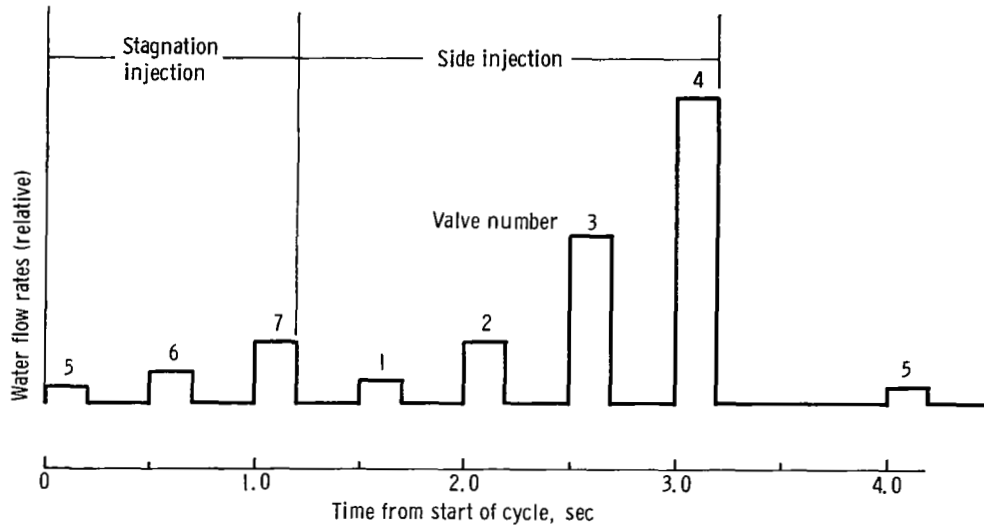
TABLE II. - POSITION OF FUNCTIONAL PARTS ON THE RAM C-I AND C-II PAYLOADS

Payload	Part and function	x		$\phi$ , deg (a)	x/D (b)
		cm (a)	in. (a)		
Water-injection nozzle					
RAM C-I	Stagnation	0	0	---	0
	Lateral	15.2	6.0	0	.48
	Lateral	15.2	6.0	180	.48
Antenna					
RAM C-II	S-band open-ended guide (3344 MHz)	4.6	1.8	90	0.15
	X-band conical horn (10 044 MHz)	4.6	1.8	330	.15
	K <sub>a</sub> -band conical horn (35 000 MHz)	4.6	1.8	210	.15
	L-band open-ended guide (1116 MHz)	23.1	9.1	195	.76
	S-band open-ended guide (3344 MHz)	23.1	9.1	15	.76
	X-band conical horn (10 044 MHz)	23.1	9.1	285	.76
	K <sub>a</sub> -band conical horn (35 000 MHz)	23.1	9.1	227	.76
	L-band open-ended guide (1116 MHz)	70.1	27.6	195	2.30
	S-band open-ended guide (3344 MHz)	70.1	27.6	15	2.30
	X-band conical horn (10 044 MHz)	70.1	27.6	285	2.30
RAM C-I	VHF axial cavity-backed slot (259.7 MHz)	75.2	29.6	0	2.36
	VHF axial cavity-backed slot (259.7 MHz)	75.2	29.6	180	2.36
RAM C-I	X-band rectangular horn (9210 MHz)	82.8	32.6	60	2.60
	X-band rectangular horn (9210 MHz)	82.8	32.6	150	2.60
	X-band rectangular horn (9210 MHz)	82.8	32.6	240	2.60
	X-band rectangular horn (9210 MHz)	82.8	32.6	330	2.60
RAM C-II	X-band rectangular horn (9210 MHz)	80.5	31.7	15	2.65
	X-band rectangular horn (9210 MHz)	80.5	31.7	105	2.65
	X-band rectangular horn (9210 MHz)	80.5	31.7	195	2.65
	X-band rectangular horn (9210 MHz)	80.5	31.7	285	2.65
RAM C-II	VHF circumferential-slot array (259.7 MHz)	97.5	38.4	---	3.20
RAM C-I	VHF circumferential-slot array (225.7 MHz)	109.2	43.0	---	3.42
RAM C-II	L-band open-ended guide (1116 MHz)	106.2	41.8	195	3.48
	S-band open-ended guide (3344 MHz)	106.2	41.8	15	3.48
	X-band conical horn (10 044 MHz)	106.2	41.8	285	3.48
	K <sub>a</sub> -band conical horn (35 000 MHz)	106.2	41.8	105	3.48
RAM C-II	C-band rectangular horn (5800 MHz)	106.7	42.0	32	3.50
RAM C-I	C-band rectangular horn (5700 MHz)	118.4	46.6	30	3.71
RAM C-II	VHF circumferential-slot array (225.7 MHz)	114.8	45.2	---	3.76
Probe rake					
RAM C-I	Electrostatic	123.4	48.6	0	3.87
	Thermocouple	123.4	48.6	180	3.87
RAM C-II	Electrostatic	123.4	48.6	0	4.05
	Thermocouple	123.4	48.6	180	4.05

<sup>a</sup> Center-line location of parts.

<sup>b</sup> Nose diameter D is 31.90 cm (12.56 in.) for RAM C-I; nose diameter D is 30.48 cm (12.00 in.) for RAM C-II.

TABLE III.- RAM C-I TYPICAL INJECTION CYCLE AND FLOW RATE HISTORY



Cycle	Valve for -		Flow rate		Altitude		Cycle	Valve for -		Flow rate		Altitude	
	Stagnation injection	Side injection	kg/sec	lb/sec	km	ft		Stagnation injection	Side injection	kg/sec	lb/sec	km	ft
1	5		0	0			5	5		0.023	0.05	61.1	200 490
	6		0	0				6		.068	.15	60.1	197 236
	7		0	0				7		.127	.28	59.1	193 982
		1	0	0					1	.045	.10	58.1	190 724
		2	0	0					2	.109	.24	57.1	187 462
2	5		0	0	85.0	278 908	6	5		0.027	0.06	53.2	174 451
	6		0	0	84.0	275 639		6		.082	.18	52.2	171 212
	7		.014	.03	83.2	273 027		7		.163	.36	51.2	167 968
		1	.004	.01	82.0	269 115			1	.059	.13	50.2	164 722
		2	.018	.04	81.0	265 866			2	.145	.32	49.2	161 466
3	5		0.009	0.02	77.1	252 861	7	5		0.032	0.07	45.2	148 484
	6		.032	.07	76.1	249 598		6		.104	.23	44.3	145 267
	7		.064	.14	75.1	246 328		7		.195	.43	43.3	142 058
		1	.027	.06	74.1	243 048			1	.068	.15	42.3	138 864
		2	.064	.14	73.1	239 771			2	.159	.35	41.4	135 684
4	5		0.018	0.04	69.1	226 690	8	5		0.036	0.08	37.5	123 137
	6		.054	.12	68.1	223 442		6		.109	.24	36.6	120 058
	7		.109	.24	67.1	220 185		7		.195	.43	35.7	117 010
		1	.036	.08	66.1	216 915			1	.068	.15	34.7	113 987
		2	.095	.21	65.1	213 635			2	.159	.35	33.8	110 986
	3	.249	.55	64.1	210 348		3	0	0				
	4	.404	.89	63.1	207 054		4	0	0				

TABLE IV.- RAM C-I AND RAM C-II RADIO-FREQUENCY SYSTEMS

Payload	Purpose	Frequency		Antenna type	Transmitter		Body location, x/D	Remarks
		Band	MHz		Approximate RF power, watts	Modulation		
RAM C-I	Real-time telemetry	VHF	259.7	Axial cavity-backed slots	5	FM	2.36	Two slots, diametrically opposed -----
RAM C-II		VHF	259.7	Circumferential-slot array	5	FM	3.20	
RAM C-I	Delayed-time telemetry	VHF	225.7	Circumferential-slot array	5	FM	3.42	Same data as real-time telemetry, but delayed by onboard tape loop for approximately 45 sec
RAM C-II		VHF	225.7	Circumferential-slot array	5	FM	3.76	
RAM C-I	Radar beacon	C	5 700	Rectangular horn	900 peak	Pulse	3.71	----- -----
RAM C-II		C	5 800	Rectangular horn	800 peak	Pulse	3.50	
RAM C-I	Real-time telemetry	X	9 210	Rectangular-horn array	500 peak	PPM	2.60	Four horns, 90° spacing Four horns, 90° spacing
RAM C-II		X	9 210	Rectangular horn	500 peak	PPM	2.65	
RAM C-II	Reflectometer experiment	L	1 116	T-fed slot	0.1	CW	---, 0.76, 2.30, and 3.48	Station number 1; x/D of 0.15
		S	3 344	Open-ended waveguide	.1	CW	0.15, 0.76, 2.30, and 3.48	Station number 2; x/D of 0.76
		X	10 044	Conical horn	.1	CW	0.15, 0.76, 2.30, and 3.48	Station number 3; x/D of 2.30
		K <sub>a</sub>	35 000	Conical horn	.1	CW	0.15, 0.76, 2.30, and 3.48	Station number 4; x/D of 3.48

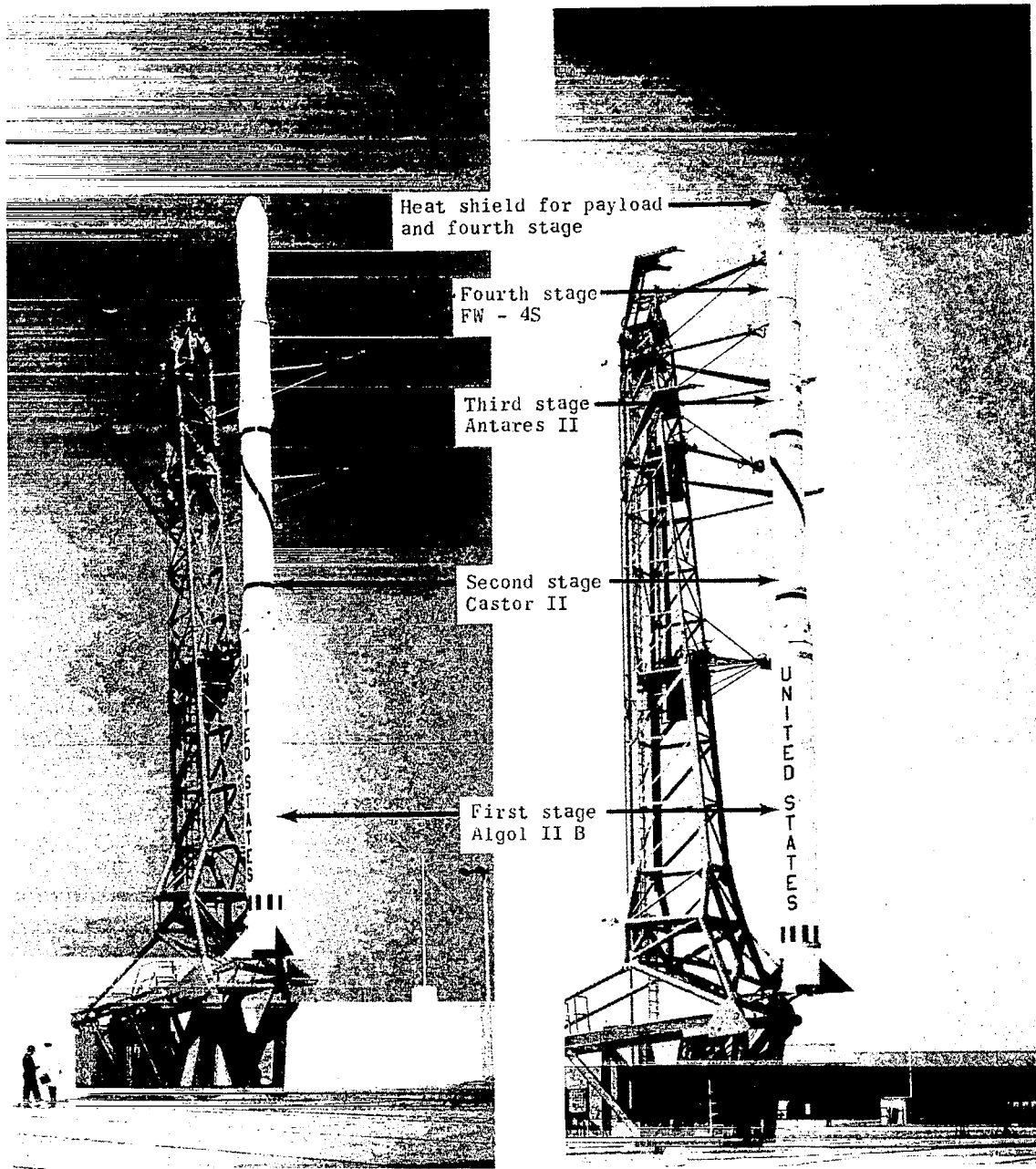
TABLE V.- COMPUTED VALUES OF IMPULSE, PRECESSION CONE ANGLE, AND  
PRECESSION FREQUENCIES (EQS. (C1) TO (C4))

Flight	L		$\theta$ , deg	$\nu_{H'}$ , Hz	$\nu_{b'}$ , Hz
	N-m-sec	lb-ft-sec			
C-I	3.7	2.7	2.48	0.704	2.25
C-II	3.2	2.3	2.00	.800	2.25

TABLE VI.- PREFLIGHT-MEASURED SPACECRAFT MOMENTS OF INERTIA\*  
AND FLIGHT-MEASURED ROTATION RATES

Flight	$I_X$		$I_Y$		$I_Z$		p, rad/sec	$\omega_L$ , rad/sec
	kg-m <sup>2</sup>	slug-ft <sup>2</sup>	kg-m <sup>2</sup>	slug-ft <sup>2</sup>	kg-m <sup>2</sup>	slug-ft <sup>2</sup>		
C-I	4.62	3.41	19.31	14.24	19.66	14.50	18.5	0.190
C-II	4.68	3.45	18.06	13.32	17.92	13.22	19.1	.175

\* Moments of inertia constant during data period.



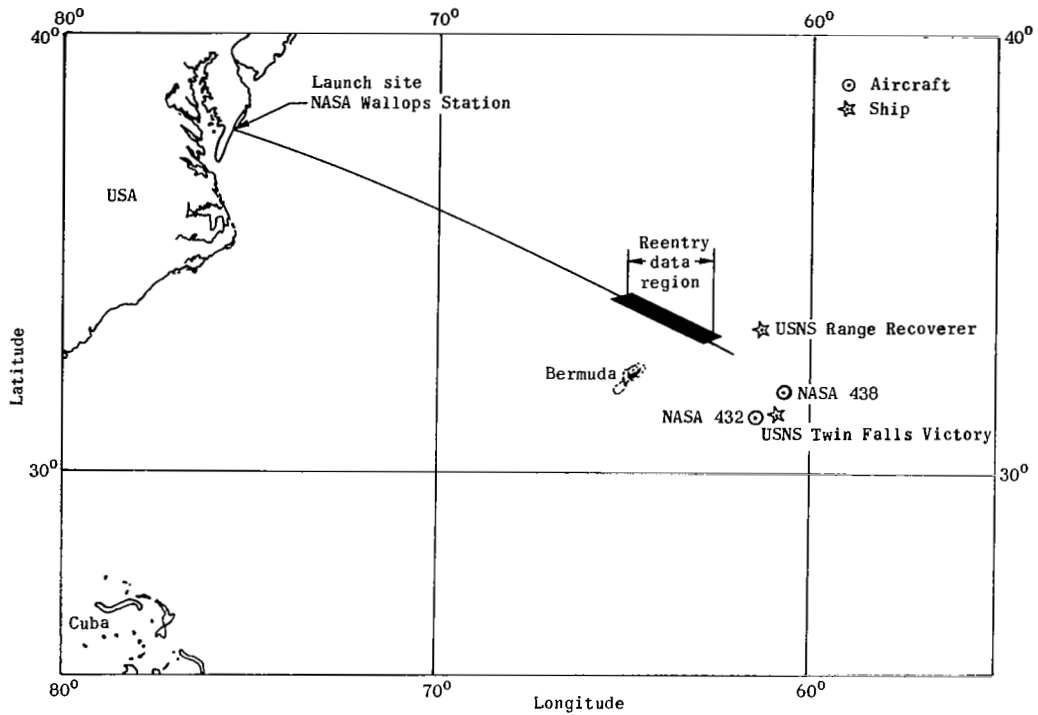
L-71-7172

(a) S-159; RAM C-I.

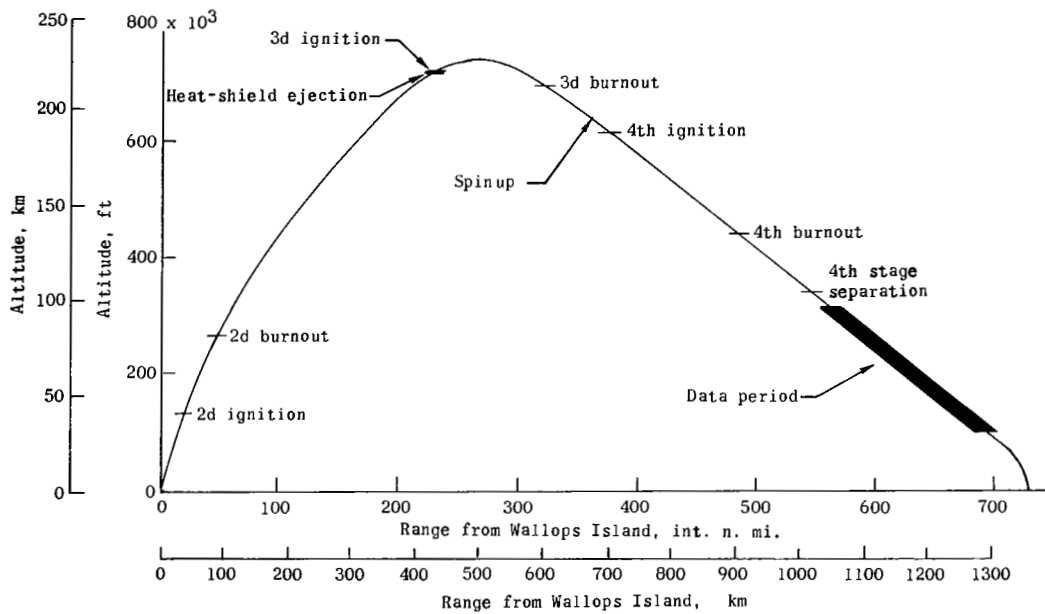
(b) S-168; RAM C-II.

Figure 1.- Launch vehicles.





(a) RAM C-II ground track.



(b) RAM C-I and C-II flight events.

Figure 2.- Ground track and flight events.

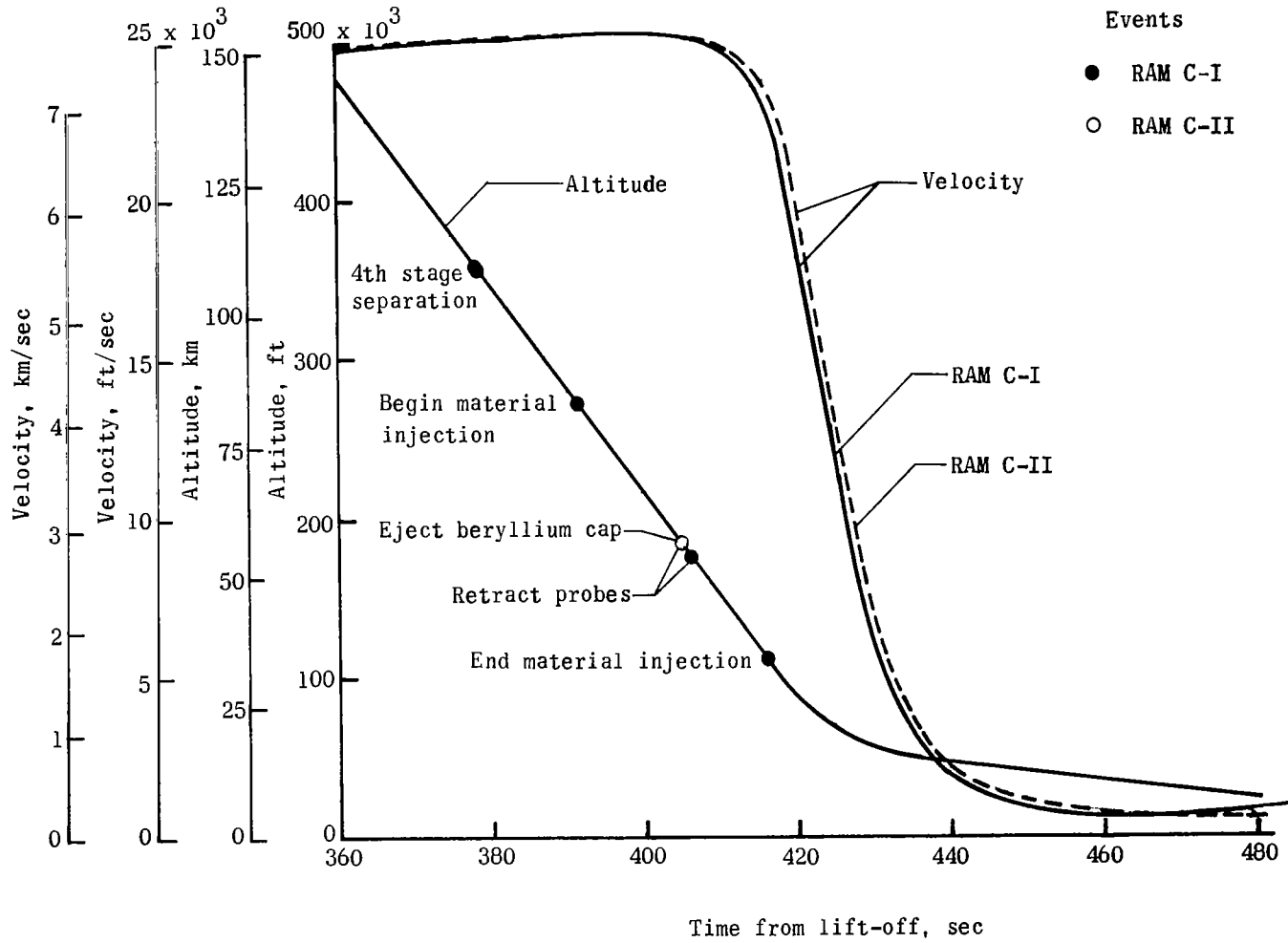
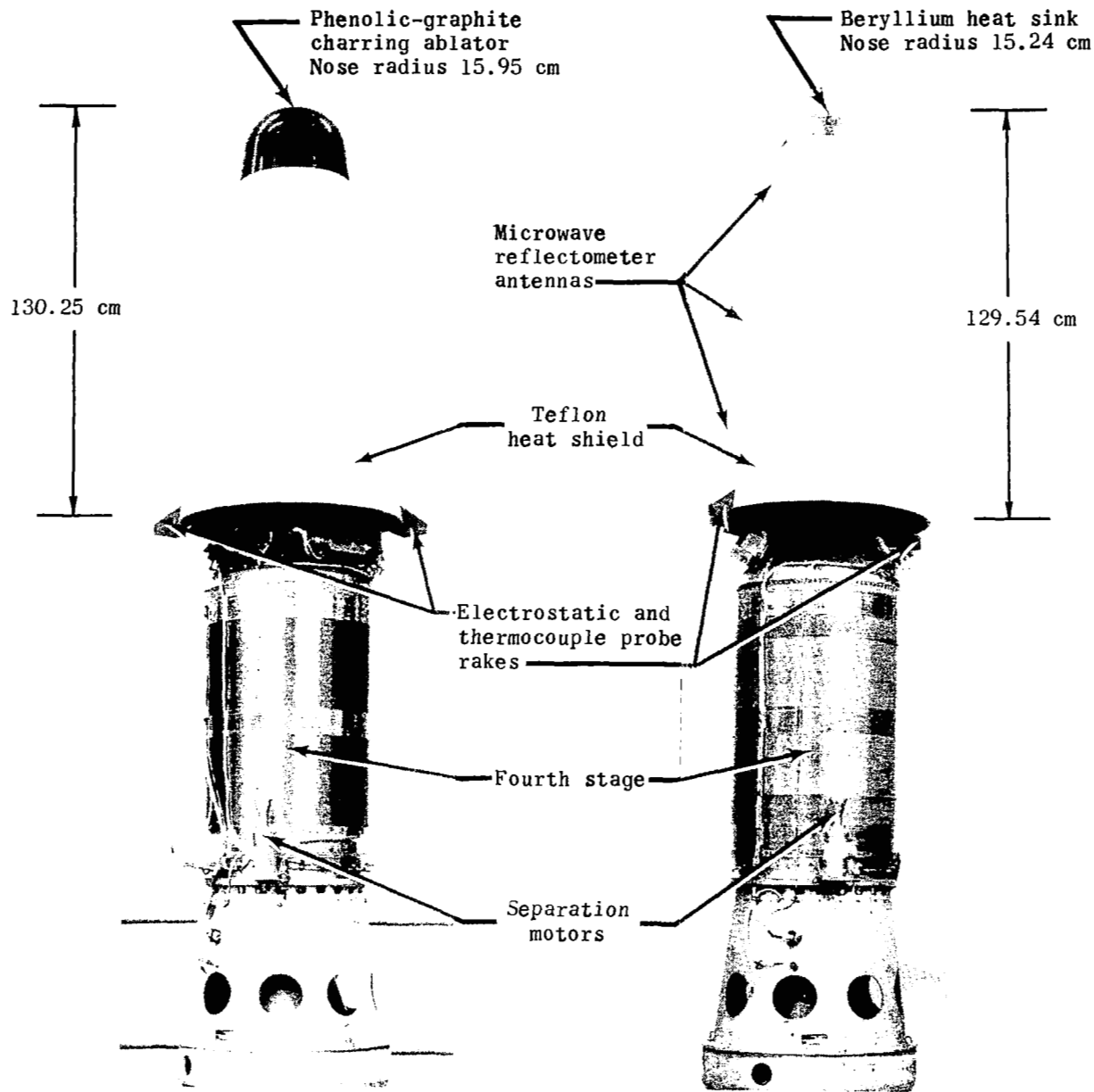


Figure 3.- Reentry trajectories.

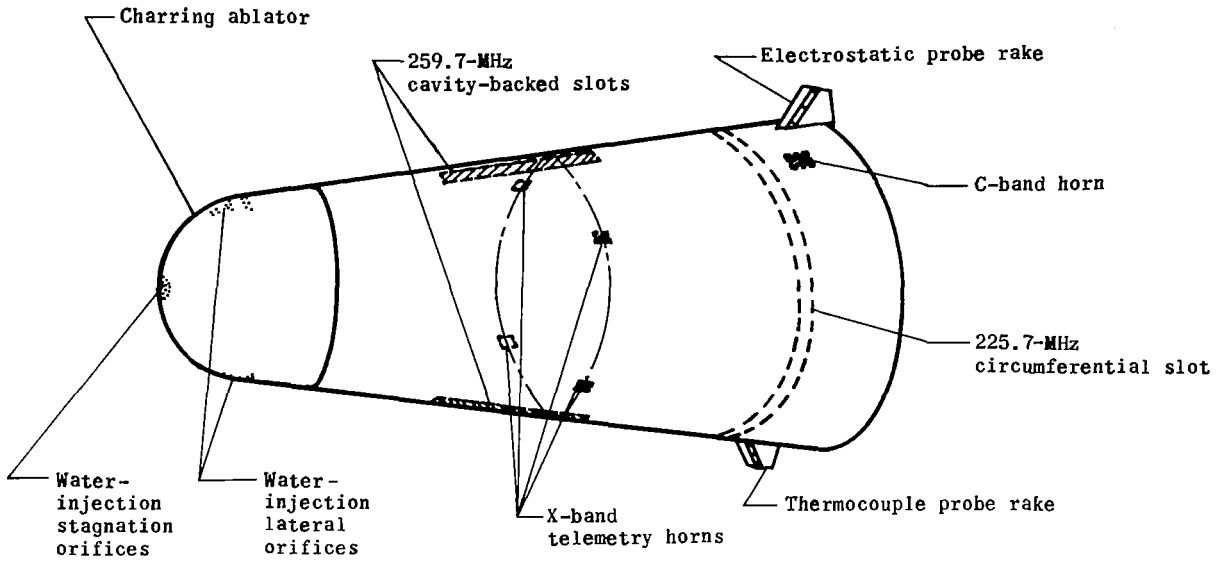


(a) RAM C-I.

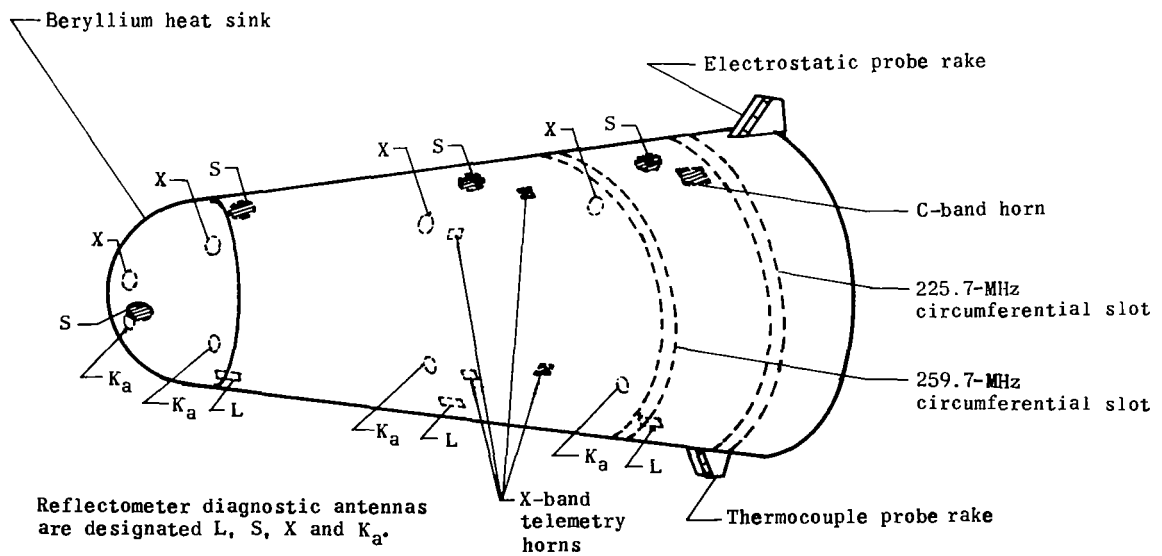
L-71-7173

(b) RAM C-II.

Figure 4.- Payload configurations shown with fourth-stage engines and separation motors.

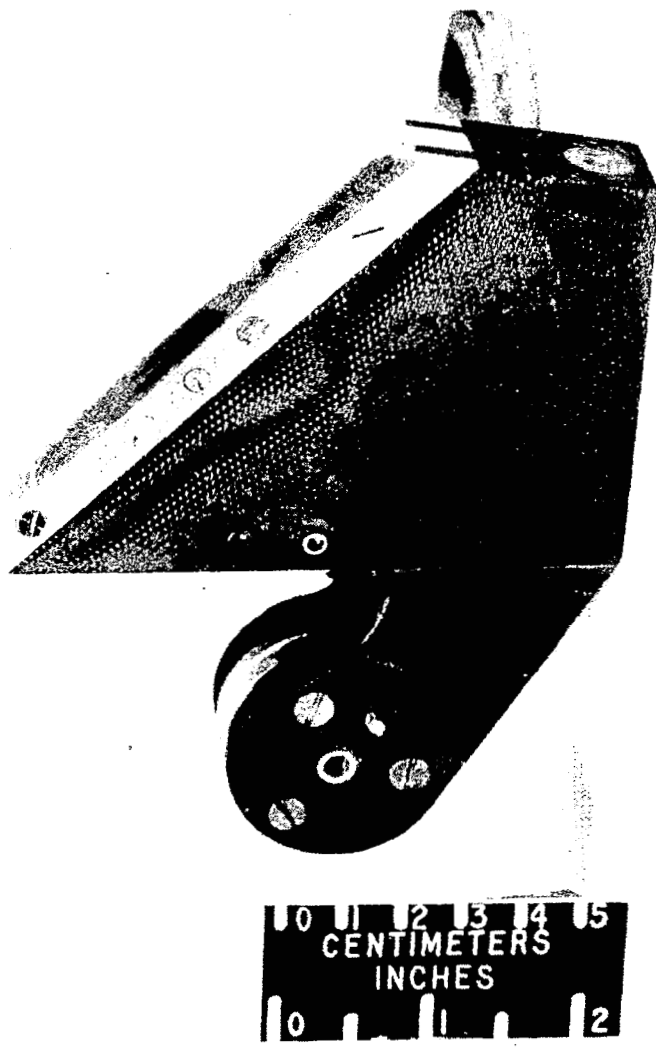


(a) RAM C-I.



(b) RAM C-II.

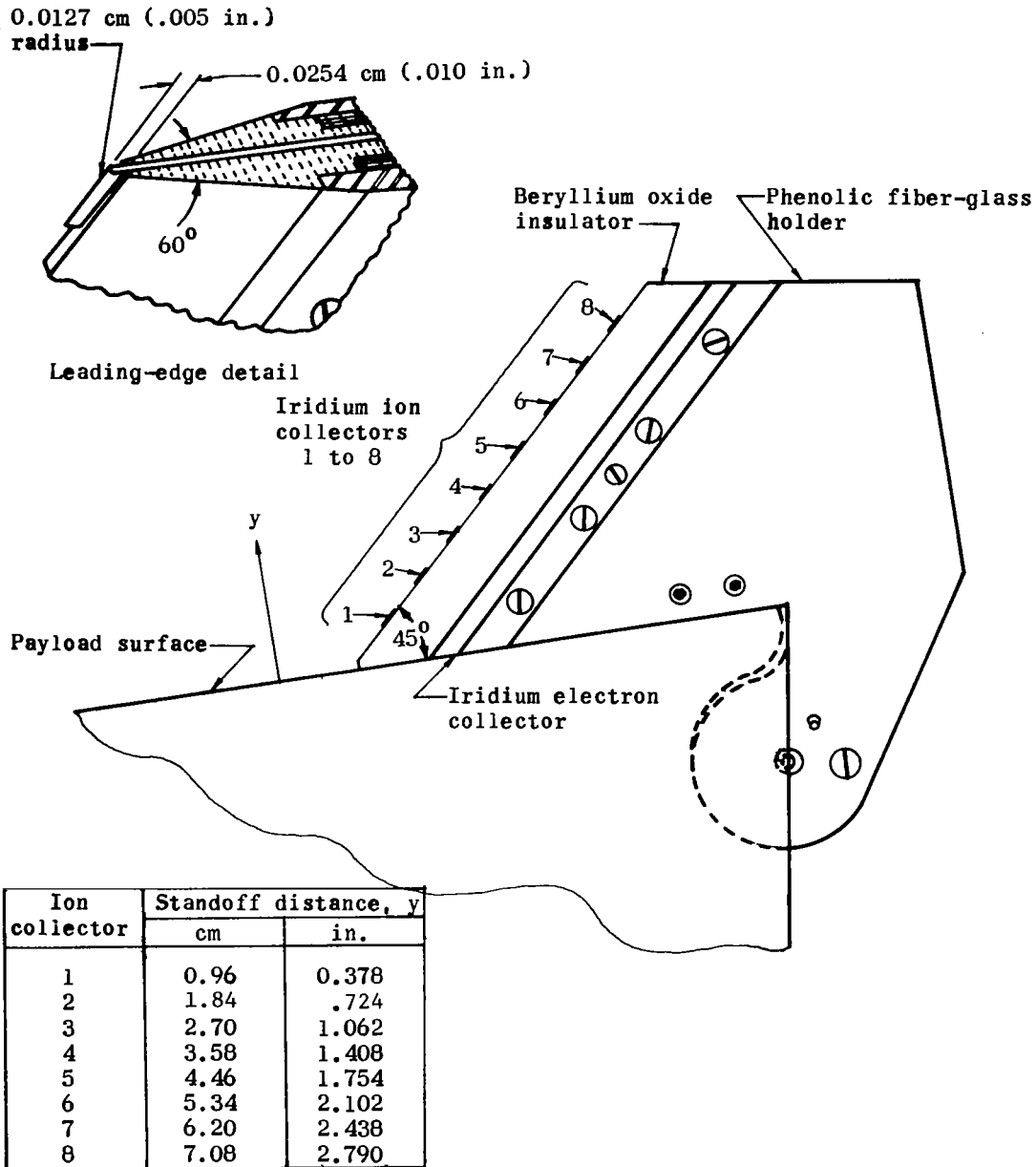
Figure 5.- Electrostatic probe and radio-frequency antenna locations.



L-67-5814

(a) Photograph of rake.

Figure 6.- Electrostatic probe rake.



(b) Detail sketch of rake. Collection area of each ion collector was 0.0420 cm<sup>2</sup> (0.006 in<sup>2</sup>).

Figure 6.- Concluded.

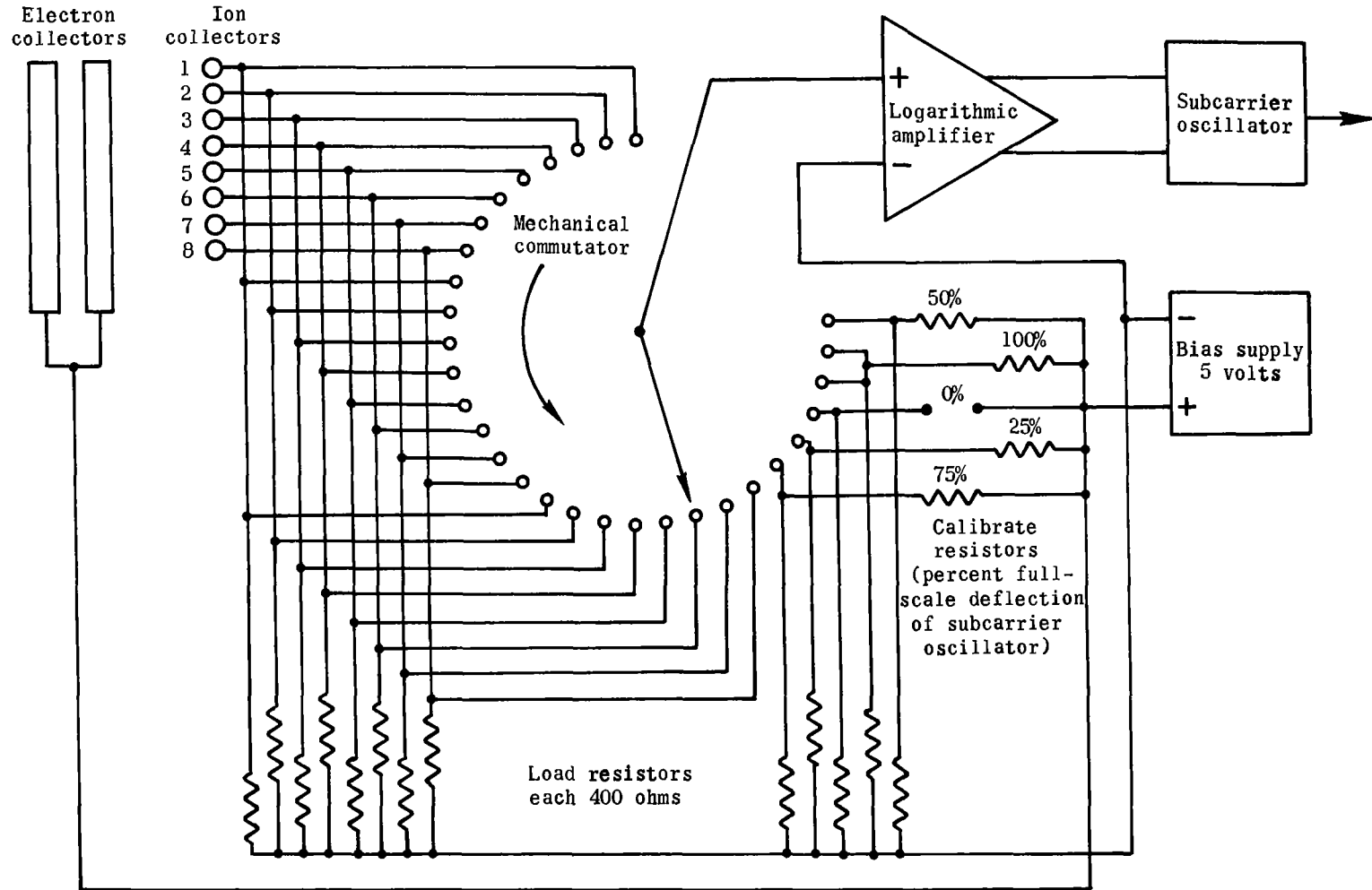
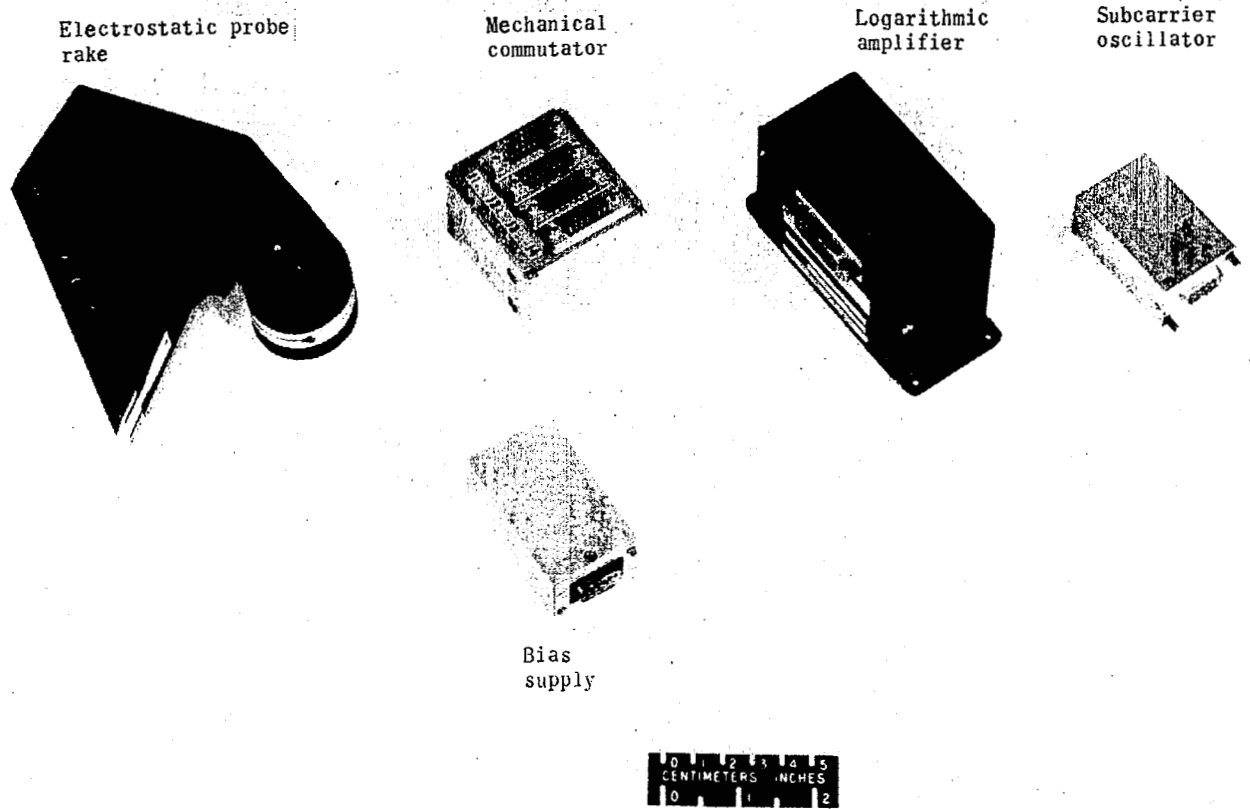


Figure 7.- Circuit diagram for electrostatic probe system.



Electrostatic probe  
rake

Mechanical  
commutator

Logarithmic  
amplifier

Subcarrier  
oscillator

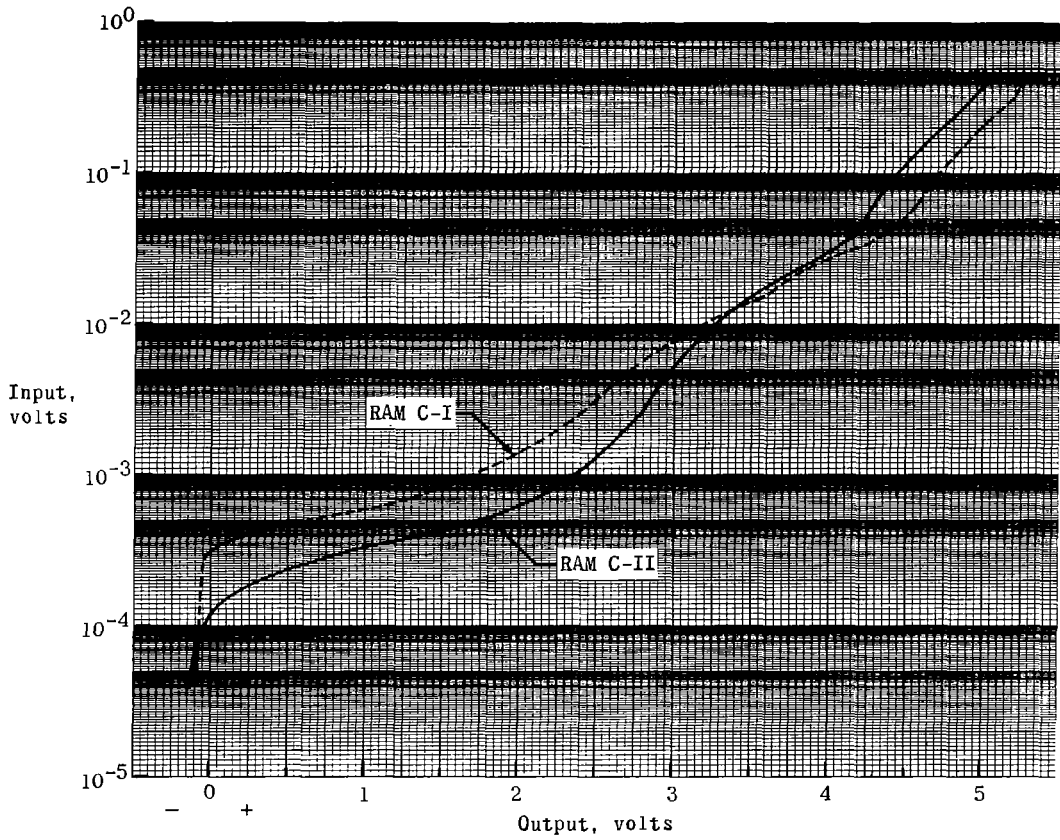
Bias  
supply



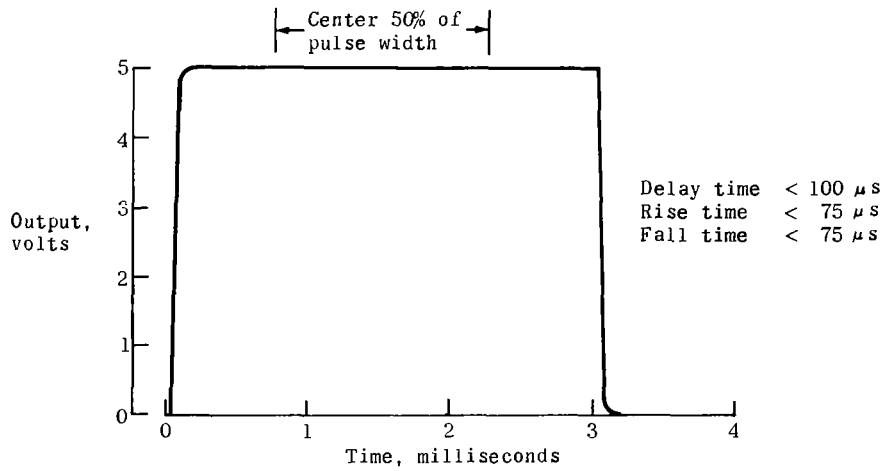
L-70-8365.1

Figure 8.- Major components of electrostatic probe system.





(a) Dynamic input-output curves.



(b) Typical pulse-response curve.

Figure 9.- Electrical characteristics of logarithmic amplifiers.

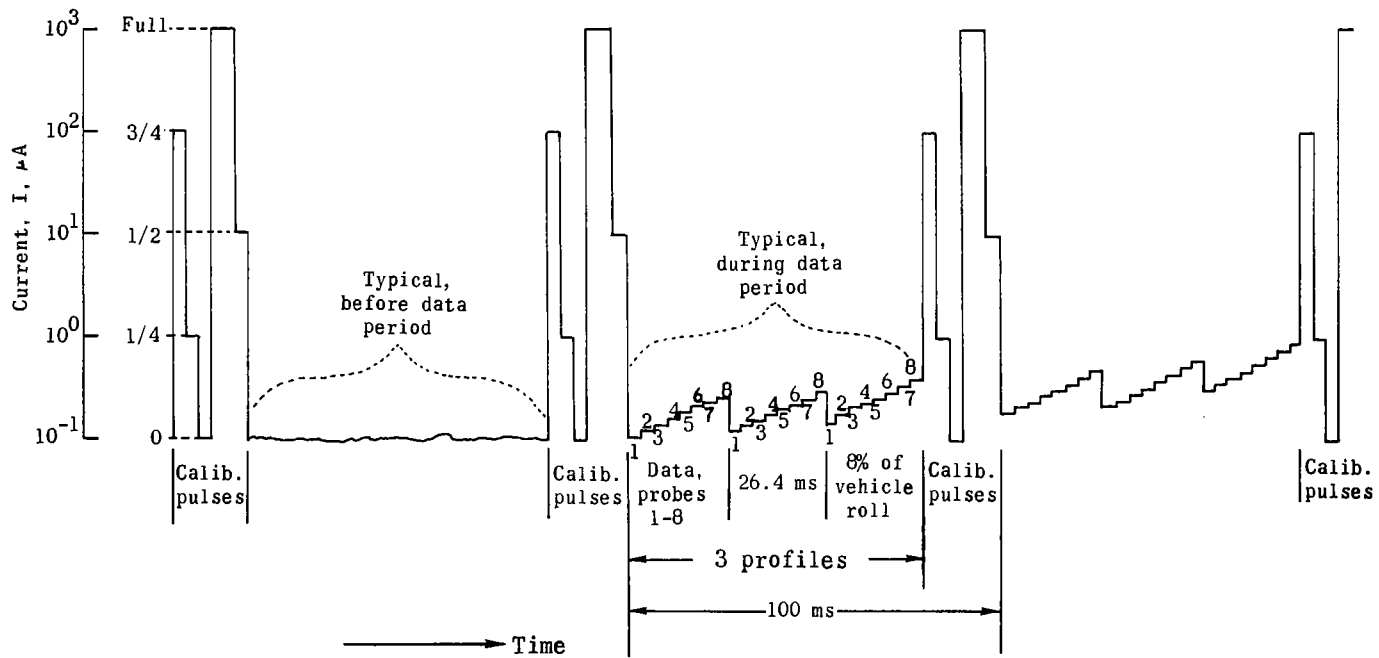
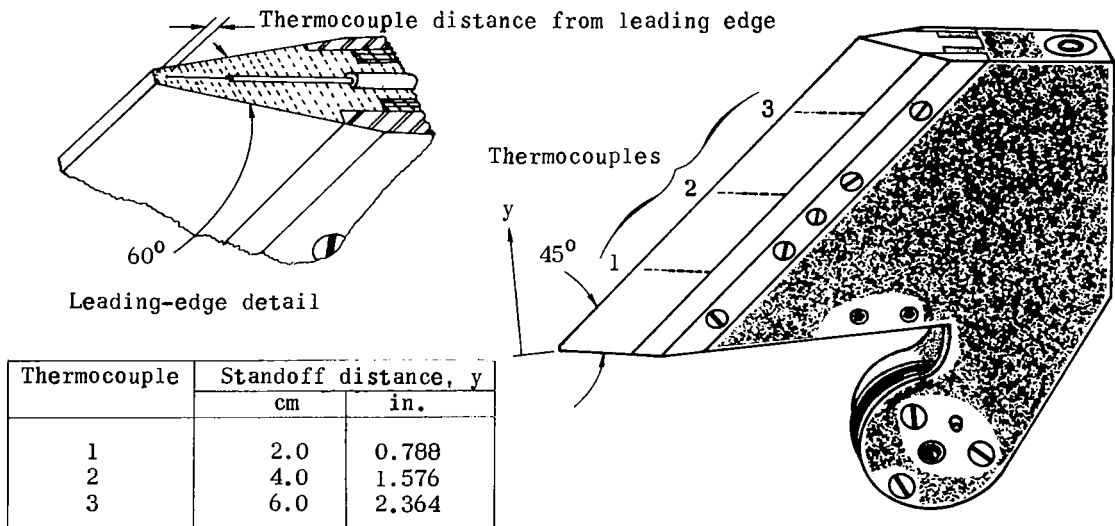


Figure 10. - Electrostatic probe data format.



L-71-7150

(a) Photograph of rake.



(b) Rake configuration. Thermocouple distance from leading edge for RAM C-I was 0.0635 cm (0.025 in.) and for RAM C-II, the distance was 0.1016 cm (0.040 in.).

Figure 11.- Thermocouple probe rake.

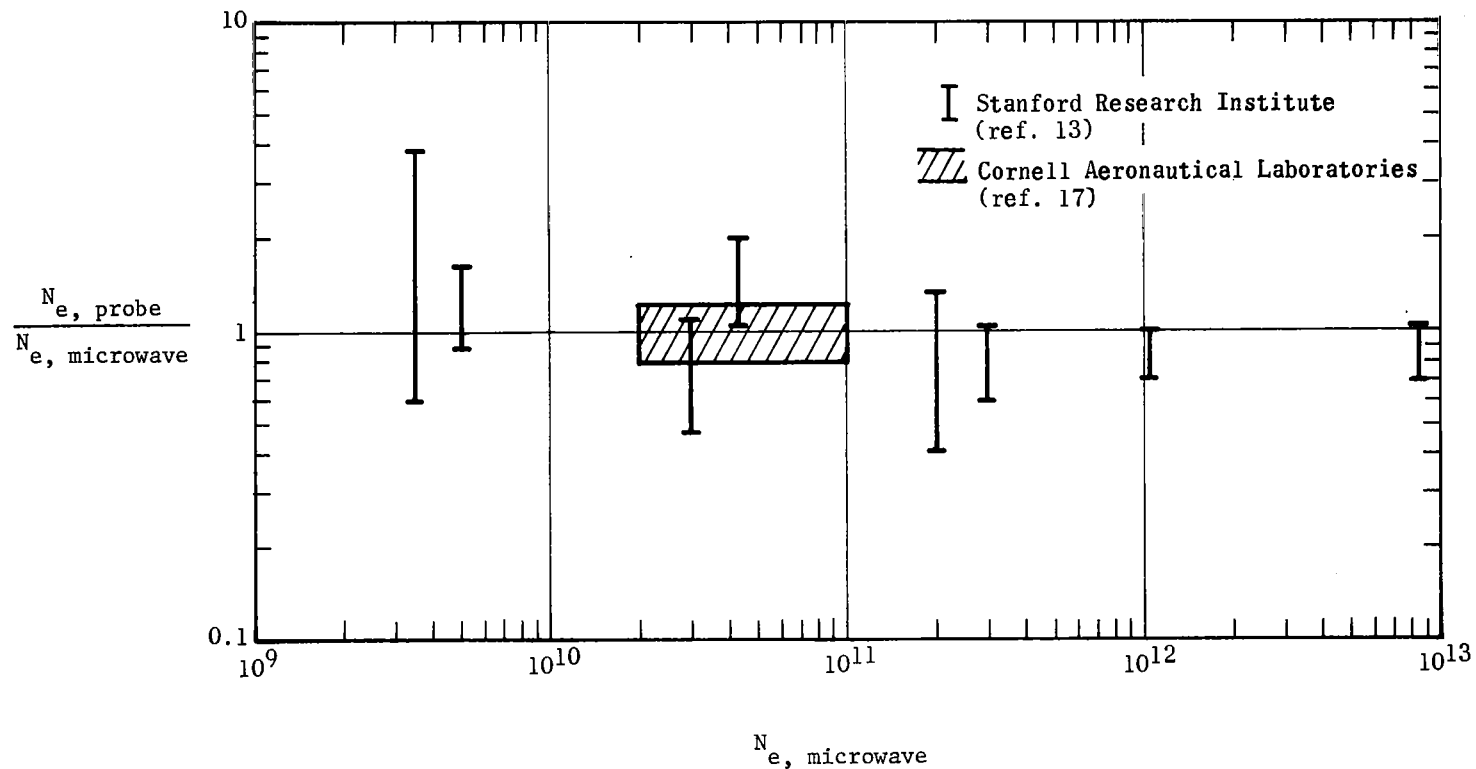
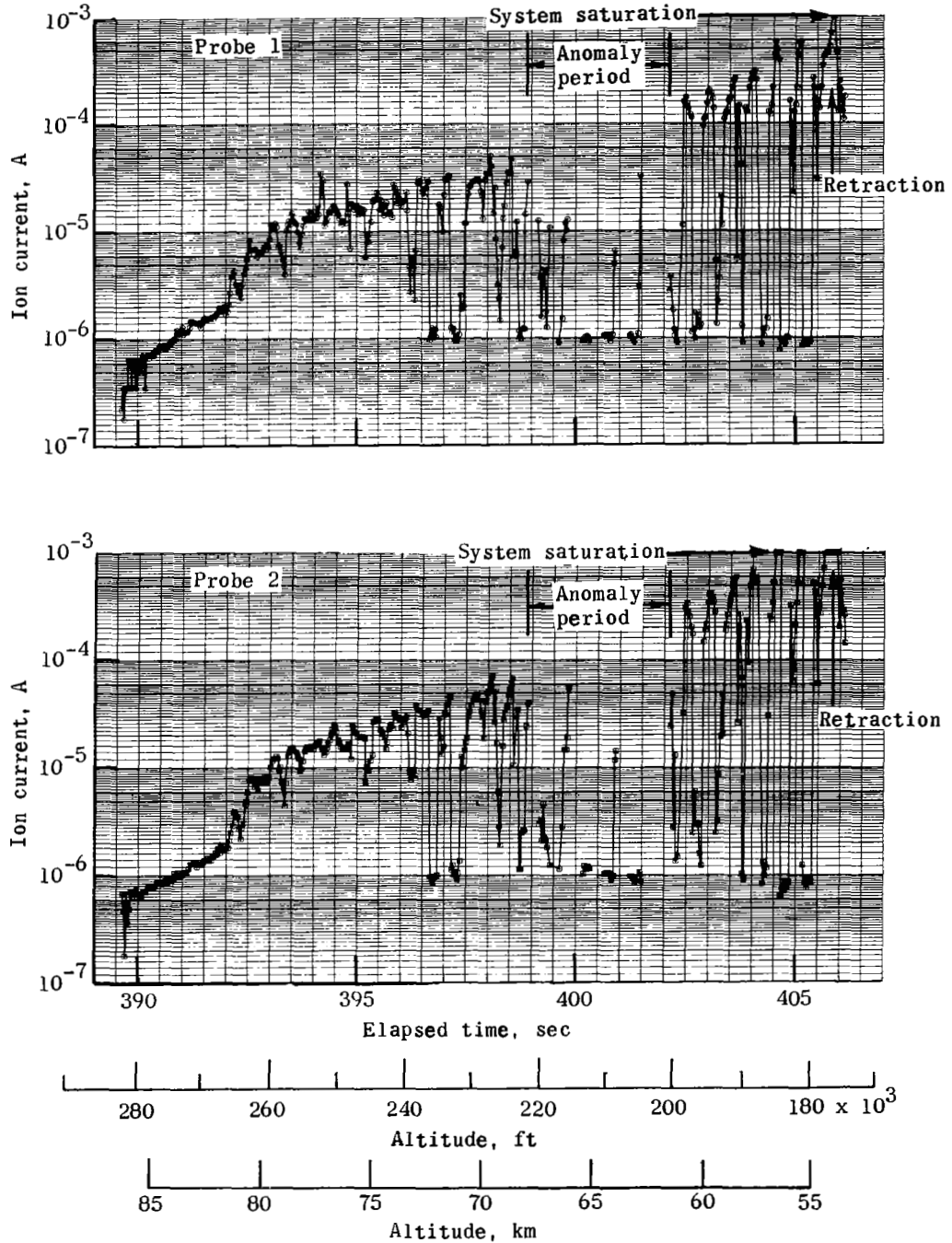
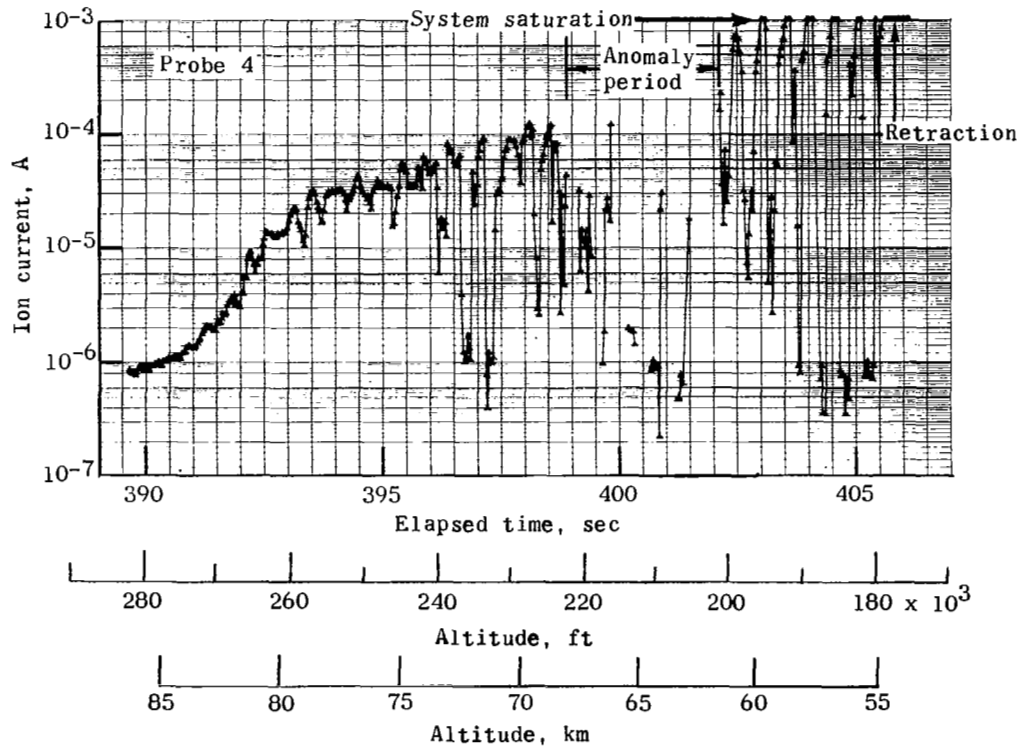
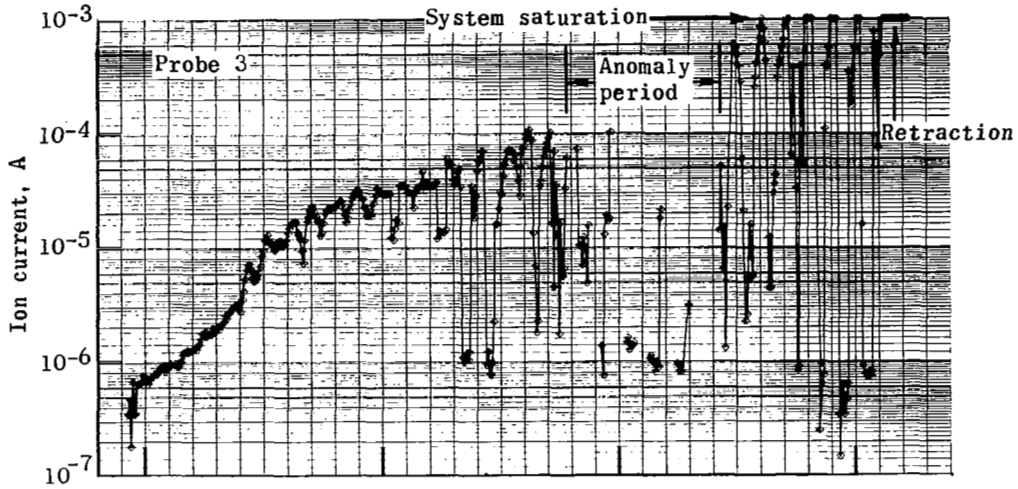


Figure 12.- Ratio of electron densities inferred from probes and from microwave data as a function of electron density inferred from microwave data.



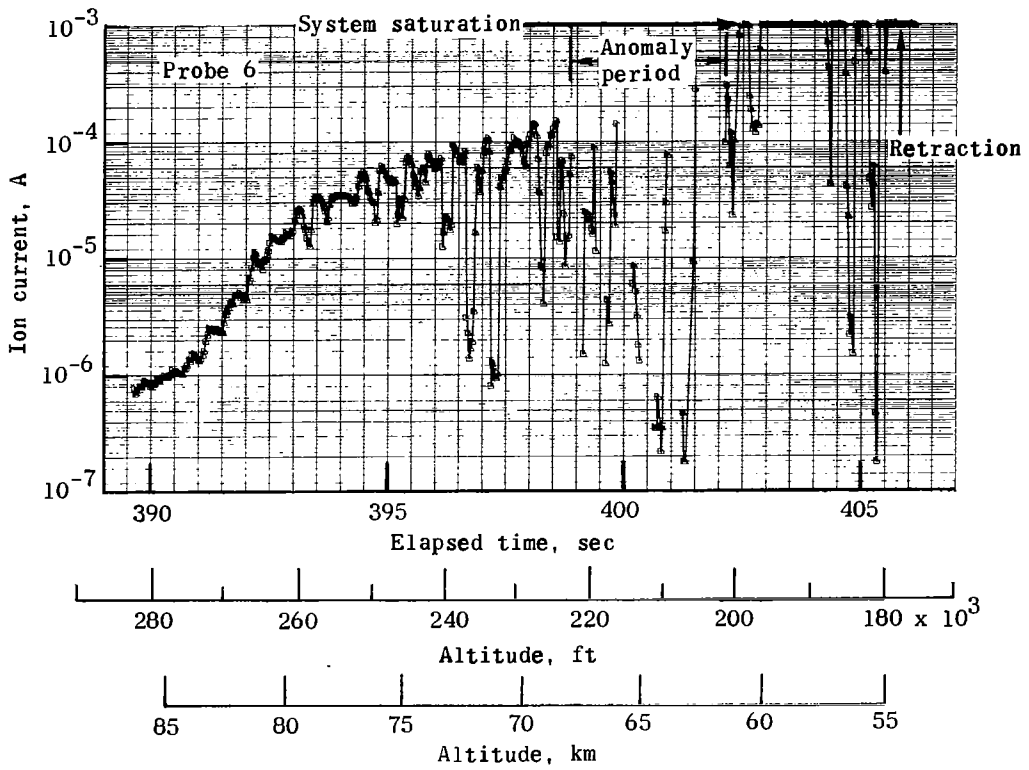
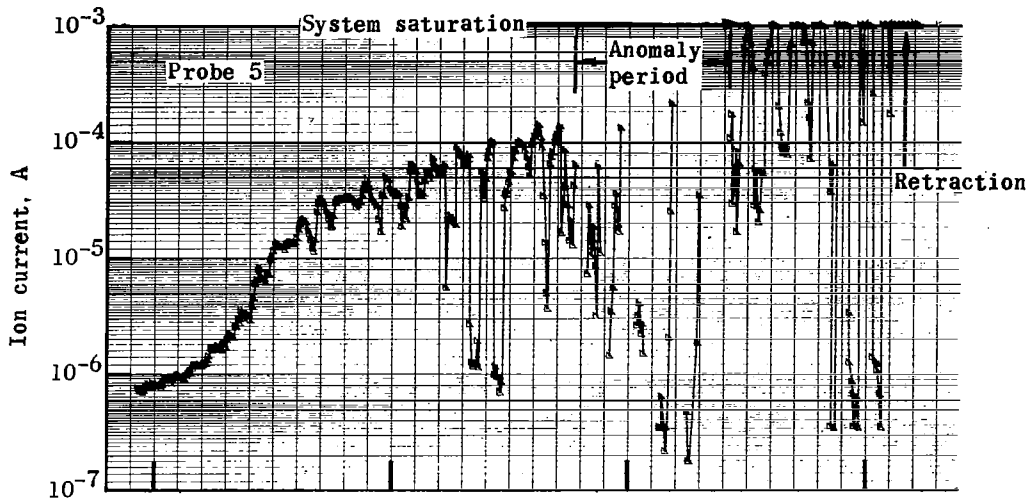
(a) Electrostatic probes 1 and 2.

Figure 13.- Ion current measurements from electrostatic probes on RAM C-I flight experiment.



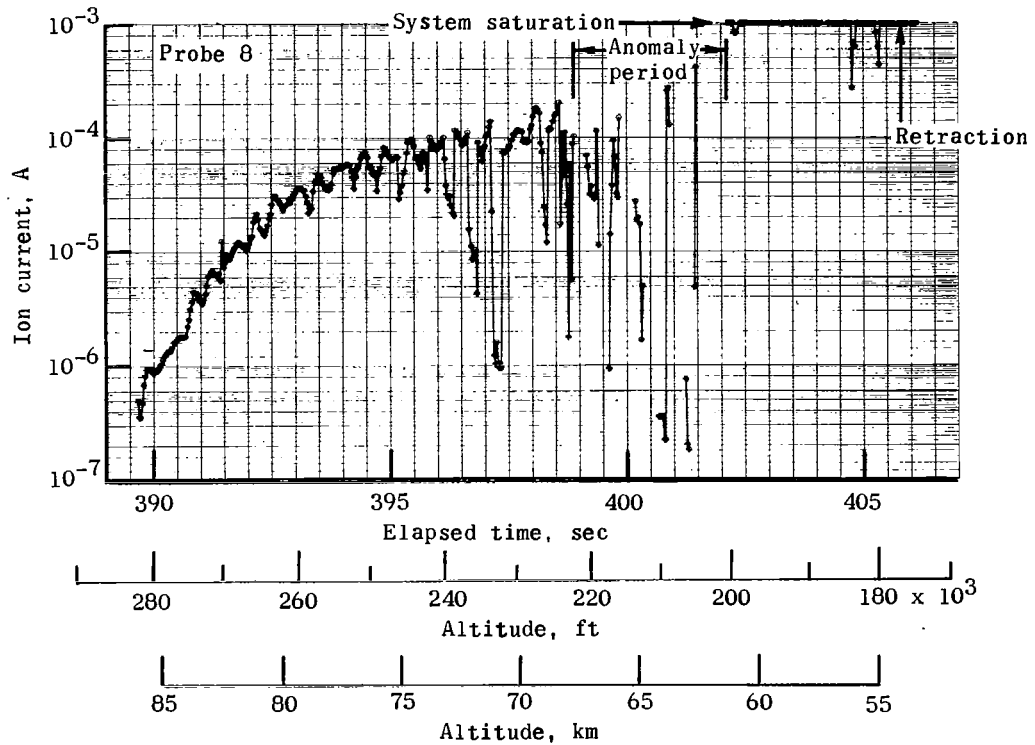
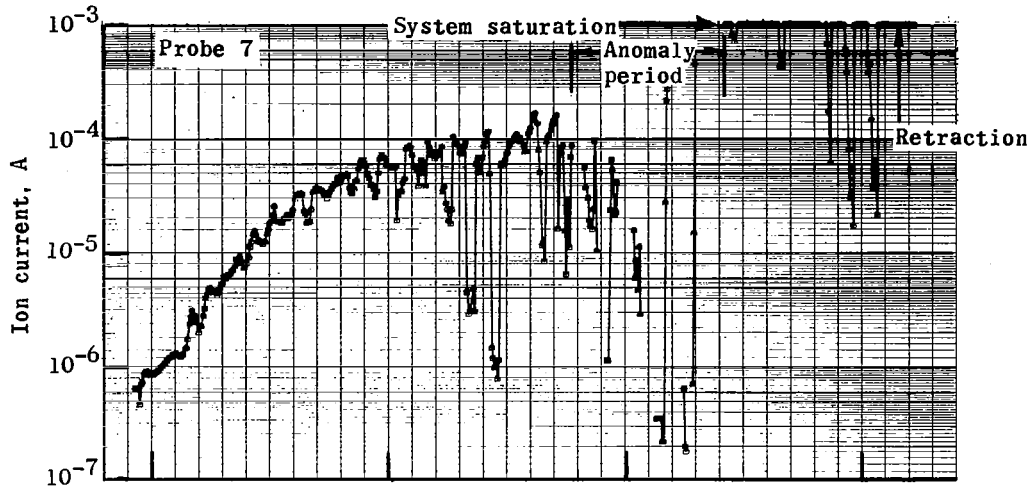
(b) Electrostatic probes 3 and 4.

Figure 13.- Continued.



(c) Electrostatic probes 5 and 6.

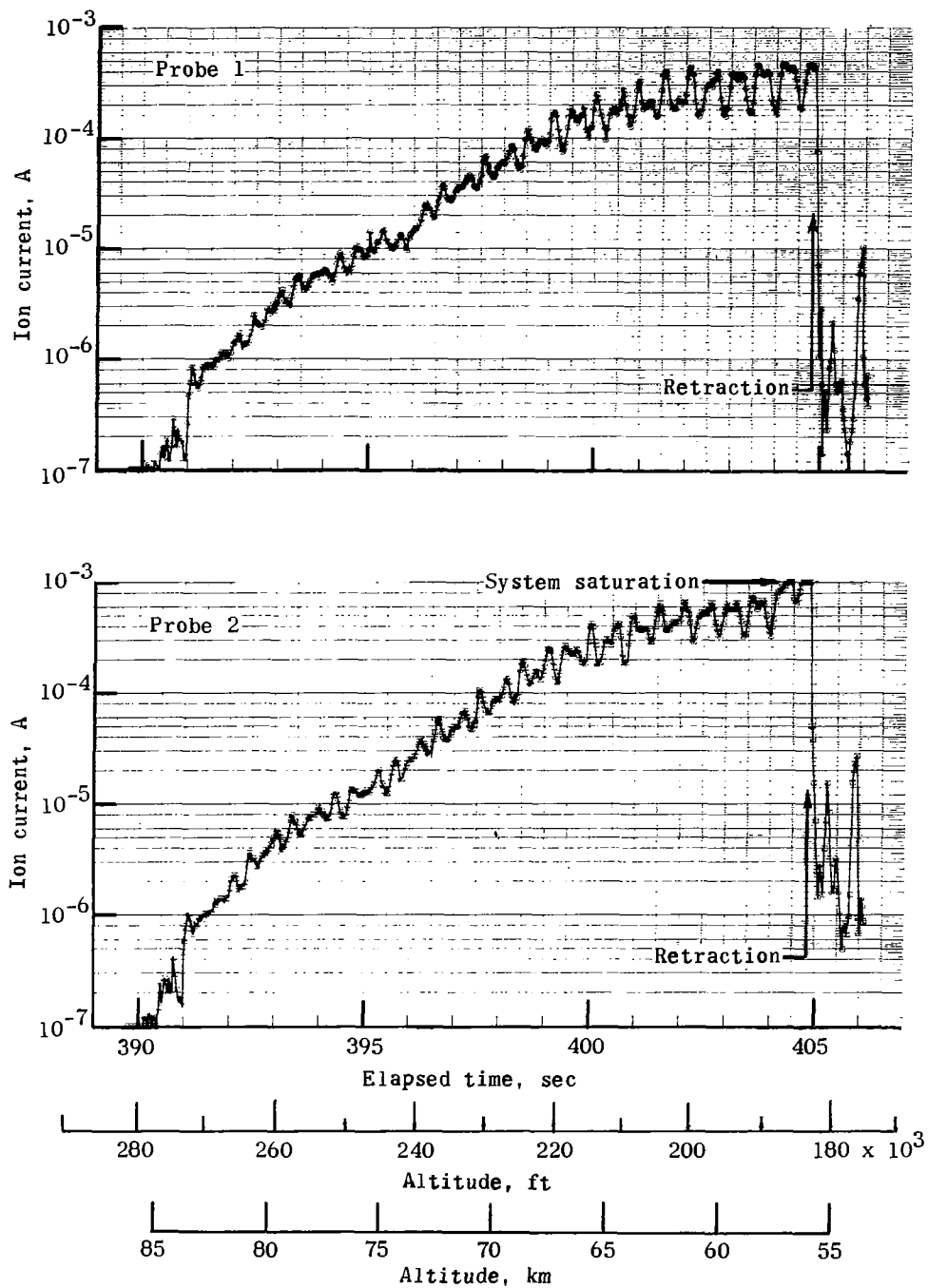
Figure 13.- Continued.



(d) Electrostatic probes 7 and 8.

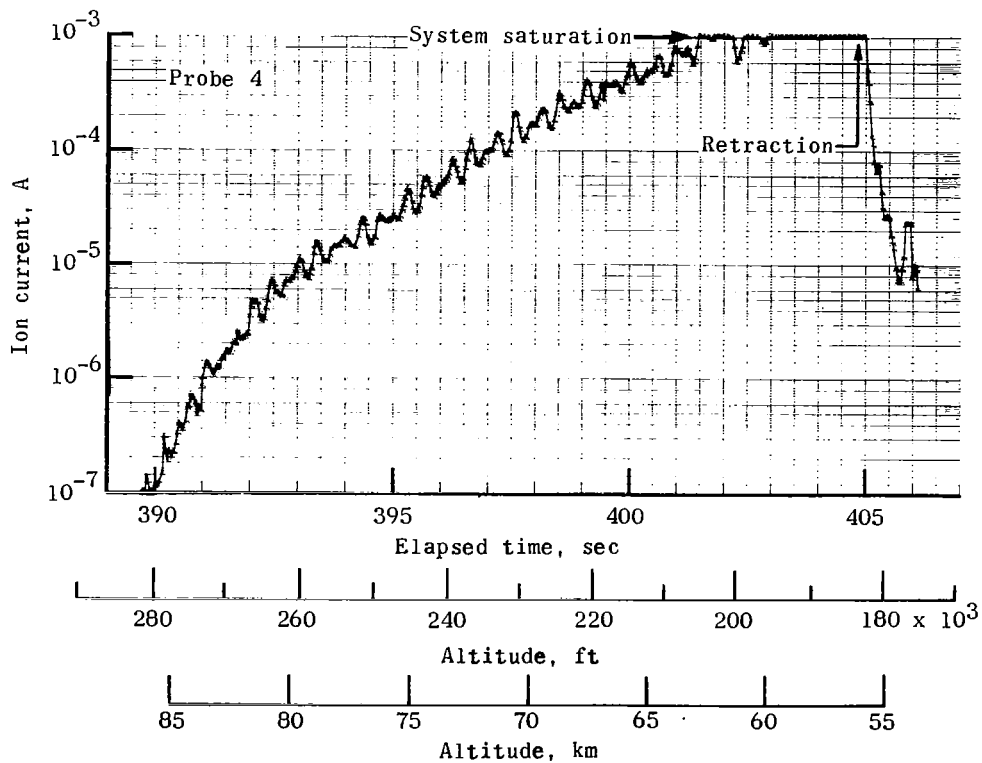
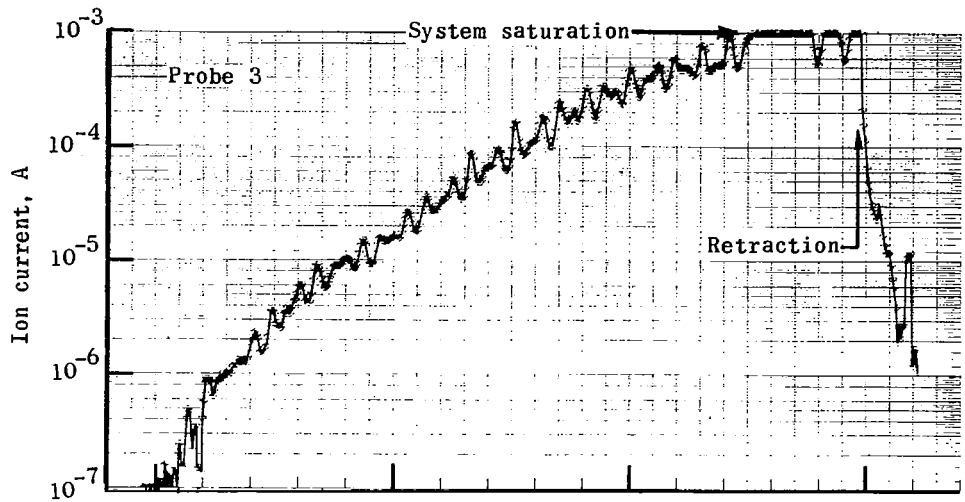
Figure 13.- Concluded.





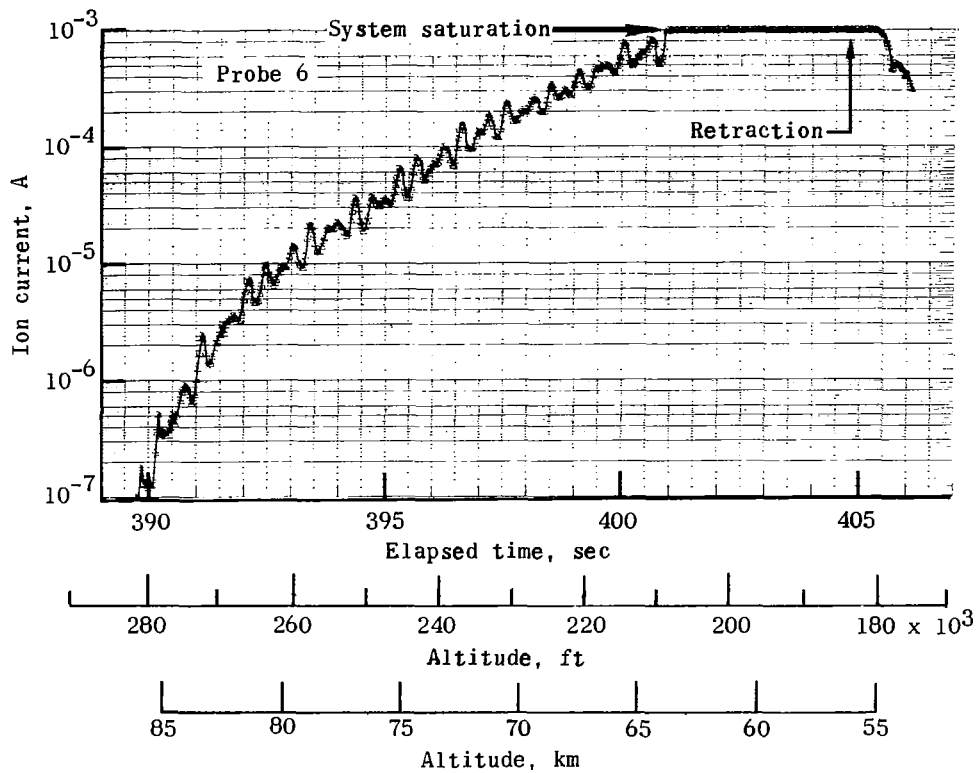
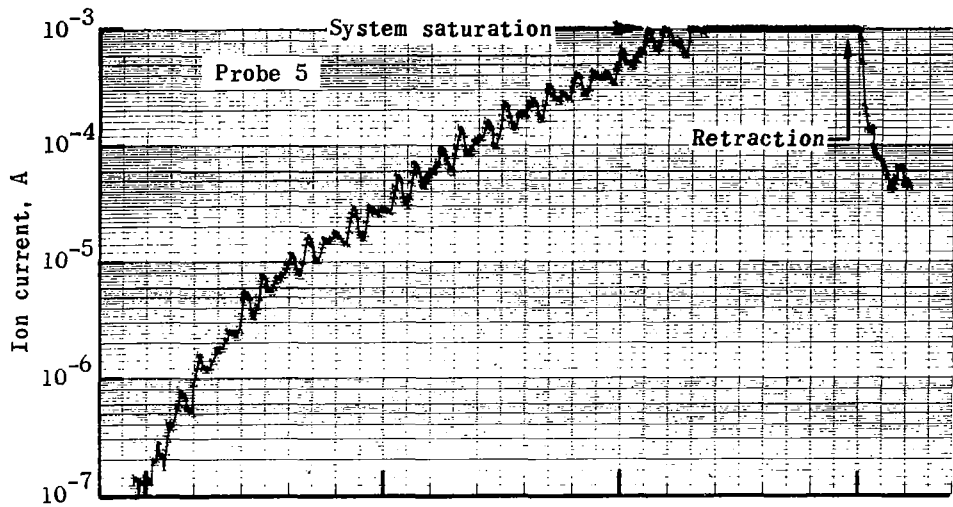
(a) Electrostatic probes 1 and 2.

Figure 14.- Ion current measurements from electrostatic probes on RAM C-II flight experiment. Altitudes shown are 0.3658 km (1200 ft) too low because of use of RAM C-I trajectory.



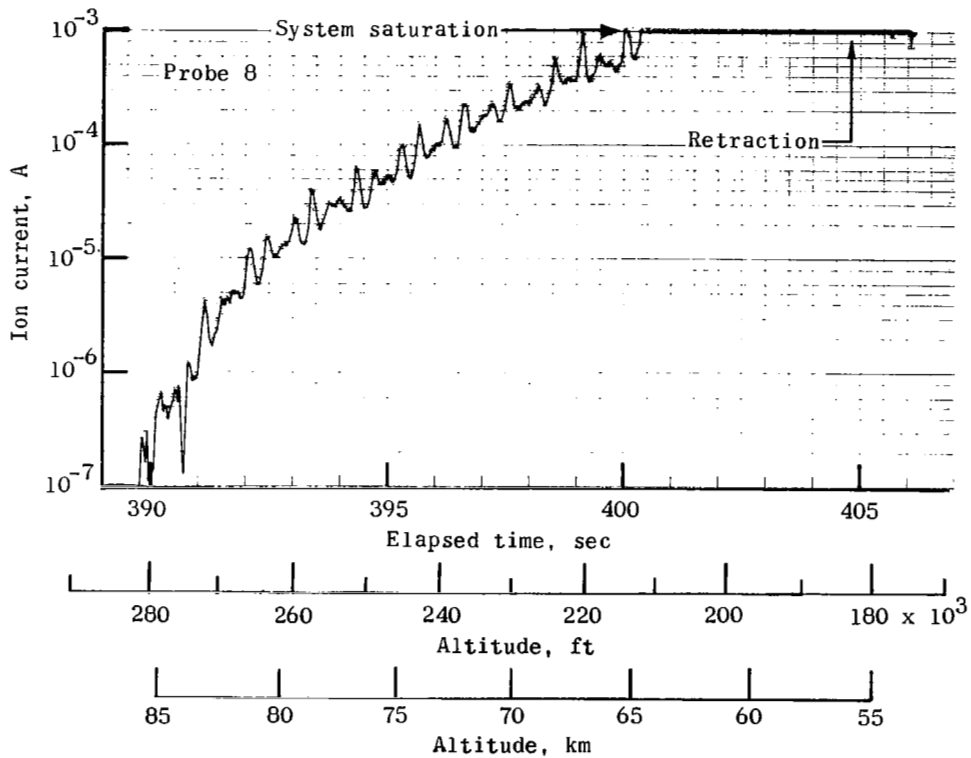
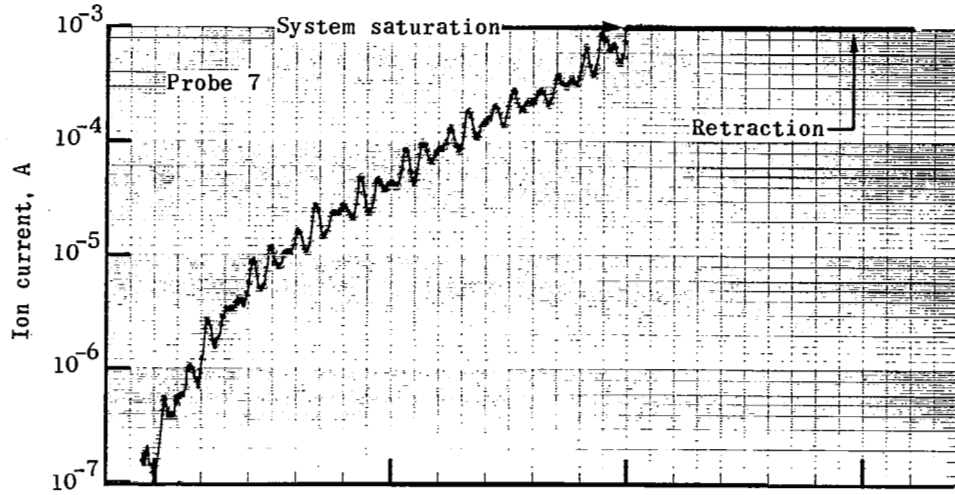
(b) Electrostatic probes 3 and 4.

Figure 14.- Continued.



(c) Electrostatic probes 5 and 6.

Figure 14.- Continued.



(d) Electrostatic probes 7 and 8.

Figure 14.- Concluded.

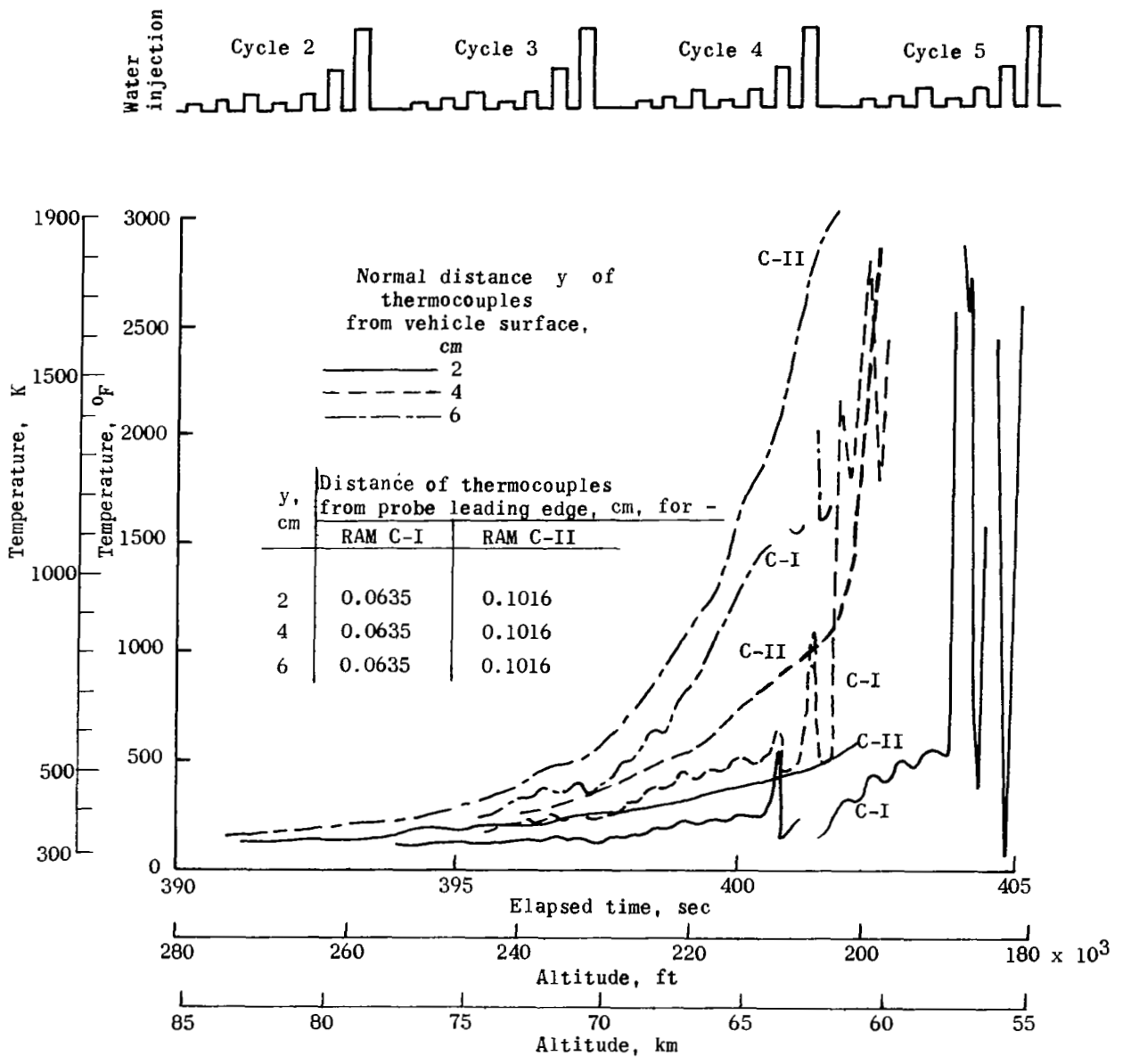


Figure 15.- Comparison of thermocouple-rake leading-edge temperatures.

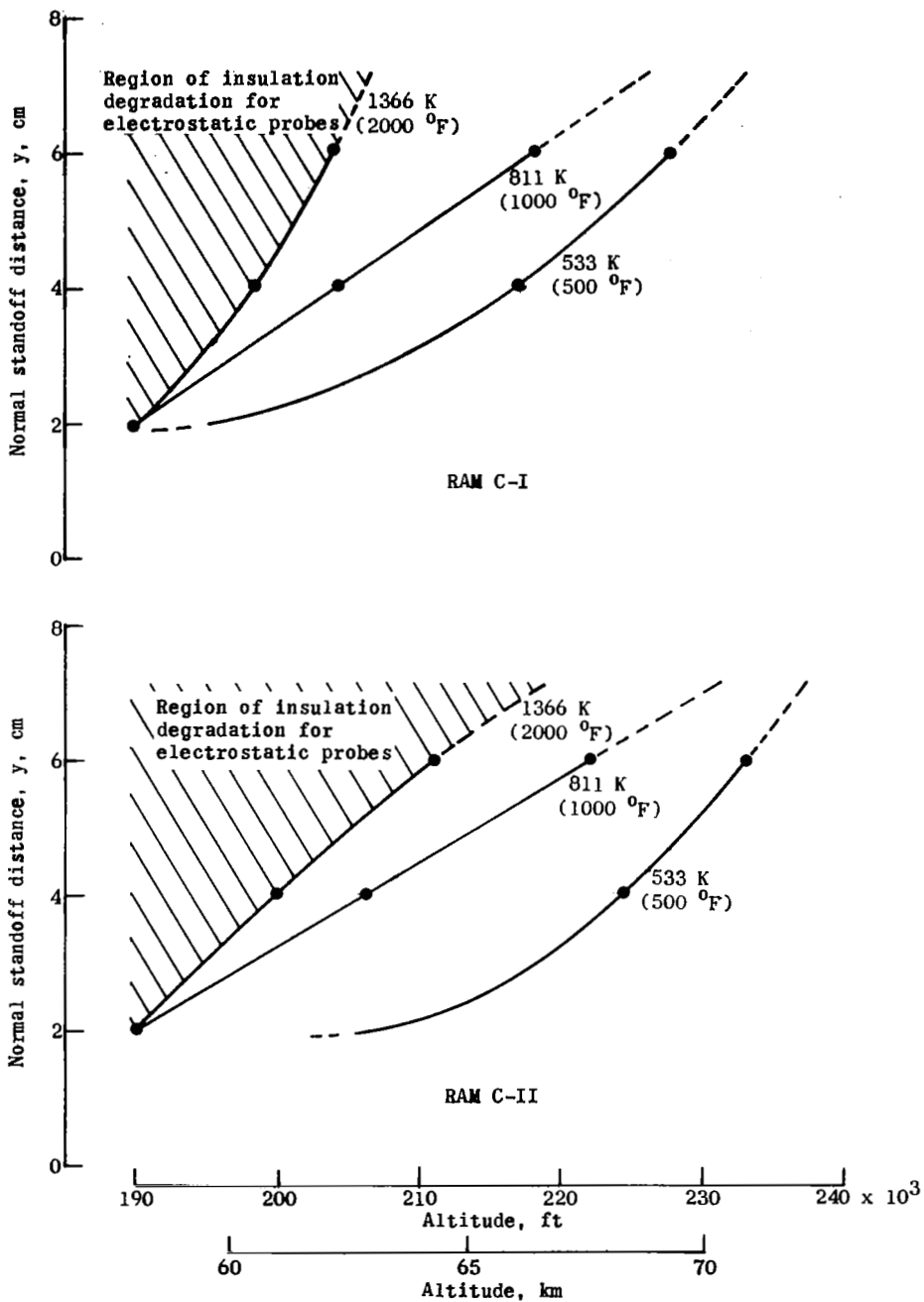
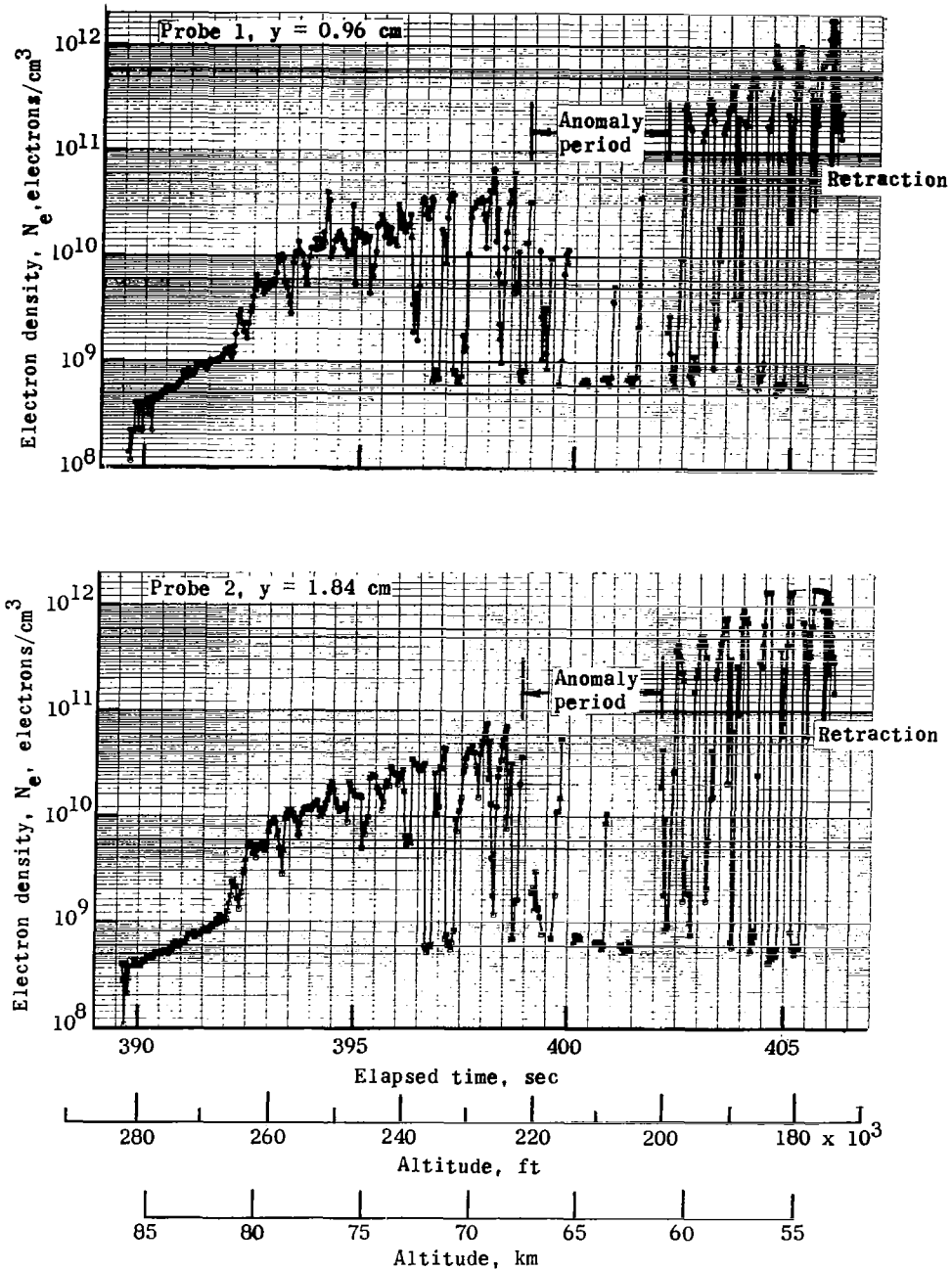
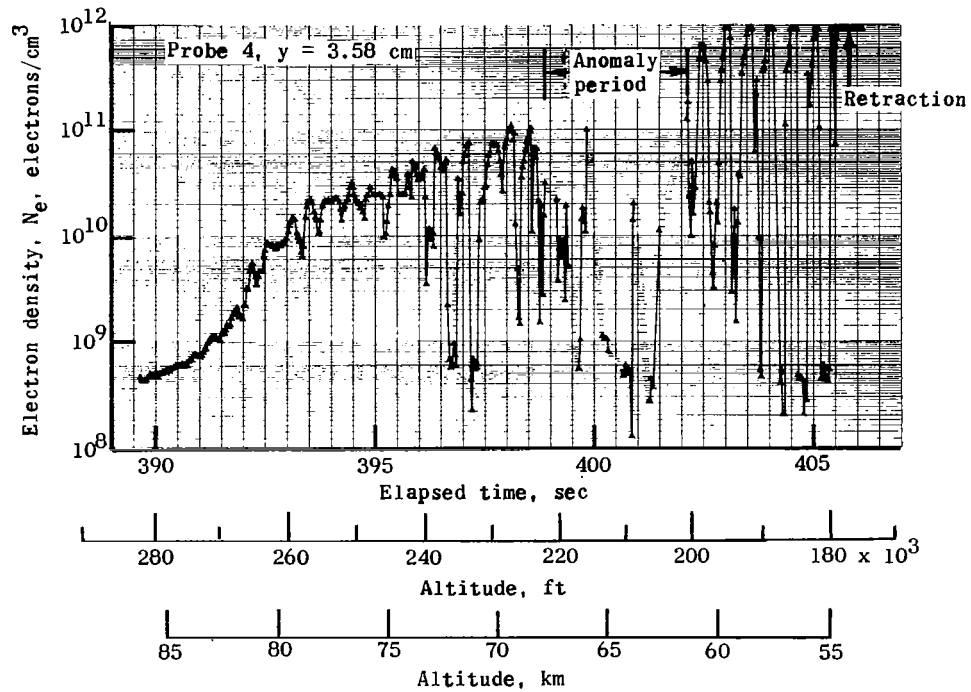
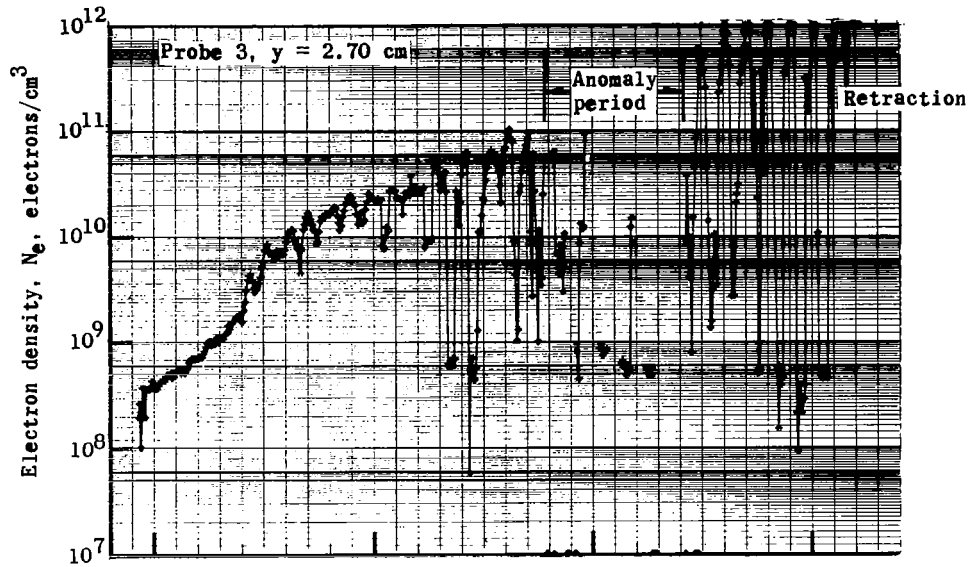


Figure 16.- Constant-temperature profiles from thermocouple measurements.



(a) Electrostatic probes 1 and 2.

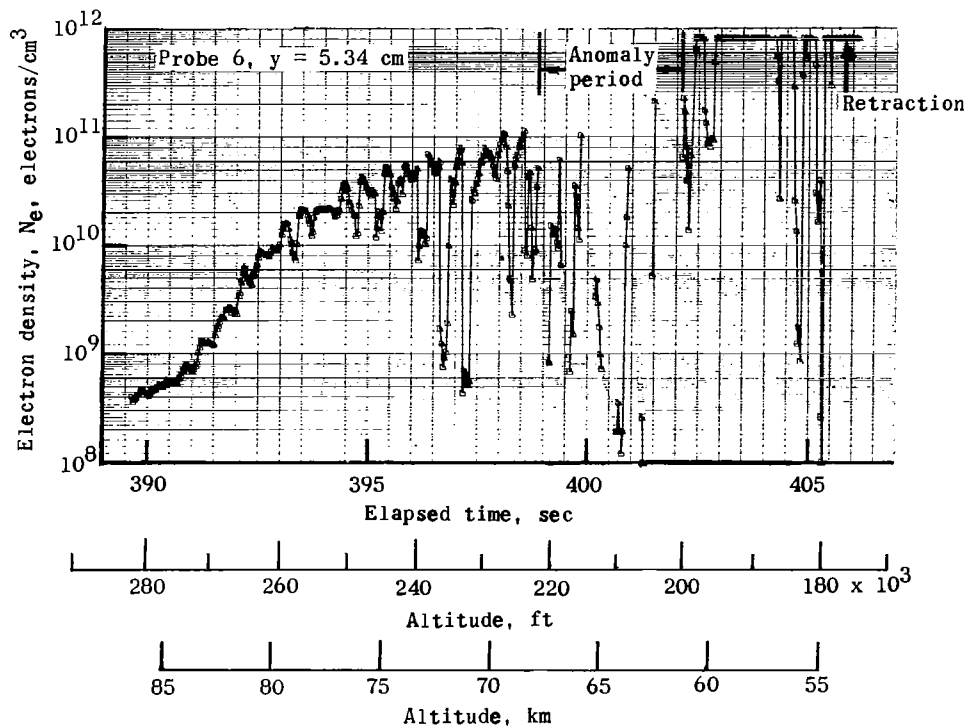
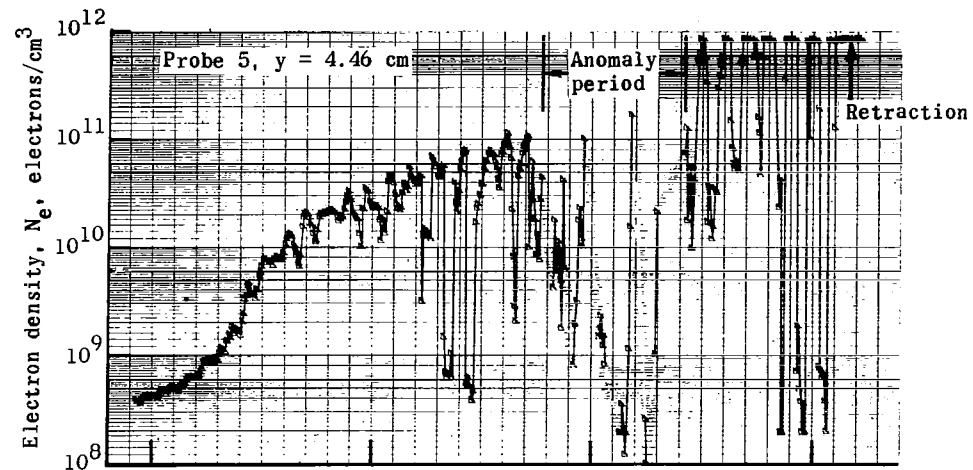
Figure 17.- Electron density of RAM C-I flow field at standoff distances  $y$  ranging between 1 and 7 cm as inferred from electrostatic probe measurements.



(b) Electrostatic probes 3 and 4.

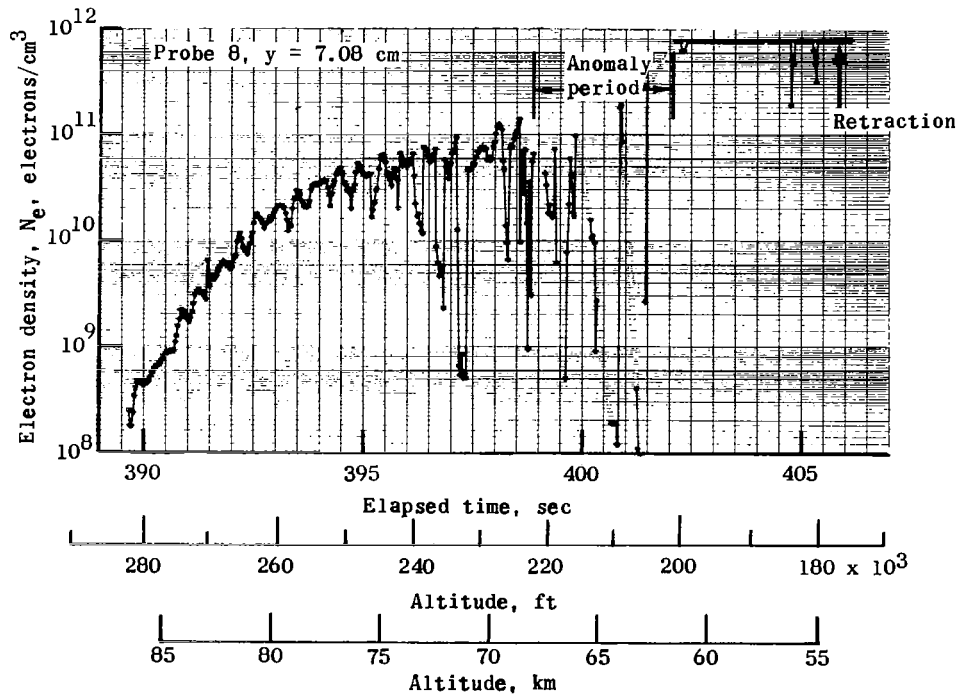
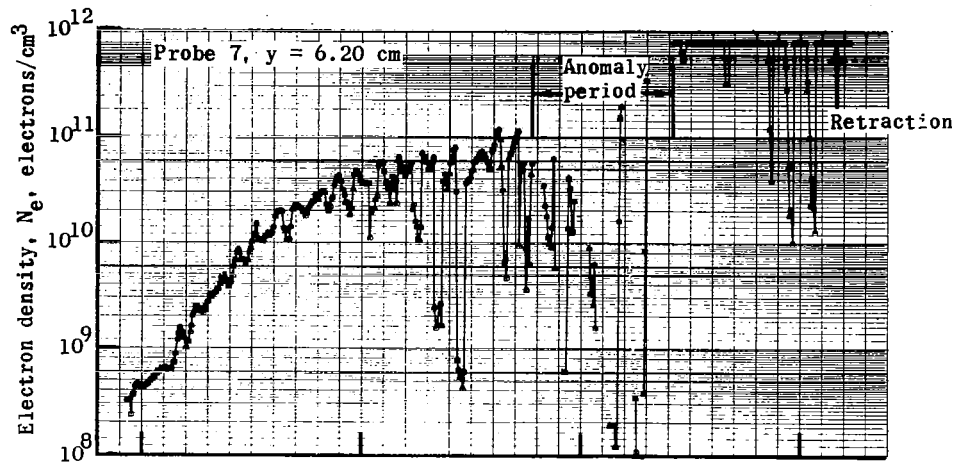
Figure 17.- Continued.





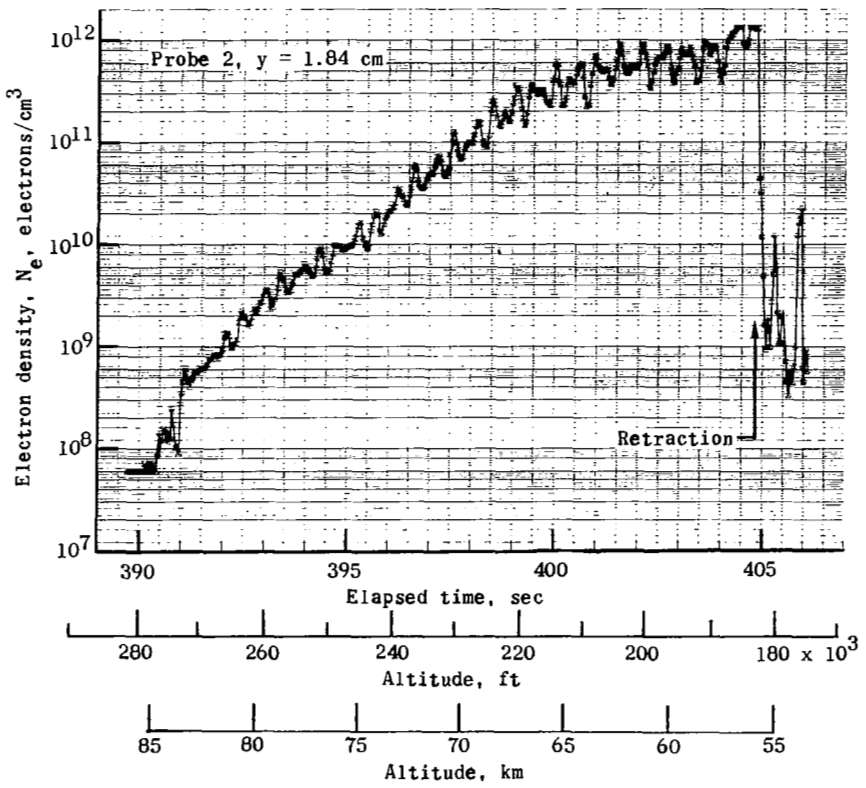
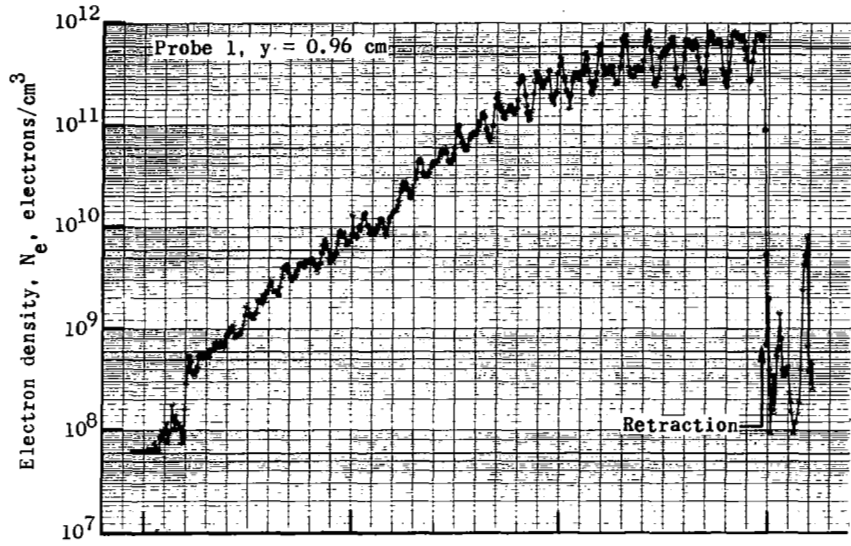
(c) Electrostatic probes 5 and 6.

Figure 17.- Continued.



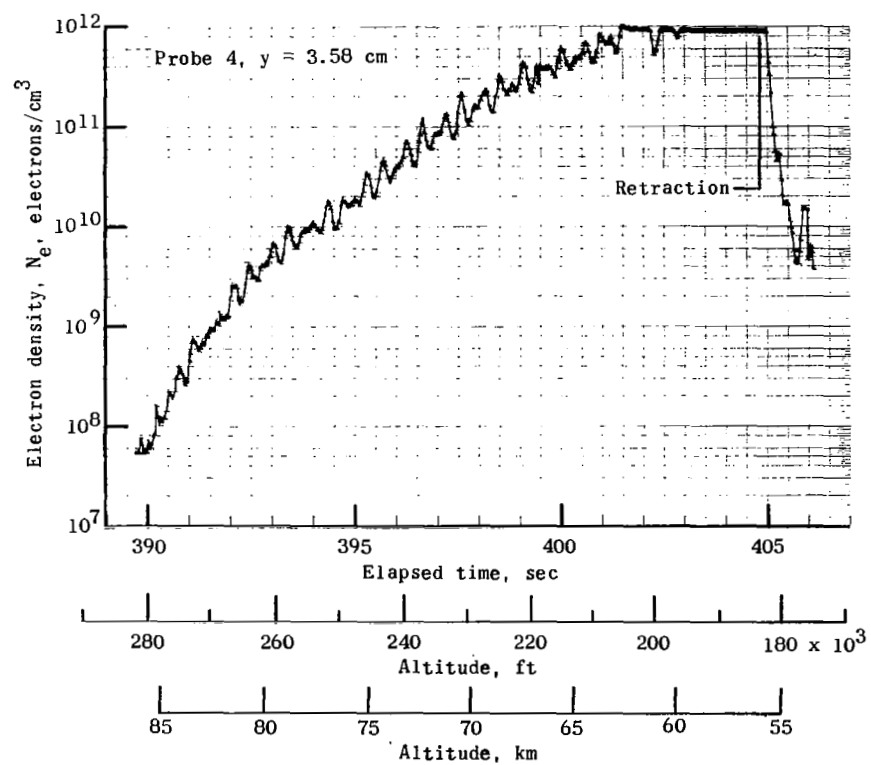
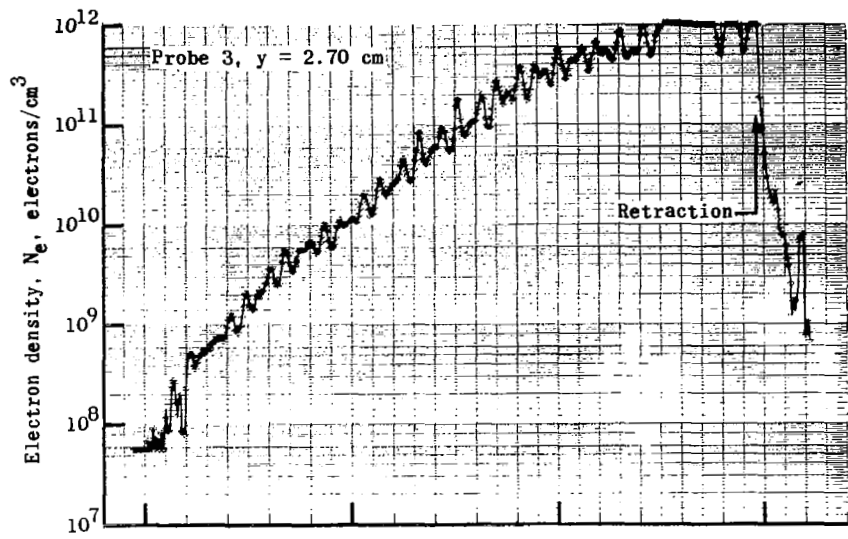
(d) Electrostatic probes 7 and 8.

Figure 17.- Concluded.



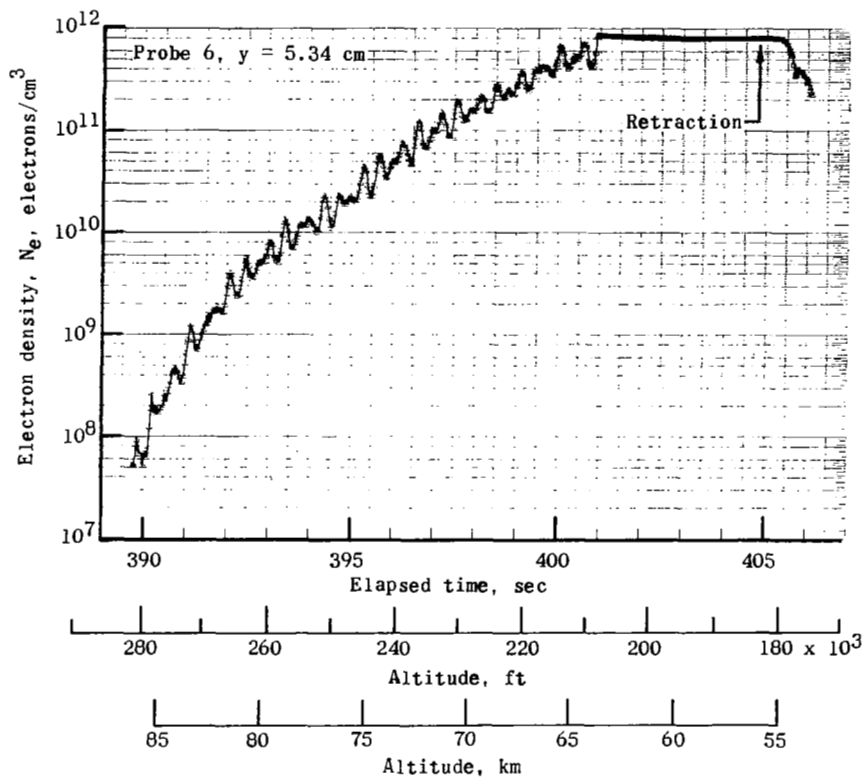
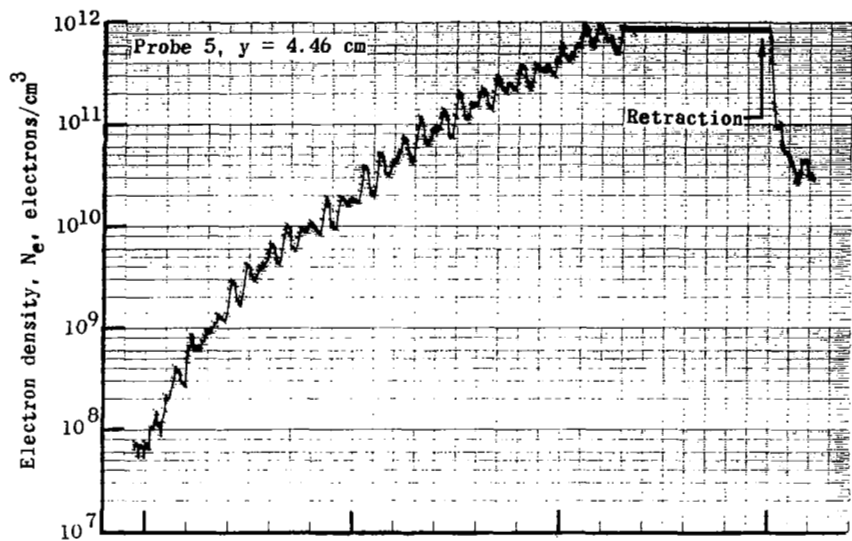
(a) Electrostatic probes 1 and 2.

Figure 18.- Electron density of RAM C-II flow field at standoff distances  $y$  ranging between 1 and 7 cm as inferred from electrostatic probe measurements. Altitudes shown are 0.3658 km (1200 ft) too low because of use of RAM C-I trajectory.



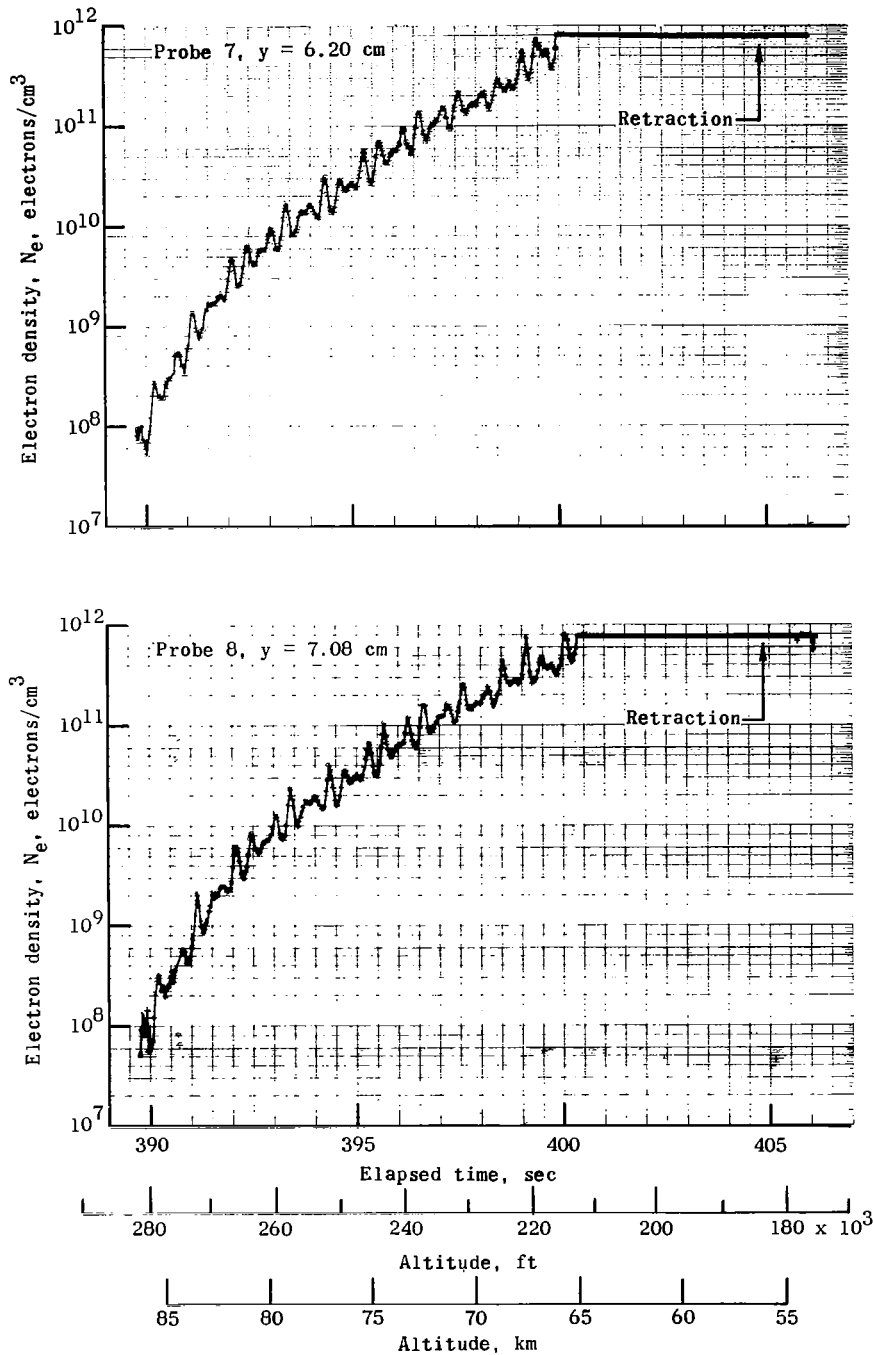
(b) Electrostatic probes 3 and 4.

Figure 18.- Continued.



(c) Electrostatic probes 5 and 6.

Figure 18.- Continued.



(d) Electrostatic probes 7 and 8.

Figure 18.- Concluded.

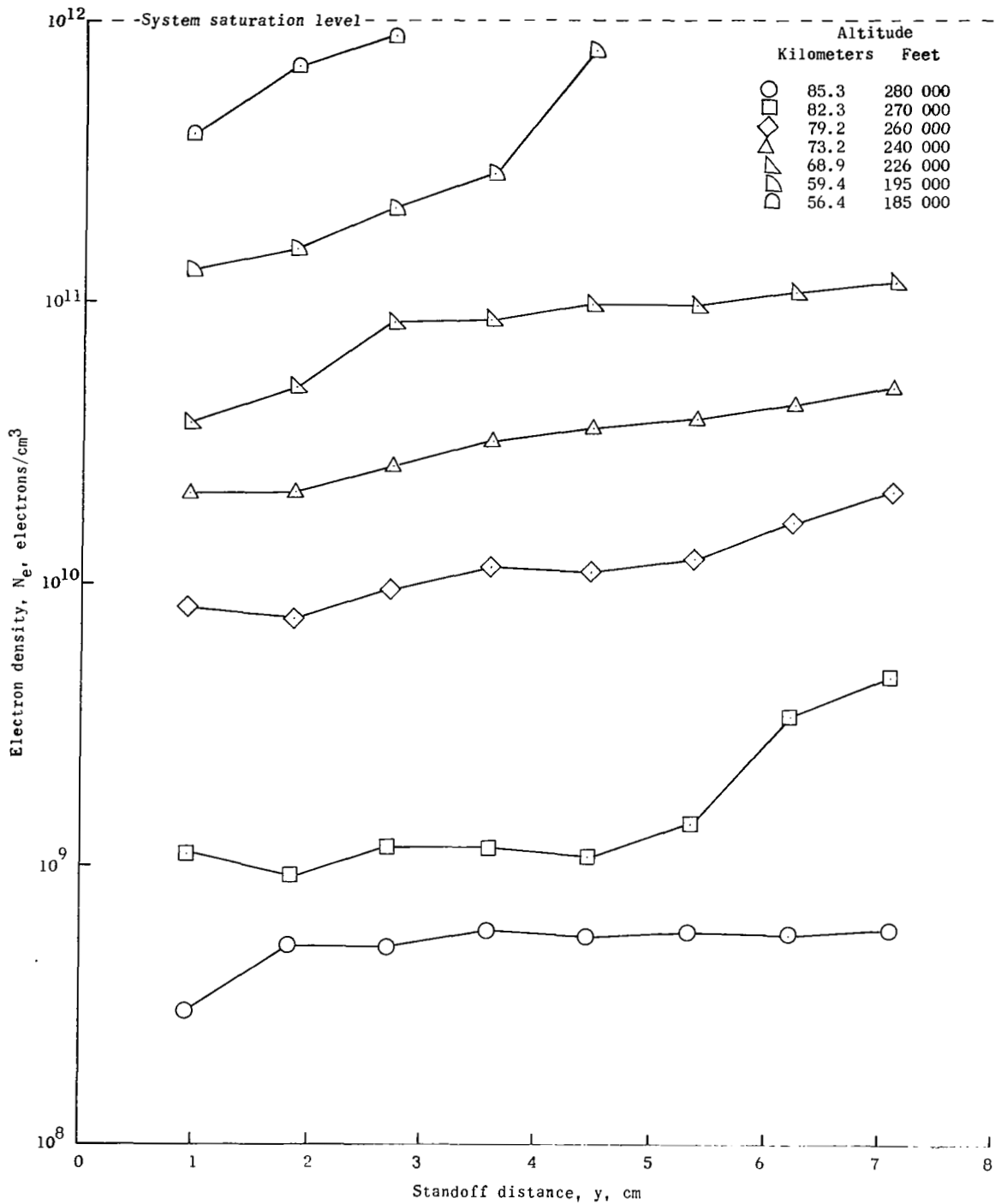


Figure 19.- Measured time-average electron density profiles for RAM C-I at selected altitudes during no water injection.

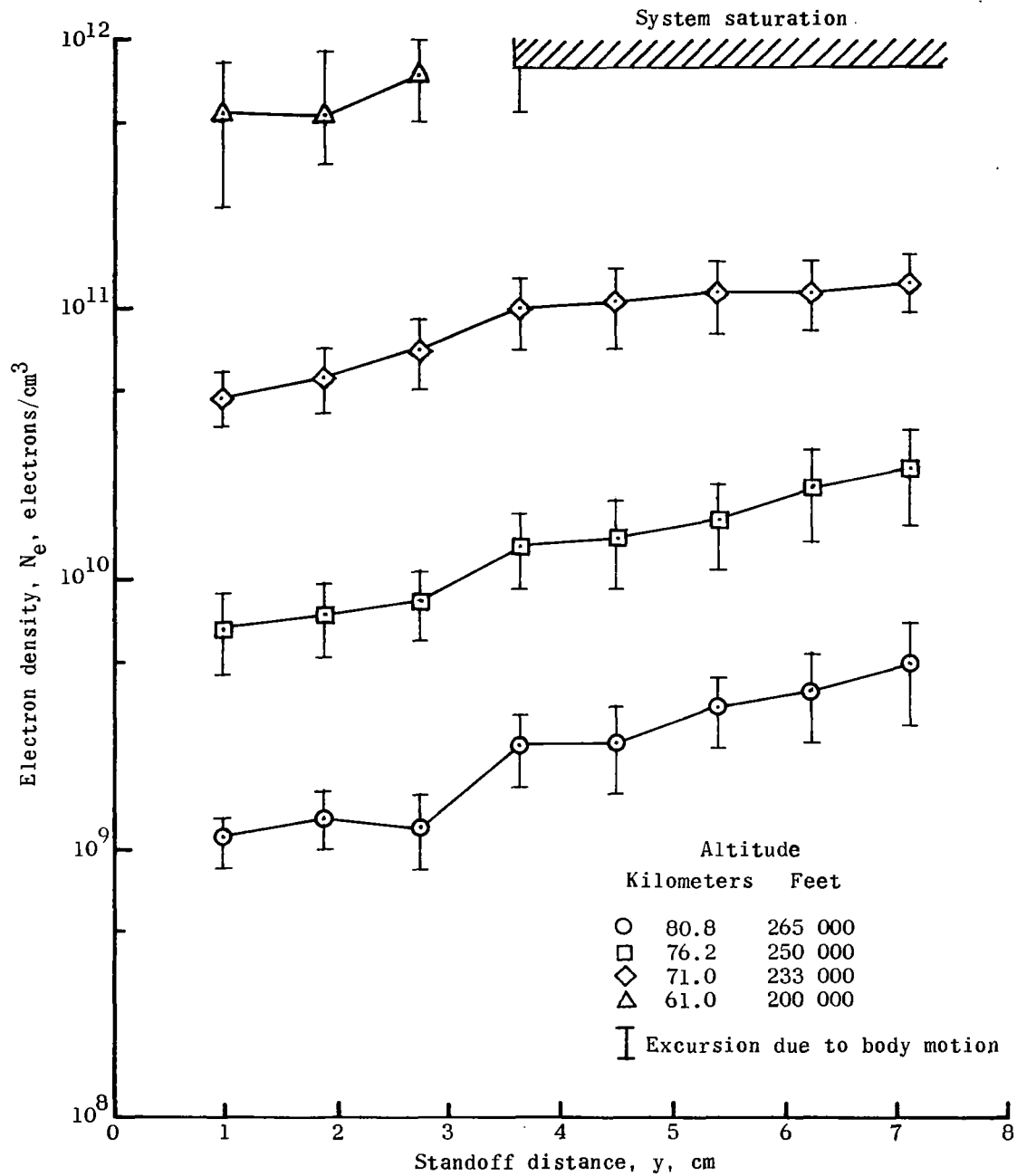
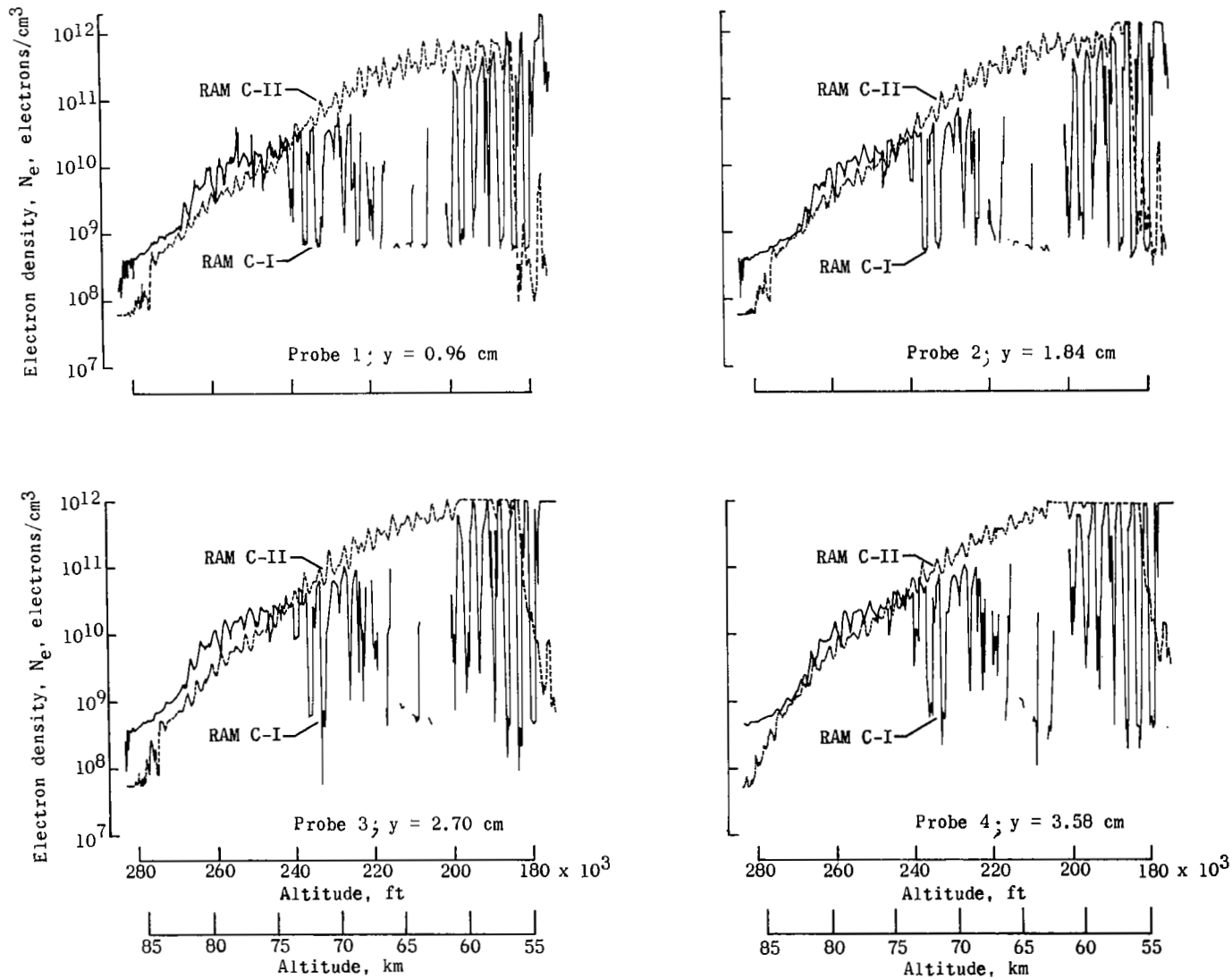


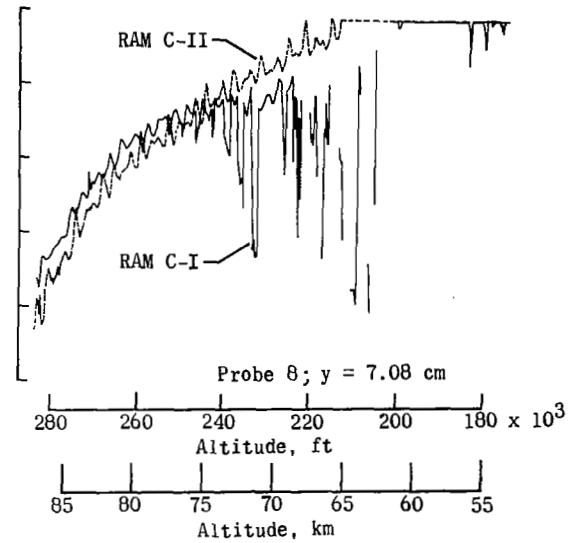
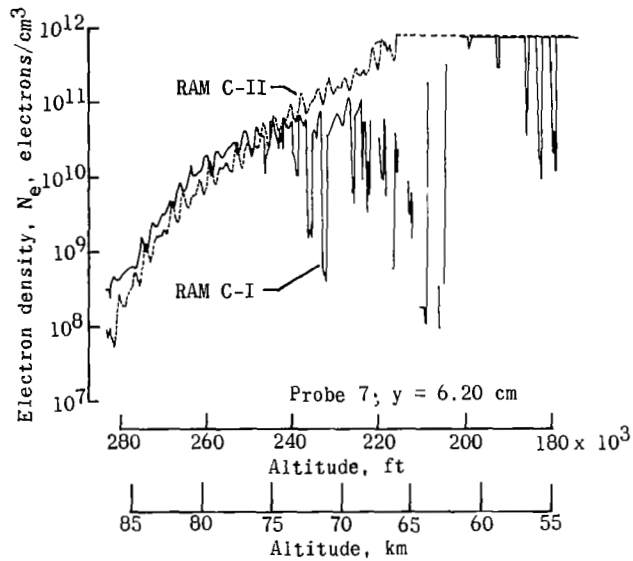
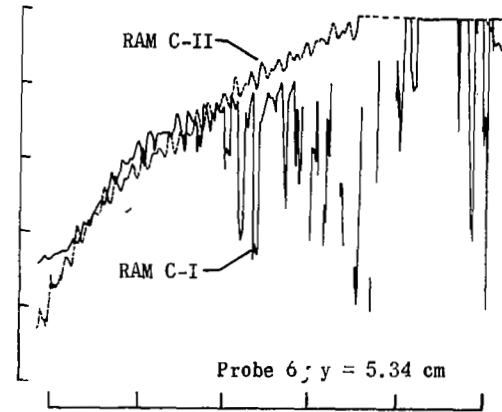
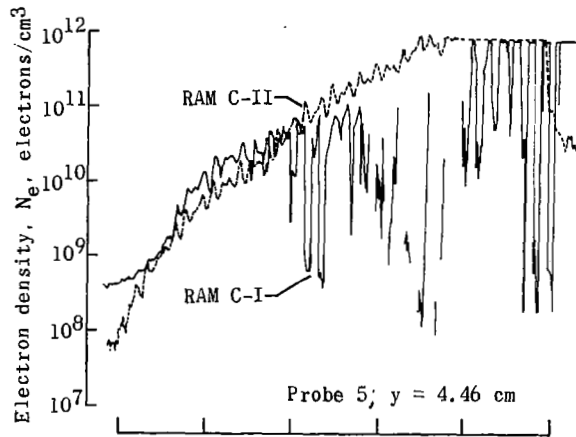
Figure 20.- Measured time-average electron density profiles for RAM C-II at four altitudes.





(a) Probes 1 to 4.

Figure 21.- Comparison of measured electron densities for individual probes on RAM C-I and C-II. Altitudes for RAM C-II data are 0.3658 km (1200 ft) too low because of use of RAM C-I trajectory.



(b) Probes 5 to 8.

Figure 21.- Concluded.

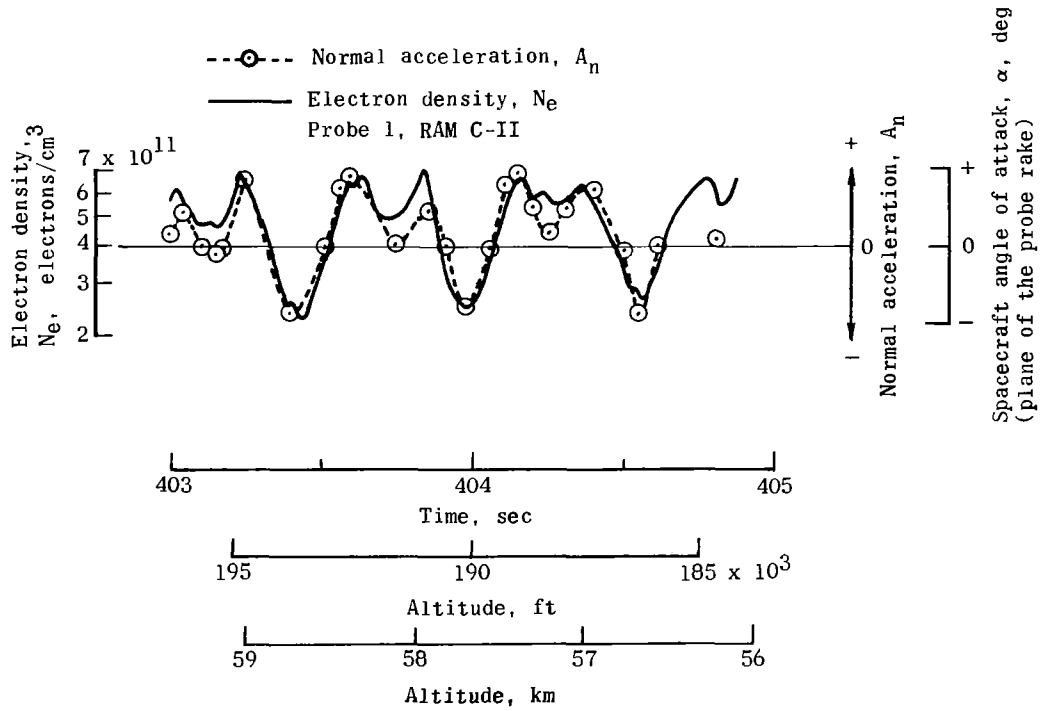
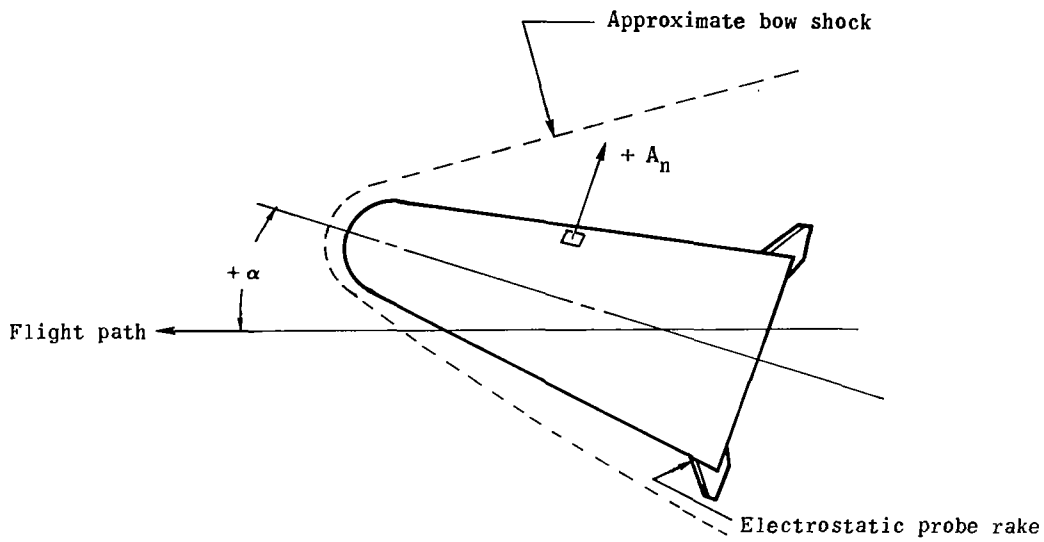


Figure 22.- Correlation of RAM C-II fixed-bias electrostatic probe measurements with spacecraft angle-of-attack motions.

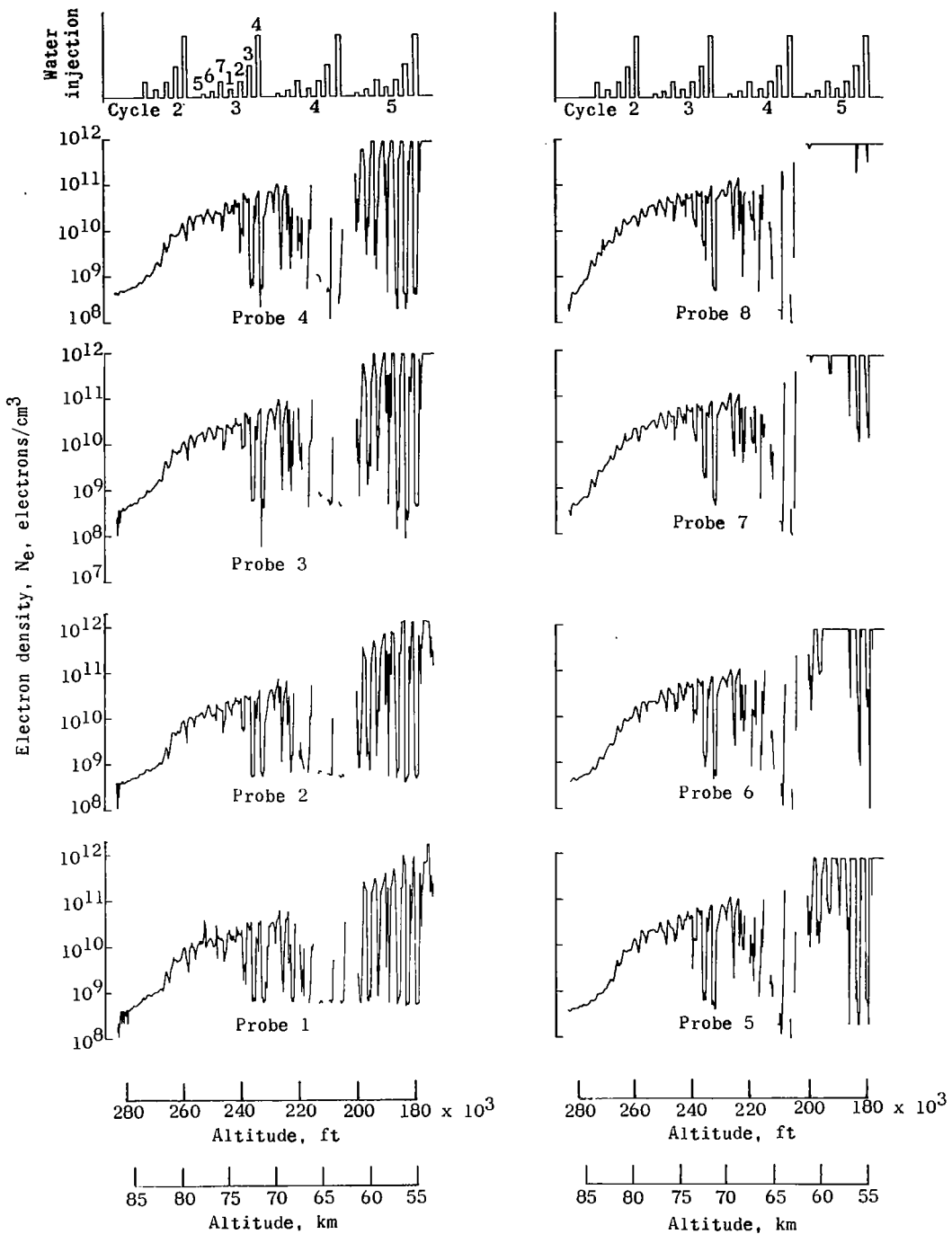


Figure 23.- Effects of water injection on electron density as inferred by RAM C-I electrostatic probes.

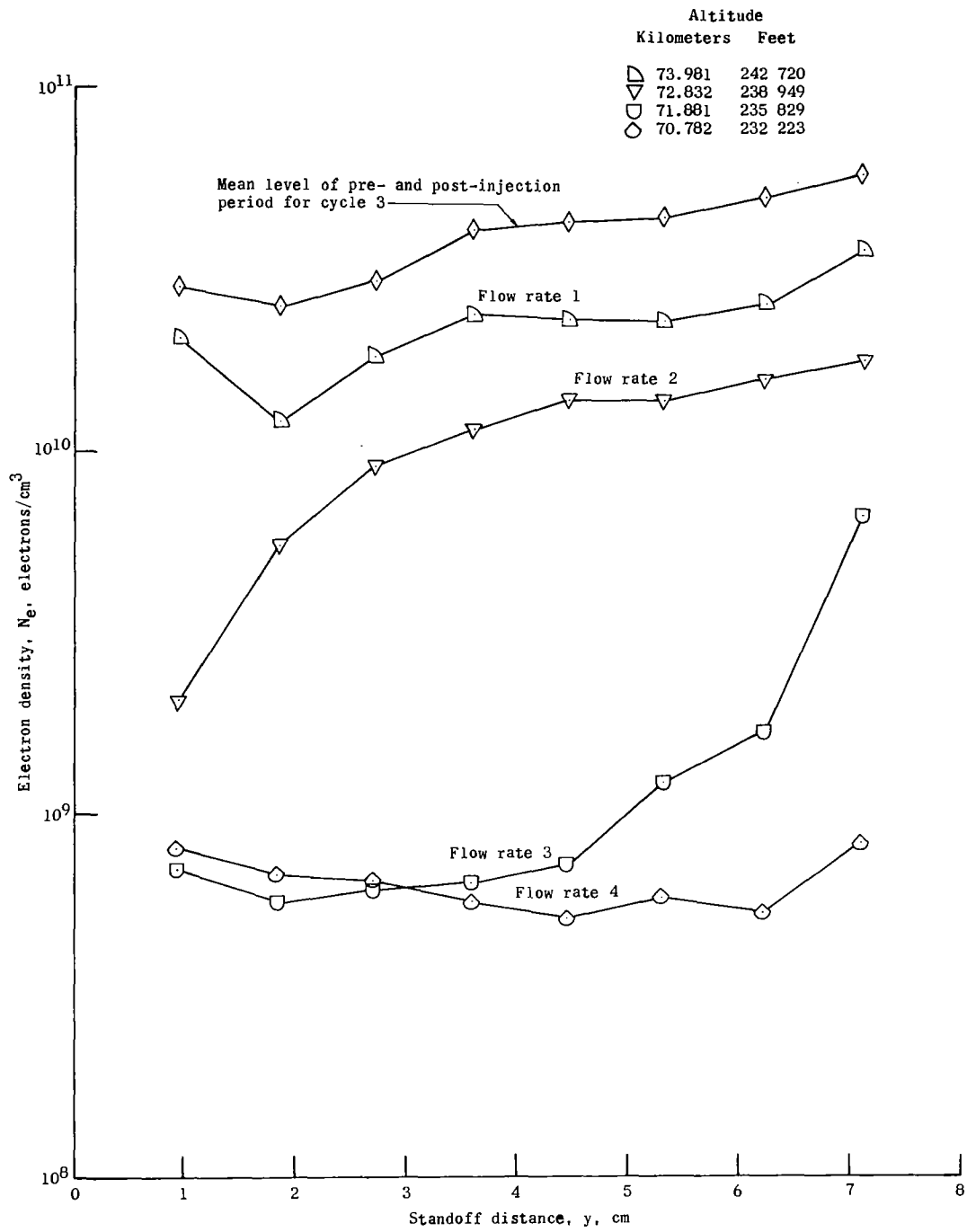


Figure 24.- RAM C-I electron-density distribution profiles during side injection portion of cycle 3.

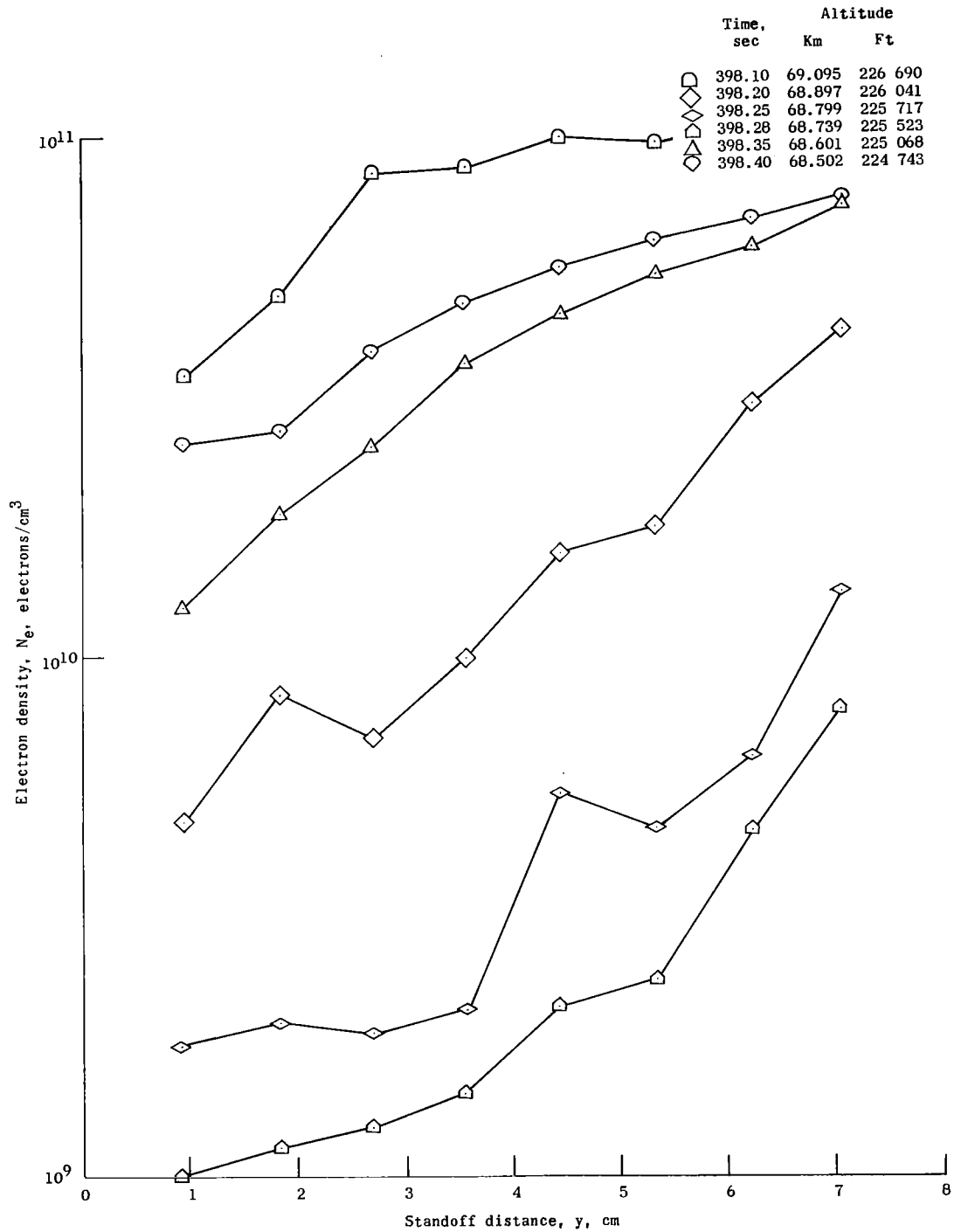


Figure 25.- Effect of stagnation injection at flow rate 5 of cycle 4 on RAM C-I electron density distribution profiles at various altitudes.

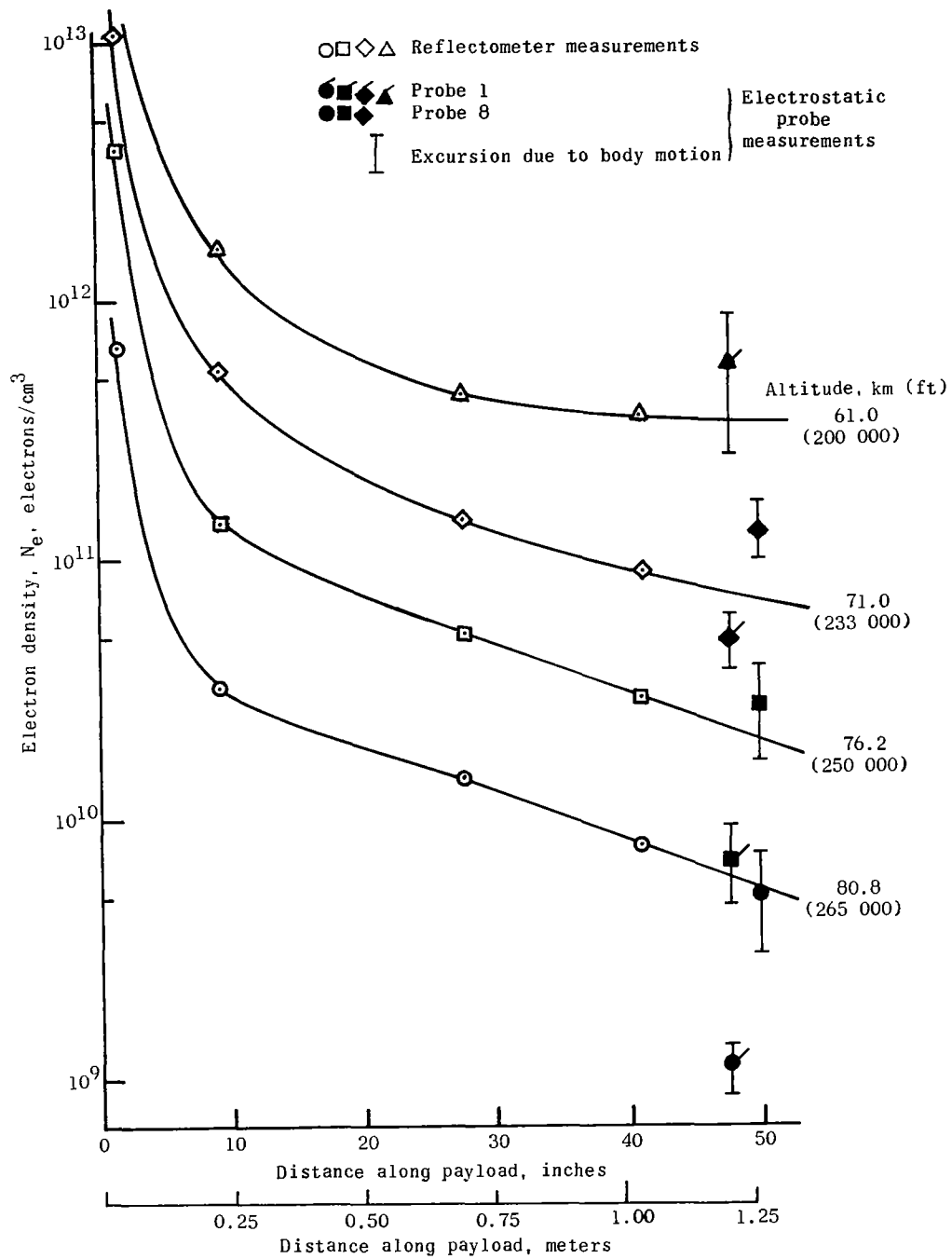


Figure 26.- RAM C-II longitudinal profiles of inferred peak electron density for constant altitudes.

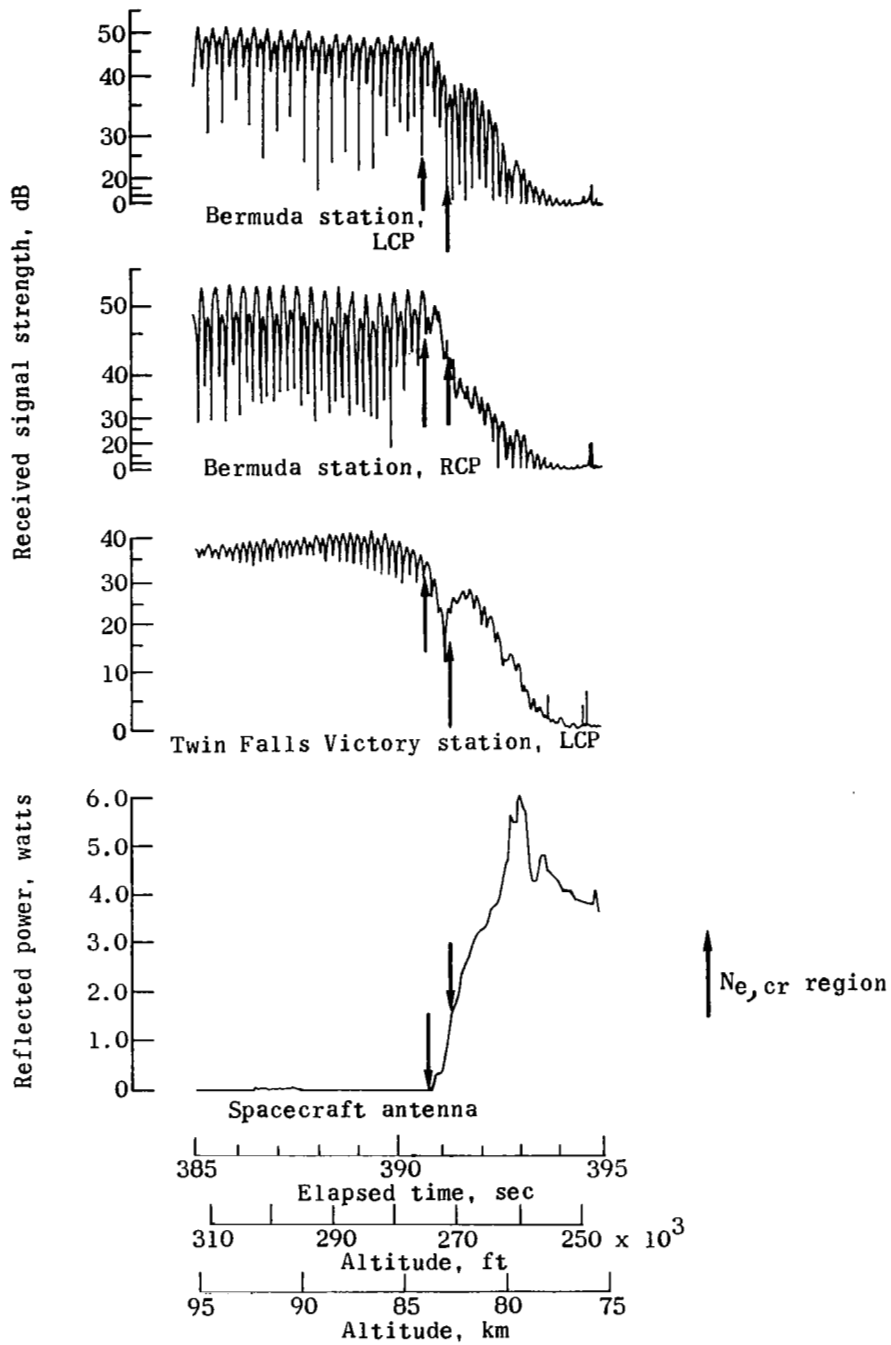


Figure 27.- Effects of RAM C-I reentry plasma on 225.7 MHz telemetry antenna. LCP, left circular polarization; RCP, right circular polarization.



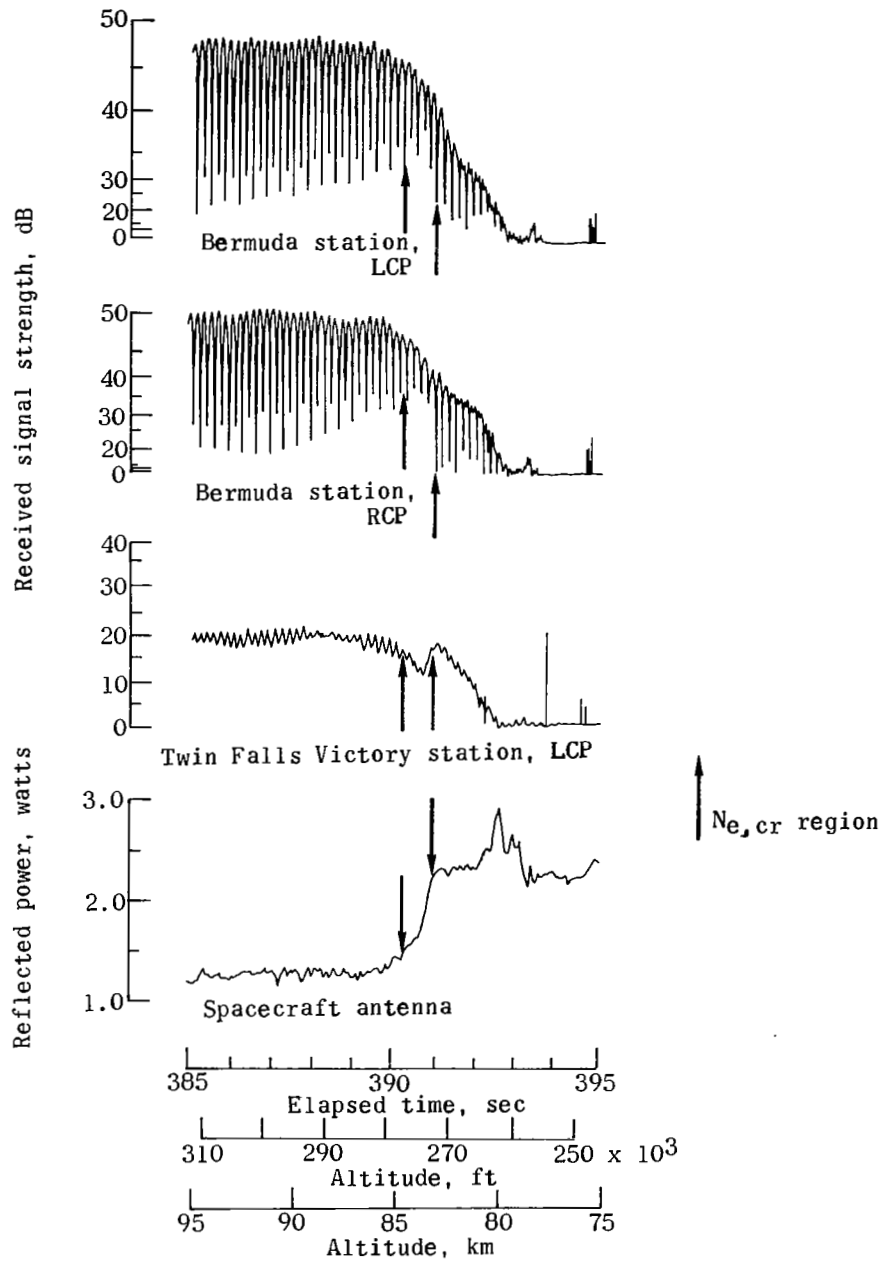


Figure 28. - Effects of RAM C-I reentry plasma on 259.7 MHz telemetry antenna. LCP, left circular polarization; RCP, right circular polarization.

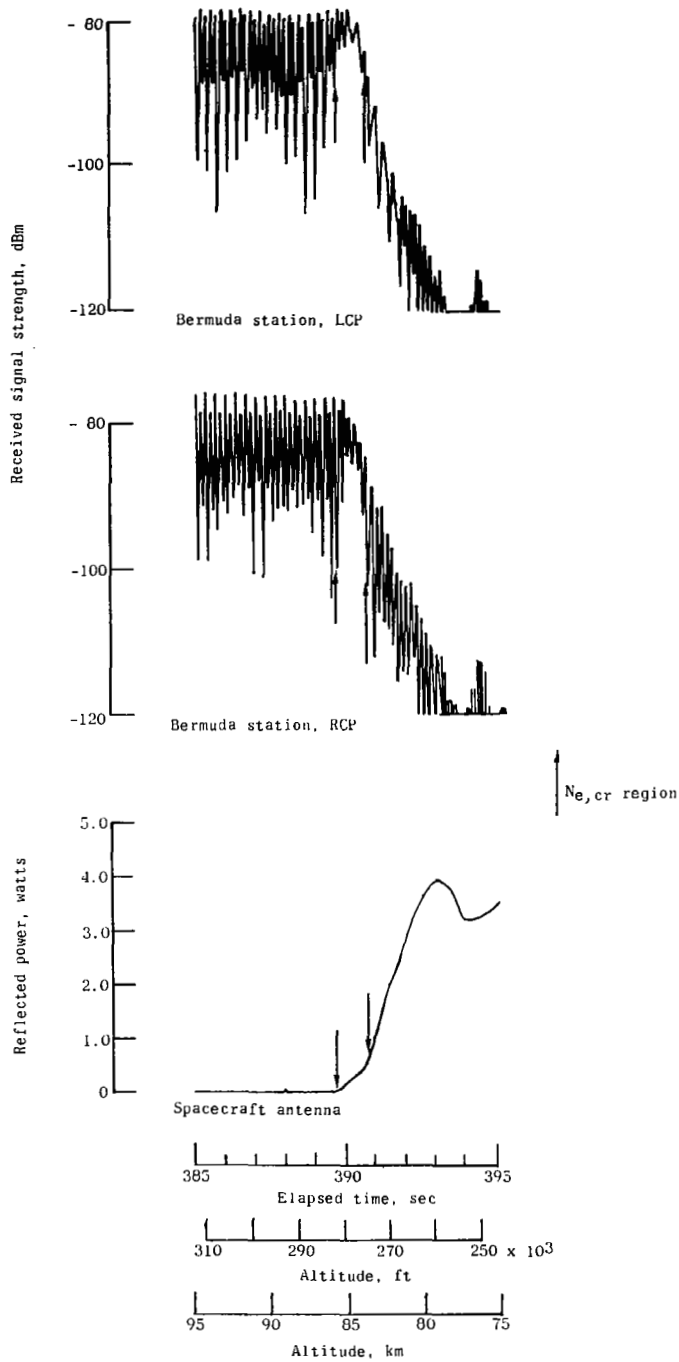


Figure 29.- Effects of RAM C-II reentry plasma on 225.7 MHz telemetry antenna. LCP, left circular polarization; RCP, right circular polarization.

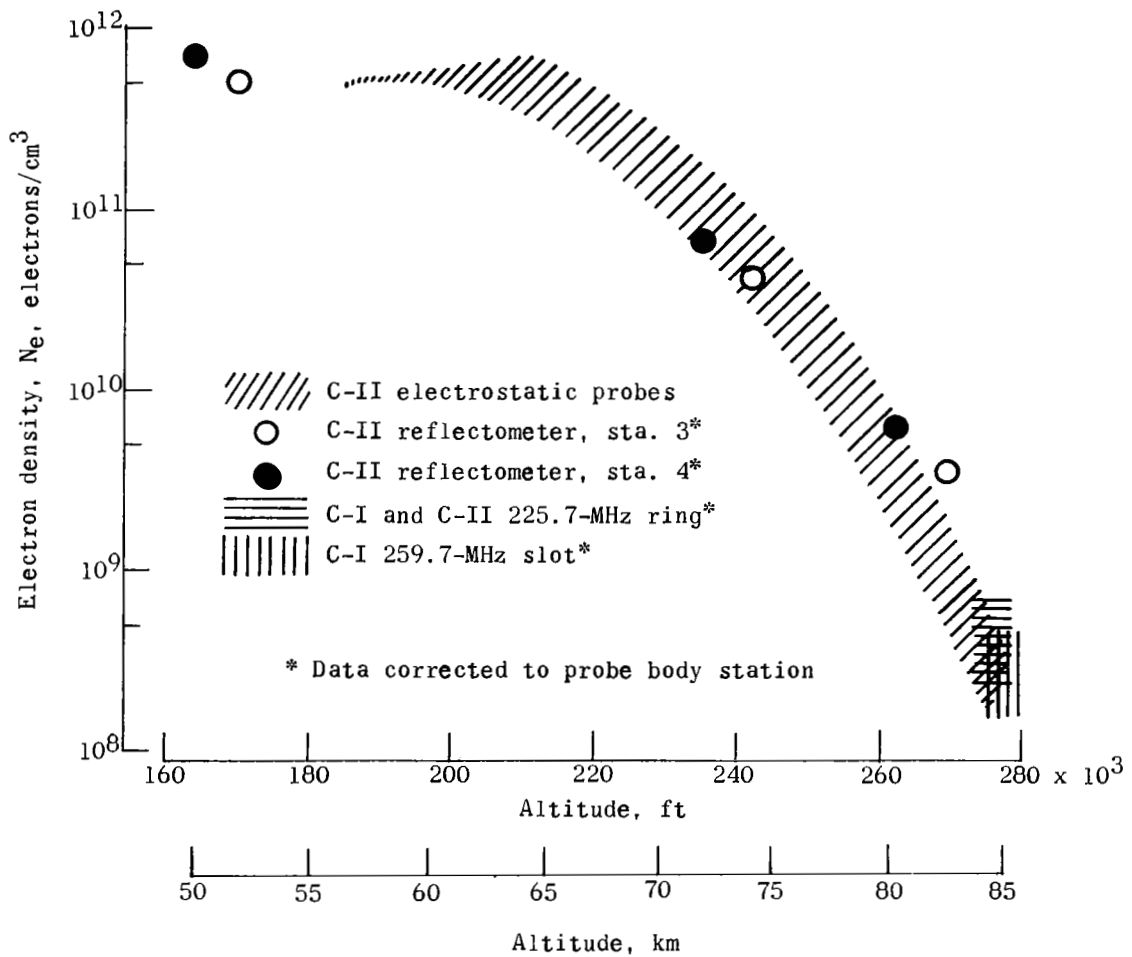


Figure 30.- Comparison of inferred electron densities.

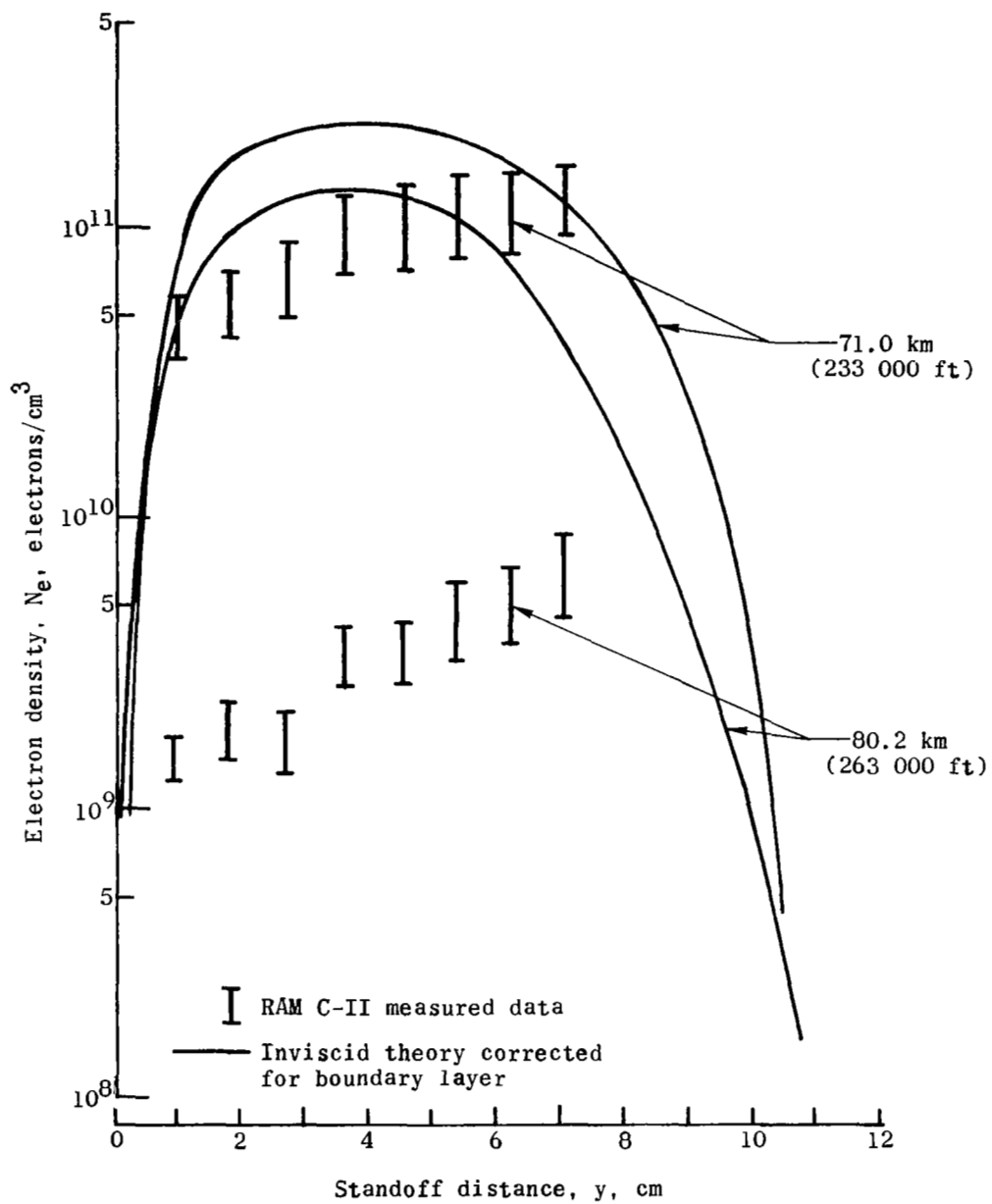


Figure 31.- Comparison of RAM C-II electrostatic probe measured data with theoretical electron density profiles.

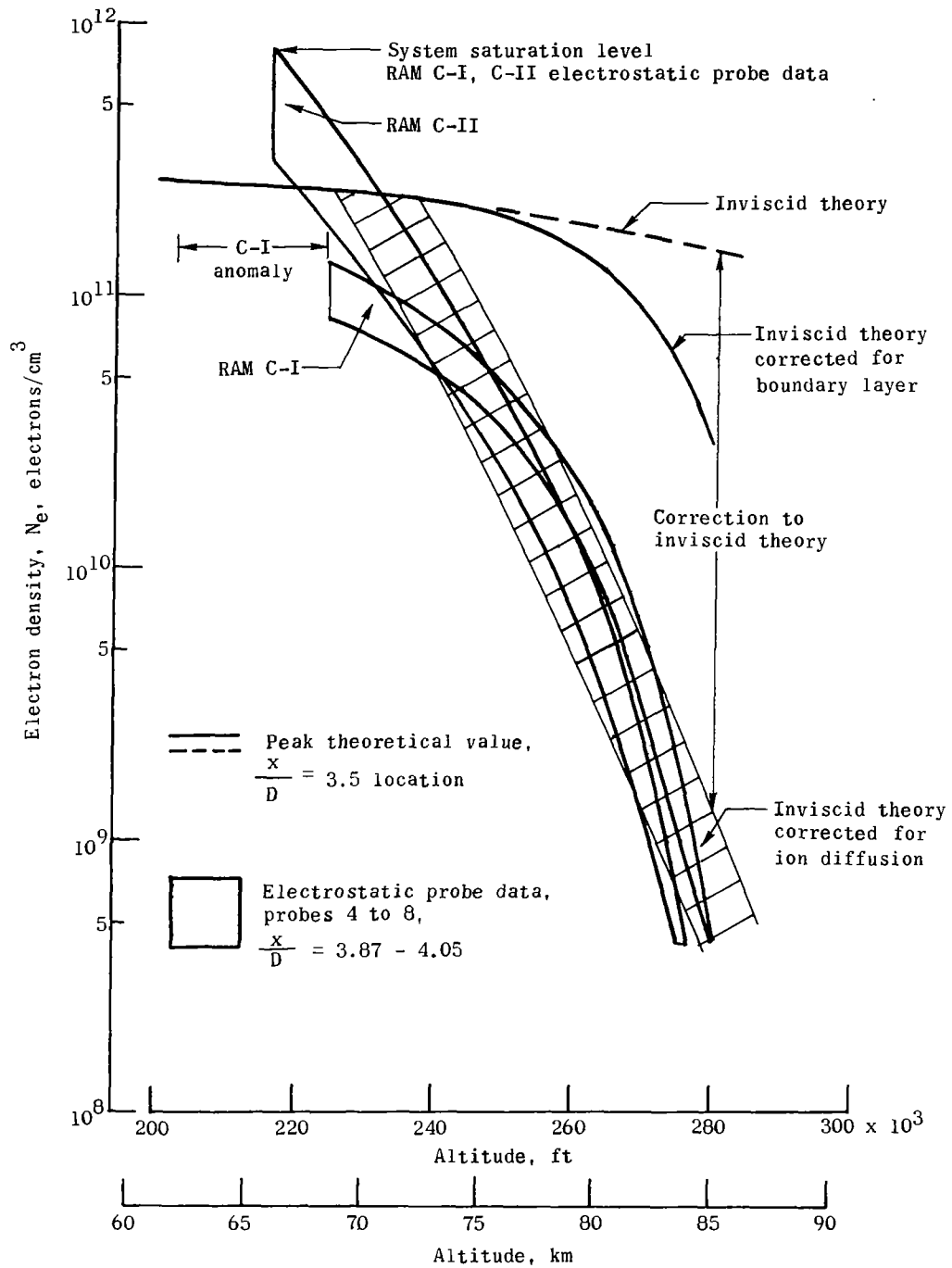


Figure 32.- Comparison of high-altitude electron density at aft body station.

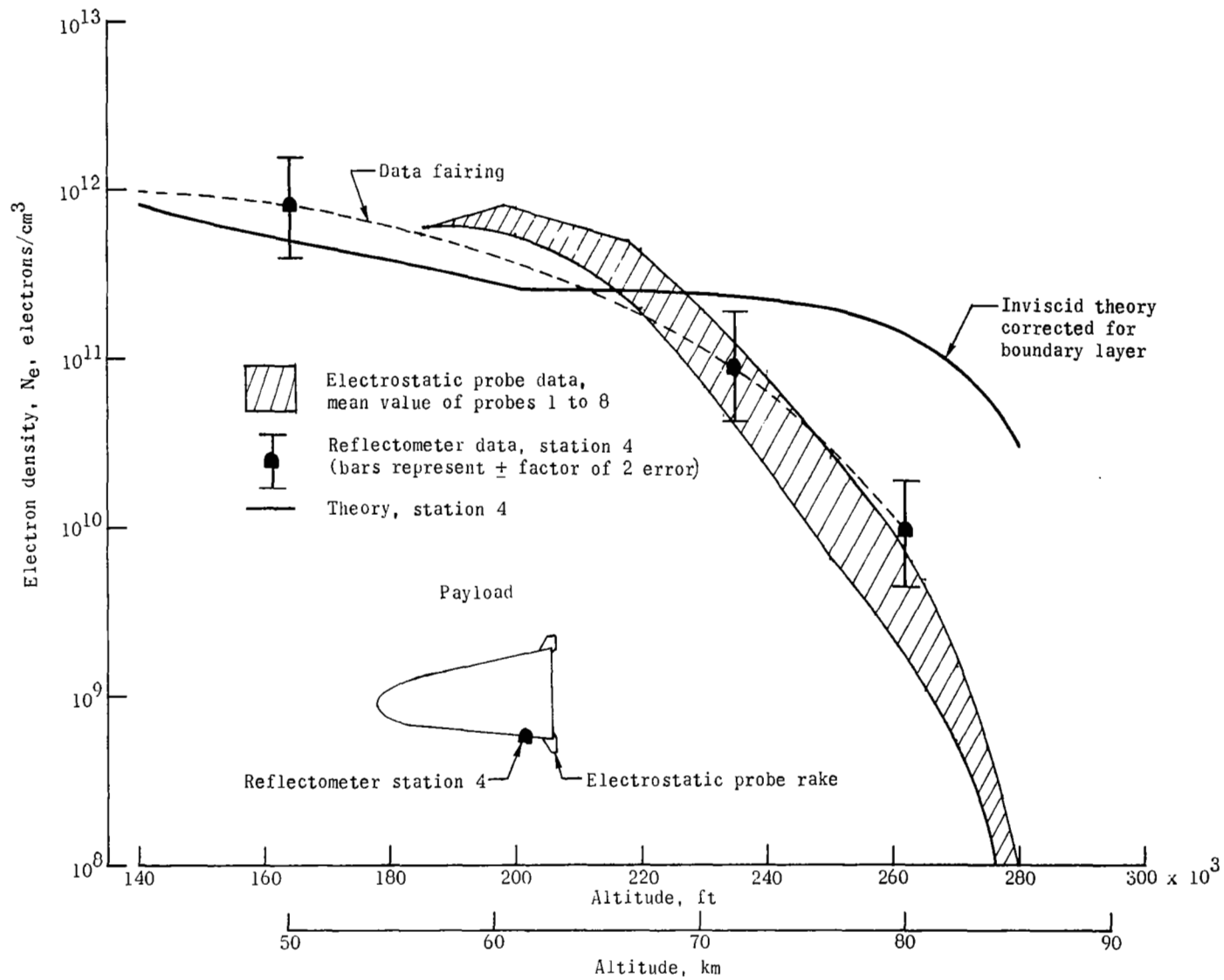


Figure 33.- Comparison of RAM C-II plasma diagnostic measurements with theoretical calculations.

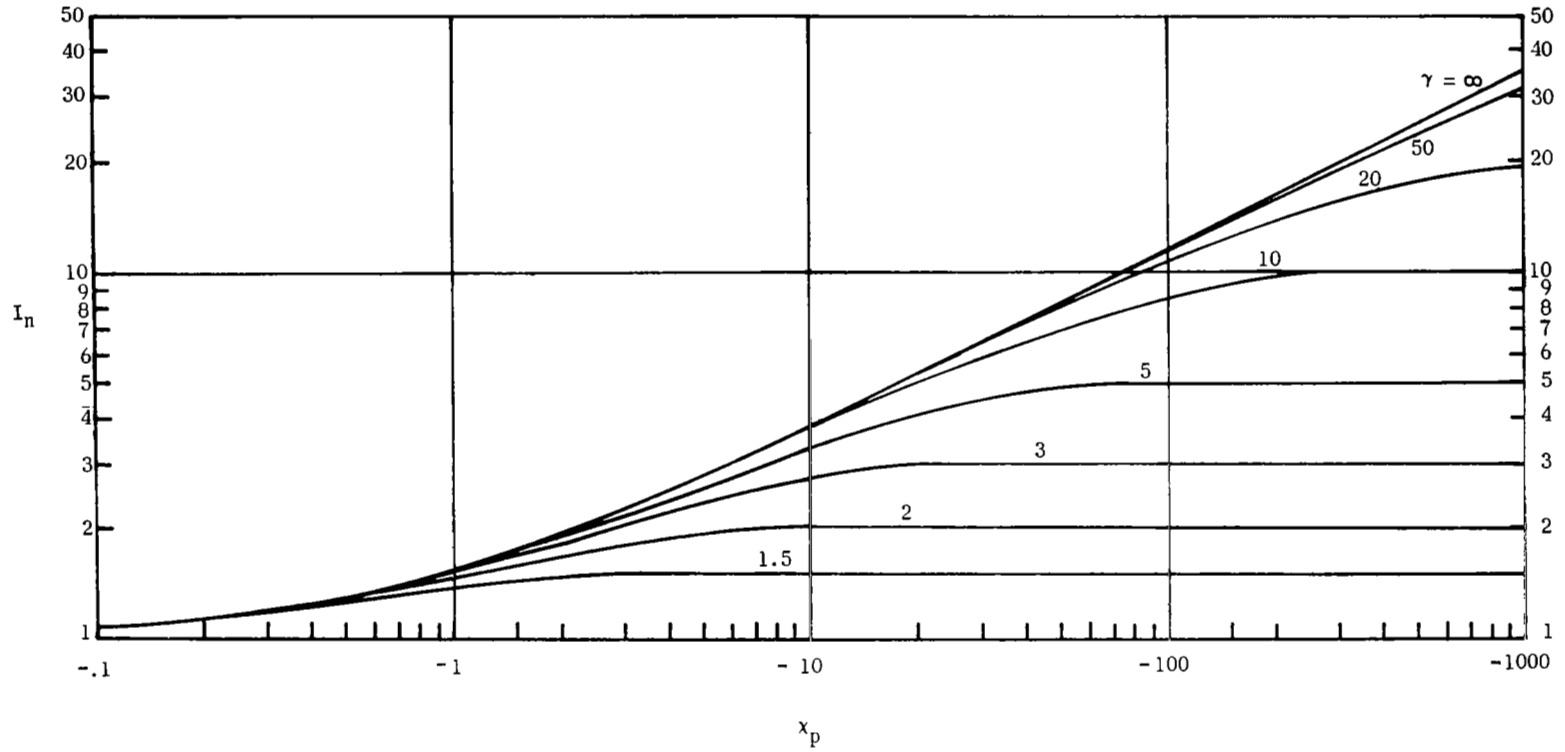


Figure 34.- Variation of normalized probe current with normalized potential difference between probe and plasma for range of  $\gamma$ .

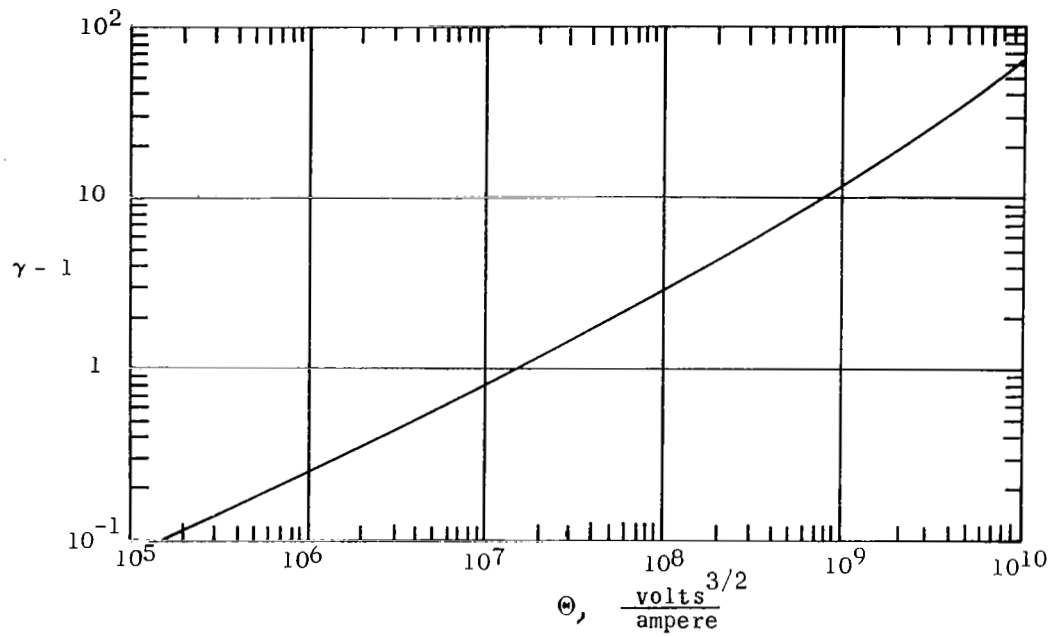


Figure 35.- Inverted form of space-charge-limited diode equation.



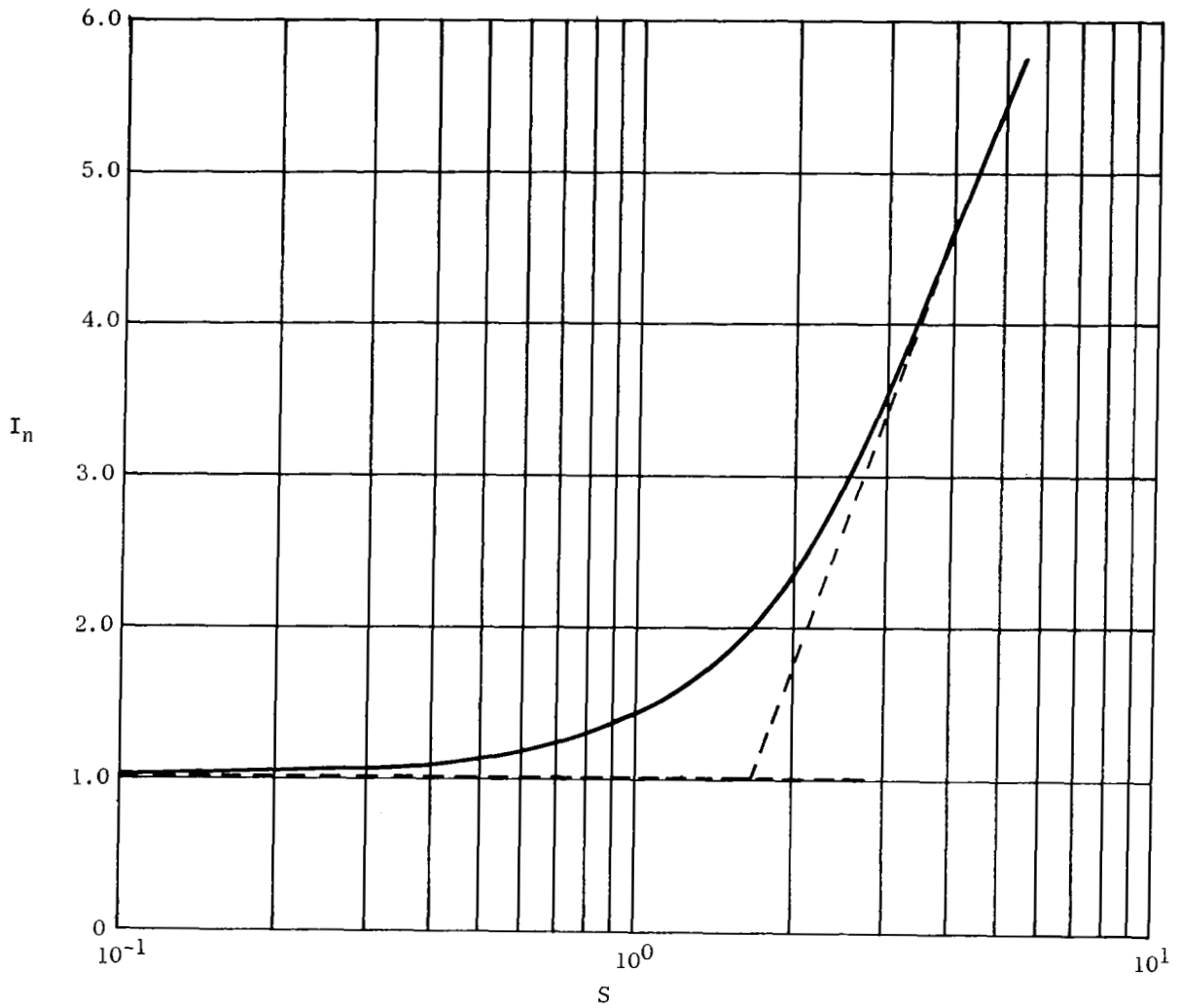


Figure 36.- Normalized current  $I_n$  collected by a probe perpendicular to the directed velocity as a function of the ratio  $S$  of directed to random velocity. Dashed lines indicate asymptotes.

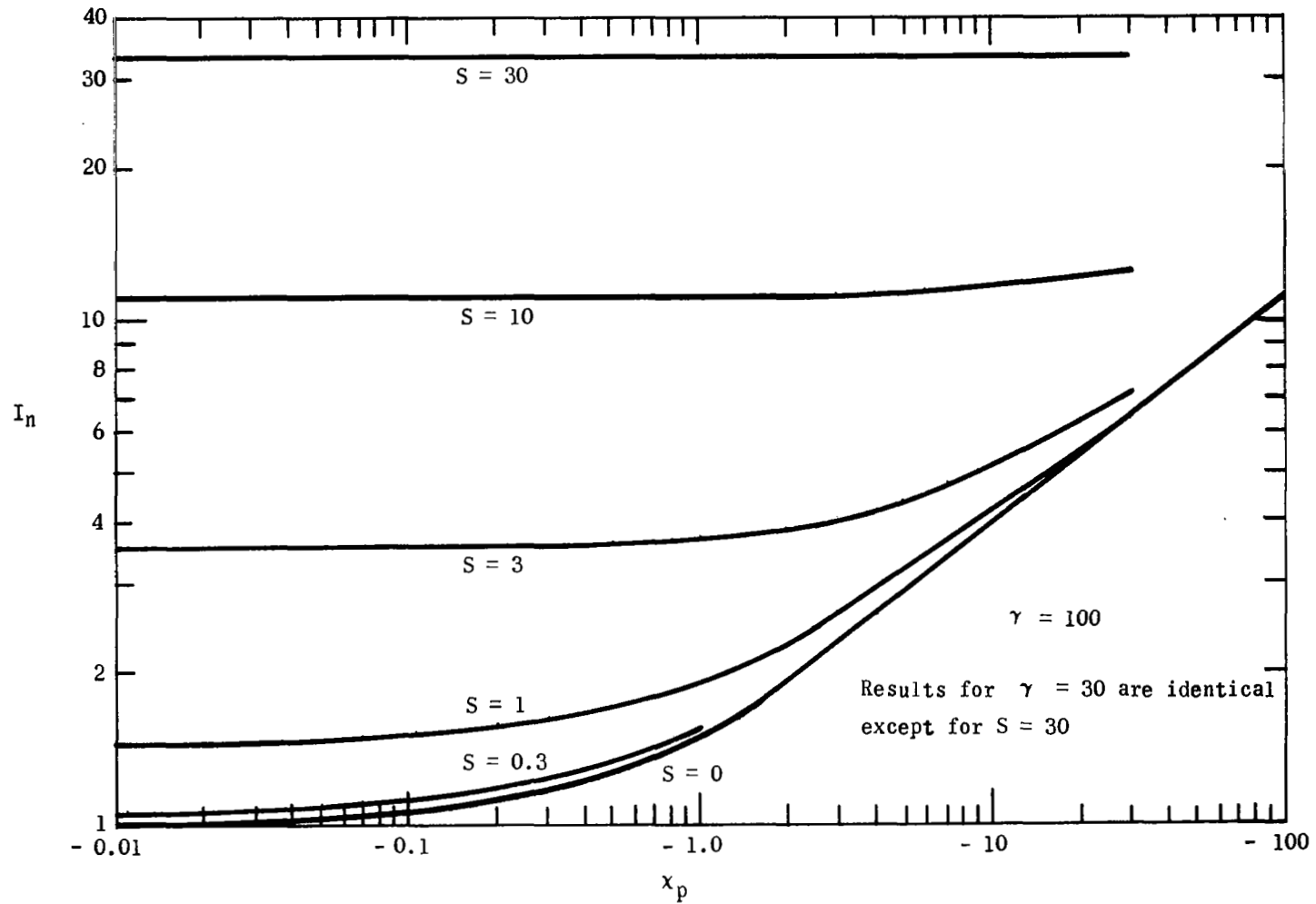


Figure 37.- Variation of normalized current with dimensionless probe potential for various speed ratios at  $\gamma = 100$ .

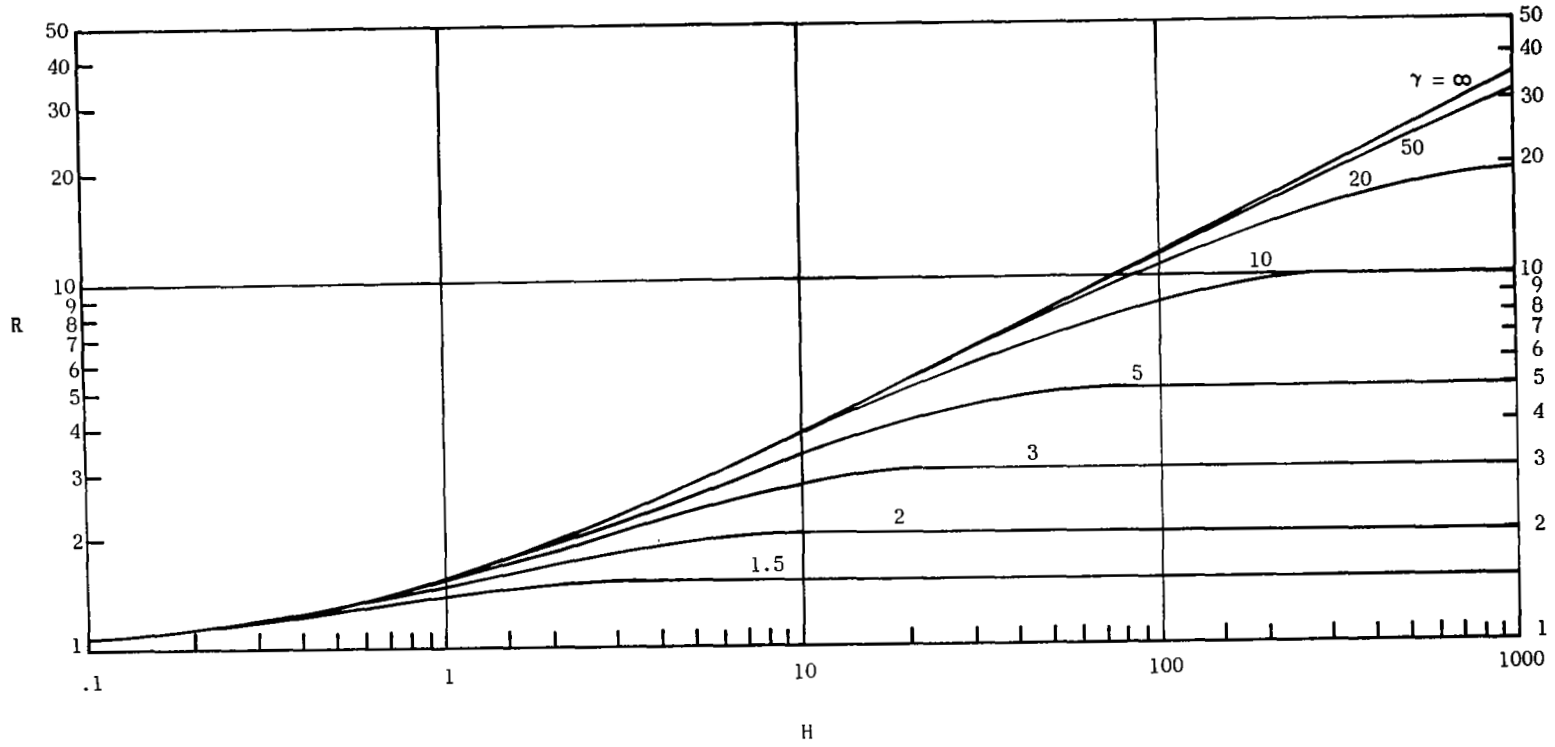


Figure 38.- Normalized probe current  $R$  as a function of the ratio of modified potential energy to the kinetic energy  $H$  for various values of  $\gamma$ .

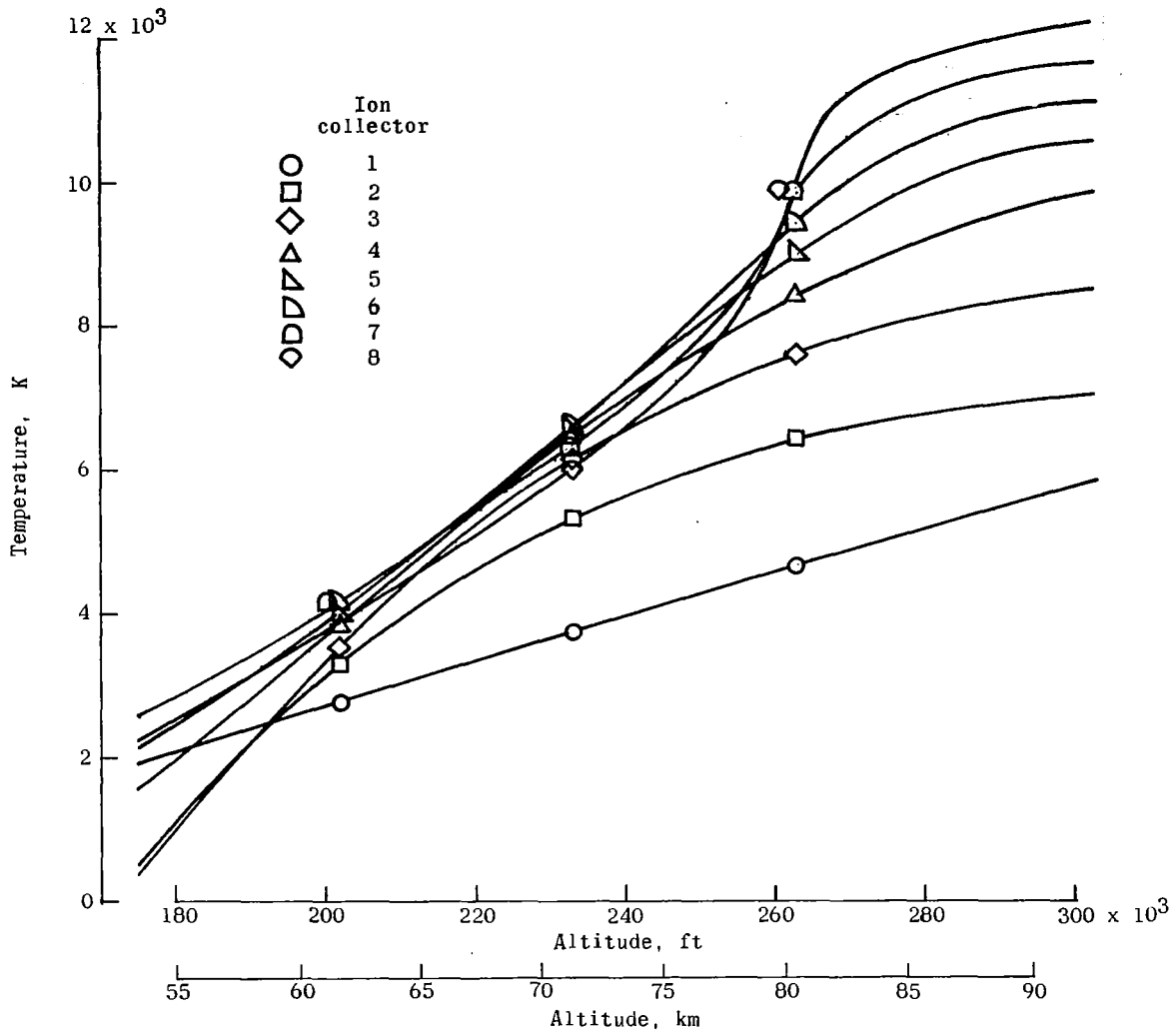


Figure 39.- Computed gas temperature as a function of altitude for electrostatic probe locations.

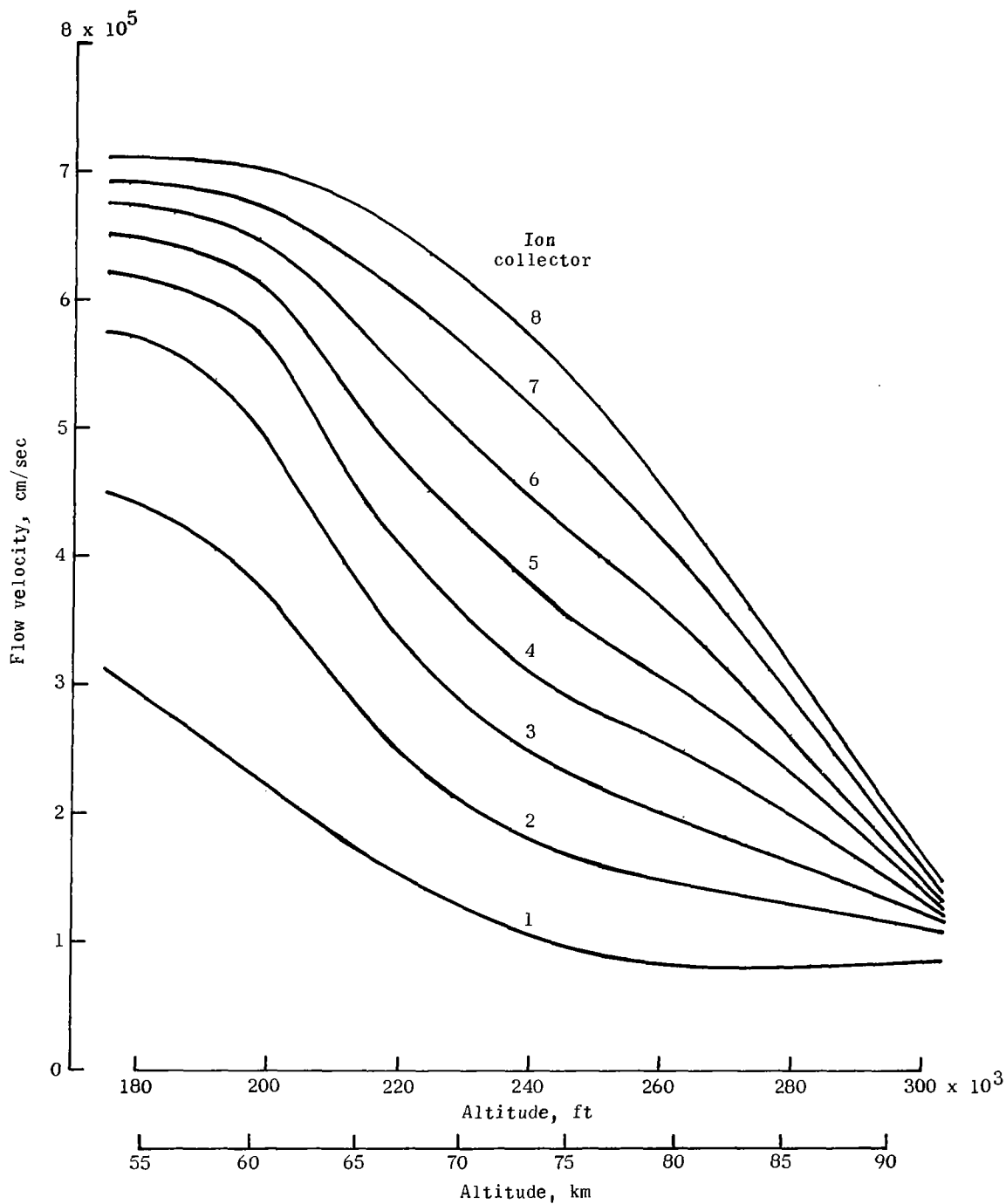
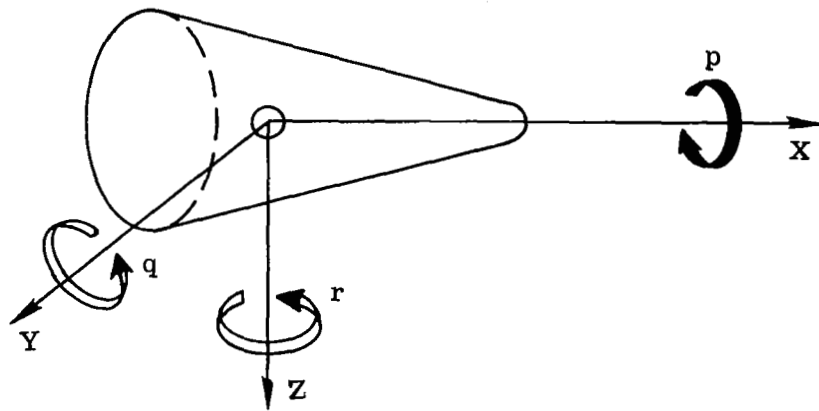
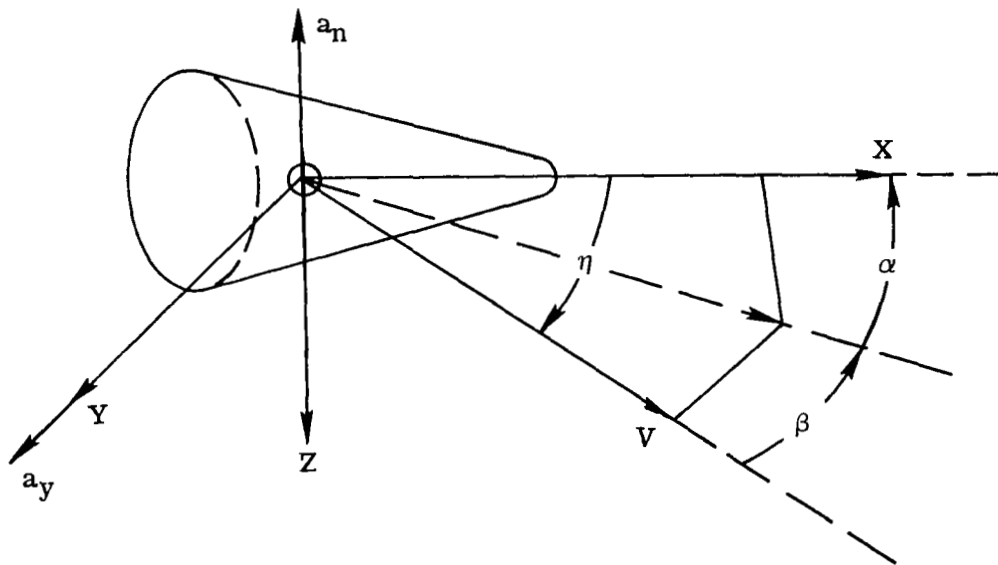


Figure 40.- Computed flow velocity as a function of altitude for electrostatic probe locations.



(a) Illustration of body rotations.



(b) Illustration of orientation with wind axis.

Figure 41.- Spacecraft axis system.

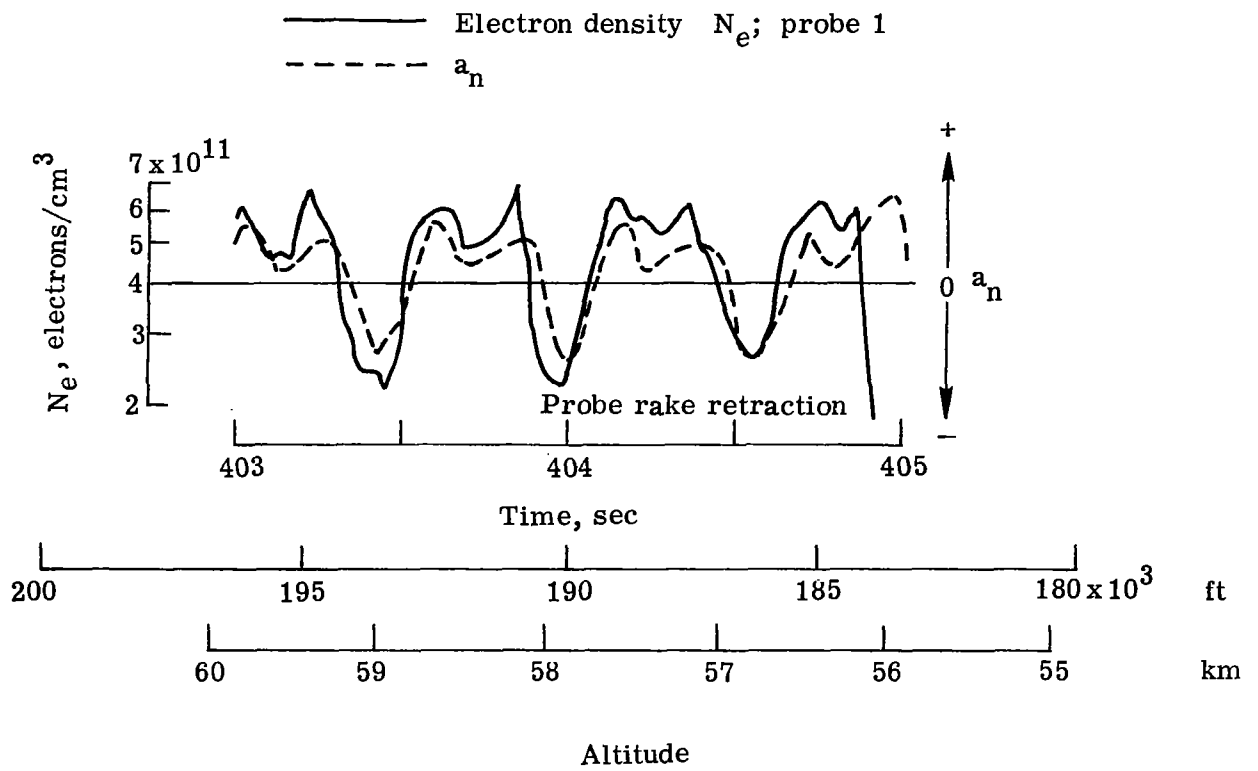


Figure 42.- Correlation of measured electron densities with measured normal acceleration on RAM C-II.

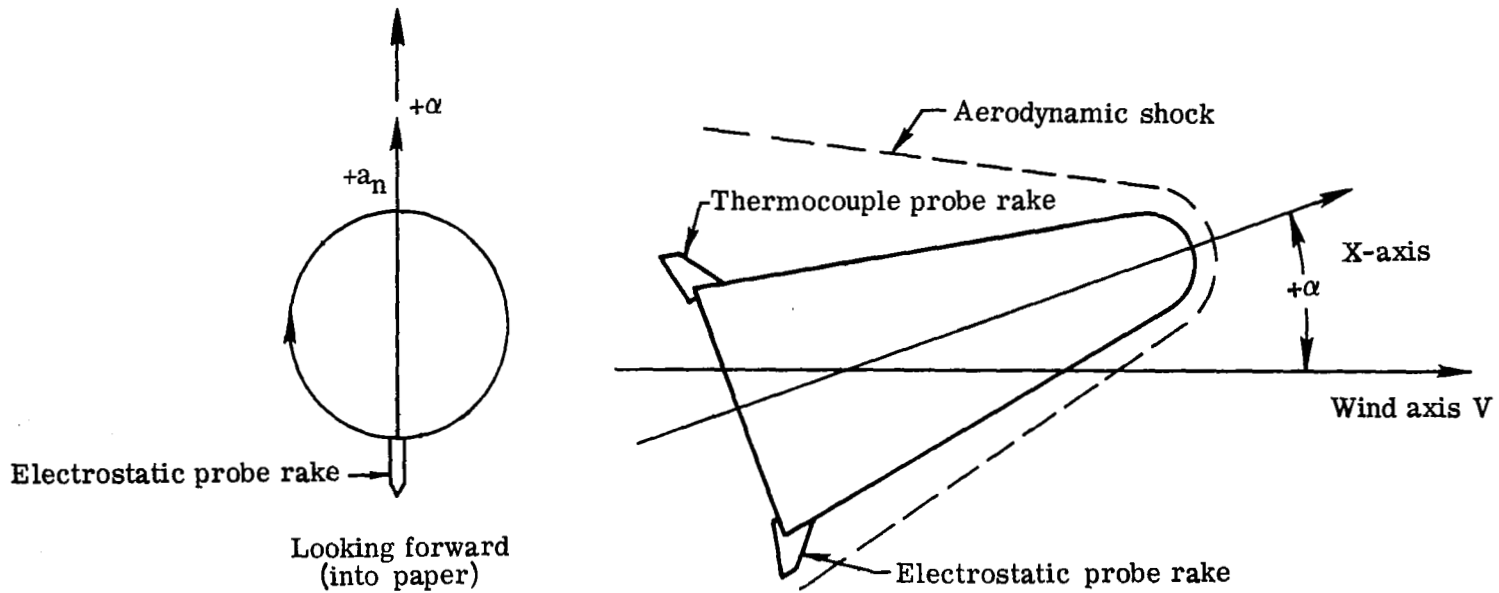


Figure 43.- Locations of probe rakes relative to axes systems.



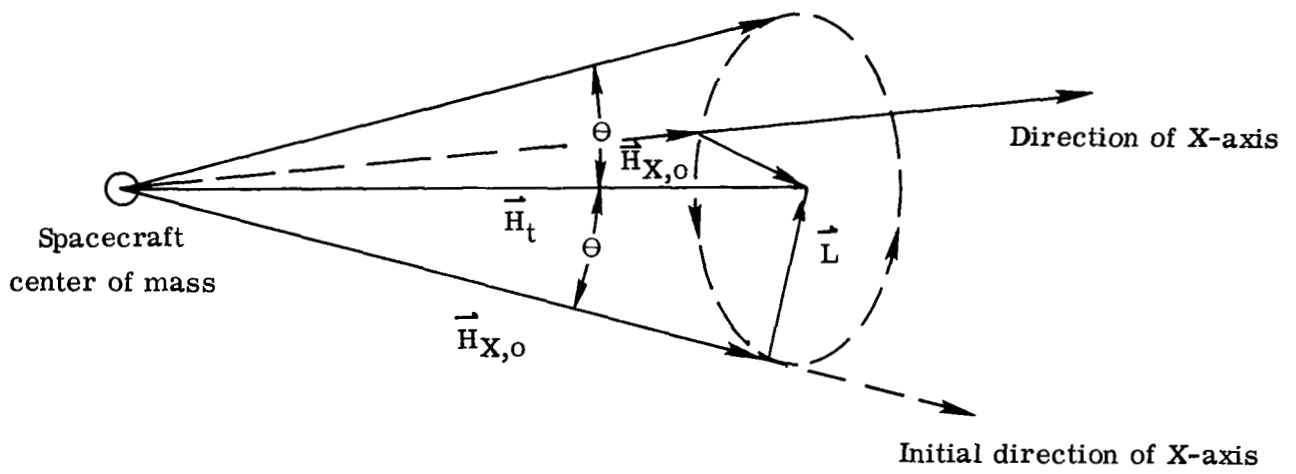
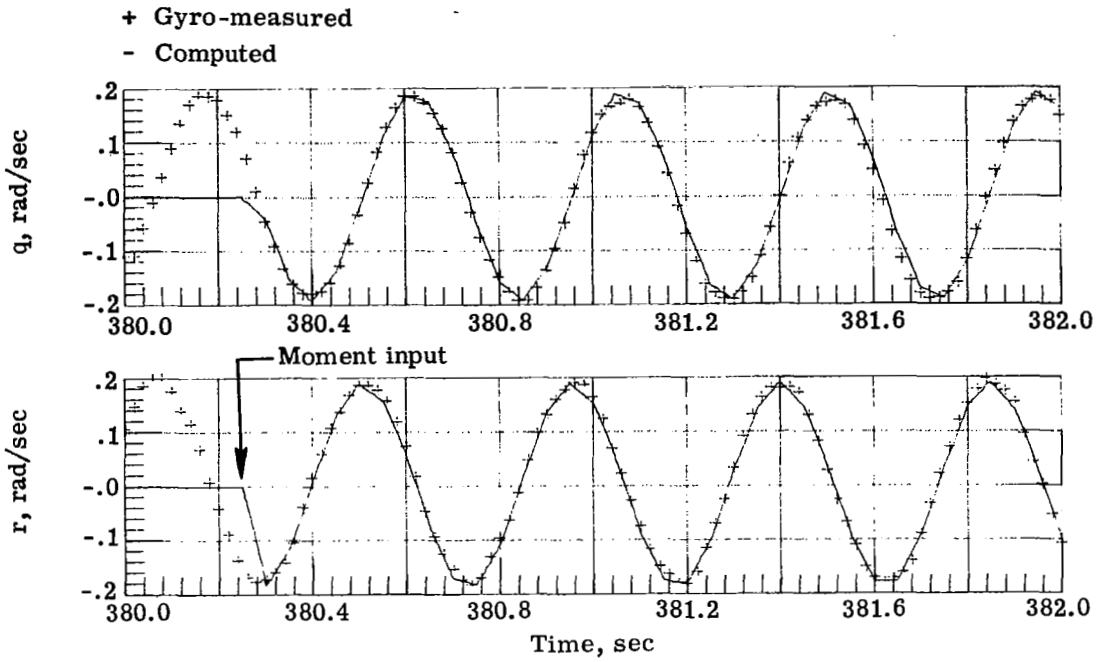
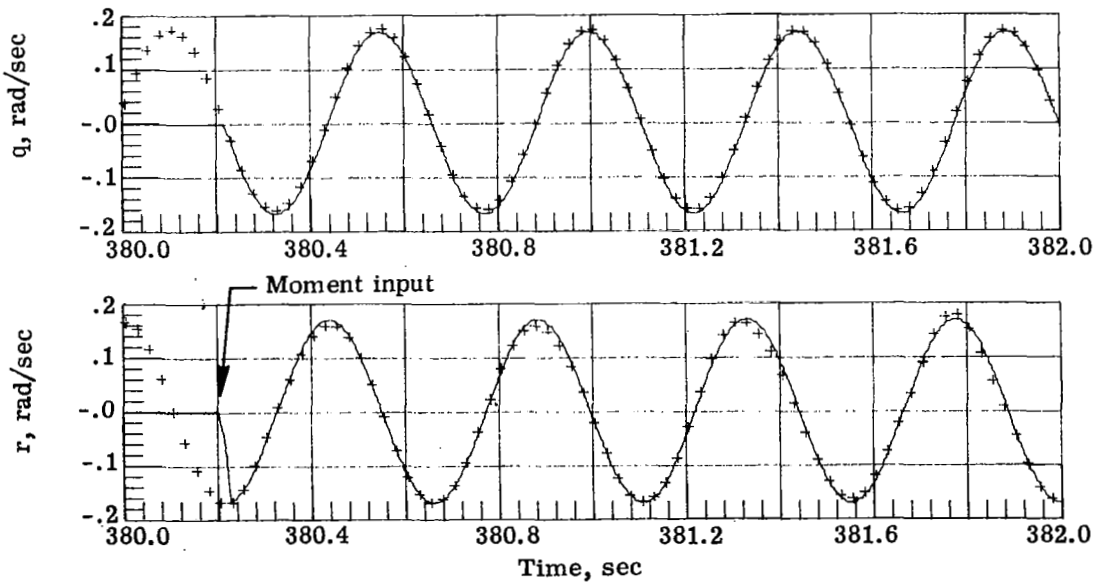


Figure 44. - Spacecraft precession in force-free space.

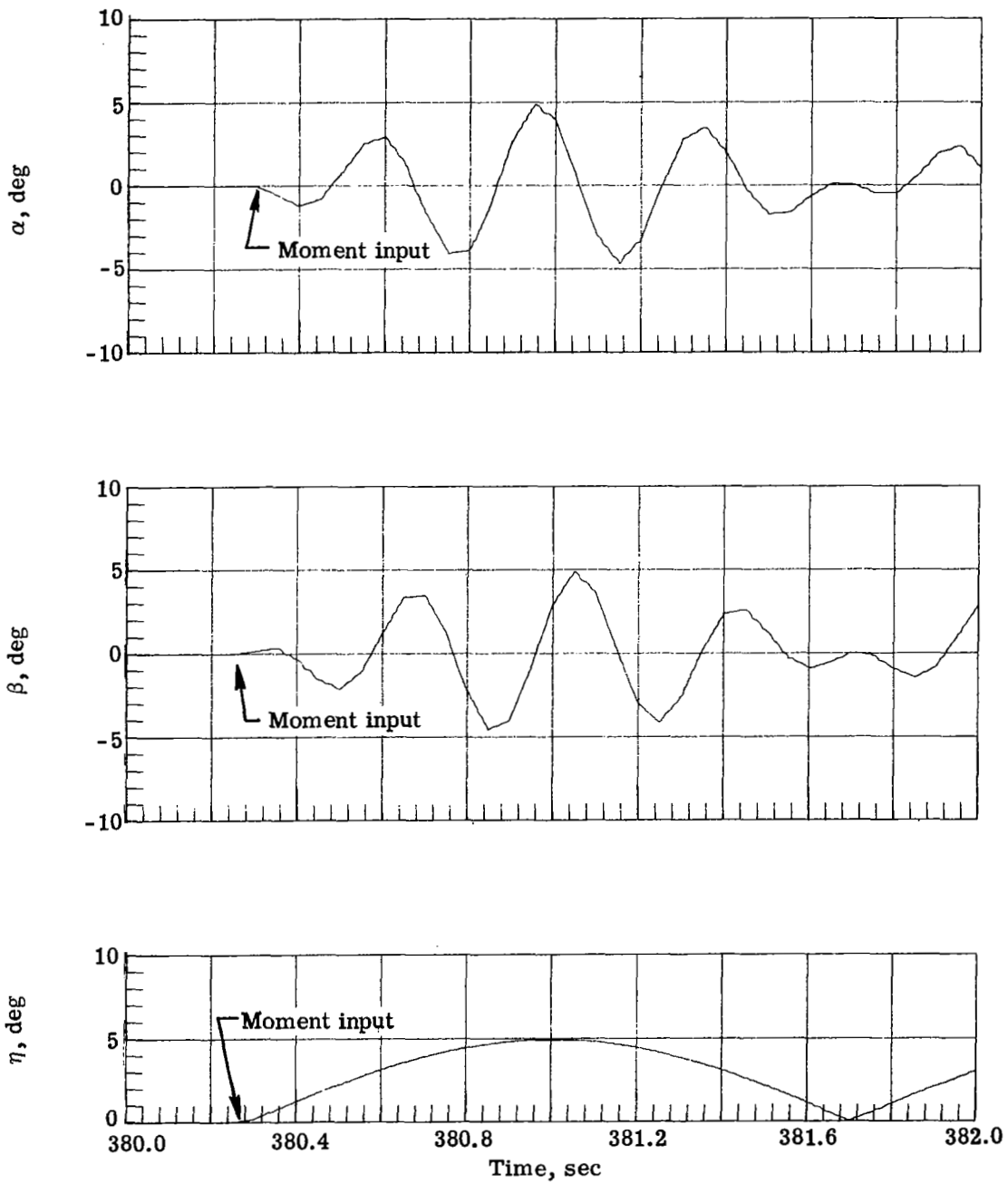


(a) RAM C-I.



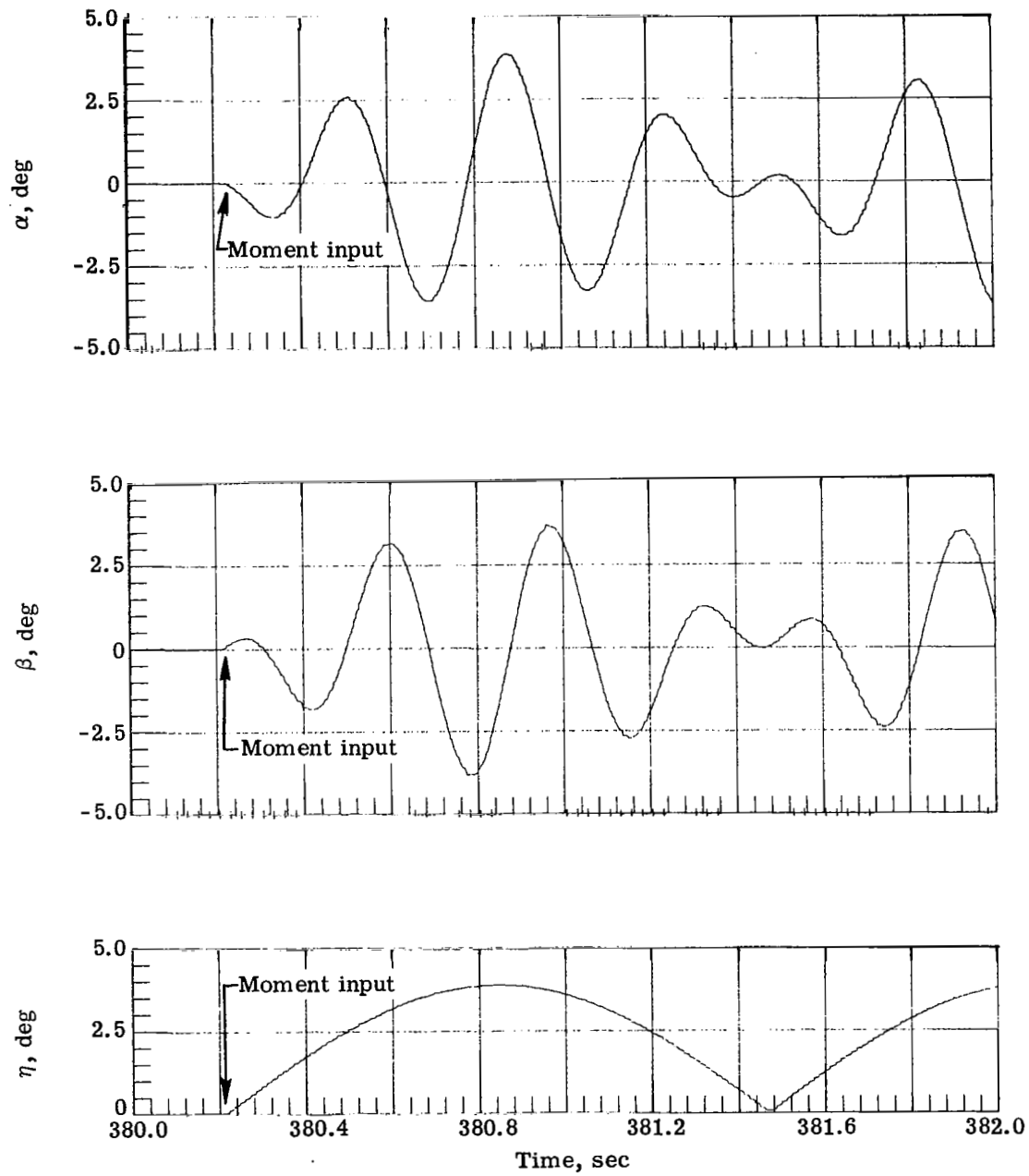
(b) RAM C-II.

Figure 45.- Comparisons of gyro-measured spacecraft rotation rates with computed rotation rates.



(a) RAM C-I.

Figure 46.- Computed characteristic wind angles.



(b) RAM C-II.

Figure 46.- Concluded.